The distribution and transport of the natural fallout radionuclide ^{210}Pb in the atmosphere and through catchment/lake systems.

Thesis submitted in accordance with the requirements of the University of Liverpool for the Degree of Doctor in Philosophy by

Panagiota Semertzidou

Department of Mathematical Sciences

School of Physical Sciences

University of Liverpool

February 2018

To my daughter Faye and my niece Fevronia.

Table of Contents

List of Figures

List of Tables

Acknowledgment

I would like to thank my supervisors, Dr Gayane Piliposyan and Professor Peter Appleby for their valuable contribution and feedback. I would like to thank them for the encouragement and advice they have provided throughout my time as their student. I would also like to thank Professor Richard Chiverrell for his help, comments and suggestions during my studies. I am very grateful for the vibrant and friendly environment that you have all offered me during the last four years.

I must also express my thankfulness to Alexandros, my husband, for his continued support and willingness to help me through my studies. Special thanks go to my parents for the huge encouragement they have given me all this years. Lastly, I want to acknowledge my sister, her support worth more than I can express on paper.

Abstract

This thesis contributes to the field of past environments and environmental radioactivity, specifically geochronology techniques and applications through lake sediment samples. Techniques used rely heavily on the analysis of isotopes, such as the natural radionuclide ^{210}Pb, which is widely used for dating environmental records stored in natural archives such as lake or marine sediments, and peat bogs.

The first part of this research investigates the atmospheric residence time of ^{210}Pb which is a key parameter controlling the distribution and fallout of this natural radionuclide over the earth's surface. A simple model was introduced for calculating the distributions of ^{210}Pb and its daughter radionuclides at northern mid-latitudes (30^{o}-65^{o}N), a region containing almost all the available empirical data. Since atmospheric fallout is the key driving force controlling the delivery of ^{210}Pb to lake sediments and other natural archives, the results of this research are an important step in the development of more reliable methodologies for dating these archives. A further important potential application is to model long time-scale studies of global circulation and the long-range transport of atmospheric pollutants. Given the constant input of the source radionuclide ^{222}Rn (measured on time-scales of a year or more), ^{210}Pb is ideally placed to serve as a tracer for these processes. The results of this study have been published in a paper, which is included in Appendix 2.

The robust atmospheric model of residence time presented here has many applications in the field of environmental science. The most immediate, ^{210}Pb dating, is of crucial importance to a very large number of environmental studies, e.g. those concerned with reconstructing historical levels of atmospheric pollution by substances such as heavy metals and Persistent Organic Pollutants (POPs). There are however relatively few studies focussing on the relationship between the sediment record and atmospheric fallout, and in particular on the pathways by which ^{210}Pb deposited on the landscape is incorporated in the sediment record.

The second part of this thesis is concerned with measuring and modelling catchment transport processes for fallout ^{210}Pb and ^{137}Cs in the lake of Brotherswater. Because of its very large catchment/lake area ratio, Brotherswater is an ideal site for studying the influence of catchment inputs. New estimates of atmospheric deposition were made using a suite of soil cores collected from two relatively stable sites near the

lake itself. Fluxes through the water column were determined from sediment samples collected in sediment trap samples placed at two different locations within the lake. Long-term supply rates to the sediment record were measured using a suite of 10 new cores collected from a range of depositional environments within the lake.

Using simple models of catchment/lake systems, results from the present study were integrated with those from two earlier multi-core studies carried out on the same lake in 1976/7 and 1988/9 in order to quantify more accurately the sources and fate of ^{210}Pb entering the water column of Brotherswater. Whereas the earlier (1976/7) study suggested that transport from the catchment accounted for 94% of all inputs, almost all of which exited the lake via the outflow, revised estimates suggest that catchment inputs were significantly lower than this and accounted for no more than around 67% of ^{210}Pb entering the water column. Further, a substantial fraction (around 40%) of these inputs were retained in the sediment record.

Analysis showed that the main reason for the difference is attributed to the fact that whereas sediments transported from the catchment include large quantities of relatively coarse material, only the fine sediments (~3 mm) play a significant role in transporting ^{210}Pb. The importance of catchment inputs is still significant, largely due to the large ratio of the catchment size relative to the size of the lake. The mass balance calculations suggest that they amount to no more than between 2.4-3.4% of the annual fallout onto the catchment. Results showed that the transport parameter used to model catchment inputs has a very similar value to that in nearby Blelham Tarn, calculated in earlier studies (Appleby et al., 2003).

The relative importance of catchment inputs raises questions about the reliability of the standard simple models used for dating lake sediments. Comparisons between the ^{210}Pb and ^{137}Cs records from the three different studies spanning nearly 40 years were used to study the long-term stability and reliability of records stored in these natural archives. Dried sediment samples from each of the present cores were analysed by gamma spectrometry for ^{210}Pb, ^{226}Ra, ^{137}Cs and ^{241}Am, following a similar protocol to that used in the 1988/9 study. The ^{137}Cs results graphically illustrate the progressive burial of a peak in concentrations recording the 1963 fallout maximum from the atmospheric testing of nuclear weapons, and its subsequent reduction due to radioactive decay. The post-1986 cores are characterised by the appearance and burial

of a second peak recording fallout from the 1986 Chernobyl accident. Identification of the 1963 137Cs peak in post-1986 cores was confirmed by the co-presence of traces of ^{241}Am, also a product of nuclear weapons test fallout. In both the 1988/9 study and the present study, ^{210}Pb dates calculated using the Constant Rate of Supply (CRS) model for the most part placed 1963 and 1986 at depths very similar to those determined from the ^{137}Cs records.

The maintenance of this agreement over a period of more than two decades provides evidence of the reliability of sediment records in this lake, and the validity of models used to interpret them. Unfortunately, the ^{137}Cs records were too indistinct and 1963 too recent to make similar comparisons in the case of the 1976/7 cores. Agreement between ^{210}Pb and ^{137}Cs dates was best at sites where the net rate of supply of ^{210}Pb to the sediment record was comparable to the atmospheric flux. Small but significant discrepancies were observed at sites where the ^{210}Pb supply rate greatly exceeded the atmospheric flux, most probably due to additional time-dependent inputs from the catchment, or post-depositional sediment redistribution within the lake. The results of this study have been submitted for publication in a paper included in Appendix 2.

Introduction

The natural radionuclide ^{210}Pb is widely used for dating environmental records stored in natural archives such as lake or marine sediments, and peat bogs. The age of any sediment later is calculated by comparing the (measured) present-day activity of ^{210}Pb in the sample with its (estimated) original activity when the sample was laid down at the sediment/water interface. Estimates of the original activity are made using models of the processes by which ^{210}Pb accumulates in the sample. Although various models have been developed to achieve this objective (Krishnaswami et al. 1971; Appleby and Oldfield 1978), they are all based on highly simplified representations of the processes governing the origins of ^{210}Pb and its distribution in the environment. Since in specific situations there may be significant discrepancies between the actual and modelled rates of supply of ^{210}Pb, in all cases it is essential to make a considered assessment as to which, if any, of the simple models is applicable to that situation. In making this assessment it is necessary to have a clear idea as to the origins of ^{210}Pb and its pathways through the environment. The ^{210}Pb cycle can be separated into two distinct stages:

- Firstly, the production of ^{210}Pb in the atmosphere by the decay of the inert gaseous radionuclide ^{222}Rn, and its subsequent distribution in and fallout from the atmosphere.
- Secondly, the transport and delivery of fallout ^{210}Pb via terrestrial and aquatic pathways and its eventual incorporation in the sediment record.

One of the key parameters controlling ^{210}Pb fallout is its residence time in the atmosphere. Part A of this thesis focuses on determining the atmospheric residence time by considering the relationship of concentrations of ^{210}Pb to those of its daughter radionuclides ^{210}Bi and ^{210}Po. Empirical measurements of these radionuclides were made in the 1970s and 1980s at a number of different locations, mainly in continental USA and western Europe. Estimates of the atmospheric residence time based on these measurements effectively assumed that the empirical data were typical of the mean global concentrations. A simple mathematical model is introduced to provide estimates of the global distribution of the ^{210}B1/^{210}Pb and ^{210}Po/^{210}Pb ratios. By fitting the empirical data at specific locations to the modelled values we have shown that the effective residence time is significantly longer than earlier estimates of between 4 and 7 days. The increase is in part attributable to the reservoir effect of radionuclides stored

in the stratosphere. The results have been published in Semertzidou et al. (2016) (see Appendix), however a more detailed account of the work is provided here. In Chapter 1 we give a brief account of the origins of ^{210}Pb in the atmosphere and review the global mass balance equations. In Chapter 2 we review the empirical data available in the literature on ^{210}Pb and its daughters in the atmosphere and estimates of the residence time are made using the global mass balance equations. Chapter 3 presents a mathematical model for determining the distribution of ^{210}Pb, ^{210}Bi and ^{210}Po, along with the details of the numerical method used to calculate the vertical and horizontal distribution due to prolonged inputs of ^{222}Rn from point and extended source. The analysis was carried out using the MATHEMATICA software package. Chapter 4 applies the methodology to a global model and determines a value for the residence time that gives a best fit with the empirical data.

The most widely used ^{210}Pb dating model assumes that fallout of this radionuclide from the atmosphere is relatively constant from year to year and results in a relatively constant supply of fallout ^{210}Pb to sediments deposited on the bed of a lake. This assumption is however questionable at sites where substantial amounts of fallout ^{210}Pb deposited on the catchment are subsequently transported to the lake by runoff or erosion. The problem is likely to be more acute at sites with large catchment/lake area ratios. Appleby et al. (2003) have shown that 47% of fallout ^{210}Pb in the sediments of Blelham Tarn (catchment/lake area ratio of 42) originates in erosive inputs from the catchment. Part B of this thesis will be concerned with a detailed study of the origins and distribution of ^{210}Pb in the sediments of Brotherswater, a nearby small lake in the English Lake District with a catchment/lake area ratio of 72. An earlier study carried out in the 1970s (Eakins et al., 1984) suggested that catchments inputs accounted for 93% of the ^{210}Pb entering Brotherswater and that only 14% of total inputs were incorporated in the sediment record. The fact that the rate of supply to the sediment record was approximately equal to the direct atmospheric inputs was believed to be fortuitous. Here the original data are revisited in the light of further studies carried out around in the late 1980s and early 1990s, and more recently during 2011-16.

Chapter 5 outlines the common models of catchment/lake systems, including transport from the catchment to the lake and thence through the water column either to the sediment record or outflow. Chapter 6 considers estimates of the atmospheric

deposition of ^{210}Pb at Brotherswater based both on direct precipitation data and on inventories in soil cores collected from stable sites in the catchment. Chapter 7 presents the results of direct measurements of the flux of fallout radionuclides through the water column of Brotherswater based on an analysis of material collected in sediment traps. The results of measurements of the rate of supply to the sediment record based on an analysis of cores collected from different locations within the lake are presented in Chapter 8, while Finally, Chapter 9 uses data both from the present and earlier studies to construct a mass balance model for fallout ^{210}Pb in Brotherswater and its catchment.

Sediment cores from the present study, together with those collected during earlier studies spanning a period of nearly 40 years, offered a unique opportunity to assess the validity of sediment records of environmental history and in particular the reliability of ^{210}Pb for dating those records. A paper on this subject has been submitted for publication and is included in Appendix 2 of this Thesis.

PART A: DETERMINING THE ATMOSPHERIC RESIDENCE TIME OF ^{210}Pb USING ^{210}Pb:^{210}Bi:^{210}Po ACTIVITY RATIOS

Chapter 1. Introduction

1.1 Rationale and Background

A good understanding of the origin and distribution of ^{210}Pb in the atmosphere is relevant not only to its application as a tool for dating environmental archives stored in natural archives such as lake and marine sediments but also to its potential role as a tracer for studies of global circulation and the long-range transport of atmospheric pollutants (Baskaran 2011; Rehfeld & Heimann, 1995). The source of ^{210}Pb is well-known and although concentrations and fallout at any particular location are highly variable on short timescales (days, weeks or months) they are relatively constant when averaged over periods of a year or more (Appleby et al. 2002). Three dimensional models operating on short time-steps (20 minutes to 30 h) have been developed by a number of authors (Feichter et al. 1991, Balkanski et al. 1993, Guelle et al. 1998a and b, Liu et al. 2001). These have two components, an established General Circulation Model that contains a detailed simulation of global atmospheric circulation over a given period of time, and a Chemistry Transport Model that computes the resulting global distribution of the relevant tracer under the impact of transport processes such as advection and diffusion. Such models suffer from two major disadvantages, they are very computationally intensive, and over many parts of the world there is very little empirical data against which they can be validated as they need monthly or yearly climatological data spanning a long period of time. They are also highly dependent on the extent to which the processes and parameterizations on which they are based are accurate representations of real world processes. An international workshop (Rasch et al. 2000) comparing different global models found that they produced significantly different results for the atmospheric distribution of ^{210}Pb.

Simpler models concerned with mean values over longer timescales have been developed by a number of authors. They include mass balance models concerned essentially (but not always explicitly) with the mean equilibrium global concentrations and fluxes (e.g. Moore et al. 1973). Although of limited value at specific locations, these models set limits on important parameters and can be used to assess the validity

of more detailed models. An earlier study by Jacobi and André (1963) modelled the equilibrium distributions of ^{222}Rn and ^{210}Pb in such a vertical column of air assuming that the spatial gradients in the concentrations are small, the vertical distributions are controlled mainly by vertical turbulent diffusion, and the ^{210}Pb removal rate (by wet and dry deposition) is proportional to the concentration. A dynamic element was introduced by Turekian et al. (1977) who presented a simple mass balance model for the evolution of the ^{222}Rn and ^{210}Pb inventories in a vertical column of air moving over the earth's surface.

Combining these two approaches, Piliposian & Appleby (2003) developed a more detailed model describing the distribution of ^{222}Rn and ^{210}Pb in a similar vertical column that also took account of the effect of the stratosphere in delaying fallout back to the earth's surface. Using a very simple model of West-to-East circulation, the results were shown capable of capturing the essential features of global fallout at mid-latitudes in the Northern Hemisphere, and also the importance of long-range intercontinental transport of ^{210}Pb.

The model required a relatively small number of key parameters, including the ^{222}Rn flux from land-surfaces, the turbulent diffusivity of ^{222}Rn and ^{210}Pb in the atmosphere, and the mean residence time for ^{210}Pb in the troposphere. Values of the ^{222}Rn flux and turbulent diffusivity were determined from measured vertical profiles of ^{222}Rn in the atmosphere available from the literature. Reliable values of the residence time were more difficult to obtain. Values were calculated using two different procedures, firstly from estimates of the ^{210}Pb/^{222}Rn inventory ratios in columns of air assumed to have reached an equilibrium distribution, and secondly from estimates of the global ^{210}Pb/^{222}Rn inventory ratio in the atmosphere.

Because of the very limited amount of data the results did however have a large degree of uncertainty. A third approach is to consider the ratios of atmospheric ^{210}Pb concentrations to those of its daughter radionuclides ^{210}Bi and ^{210}Po. Although this approach has been used in a number of earlier studies (Poet et al. 1972, Moore et al. 1973), the equations used to calculate the residence time were the global equilibrium equations and not strictly applicable to data from specific locations on the earth's surface. The main objective of this first part of my thesis was to extend the model developed by Piliposian & Appleby to the ^{210}Pb daughters ^{210}Bi and ^{210}Po and

determine a more reliable value for the residence time by fitting the modelled concentration ratios to the empirical data.

The following section provides a brief account of the origins of atmospheric ^{210}Pb and the global equilibrium equations and introduces the way in which they can be used to give a first order estimate of the ^{210}Pb residence time.

1.2 Origin of ^{222}Rn and ^{210}Pb in the atmosphere

Lead 210 occurs in naturally as a member of the ^{238}U decay series. Its immediate long-lived precursor ^{226}Ra (half-life 1602 years) decays by alpha emission to the inert gaseous radionuclide ^{222}Rn (half-life 3.82 days). This in turn decays via a number of short-lived radionuclides to ^{210}Pb (half-life 22.26 years). ^{210}Pb decays by beta emissions first to ^{210}Bi (half-life 5.013 days) and then to ^{210}Po (half-life 138.38 days). This decays by alpha emission to the stable lead isotope ^{206}Pb. ^{210}Pb in sediments consists of two components: supported ^{210}Pb, which is present due to autogenic material of the sediment and unsupported ^{210}Pb, which originates from the atmospheric deposition. Unsupported ^{210}Pb can be determined by subtracting supported activity from the total activity.

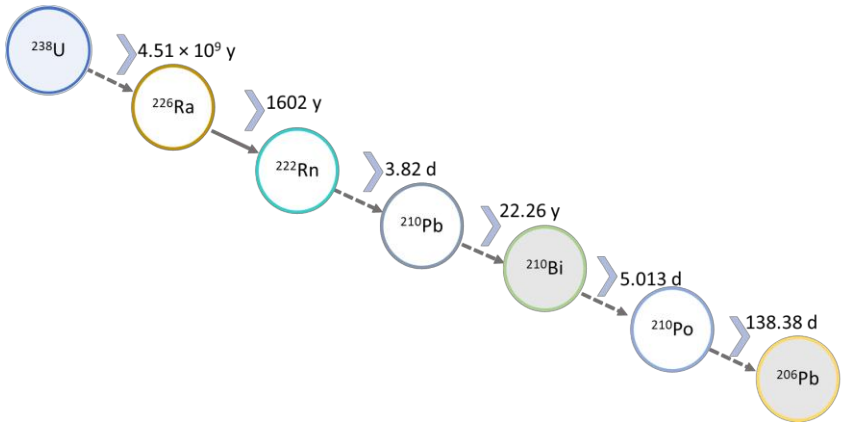

Figure 1.1: ^{238}U decay series.

Radium 226 is present in most soils in concentrations typically of around 30-50 Bq kg^{-1}. The recoil caused by the emission of an alpha particle from a ^{226}Ra atom near the surface of a particle may result in the ejection the newly produced ^{222}Rn atom into the interstices of the soil. Assuming a homogeneous soil and a simple 1-dimensional diffusion model, it is readily shown (Appleby & Piliposyan 2010) that the interstitial ^{222}Rn activity per unit volume C is controlled by the equation

$$\frac{\partial C}{\partial t} = -\lambda_{Rn} C + f_e \lambda_{Rn} C_{Ra} + D \frac{\partial^2 C}{\partial z^2} \tag{1.1}$$

where C_{Ra} is the ^{226}Ra activity per unit volume of soil (Bq cm^{-3}), f_e the fraction of ^{222}Rn atoms escaping into the interstices, λ_{Rn} (d^{-1}) the ^{222}Rn decay constant, D (cm^2 d^{-1}) a diffusion coefficient for ^{222}Rn through soil, and z (cm) depth below the soil surface. The value of D will depend on the molecular diffusivity of ^{222}Rn through the interstitial fluid (water and/or air) and the porosity of soil. Although ^{222}Rn concentrations on short timescales may vary significantly with the time of year and degree of saturation of the soil, mean concentrations over the longer timescales appropriate to ^{210}Pb studies are likely to satisfy a steady state solution. Assuming the soil depth sufficiently great for ^{222}Rn/^{226}Ra equilibrium to be reached near the soil base this may be written

$$C = f_e C_{Ra} \left(1 - \mathrm{e}^{-\sqrt{\frac{\lambda_{Rn}}{D}} z} \right). \tag{1.2}$$

The flux of ^{222}Rn across the soil surface to the atmosphere will be

$$\mathcal{F} = -D \left. \frac{\partial C}{\partial z} \right|_{z=0} = f_e C_{Ra} \sqrt{\lambda_{Rn} D}\,. \tag{1.3}$$

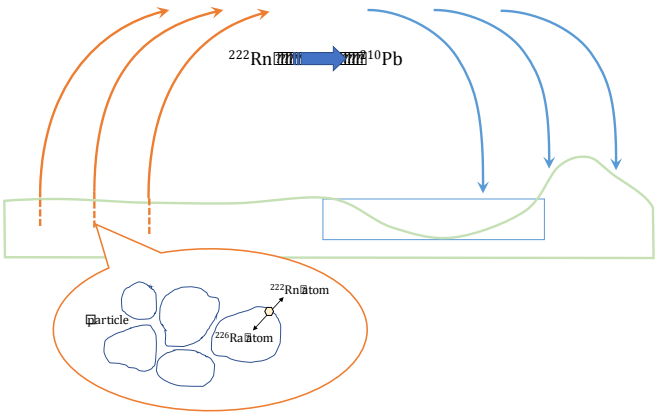

Figure 1.2: ^{222}Rn escape.

Measured values of ^{226}Ra activity in soils show that it is typically in the range 30-50 Bq kg^{-1} (Lauer et al. 1995; Garcia-leon et al. 1994). Measurements of the escape fraction give widely varying results but suggest a value of around 10% (Krishnaswami et al. 1998). The diffusivity depends strongly on the water content of the soil and varies substantially during the course of a year. A best estimate for reasonably dry soils is 0.06-0.08 cm^2 s^{-1}. ^{222}Rn emanation rates calculated using these values, ranging from 900-1800 Bq m^{-2} d^{-1}, are reasonably consistent with results obtained by direct

measurements on soils (Wilkening et al. 1975). Additional sources of atmospheric ^{222}Rn include emissions from groundwater and, to a much lesser extent, from the oceans.

Integrating these data we obtain a good estimate of the mean exhalation rate involves a great deal of uncertainty. An alternative approach to this calculation is based on measurements of ^{222}Rn in the atmosphere. In the interior of a large land mass, since the rate of supply of ^{222}Rn into the base of a vertical column of air by emanation from the land surface is to a good approximation balanced by the rate of loss of ^{222}Rn from the column by radioactive decay, the emanation rate can be estimated directly from the ^{222}Rn inventory. Using published data on vertical ^{222}Rn profiles at sites in continental USA and Eurasia, Piliposian and Appleby (2003) estimated the mean ^{222}Rn flux from the land surface to be 1570 Bq m^{-2} d^{-1}. This figure is relatively consistent with the emissions data and, in spite of the large uncertainties, may be regarded as representing a reasonable estimate of the mean exhalation rate from land surfaces free of ice cover or water.

1.3 Global mass balance equations for ^{222}Rn and ^{210}Pb in the atmosphere

The global cycle of ^{222}Rn and ^{210}Pb in the atmosphere is illustrated in Figure 1.3. ^{222}Rn emanating from soils is rapidly transported to all levels of the atmosphere (in spite of its relatively short half-life of just 3.82 days) and, being chemically inactive, can only be removed from the atmosphere by the process of radioactive decay. In contrast, its daughter radionuclide ^{210}Pb (half-life 2.26 years) is highly reactive and quickly becomes attached to airborne particulates that are readily removed from the atmosphere by washout or dry deposition (Junge 1963; Gillette et al. 1972).

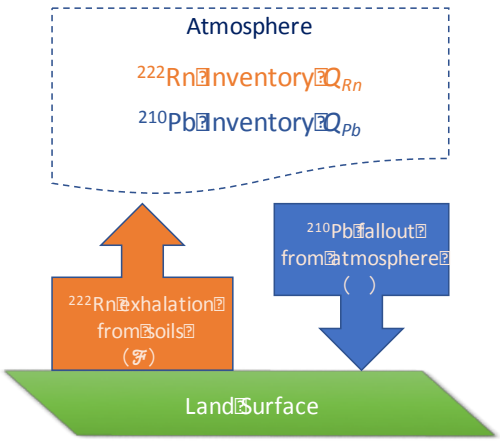

Figure 1.3: The global balance of ^{222}Rn and ^{210}Pb in the atmosphere.

Since the atmosphere as a whole can reasonably be assumed to be in a state of near equilibrium (when measured on timescales of a year or more), the global rate of supply of ^{222}Rn will be balanced by the global loss rate by radioactive decay. Writing $\mathcal{F}$ (Bq m^{-2} d^{-1}) for the mean global flux per unit area from the earth's land surfaces, it follows that,

$$A_L \mathcal{F} = \lambda_{Rn} Q_{Rn},$$

where A_L (m^3) is the effective area of the earth's land surface contributing to the flux, λ_{Rn} (d^{-1}) is the ^{222}Rn decay constant and Q_{Rn} (Bq) the global ^{222}Rn inventory. The rate of production of ^{210}Pb by ^{222}Rn decay will similarly be balanced by the losses in this case due fallout from the atmosphere as well as radioactive decay. Writing $\mathcal{P}$ for the mean atmospheric flux per unit area it follows that the global ^{210}Pb inventory Q_{Pb} will satisfy the balance equation

$$\lambda_{Pb} Q_{Rn} = \lambda_{Pb} Q_{Pb} + A_E \mathcal{P},$$

where λ_{Pb} is the ^{210}Pb decay constant and A_E the total area of the earth's surface. Assuming that the mean global ^{210}Pb fallout rate is proportional to the global ^{210}Pb inventory it can further be written that

$$A_E \mathcal{P} = k_g Q_{Pb},$$

where k_g is a mean global loss-rate coefficient. The reciprocal $\tau_g = 1/k_g$ provides a measure of the mean global residence time of ^{210}Pb in the atmosphere. Eliminating the ^{210}Pb flux from these equations it follows that the global ^{222}Rn and ^{210}Pb inventories are related by the equation

$$Q_{Pb} = \frac{\lambda_{Pb}}{\lambda_{Pb} + k_g} Q_{Rn}. \qquad (1.4)$$

Since the ^{210}Pb residence is estimated to be no more than a couple of weeks and so negligible compared to the radioactive half-life (22.26 years), the ^{210}Pb decay constant λ_{Pb} will be negligible compared to k_g and to a close approximation

$$k_g = \lambda_{Pb} \frac{Q_{Rn}}{Q_{Pb}}. \qquad (1.5)$$

Given empirical values for the ^{222}Rn and ^{210}Pb inventories this equation can be used to estimate the loss-rate coefficient k_g (d) and hence the ^{210}Pb residence time. Substituting into the equation for $\mathcal{P}$ (Bq m^{-2}y^{-1}) we obtain

$$A_E \mathcal{P} = \lambda_{Pb} Q_{Rn} = \lambda_{Pb} \left(\frac{A_L \mathcal{F}}{\lambda_{Rn}} \right),$$

whence to a close approximation

$$\mathcal{P} = \frac{\lambda_{Pb}}{\lambda_{Rn}} \frac{A_L}{A_E} \mathcal{F} . \tag{1.6}$$

Assuming a mean ^{222}Rn exhalation rate of ~1570 Bq m^{-2} d^{-1} from the c.74% of earth's continental land surface free of ice sheets and permafrost and fresh water bodies and ~10 Bq m^{-2} d^{-1} from the oceans, and given that ~70% of the ice free land is in the Northern Hemisphere, the mean ^{210}Pb flux from atmosphere is calculated to be ~82 Bq m^{-2} y^{-1} in the Northern Hemisphere and ~37 Bq m^{-2} y^{-1} in the Southern Hemisphere. These values are relatively consistent with those in the ERRC global data base on ^{210}Pb fallout which suggest a mean ^{210}Pb flux of ~70 Bq m^{-2} y^{-1} in the Northern Hemisphere and ~41 Bq m^{-2} y^{-1} in the Southern Hemisphere.

1.4 Global mass balance equations for ^{210}Bi and ^{210}Po in the atmosphere

The radioactive daughters of ^{210}Pb are both relatively short-lived. The first daughter ^{210}Bi decays with a half-life of 5.013 days to ^{210}Po and this in turn decays with a half-life of 138.38 days to ^{206}Pb. Writing Q_{Bi}, Q_{Po} for their global inventories and λ_{Bi}, λ_{Po} for their decay constants, their respective production rates are $\lambda_{Bi}Q_{Pb}$, $\lambda_{Po}Q_{Bi}$, and their decay rates $\lambda_{Bi}Q_{Bi}$, $\lambda_{Po}Q_{Po}$. Since they will be attached to particulates in the same way as ^{210}Pb (Wójcik & Zuzel 2013), it is reasonable to suppose that their fallout rates from the atmosphere will be governed by the same processes and so may be written k_gQ_{Bi}, k_gQ_{Po}. Their global inventories (averaged of periods of a year or more) will therefore satisfy similar mass balance equations

$$\lambda_{Bi} Q_{Pb} = \lambda_{Bi} Q_{Bi} + k_g Q_{Bi}$$

$$\lambda_{Po} Q_{Bi} = \lambda_{Po} Q_{Po} + k_g Q_{Po} .$$

It follows immediately that the inventory ratios will satisfy the equations

$$\frac{Q_{Bi}}{Q_{Pb}} = \frac{\lambda_{Bi}}{\lambda_{Bi} + k_g},$$

$$\frac{Q_{Po}}{Q_{Bi}} = \frac{\lambda_{Po}}{\lambda_{Po} + k_g},$$

$$\frac{Q_{Po}}{Q_{Pb}} = \frac{\lambda_{Po}\lambda_{Bi}}{(\lambda_{Po} + k_g)(\lambda_{Bi} + k_g)} .$$

Rearranging yields three equations for the removal rate constant:

$$k_g = \lambda_{Bi}\left(\frac{Q_{Pb}}{Q_{Bi}} - 1\right), \tag{1.7}$$

$$k_g = \lambda_{Po}\left(\frac{Q_{Bi}}{Q_{Po}} - 1\right), \tag{1.8}$$

$$k_g{}^2 + (\lambda_{Po} + \lambda_{Bi})k_g - \lambda_{Po}\lambda_{Bi}\left(\frac{Q_{Pb}}{Q_{Po}} - 1\right) = 0.$$

The third equation can be solved to give k_g explicitly in the form

$$k_g = \frac{1}{2}\left(-b + \sqrt{b^2 + 4c\left(\frac{Q_{Pb}}{Q_{Po}} - 1\right)}\right). \tag{1.9}$$

where $b=\lambda_{Po}+\lambda_{Bi}$ and $c = \lambda_{Po}\lambda_{Bi}$. Equations essentially similar to these were used by Poet et al. (1972) and Moore et al. (1973) to estimate the ^{210}Pb residence time, though since their calculations were based on measurements at specific locations rather than global inventories, the validity of their results is questionable. The next chapter summarises the available empirical data on ^{222}Rn and its daughter radionuclides in the atmosphere and the extent to which it may be used to make estimates of the mean global residence times of ^{210}Pb, ^{210}Bi and ^{210}Po.

Chapter 2. Empirical data on ^{222}Rn and its daughters in the atmosphere

Empirical investigations of the distribution of ^{222}Rn and its daughter radionuclides ^{210}Pb, ^{210}Bi and ^{210}Po in the atmosphere have been carried out by a number of investigators, mainly from the late 1960s through to the 1990s and at sites in continental USA, Western Europe and Eurasia. In this chapter we present a brief summary of the extent and nature of this data. The objective of succeeding chapters will be to find a value of the ^{210}Pb residence time that gives the best possible match between the modelled data and the empirical data.

2.1 ^{222}Rn concentrations

Continental USA

Measurements of the vertical distribution of ^{222}Rn in the atmosphere have been carried out at a number of locations in the interior of the USA including Arizona and Utah in the south west (Larson & Hoppel 1973; Moore *et al*. 1973), New Mexico, Colorado and Nebraska in the centre (Wilkening 1970; Jonassen & Wilkening 1970; Moore *et al*. 1974) and Illinois further to the northeast (Bradley & Pearson, 1970). Below we give brief summaries of the nature and extent of these data sets.

Wilkening 1970: Vertical profiles to a height of 7 km were measured over relatively flat terrain in the Rio Grande Valley (New Mexico) in 1967. Data have been extracted from Figure 3 in their paper which plots mean results from 6 different flights, three in early morning and three in early afternoon.

Jonassen & Wilkening 1970: Vertical profiles to a height of 3.5 km over the Rio Grande Valley (New Mexico) were measured on three occasions during July 1968. The first on 16th July was measured above the valley floor. The second on 18th July was measured above both the valley floor and a mountain ridge 40 km to the west. The third on 27th July was only measured above the mountain ridge. Data have been extracted from the results presented in Figures 5–7 in their paper.

Bradley & Pearson, 1970: Vertical profiles to a height of 4.7 km over the Illinois were measured on five occasions between March–September 1967. Data have been extracted from the results plotted in Figure 1 of their paper.

Moore et al. 1973: Vertical profiles to a height of 13.1 km were measured at sites in Utah (Salt Lake City, 31st August 1971), Colorado (Limon, 2nd April 1971) and Nebraska (Scottsbluff). The measurements at Scottsbluff were carried out on four separate occasions, 18th May 1971, 18th August 1971, 12th November 1971 and 25th January 1972). The results have been presented in detail in Table 3 of their article.

Larson & Hoppel 1973: Vertical profiles to an altitude of around 4 km above a flat desert region in southwest Arizona were measured 7 different occasions during August 1971. Data have been extracted from Figures 1-3 in their paper which plot results from four early morning flights, an afternoon flight, and two evening flights.

Figure 2.1 plots summaries of data from each of the above sites. The mean concentration declines from 3.7 Bq m^{-3} at altitudes below 0.5 km to 0.08 Bq m^{-3} at altitudes above 11 km. Although there is a lot of scatter in the data the general trend approximates that of an exponential relationship

$$C_{Rn} = 2.48\,e^{-0.28z}\ \text{Bq m}^{-3}\ . \qquad (2.1)$$

Although the ^{222}Rn inventory in the column can be calculated from the parameters of this fit, since each of the data points is a snapshot of quantity undergoing large fluctuations on short-timescales a more reliable estimate of the long-term average is obtained by carrying out a direct numerical integration of a raw concentration versus depth profiles. The two methods are however good agreement and yield a mean value of 8850 Bq m^{-2} with an uncertainty of 3%.

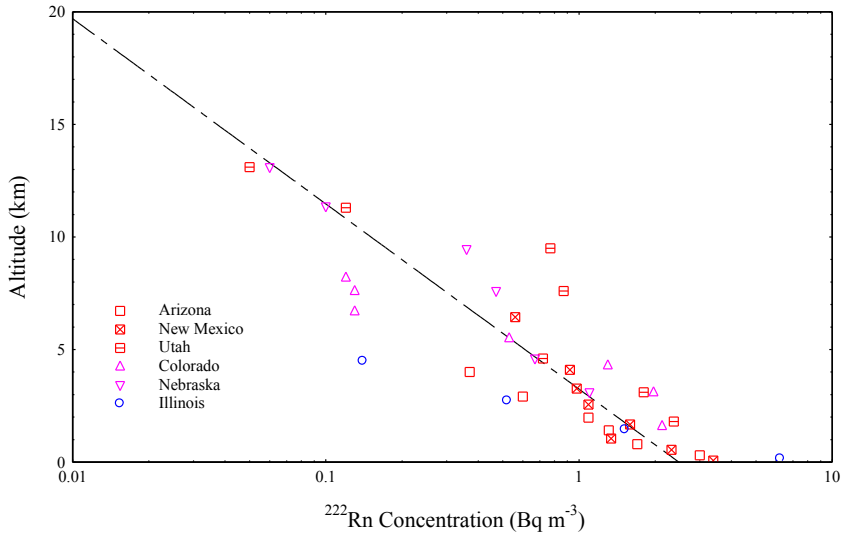

Figure 2.1: ^{222}Rn concentrations versus altitude in continental USA.

Central Eurasia

Measured atmospheric ^{222}Rn profiles from sites in the interior of Eurasia were published by Nazarov *et al.* (1970) and Kirichenko (1970). Although the data are sparse the overall results, shown in Figure 2.2, are broadly similar to those from continental USA. The mean concentration varies from 4.5 Bq m^{-3} at an altitude of 0.5 km to 0.29 Bq m^{-3} at 9 km. Fitting an exponential relation to the data gives the relation

$$C_{Rn} = 2.05\,e^{-0.24z}\ \text{Bq m}^{-3}\ . \qquad (2.2)$$

Estimates of the value of the ^{222}Rn inventory in the atmosphere above these sites calculated by the above methods were again in relatively good agreement. The mean value was 8,320 Bq m^{-2}, with an uncertainty of 5%.

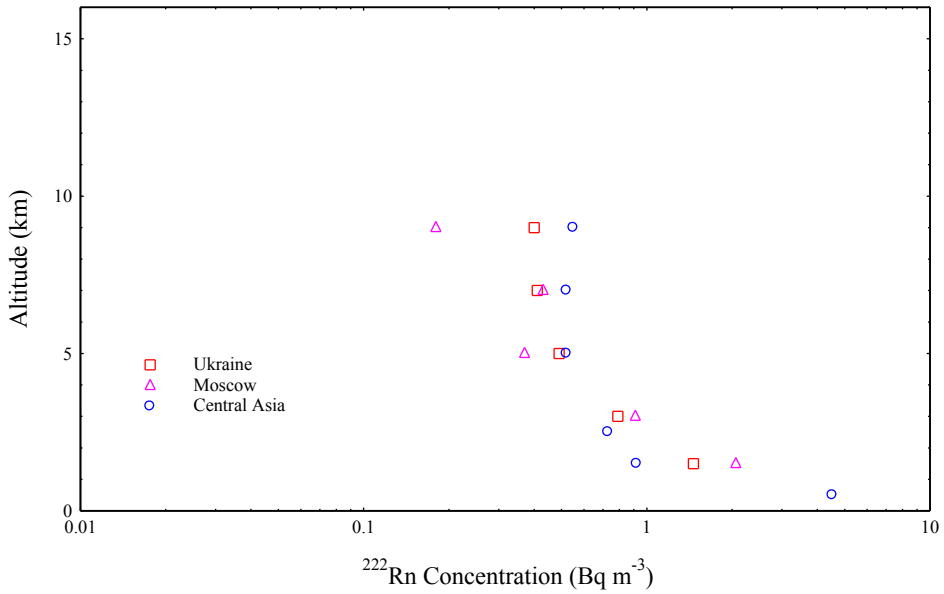

Figure 2.2: ^{222}Rn concentrations versus altitude at sites in central Eurasia.

Pacific region

A small number of studies have been carried out at sites in and around the northeastern Pacific between Hawaii and the north-American seaboard.

Larson (1974) and Anderson & Larson (1974): ^{222}Rn profiles to altitude of 4.6 km were measured on 6th, 7th February 1972 at sites approximately 65 miles northeast of Oahu (~157^{o}W, ~22^{o}N). Near ground level measurements were made on 8th, 9th February from a 4 m high tower 50 m inland from the northern coast of Oahu. On 10th February three measurements were made on air samples within the plume of Kilauea volcano at an altitude of 1 km. Eighteen over-ocean measurements at an altitude of

between 2-3 km were then made during a flight from Hawaii to Alaska. In Alaska ^{222}Rn profiles to altitude of between 4–5 km were measured on the 15th, 20th, 21st, 22nd February 1972 at sites in the Yukon valley ~500 miles inland between Stevens and Fort Yukon. Since ground-level temperatures were around –30ºC, there would have been little ^{222}Rn exhalation from the local soils. A further set of 12 measurements were made at an altitude of ~3.5 km over the Gulf of Alaska. Data for the two Hawaiian and four Alaskan profiles have been extracted from the results plotted in Figures 1 and 2 of Larson (1974) and Figure 2 in Anderson & Larson (1974). Values reported in Larson (1974) include the mean values of:

1. the ground-level measurements in Hawaii (2.65 pCi m^{-3} or 0.098 Bq m^{-3}),
2. the measurements in the volcanic plume (3.26 pCi m^{-3} or 0.121 Bq m^{-3}),
3. the measurements collected during the flight from Hawaii to Alaska (3.57 pCi m^{-3} or 0.132 Bq m^{-3}),
4. the measurements over the Gulf of Alaska (3.4 pCi m^{-3} or 0.126 Bq m^{-3}).

Kritz (1990): ^{222}Rn measurements at altitudes of between 11.3–12.5 km were made during the course of a series of flights over the eastern Pacific and west coast of North America carried out between 14th July –10th August 1983 and 7th June–24th July 1984. They included flights to the north-west of Hawaii (28th July 1983) and from Hawaii to Moffett airfield (near San Francisco, 31st July 1983).

Data summaries from all these measurements are shown in Figure 2.3. In contrast to the continental sites concentrations show little decline with altitude. Values from near Hawaii (up to an altitude of 4.6 km) are very low and almost constant, with a mean value of 0.14 Bq m^{-3}. The high-altitude measurements (mean height 12.1 km) had a slightly higher mean concentration of 0.27 Bq m^{-3}, possibly indicating inputs from the stratosphere. The inventory up to an altitude of 12.1 km (including the high-altitude data point) is calculated to be 2285 Bq m^{-2}. The large reduction and flat gradient compared to continental sites is attributable to its isolation from large land masses and the resulting absence of fresh inputs of ^{222}Rn. At the Alaskan sites, relatively high values below an altitude of 2 km suggest significant exhalation rates at ground level in spite of the frozen ground. The influence of the predominantly west to east global circulation is shown by the fact that concentrations above 2 km are very

similar to those at Hawaii. The inventory up to an altitude of 12.1 km (again including the high-altitude data point) is calculated to be 5,599 Bq m^{-2}.

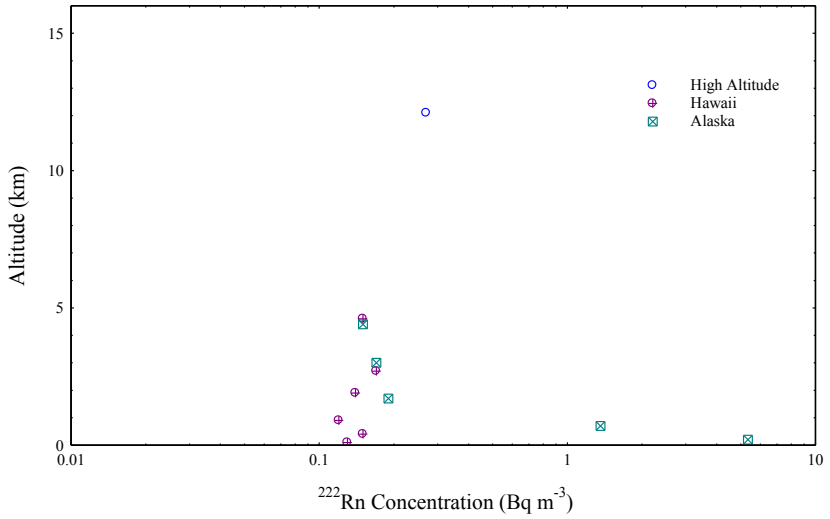

Figure 2.3: ^{222}Rn concentrations versus altitude at sites around the Pacific.

2.2 Vertical distributions of ^{210}Pb and its daughters in the atmosphere

There have been relatively few measurements of the vertical distribution of ^{210}Pb and its daughters in the atmosphere, mostly carried out in the late 1960s and early 1970s at sites in continental USA and the UK. More recently, a number of measurements were carried out in the 1990s at sites in the western Pacific.

Continental USA

The study by Moore *et al*. (1973) on the vertical distribution of ^{222}Rn included measured vertical profiles of the daughter radionuclides ^{210}Pb, ^{210}Bi and ^{210}Po to altitudes of up to 13.1 km at sites in Utah, Colorado, Kansas and Nebraska, and also at a site in Central United States at altitudes of between 15.2–17 km. A summary of the ^{210}Pb results is shown in Figure 2.4. Mean values of the ^{210}Pb concentration decline from ~340 μBq m^{-3} near ground level to ~50 μBq m^{-3} at 13 km. Although there is a lot of scatter in the data, the general trend up to this altitude is reasonably approximated by an exponential relationship. The mean value of the ^{210}Pb inventory in the atmosphere up to this height is calculated to be 2.05 Bq m^{-2}. Above 13 km (in the stratosphere) the decline is reversed and concentrations increase to values at around 16 km comparable to those at ground level. The mean value is ~380 μBq m^{-3}. The stratospheric inventory to an altitude of 17 km is calculated to be 1.1 Bq m^{-2}.

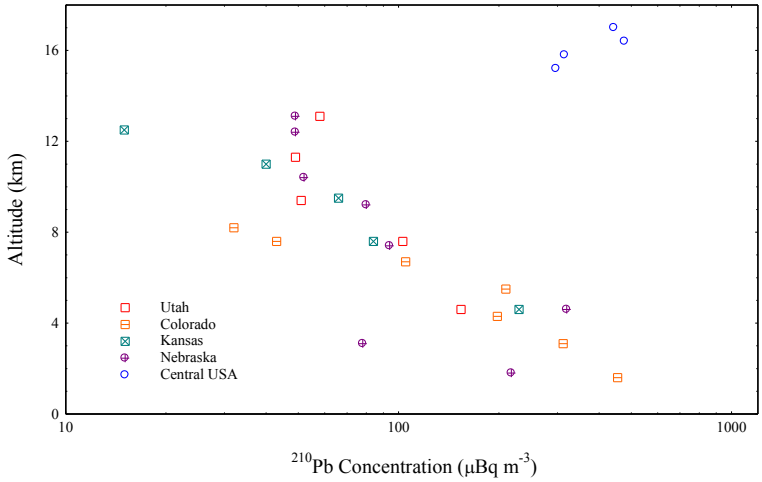

Figure 2.4: ^{210}Pb concentrations versus altitude in continental USA.

Figure 2.5 plots values of the ^{210}Bi/^{210}Pb, ^{210}Po/^{210}Bi and ^{210}Po/^{210}Pb concentration ratios versus altitude. Although values of the ^{210}Bi/^{210}Pb concentration ratio vary irregularly with altitude there is little net change up to an altitude of 10 km. The mean value up to this height is 0.53, indicating a significant ^{210}Bi deficit. At higher altitudes there is a relatively rapid increase to near equilibrium values. (When a state of equilibrium is reached, the activity of the radioactive daughter is determined by the activity of the parent.) The mean value between 10–13 km is 0.92. The stratospheric values (up to 17 km) all appear to suggest ^{210}Bi/^{210}Pb equilibrium, i.e., they have an activity ratio close to 1..

Mean values of the ^{210}Po/^{210}Bi and ^{210}Po/^{210}Pb ratios in the troposphere (up to 10 km) are 0.14 and 0.09 respectively, indicating a large ^{210}Po deficit. Above 10 km the trend for both these ratios is a general increase to a mean stratospheric value of around 0.52.

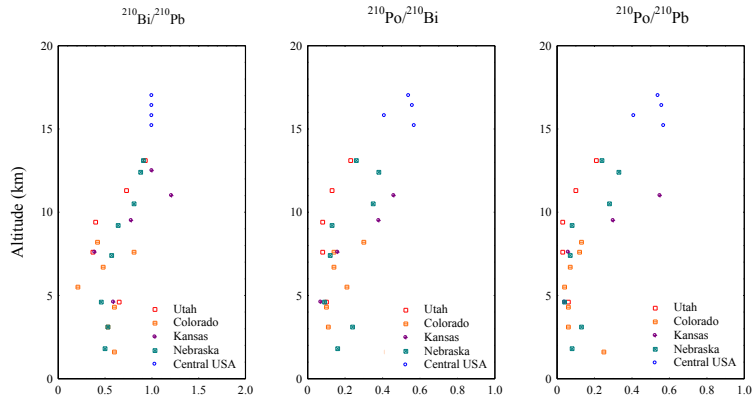

Figure 2.5: ^{210}Bi/^{10}Pb, ^{210}Po/^{210}Bi and ^{210}Po/^{210}Pb concentration ratios versus altitude in continental USA.

UK

Measurements of ^{210}Pb (Radium-D) and ^{210}Po (Radium-F) as dpm kg^{-1} were made at a site near Harwell by Burton & Stewart (1960). Samples were collected at ground level between May 1954 and January 1957, and at altitudes of 3–14 km between July 1954 and July 1956. In a further study at the same location Peirson et al. (1966) carried out measurements of ^{210}Pb and ^{210}Po on samples collected at ground level in 1958 and during 1961/5, and of ^{210}Pb on samples collected at altitudes of between 1.3–14.3 km during 1957/8. Concentrations have been converted to μBq m^{-3} by multiplying by the density of air. Figure 2.6 plots results from both studies (a) as ^{210}Pb concentrations and (b) ^{210}Po/^{210}Pb concentration ratios versus altitude. The mean ground level ^{210}Pb concentration is 197 μBq m^{-3} and the mean ^{210}Po/^{210}Pb ratio 0.091. Both are significantly lower than the corresponding USA values. Whereas ^{210}Pb concentrations determined from the Burton & Stewart study show little variation with height, those from Peirson et al. show a slight decreasing trend with a mean stratospheric concentration around 40% of the ground-level value. Stratospheric concentrations range from 84–188 μBq m^{-3}, again significantly lower than the corresponding USA value, though the mean stratospheric ^{210}Po/^{210}Pb ratio (0.67) is a little higher. Combining the two data sets the atmospheric ^{210}Pb inventory up to an altitude of 14 km is calculated to be 2.79 Bq m^{-2}.

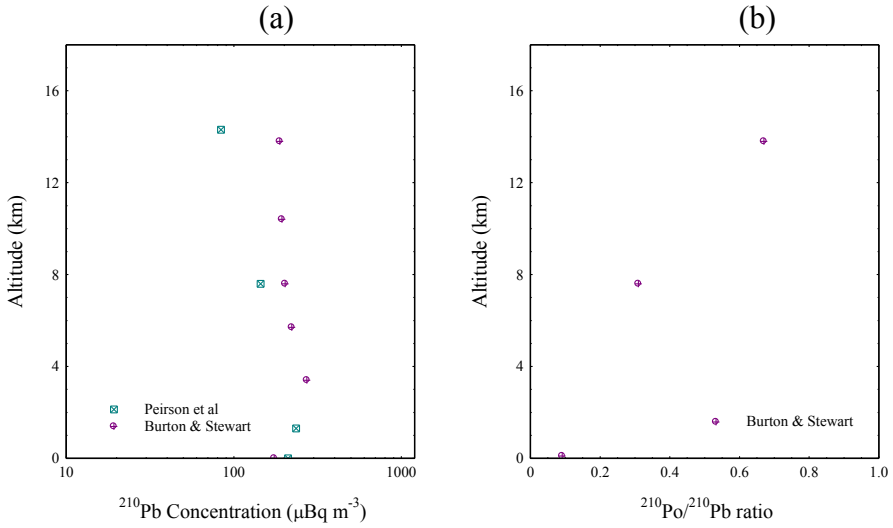

Figure 2.6: ^{210}Pb concentrations (a) and ^{210}Po/^{210}Pb concentrations ratios (b) versus altitude above Harwell, UK.

Western Pacific

A substantial number of ^{210}Pb profiles were measured during the course of the NASA/Global Tropospheric Experiment Pacific Exploratory Missions conducted over the western Pacific. They included 17 flights made during September/October 1991 as part of the PEM-West A program, 16 flights made during September/October 1996 as part of the PEM-West B program, and 12 flights made during February/March 1994 as part of the PEM-Tropics program. The PEM-West A results were reported in Dibb *et al.* (1996), the PEM-West A results in Dibb *et al.* (1997), and the PEM-Tropics results in Dibb *et al.* (1999). From the plots in these papers it was not however possible to identify profiles from individual flights. Individual profiles were however published in Guelle *et al*. (1998b), 8 from 8 PEM-West A and 13 from PEM-West A. They included

- 4 from the Sea of Japan (Profiles 19, 21-23),
- 6 from off the SE coast of China (Profiles 4-6, 15-17),
- 3 from off E coast of Japan (Profiles 2, 18, 20),
- 4 from the N Marianas (Profiles 1, 3, 7, 11-14),
- 1 from Midway (Profile 8).

Summary values of ^{210}Pb concentration versus altitude are plotted in Figure 2.7 for results from the West Pacific (Sea of Japan and coasts of Japan and China), Northern Marianas and Midway.

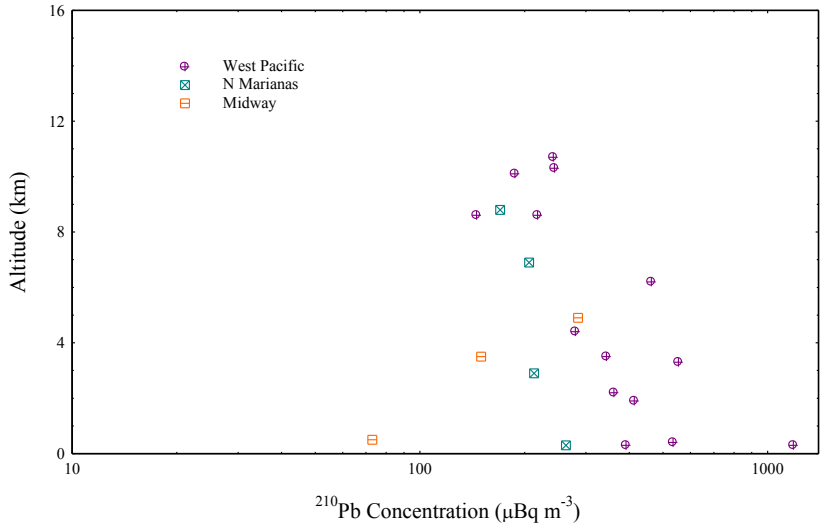

Figure 2.7: ^{210}Pb concentrations versus altitude in the Western Pacific

Although there is a lot of scatter in the data the general trends for the three west Pacific sites close to the Asian mainland are broadly similar. Concentrations decrease in a roughly exponential way with height from a mean value of 704 μBq m^{-3} at altitudes below 0.5 km to 224 μBq m^{-3} at altitudes above 10 km. The mean value of the ^{210}Pb inventory in the atmosphere above these sites is estimated to be 5.57 Bq m^{-2}. Concentrations are significantly lower further to the east at the sites along the line of the Northern Marianas, particularly at ground-level where the mean value is around 40% of that at sites close to the Asian mainland. A general west-to-east decline appears to be further illustrated by the Midway results where ground-level concentrations are just 10% of those on the western margin of the Pacific. Mean values of ^{210}Pb inventories over of the Northern Marianas and Midway sites are calculated to be 1.90 Bq m^{-2} and 0.67 Bq m^{-2}.

A summary of the vertical distributions of ^{210}Pb, ^{210}Bi and ^{210}Po concentrations in air and their ratios at all three locations is given in Table 2.1.

2.3 Ground-level measurements of ^{210}Pb, ^{210}Bi and ^{210}Po

Separately from the above studies, a number of measurements of ^{210}Pb, ^{210}Bi and ^{210}Po concentrations in ground-level concentrations air and rainwater have been reported in the literature.

Continental USA

Ground-level measurements of ^{210}Pb, ^{210}Bi and ^{210}Po have been carried at Colorado (Poet et al. 1972) both on air samples collected during 4th June 1969 to 2nd January 1972 and on rainwater and snow samples collected during 25th September 1970 to 27th March 1971. Gavini et al. (1974) carried out similar measurements on rainwater samples collected at Fayetteville, Arkansas, during April 1973 to April 1974.

Europe

Carvalho (1995) carried out measurements of ^{210}Pb, ^{210}Bi and ^{210}Po in surface air at Sacavem, near Lisbon during 1986/89.

Enewetak (Marshall Island)

Turekian & Cochran (1981) carried out ground-level measurements of ^{210}Pb and ^{210}Po in ground-level air at Enewetak (11ºN, 162º 20′E, at the north-western end of the Marshall Islands) during 18th April to 4th August 1979. ^{210}Pb concentrations varied from 13–64 μBq m^{-3} with a mean value of 34 μBq m^{-3}, just 13% of the near ground-level concentration in the lower level in the Northern Marianas nearer to the Asian land mass and 47% of that at Midway. These results presumably reflect the remoteness of this site from any significant landmass. ^{210}Po concentrations were effectively zero.

Hawaii

Moore *et al.* (1974) carried out measurements of ^{222}Rn, ^{210}Pb, ^{210}Bi and ^{210}Po in ground-level air at three coastal sites on the windward side of the island of Hawaii, a site 35 km inland at an altitude of 1500 m (Kulani), and a site 56 km inland at an altitude of 3,300 m (Mauna Loa). Sampling was carried out during the period 30th May to 22nd June 1971. At each site samples were collected both at night and during the day. Mean values of the ^{222}Rn concentrations at the three sites ranged from 0.37 Bq m^{-3} at Mauna Loa to 0.68 Bq m^{-3} at Kulani. The overall mean value of 0.50 Bq m^{-3} was significantly higher than the mean concentration of 0.15 Bq m^{-3} in air samples over the ocean to the north west of Hawaii (Larson 1974), suggesting that the main source was ^{222}Rn exhalation from local soils. Much lower ^{222}Rn concentrations during the day time at coastal sites presumably reflect the influence of sea breezes carrying oceanic air from the sea to the land. The contrast between night and day is greatly reduced at the inland sites, and almost non-existent at Mauna Loa.

Concentrations of ^{210}Pb and its daughters at the coastal sites are similar to those at Kulani, and also to those at Chilton and Lisbon on the western margin of the Atlantic Ocean. Much higher ^{210}Pb concentrations were however recorded at the Mauna Loa site, possibly due to contamination by local sources of dust. ^{210}Bi and ^{210}Po concentrations were also affected though to a lesser extent.

Arctic

Dibb *et al.* (1994) carried out measurements of ^{210}Pb in surface-level air at Alert in the Canadian Arctic at weekly intervals over a period of 2 years, from August

1990 to October 1992. Concentrations showed seasonal variations from lows of around 65 μBq m^{-3} during the summer months to peak values of around 1100 μBq m^{-3} during the winter. Similar data for Barrow in Alaska were reported in Feely et al. (1988).

A summary of the ground-level concentrations of ^{210}Pb, ^{210}Bi and ^{210}Po and their ratios in air and rainwater at all the locations reported above is given in Table 2.2.

Summary Tables

Table 2.1: ^{210}Pb, ^{210}Bi and ^{210}Po concentrations and ratios versus altitude

(a) Over continental USA

Altitude	Concentrations (μBq m^{-3})			Ratios		
	^{210}Pb	^{210}Bi	^{210}Po	^{210}Bi/^{210}Pb	^{210}Po/^{210}Bi	^{210}Po/^{210}Pb
0-2 km	337	192	67	0.55	0.29	0.17
2-5 km	215	118	12	0.56	0.12	0.07
5-8 km	107	42	6	0.47	0.14	0.06
8-11 km	58	37	10	0.61	0.25	0.16
11-13 km	43	40	15	0.92	0.45	0.48
13-17 km	383	383	201	1.00	0.52	0.52

(b) Over southern England

Altitude	Concentrations (μBq m^{-3})		Ratio
	^{210}Pb	^{210}Po	^{210}Po/^{210}Pb
0-2 km	210	18	0.09
3-6 km	247		
7-8 km	173	63	0.31
10-14 km	191	126	0.67
14-15 km	84		

(c) Over the Pacific Ocean

	^{210}Pb Concentrations (μBq m^{-3})		
	Western Pacific	N Marianas	Midway
0-1 km	704	263	73
2-4 km	418	213	150
4-5 km			285
6-7 km	277	206	
8-9 km		171	
10-11 km	224		

Table 2.2: Ground-level ^{210}Pb, ^{210}Bi and ^{210}Po concentrations and ratios

(a) In surface air

Location	Concentrations (μBq m^{-3})			Ratios		
	^{210}Pb	^{210}Bi	^{210}Po	^{210}Bi/ ^{210}Pb	^{210}Po/^{210}Bi	^{210}Po/^{210}Pb
Colorado	412	170	35	0.41	0.20	0.083
Colorado (<2km)	455	273	115	0.60	0.42	0.25
Nebraska (<2km)	218	110	18	0.50	0.16	0.082
Chilton (UK)	220		40			0.18
Lisbon (Portugal)	192	105	31	0.57	0.31	0.17
Western Pacific (<1 km)	704					
N Marianas (<1 km)	263					
Enewetak	34		0			0
Midway (<1 km)	73					
Hawaii (sea level)	183	153	17	0.84	0.12	0.10
" (1500 m)	108	90	17	0.81	0.17	0.14
" (3300 m)	758	372	28	0.55	0.08	0.041
Barrow (Alaska)	446					
Alert (N Canada)	557					

(b) In precipitation

Location	Concentrations (Bq kl^{-1})			Ratios		
	^{210}Pb	^{210}Bi	^{210}Po	^{210}Bi/^{210}Pb	^{210}Po/^{210}Bi	^{210}Po/^{210}Pb
Colorado	186	112	11	0.61	0.10	0.061
Arkansas	99	82	14	0.70	0.17	0.13

Table 2.3 summarises mean values of the ^{210}Pb residence time calculated from the ^{210}Bi/^{210}Pb and ^{210}Po/^{210}Pb activity ratios in surface air and rainwater from the above studies. Possible causes of the large discrepancy between residence times calculated from ^{210}Bi/^{210}Pb ratios and those calculated from ^{210}Po/^{210}Pb ratios were thought to be inputs of older stratospheric air, or contamination by dust particles containing ^{210}Pb, ^{210}Bi and ^{210}Po in secular equilibrium (Poet et al. 1972; Gavini et al. 1974). Assuming the main cause to be dust contamination, Poet et al. (1972) corrected their estimates of the mean atmospheric residence time to ~4 days for particles in the lower troposphere and ~7 days for particles in precipitation. Using various arguments, Gavini et al. (1974) suggested mean residence times of ~30 days for aerosols in the troposphere and ~1 year for the stratosphere. While some of the reasons advanced may be factors, the main cause of error is almost certainly failure of the ^{210}Pb, ^{210}Bi and ^{210}Po activities in the samples to satisfy the equilibrium conditions implicit in

equations (1.7 – 1.9). Since the concentrations of these radionuclides vary considerably with both geographical location and altitude, it is likely that their ratios will show similar variations. The main objective of this research is to model these variations and match the results to empirical data. This will provide a more accurate estimate of the ^{210}Pb atmospheric residence time, while also producing a simple yet reliable model of the distribution of fallout ^{210}Pb over the landscape.

Table 2.3: Atmospheric residence times calculated from ^{210}Pb, ^{210}Bi and ^{210}Po activity ratios in surface air and rainwater.

	Residence time from			
	^{210}Bi/^{210}Pb	^{210}Po/^{210}Pb	Location	Reference
Surface air	5 d	24 d	Boulder, Co	Poet et al. 1972
	9 d	24 d	Continental USA	Moore et al. 1973
	6 d	33 d	Lisbon, Portugal	Carvalho 1995
		36 d	Chilton, UK	Burton & Stewart 1960
		40 d	Chilton, UK	Peirson et al. 1966
Rainwater	8 d	19 d	Boulder, Co	Poet et al. 1972
	17 d	32 d	Fayetteville, Ark	Gavini et al. 1974
		22-29 d	Chilton, UK	Burton & Stewart 1960

Most of these datasets were collected during the 1970s and 1980s in studies that arose from the interest at that time on the atmospheric impact of nuclear weapon tests and accidents. In spite of the widespread and continued use of ^{210}Pb as a tool for dating environmental records in natural archives, very little work has been done since then linking the atmospheric part of the ^{210}Pb cycle to the terrestrial and aquatic parts.

Chapter 3. Mathematical modelling

3.1 Introduction

The distribution of ^{222}Rn in the atmosphere is controlled initially by the boundary conditions at the surface of the Earth, and subsequently by the processes of advection, diffusion, and radioactive decay. On short time-scales (hours or days), these processes can only be described in any accuracy by using detailed 3-dimensional models. As pointed out above these models however suffer from two major disadvantages, they are very computationally expensive, and there is very little data against which they can be validated. On longer time-scales (time-averaged over months or years), some of the essential features of the available empirical data have been captured using simpler models in which conservation principles are applied to a vertical column of air moving horizontally over the earth's surface, with little net transfer between adjacent columns (Jacobi and André 1963; Turekian et al. 1977; Piliposian and Appleby 2003). Since ^{222}Rn is an inert gas and removed from the column only by radioactive decay, its vertical distribution in the column is assumed to be governed by the partial differential equation

$$\frac{\partial C_{Rn}}{\partial t} = \frac{\partial}{\partial z}\left(D \frac{\partial C_{Rn}}{\partial z} \right) - \lambda_{Rn} C_{Rn} , \tag{3.1}$$

where $C_{Rn}(z,t)$ denotes the ^{222}Rn concentration (in Bq m^{-3}) at altitude z and time t, D is an effective vertical diffusivity, and λ_{Rn} is the ^{222}Rn radioactive decay constant. The boundary conditions for this equation are

$$-D \frac{\partial C_{Rn}}{\partial z}\bigg|_{(0,t)} = \mathcal{F}, \qquad C_{Rn}(z,t) \to 0 \text{ as } z \to \infty , \tag{3.2}$$

where $\mathcal{F}$ denotes the ^{222}Rn flux (in Bq m^{-2}d^{-1}) into the base of the column.

^{222}Rn decays via a number of intermediate short-lived radionuclides to ^{210}Pb. In contrast to ^{222}Rn, ^{210}Pb atoms are highly reactive and readily adsorbed onto dust particles. They may be removed from the atmosphere by wet and dry deposition, as well as by radioactive decay to its daughter radionuclides ^{210}Bi and ^{210}Po. In the above model the ^{210}Pb concentration $C_{Pb}(z,t)$ in the atmosphere is assumed to be governed by the partial differential equation

$$\frac{\partial C_{Pb}}{\partial t} = \frac{\partial}{\partial z}\left(D\frac{\partial C_{Pb}}{\partial z} \right) + \lambda_{Pb}(C_{Rn} - C_{Pb}) - \Lambda(C_{Pb}), \tag{3.3}$$

and boundary conditions

$$\left.\frac{\partial C_{Pb}}{\partial z}\right|_{(0,t)} = 0, \qquad C_{Pb}(z,t) \to 0 \text{ as } z \to \infty, \tag{3.4}$$

where D is the turbulent diffusivity, and $\Lambda(C_{Pb})$ a term characterizing the rate at which ^{210}Pb condenses from the aerosol state, dominated by turbulent diffusion, to incipient precipitation, dominated by gravity (Piliposian and Appleby 2003). Since the transport processes for ^{210}Bi and ^{210}Po can reasonably be presumed to follow those of ^{210}Pb, the atmospheric concentrations of ^{210}Bi and ^{210}Po are assumed to be similarly governed by the partial differential equations

$$\frac{\partial C_{Bi}}{\partial t} = \frac{\partial}{\partial z}\left(D\frac{\partial C_{Bi}}{\partial z} \right) + \lambda_{Bi}(C_{Bi} - C_{Pb}) - \Lambda(C_{Bi}) \tag{3.5}$$

$$\frac{\partial C_{Po}}{\partial t} = \frac{\partial}{\partial z}\left(D\frac{\partial C_{Po}}{\partial z} \right) + \lambda_{Po}(C_{Po} - C_{Bi}) - \Lambda(C_{Po}) \tag{3.6}$$

together with the boundary conditions

$$\left.\frac{\partial C_{Bi}}{\partial z}\right|_{(0,t)} = 0, \qquad C_{Bi}(z,t) \to 0 \text{ as } z \to \infty, \tag{3.7}$$

$$\left.\frac{\partial C_{Po}}{\partial z}\right|_{(0,t)} = 0, \qquad C_{Po}(z,t) \to 0 \text{ as } z \to \infty. \tag{3.8}$$

The purpose of the next two chapters will be to solve these equations for C_{Rn}, C_{Pb}, C_{Bi}, C_{Po} and by comparing the concentrations and their ratios to the available empirical data, determine a best estimate of the atmospheric residence times of ^{210}Pb and its daughters.

3.2 Analytical solutions

Although a full solution to the above equations can only be achieved using a numerical approach there are a number of situations where the equations governing the ^{222}Rn distribution can be solved analytically. Apart from giving some useful insights into the nature of the ^{222}Rn distribution, they also provide a means for validating solutions obtained by numerical means.

^{222}Rn inventory

From simple mass balance considerations, the ^{222}Rn inventory

$$A_{Rn}(t) = \int_0^\infty C_{Rn}(z,t)\,\mathrm{d}z$$

in a column satisfies the ordinary differential equation

$$\dot{A}_{Rn} = \mathcal{F} - \lambda_{Rn} A_{Rn} \,. \tag{3.9}$$

Writing $A_{Rn}(0)$ for the initial inventory at time t=0, this has the general solution

$$A_{Rn}(t) = A_{Rn}(0)\,\mathrm{e}^{-\lambda_{Rn} t} + \int_0^t \mathcal{F}(\tau)\,\mathrm{e}^{-\lambda_{Rn}(t-\tau)}\,\mathrm{d}\tau \,,$$

or equivalently

$$A_{Rn}(t) = A_{Rn}(0)\,\mathrm{e}^{-\lambda_{Rn} t} + \int_0^t \mathcal{F}(t-s)\,\mathrm{e}^{-\lambda_{Rn} s}\,\mathrm{d}s \,. \tag{3.10}$$

In the case of a column of air moving over a large land mass, assuming a constant flux of ^{222}Rn into the base of the column and that there is no initial inventory, the above solution reduces to

$$A_{Rn}(t) = \frac{\mathcal{F}}{\lambda_{Rn}}(1 - \mathrm{e}^{-\lambda_{Rn} t}). \tag{3.11}$$

As $t \to \infty$, this tends to a steady state value $\mathcal{F}/\lambda_{Rn}$. Since ^{222}Rn has a half-life of 3.82 days, 90% equilibrium will be achieved after a period of about 13 days, and 99% equilibrium after ~25 days.

For a column passing from a land mass out over a large ocean, assuming zero flux from the ocean the inventory will be steadily depleted by radioactive decay. The solution in this case is

$$A_{Rn}(t) = A_{Rn}(0)\,\mathrm{e}^{-\lambda_{Rn} t} \,,$$

where $A_{Rn}(0)$ is the inventory at the point at which the column crosses the land/ocean boundary, and t the elapsed time over the ocean. The inventory will have declined by 50% after just 4 days, and 90% after around 13 days.

Combining these two situations, for a column of air with zero initial concentration moving overland for the time $0 < t < t_1$ and then out over the ocean the boundary condition is

$$\mathcal{F}(t)= \mathcal{F}\{\mathrm{H}(t)\text{-}\mathrm{H}(t\text{-}t_1)\},$$

where

$$\mathrm{H}(t) = \begin{cases} 0 & \text{for } t < 0 \\ 1 & \text{for } t \geq 0 \end{cases}$$

is the Heaviside step function. The solution in this case is

$$\left.\begin{aligned} A_{Rn}(t) &= \mathcal{F}\,\mathrm{e}^{-\lambda_{Rn}t}\int_0^t \{\mathrm{H}(\tau)-\mathrm{H}(\tau-t_1)\}\,\mathrm{e}^{\lambda_{Rn}\tau}\,\mathrm{d}\,\tau \\ &= \mathcal{F}\begin{cases} \mathrm{e}^{-\lambda_{Rn}t}\int_0^t \mathrm{e}^{\lambda_{Rn}\tau}\,\mathrm{d}\,\tau & 0<t<t_1 \\ \mathrm{e}^{-\lambda_{Rn}t}\int_0^{t_1} \mathrm{e}^{\lambda_{Rn}\tau}\,\mathrm{d}\,\tau & t>t_1 \end{cases} \\ &= \frac{\mathcal{F}}{\lambda_{Rn}}\begin{cases} 1-\mathrm{e}^{-\lambda_{Rn}t} & 0<t<t_1 \\ \mathrm{e}^{-\lambda_{Rn}(t-t_1)}-\mathrm{e}^{-\lambda_{Rn}t} & t>t_1 \end{cases} \end{aligned}\right\} \tag{3.12}$$

If we now suppose that the column circumnavigates the globe at a fixed latitude[1] with a global travel time t_g, since at any given location the ^{222}Rn exhalation rate will be relatively constant when measured on annual timescales, after a relatively short time a steady state will be reached where the solution is a periodic function of time with period t_g, whence $A_{Rn}(t_g) = A_{Rn}(0)$. From the general solution we also have

$$A_{Rn}(t_g) = A_{Rn}(0)\,\mathrm{e}^{-\lambda_{Rn}t_g} + \int_0^{t_g} \mathcal{F}(\tau)\,\mathrm{e}^{-\lambda_{Rn}(t_g-\tau)}\,\mathrm{d}\,\tau\,.$$

It follows that the inventory at time $t = 0$ must satisfy the equation

$$A_{Rn}(0) = \frac{1}{1-\mathrm{e}^{-\lambda_{Rn}t_g}}\int_0^{t_g} \mathcal{F}(\tau)\,\mathrm{e}^{-\lambda_{Rn}(t_g-\tau)}\,\mathrm{d}\,\tau\,. \tag{3.13}$$

Assuming that the column passes over two land masses (North America and Eurasia) and two oceans (Atlantic and Pacific) the exhalation function can be written

$$\mathcal{F}(t) = \mathcal{F}\{\mathrm{H(t)}\text{–}\mathrm{H}(t\text{–}t_1)+\mathrm{H}(t\text{–}t_2)\ )\text{–}\mathrm{H}(t\text{–}t_3)\},$$

where t_1, t_2, t_3 are the times at which it crosses the respective boundaries. Since

$$\int_0^{t_g} \mathcal{F}(\tau)\,\mathrm{e}^{\lambda_{Rn}\tau}\,\mathrm{d}\,\tau = \mathcal{F}\left\{\int_0^{t_1} \mathrm{e}^{\lambda_{Rn}\tau}\,\mathrm{d}\,\tau + \int_{t_2}^{t_3} \mathrm{e}^{\lambda_{Rn}\tau}\,\mathrm{d}\,\tau\right\} = \frac{\mathcal{F}}{\lambda_{Rn}}\left(\mathrm{e}^{\lambda_{Rn}t_1}-1+\mathrm{e}^{\lambda_{Rn}t_3}-\mathrm{e}^{\lambda_{Rn}t_2}\right),$$

it follows that

[1] It is not assumed that the column literally circumnavigates the globe. The concept here is of a notional column the motion of which is defined by the mean velocity of circulation time-averaged over a period of years.

$$A_{Rn}(0) = \frac{\mathcal{F}}{\lambda_{Rn}} \frac{e^{-\lambda_{Rn} t_g}}{1 - e^{-\lambda_{Rn} t_g}} (e^{\lambda_{Rn} t_1} - 1 + e^{\lambda_{Rn} t_3} - e^{\lambda_{Rn} t_2}) = \varepsilon \frac{\mathcal{F}}{\lambda_{Rn}}, \qquad (3.14)$$

where

$$\varepsilon = \frac{e^{-\lambda_{Rn}(t_g - t_1)} - e^{-\lambda_{Rn} t_g} + e^{-\lambda_{Rn}(t_g - t_3)} - e^{-\lambda_{Rn}(t_g - t_2)}}{1 - e^{-\lambda_{Rn} t_g}}.$$

Using the values t_1=11 days, t_2=26 days, t_3=55 days, t_g=78 days (Piliposian & Appleby 2003), it follows that the residual inventory on completing one full circuit is 1.5% of the equilibrium value. The inventory at time t is thus

$$A_{Rn}(t) = \frac{\mathcal{F}}{\lambda_{Rn}} \{1 - (1 - \varepsilon) e^{-\lambda_{Rn} t}\} \qquad 0 < t < t_1$$

$$A_{Rn}(t) = \frac{\mathcal{F}}{\lambda_{Rn}} \{e^{-\lambda_{Rn}(t - t_1)} - (1 - \varepsilon) e^{-\lambda_{Rn} t}\} \qquad t_1 < t < t_2$$

$$A_{Rn}(t) = \frac{\mathcal{F}}{\lambda_{Rn}} \{e^{-\lambda_{Rn}(t - t_1)} - (1 - \varepsilon) e^{-\lambda_{Rn} t} + 1 - e^{-\lambda_{Rn}(t - t_2)}\} \qquad t_2 < t < t_3$$

$$A_{Rn}(t) = \frac{\mathcal{F}}{\lambda_{Rn}} \{e^{-\lambda_{Rn}(t - t_1)} - (1 - \varepsilon) e^{-\lambda_{Rn} t} + e^{-\lambda_{Rn}(t - t_3)} - e^{-\lambda_{Rn}(t - t_2)}\} = \frac{\varepsilon \mathcal{F}}{\lambda_{Rn}} e^{-\lambda_{Rn}(t - t_g)} \qquad t_3 < t < t_g.$$

The following diagram shows how the inventory varies as a fraction of the equilibrium value during the course of one circuit. Values rise sharply over the land masses and fall rapidly over the oceans.

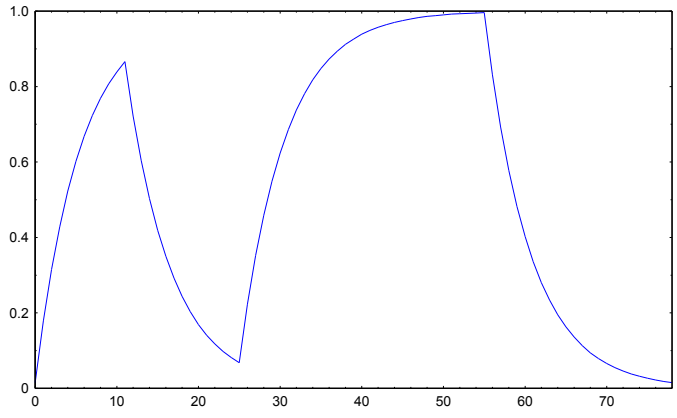

Figure 3.1: ^{222}Rn inventory versus time in a vertical column of air circumnavigating the Earth.

Laplace's general solution for constant diffusivity

In this and the next two sub-sections we consider analytical solutions for the distribution of ^{222}Rn within the column. We suppose that ^{222}Rn has a constant diffusivity and hence that the governing equation reduces to

$$\frac{\partial C_{Rn}}{\partial t} = D\frac{\partial^2 C_{Rn}}{\partial z^2} - \lambda_{Rn} C_{Rn}\,.$$

Under the boundary conditions

$$-D\frac{\partial C_{Rn}}{\partial z}\bigg|_{(0,t)} = \mathcal{F}, \qquad C_{Rn}(z,t) \to 0 \text{ as } z \to \infty\,,$$

this problem can be solved analytically using the solution

$$C_{Rn}(z,t) = \frac{M\,\mathrm{e}^{-\lambda_{Rn}t}}{\sqrt{\pi D t}}\,\mathrm{e}^{-\frac{z^2}{4Dt}} \tag{3.15}$$

of the diffusion equation for a radioactive plane source of strength M placed at z=0 at time t=0 (c.f. Crank 1975, p.13). ^{222}Rn injected into the base of the column by exhalation from the land surface during the time interval (τ, τ+dτ) can be regarded as a plane source of strength $\mathcal{F}(\tau)\,\mathrm{d}\tau$ placed at z=0 at time τ. From the above equation the contribution that this increment makes to the total concentration at time t is

$$\mathrm{d}C_{Rn}(z,t) = \begin{cases} 0 & t \le \tau, \\ \dfrac{\mathcal{F}(\tau)\,\mathrm{d}\tau\,\mathrm{e}^{-\lambda_{Rn}(t-\tau)}}{\sqrt{\pi D(t-\tau)}}\,\mathrm{e}^{-\frac{z^2}{4D(t-\tau)}} & t > \tau. \end{cases}$$

The solution due to a continuous flux $\mathcal{F}$ across the boundary z=0 is thus

$$C_{Rn}(z,t) = \frac{1}{\sqrt{\pi D}}\int_0^t \mathcal{F}(\tau)\frac{\mathrm{e}^{-\lambda_{Rn}(t-\tau)}}{\sqrt{(t-\tau)}}\,\mathrm{e}^{-\frac{z^2}{4D(t-\tau)}}\,\mathrm{d}\tau\,. \tag{3.16}$$

Writing $s = t-\tau$, this can be written

$$C_{Rn}(z,t) = \frac{1}{\sqrt{\pi D}}\int_0^t \mathcal{F}(t-s)\frac{\mathrm{e}^{-\lambda_{Rn}s}}{\sqrt{s}}\,\mathrm{e}^{-\frac{z^2}{4Ds}}\,\mathrm{d}s\,.$$

Over a continental land mass, assuming a constant flux this reduces to

$$C_{Rn}(z,t) = \frac{\mathcal{F}}{\sqrt{\pi D}}\int_0^t \frac{\mathrm{e}^{-\lambda_{Rn}s}}{\sqrt{s}}\,\mathrm{e}^{-\frac{z^2}{4Ds}}\,\mathrm{d}s\,.$$

Equilibrium ^{222}Rn profiles

Under a constant flux the ^{222}Rn distribution will over a period of time reach an equilibrium state in which the governing partial differential equation reduces to a simple ordinary differential equation

$$D\frac{\partial^2 C_{Rn}}{\partial z^2} - \lambda_{Rn} C_{Rn} = 0 .$$

Solving this equation subject to the boundary conditions

$$-D\frac{\partial C_{Rn}}{\partial z}\bigg|_{(0,t)} = \mathcal{F}, \qquad C_{Rn}(z,t) \to 0 \text{ as } z \to \infty ,$$

the equilibrium ^{222}Rn distribution satisfies a simple exponential relation

$$C_{Rn}(z) = \frac{\mathcal{F}}{\sqrt{\lambda_{Rn} D}} \mathrm{e}^{-\sqrt{\frac{\lambda_{Rn}}{D}} z} . \tag{3.17}$$

^{222}Rn profiles might be expected to approach this equilibrium distribution in the interior of large continental land masses where there has been sufficient time for the equilibrium state to develop. The empirical data shown in Figures 2.1 and 2.2 suggest that this is the case for ^{222}Rn profiles from sites in the interior of the USA and Eurasia. In most cases the data points shown are mean values from measurements carried out over a period of several days. Although there is, as might be expected, a lot of scatter within the data, an exponential trend can be observed with similar gradients and intercepts. Fitting an exponential relation to both data sets gave the relations (equations . 2.1-2.2):

$C_{Rn} = 2.48\ \mathrm{e}^{-0.28\,z}$ Bq m^{-3} for continental USA

$C_{Rn} = 2.05\ \mathrm{e}^{-0.24\,z}$ Bq m^{-3} for Eurasia

Assuming that these profiles are close to equilibrium, equating their mean gradient (0.26 km^{-1}) to the equilibrium expression $\sqrt{\lambda_{Rn}/D}$ (Piliposian & Appleby 2003), the mean vertical diffusivity for ^{222}Rn in the atmosphere is calculated to be D = 2.7 km^2 d^{-1} (3.1×10^5 cm^2 s^{-1}). Equating the mean ground level concentration (2.27 Bq m^{-3}) to the equilibrium expression $\mathcal{F}/\sqrt{\lambda_{Rn} D}$, the mean ^{222}Rn flux from the land surface is calculated to be 1570 Bq m^{-2} d^{-1} (0.88 atoms cm^{-2} s^{-1}). This figure is comparable with

the estimates of between 1310-1815 Bq m^{-2} d^{-1} (0.72-1.00 atoms cm^{-2} s^{-1}) used in global circulation models (Feichter et al. 1991; Balkanski et al. 1993).

Decay of ^{222}Rn profiles over a large ocean

Air masses passing over the eastern seaboard of a continent with an initial concentration $C_{Rn}^{0}(z)$ will become depleted in ^{222}Rn as they pass over the ocean. The vertical distribution of ^{222}Rn profile in such an air mass must again satisfy the equation

$$\frac{\partial C_{Rn}}{\partial t} = D\frac{\partial^2 C_{Rn}}{\partial z^2} - \lambda_{Rn} C_{Rn},$$

though in this case the solution will be subject to the initial and boundary conditions:

$$\text{(i)} \quad C_{Rn} = C_{Rn}^{0}(z) \text{ at } t = 0 \text{ for } 0 \le z < \infty,$$

$$\text{(ii)} \quad \frac{\partial C_{Rn}}{\partial z} = 0 \quad \text{over } z = 0 \text{ for } t > 0.$$

The general solution to this homogeneous Neumann boundary value problem in the half-space $z > 0$ can be written

$$C_{Rn}(z,t) = \frac{e^{-\lambda_{Rn} t}}{\sqrt{4\pi D t}} \int_0^\infty C_{Rn}^{0}(\varsigma)\left(e^{-\frac{(z-\varsigma)^2}{4Dt}} + e^{-\frac{(z+\varsigma)^2}{4Dt}} \right) d\varsigma. \qquad (3.18)$$

Figure 3.2 plots the evolution of theoretical ^{222}Rn profiles (a) over a continental land mass assuming a zero initial concentration, and (b) over a large ocean assuming an initial equilibrium concentration for times ranging from $t = 0$ to $t = 12.5$ days, calculated using the above-determined values for $\mathcal{F}$ and D. Over land, the ^{222}Rn inventory will reach 90% of the equilibrium inventory after ~13 days. Over the ocean the ^{222}Rn inventory will be 90% depleted after this time. Figure (b) also plots measured data from a site in the Pacific near Hawaii (Larson 1974). The results suggest an elapsed time between 8-10 days.

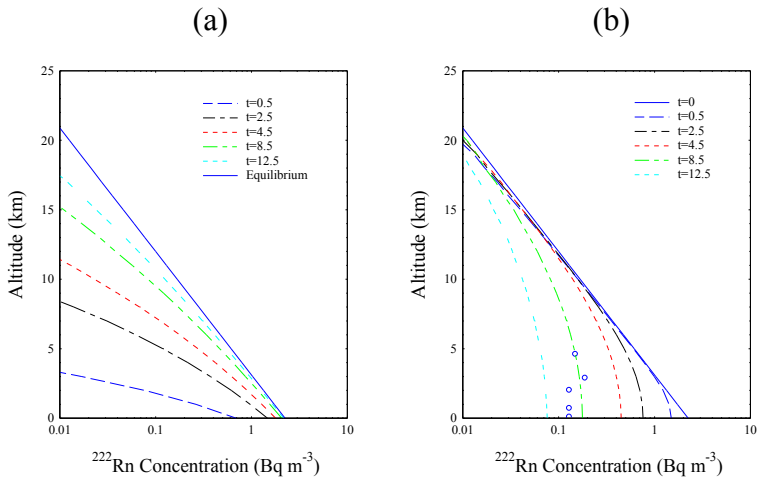

Figure 3.2: ^{222}Rn inventory versus time in a vertical column of air circumnavigating the Earth.

3.3 Numerical solutions

It is not possible to obtain analytical solutions for ^{210}Pb and its daughter radionuclides. These must be obtained by solving numerically the system of equations (3.1)-(3.4):

$$\frac{\partial C_{Rn}}{\partial t} = \frac{\partial}{\partial z}\left(D\frac{\partial C_{Rn}}{\partial z}\right) - \lambda_{Rn} C_{Rn}\,,$$

$$\frac{\partial C_{Pb}}{\partial t} = \frac{\partial}{\partial z}\left(D\frac{\partial C_{Pb}}{\partial z}\right) + \lambda_{Pb}(C_{Rn} - C_{Pb}) - \Lambda(C_{Pb})$$

$$\frac{\partial C_{Bi}}{\partial t} = \frac{\partial}{\partial z}\left(D\frac{\partial C_{Bi}}{\partial z}\right) + \lambda_{Bi}(C_{Bi} - C_{Pb}) - \Lambda(C_{Bi})$$

$$\frac{\partial C_{Po}}{\partial t} = \frac{\partial}{\partial z}\left(D\frac{\partial C_{Po}}{\partial z}\right) + \lambda_{Po}(C_{Po} - C_{Bi}) - \Lambda(C_{Po})$$

for the ^{222}Rn, ^{210}Pb, ^{210}Bi, and ^{210}Po concentrations $C_{Rn}(z,t)$, $C_{Pb}(z,t)$, $C_{Bi}(z,t)$, $C_{Po}(z,t)$ subject to the boundary conditions (3.5)-(3.8):

$$-D\frac{\partial C_{Rn}}{\partial z}\bigg|_{(0,t)} = \mathcal{F}, \qquad C_{Rn}(z,t) \to 0 \text{ as } z \to \infty\,,$$

$$\frac{\partial C_{Pb}}{\partial z}\bigg|_{(0,t)} = 0, \qquad C_{Pb}(z,t) \to 0 \text{ as } z \to \infty\,,$$

$$\frac{\partial C_{Bi}}{\partial z}\bigg|_{(0,t)} = 0, \qquad C_{Bi}(z,t) \to 0 \text{ as } z \to \infty\,,$$

$$\left.\frac{\partial C_{Po}}{\partial z}\right|_{(0,t)} = 0, \qquad C_{Po}(z,t) \to 0 \text{ as } z \to \infty .$$

Solution will be implemented using the software package MATHEMATICA (with Runge-Kutta method). In carrying out the solution we shall assume a constant diffusivity $D = 2.7\ km^2\ d^{-1}$ and a mean ^{222}Rn flux from the land surface of $1590\ Bq\ m^{-2}\ d^{-1}$. The term $\Lambda(C_{Pb})$ characterizes the rate at which ^{210}Pb and its daughters condense from the aerosol state dominated by turbulent diffusion to incipient precipitation dominated by gravity. Since the processes of condensation is effectively confined to the troposphere, it may be written

$$\Lambda(C_{Pb}) = \kappa\, C_{Pb}\, (1 - H(z - z_1)), \tag{3.19}$$

(Piliposian and Appleby 2003) where κ is a rate constant, $H(z)$ is the Heaviside function, defined by

$$H(z) = \begin{cases} 0 & z \le 0 \\ 1 & z > 0 \end{cases}, \tag{3.20}$$

and z_1 is the height of the tropopause. For numerical calculations it is more practical both from a mathematical and physical point of view to replace the Heaviside function by the differentiable function

$$\frac{1}{2}(1 + \tanh(\beta z)) . \tag{3.21}$$

This will give a transition zone of thickness δ in which the value of the function

$$\frac{1}{2}(1 - \tanh(\beta(z - z_1)) \tag{3.22}$$

varies from a value 0.95 to 0.05 provided β is chosen so that $\beta > 3/\delta$.

Solution for an impulsive input (Green's function)

Although MATHEMATICA can be run for any defined input function $\mathcal{F}(t)$, it was found do be numerically more stable to use a Green's function type approach, and first consider the response of the system to a brief impulsive input of ^{222}Rn

$$\mathcal{F}(t) = I_0 \delta(t) .$$

In this case the ^{222}Rn distribution has the exact analytical solution

$$C_{Rn}(z,t) = I_0 \, \mathrm{e}^{-\lambda_{Rn} t} \frac{1}{\sqrt{\pi D t}} \mathrm{e}^{-\frac{z^2}{4Dt}} = I_0 G(z,t) \quad , \tag{3.23}$$

where

$$G(z,t) = \frac{\mathrm{e}^{-\lambda_{Rn} t}}{\sqrt{\pi D t}} \mathrm{e}^{-\frac{z^2}{4Dt}} \tag{3.24}$$

is the response to a unit input at time $t = 0$. This solution can be used as a given input when using MATHEMATICA to solve the partial differential equations for the daughter radionuclides ^{210}Pb, ^{210}Bi and ^{210}Po.

The validity and accuracy of the calculations can be checked by comparing the value of the inventories calculated from the MATHEMATICA results with the theoretical values calculated directly from the known ^{222}Rn inventory, given by

$$A_{Rn}(t) = I_0 \, \mathrm{e}^{-\lambda_{\mathrm{Rn}} t}$$

The ^{210}Pb inventory (including both the stratosphere and the troposphere and also the fallout component) will satisfy the radioactive decay equation

$$\dot{A}_{Pb}(t) = \lambda_{Pb}(A_{Rn} - A_{Pb}) \, .$$

This has the solution

$$A_{Pb}(t) = \frac{\lambda_{Pb} I_0}{\lambda_{Rn} - \lambda_{Pb}} (\mathrm{e}^{-\lambda_{Pb} t} - \mathrm{e}^{-\lambda_{\mathrm{Rn}} t}) \, . \tag{3.25}$$

The corresponding ^{210}Bi and ^{210}Po inventories will similarly satisfy the equations

$$\dot{A}_{Bi}(t) = \lambda_{Bi}(A_{Pb} - A_{Bi})$$

$$\dot{A}_{Po}(t) = \lambda_{Po}(A_{Bi} - A_{Po}) \, .$$

The analytical solutions of these equations are more complicated but were obtained using MATHEMATICA.

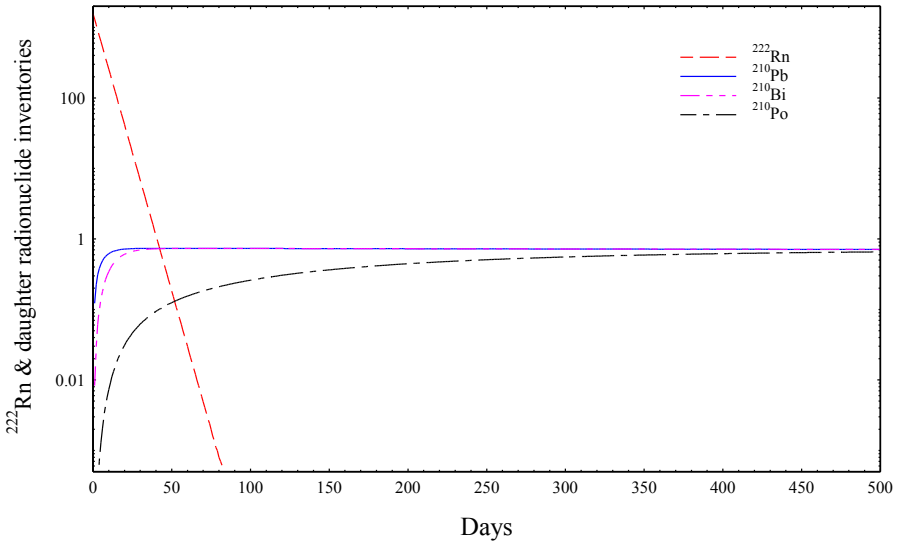

Figure 3.3: Evolution of the ^{222}Rn, ^{210}Pb, ^{210}Bi and ^{210}Po inventories following an impulsive input of ^{222}Rn into a vertical column of air at time $t = 0$.

Figure 3.3 plots the evolution of the inventories of all four radionuclides assuming an impulsive ^{222}Rn input of 1570 Bq m^{-2} at time $t = 0$. The ^{222}Rn inventory has declined by 90% after 26 days, and 99% after 38 days. Since λ_{Rn} is three orders of magnitude larger than λ_{Pb} the exact solution for the ^{210}Pb inventory can be closely approximated by

$$A_{Pb}(t) = I_0 \frac{\lambda_{Pb}}{\lambda_{Rn}}(e^{-\lambda_{Pb}t} - e^{-\lambda_{Rn}t}) = I_0 \frac{\tau_{Rn}}{\tau_{Pb}}(e^{-\lambda_{Pb}t} - e^{-\lambda_{Rn}t}),$$

where τ_{Rn} and τ_{Pb} are the ^{222}Rn and ^{210}Pb half-lives. After ~6 ^{222}Rn half-lives (23 days) the ^{222}Rn exponential term will be negligible. To a close approximation the ^{210}Pb inventory will then satisfy the simple exponential relationship

$$A_{Pb}(t) = I_0 \frac{\tau_{Rn}}{\tau_{Pb}} e^{-\lambda_{Pb}t}. \qquad (3.26)$$

The theoretical maximum of 0.736 Bq m^{-2} is essentially reached after around 40 days after which time it slowly declines in accordance with the above simple exponential relationship.

The ^{210}Bi inventory reaches 90% equilibrium with ^{210}Pb after 24 days and 99% equilibrium after 40 days (~8 ^{210}Bi half-lives). Due to its longer half-life ^{210}Po takes over 400 days ((~3 ^{210}Po half-lives) to reach 90% equilibrium.

Numerical results for an impulsive input

Numerical calculations using MATHEMATICA were made of the ^{210}Pb, ^{210}Bi, and ^{210}Po concentrations $C_{Rn}(z,t)$, $C_{Pb}(z,t)$, $C_{Bi}(z,t)$, $C_{Po}(z,t)$ following an impulsive ^{222}Rn input of 1570 Bq m^{-2} at time $t = 0$. For the purpose of these calculations the fallout coefficient κ (defined in equation 3.9) has been given the value 0.2 d^{-1}, corresponding to a residence time of 5 days. As a test of the reliability of the results, values of the stratospheric, tropospheric, total atmospheric and total (including fallout) radionuclide inventories were made by numerically integrating the vertical profiles and the results compared with the numerical values of the calculated from the above decay equations.

The results for ^{210}Pb are shown in Figure 3.4. The total inventory calculated in this way is in good agreement with the exact value. After 25 days it reached a maximum value of 0.71 Bq m^{-2}, 98% of the theoretical value. After 35 days it was 96% of the theoretical value. The small discrepancy shown in the diagram appears to be due to a small error in the numerical procedure for calculating the fallout component. This was determined using the time step calculation

$$A_{Pb}^{F}(t+h) = A_{Pb}^{F}(t)\mathrm{e}^{-\lambda_{Pb}h} + \kappa\tfrac{1}{2}\{A_{Pb}^{T}(t) + A_{Pb}^{T}(t+h)\}h, \qquad (3.27)$$

where A_{Pb}^{T} is the tropospheric inventory.

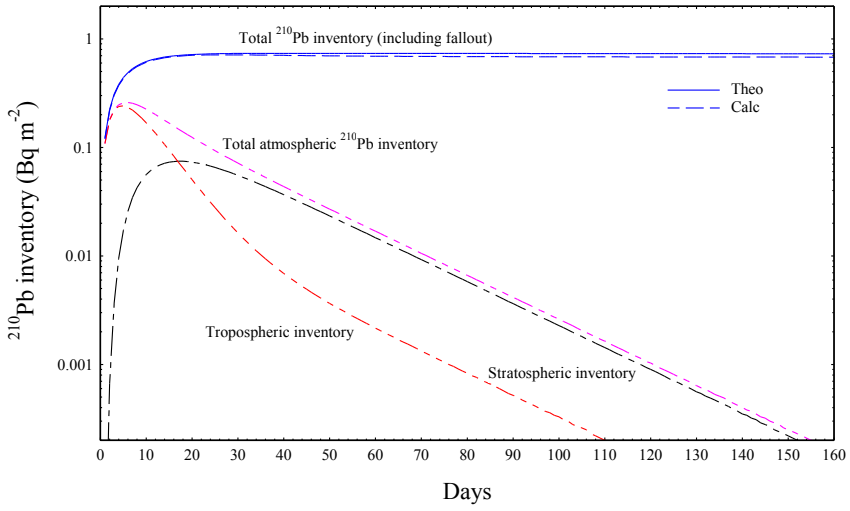

Figure 3.4: Evolution of the tropospheric, stratospheric and total ^{210}Pb inventories in a vertical column of air assuming a 5 day residence time, calculated from the numerically determined ^{210}Pb profiles following an impulsive input of ^{222}Rn at time $t = 0$. Also shown is the exact total inventory determined from the decay equations.

The results show that the initial rapid increase in the ^{210}Pb inventory takes place mainly in the troposphere where it reaches a maximum value of 0.24 Bq m^{-2} after just 5 days. Over the next 26 days it then declines rapidly (with a half-life of around 6 days) due mainly to a combination of reduced creation by ^{222}Rn decay and loss by fallout. After around 16 days the tropospheric inventory falls below that of the stratosphere causing a reverse flux from the stratosphere. This becomes significant after around 30 days, slowing down the rate of decline in the troposphere and increasing the half-life of the remaining tropospheric inventory to around 15 days. The stratospheric inventory reaches a maximum value of around 0.075 Bq m^{-2} after 17 days (at which point it is about equal to that in the troposphere). It then begins a long slow decline due to depletion of the ^{222}Rn and the reverse flux to the troposphere. This decline has a half-life of 15 days, similar to that of the tropospheric inventory. The fallout from the atmosphere is 90% complete after around 30 days, and 99% complete after around 75 days.

Similar results for the inventories of the daughter radionuclides ^{210}Bi and ^{210}Po are shown in Figures 3.5 and 3.6. Because of the short half-life of ^{210}Bi, the fallout component was determined from the decay equation

$$\dot{A}^F_{Bi}(t) = \lambda_{Bi}(A^F_{Pb} - A^F_{Bi}) + \kappa A^T_{Bi}$$

where A^T_{Bi} is the tropospheric inventory. Assuming that the time step h is sufficiently small so that the terms $\lambda_{Bi} A^F_{Pb}$ and κA^T_{Bi} are reasonably constant over the time interval $[t,t+h]$, rewriting in the form

$$\frac{\mathrm{d}}{\mathrm{d}t}\left(A^F_{Bi}(t)\,\mathrm{e}^{\lambda_{Bi}t}\right) = \mathrm{e}^{\lambda_{Bi}t}\left\{\lambda_{Bi} A^F_{Pb} + \kappa A^T_{Bi}\right\}$$

and then integrating over this time interval we obtain

$$A^F_{Bi}(t+h) - A^F_{Bi}(t)\,\mathrm{e}^{-\lambda_{Bi}h} = \frac{1}{\lambda_{Bi}}(1-\mathrm{e}^{-\lambda_{Bi}h})\{\lambda_{Bi} A^F_{Pb} + \kappa A^T_{Bi}\}.$$

Setting

$$A^F_{Pb} = A^F_{Pb}(t) \quad \text{and} \quad A^T_{Bi} = \tfrac{1}{2}\{A^T_{Bi}(t) + A^T_{Bi}(t+h)\}$$

the fallout ^{210}Bi inventory at time $t+h$ can thus be determined using the time step calculation

$$A_{Bi}^{F}(t+h) = A_{Bi}^{F}(t)\,\mathrm{e}^{-\lambda_{Bi}h} + A_{Pb}^{F}(t)(1-\mathrm{e}^{-\lambda_{Bi}h}) + \kappa\tfrac{1}{2}\{A_{Bi}^{T}(t) + A_{Bi}^{T}(t+h)\}\frac{1}{\lambda_{Bi}}(1-\mathrm{e}^{-\lambda_{Bi}h}). \quad (3.28)$$

Using similar arguments, the fallout ^{210}Po inventory can be determined using the time step calculation

$$A_{Po}^{F}(t+h) = A_{Po}^{F}(t)\,\mathrm{e}^{-\lambda_{Po}h} + A_{Bi}^{F}(t)(1-\mathrm{e}^{-\lambda_{Po}h}) + \kappa\tfrac{1}{2}\{A_{Po}^{T}(t) + A_{Po}^{T}(t+h)\}\frac{1}{\lambda_{Po}}(1-\mathrm{e}^{-\lambda_{Po}h}). \quad (3.29)$$

The production of ^{210}Bi is driven by ^{210}Pb decay and the two radionuclides should reach 90% radioactive equilibrium after around 25 days and 99% radioactive equilibrium after around 40 days. MATHEMATICA results are again in good agreement. The total ^{210}Bi inventory (including fallout) reached a maximum value of 0.70 Bq m^{-2} after 44 days, 95% of the theoretical value. The initial rapid increase in the ^{210}Bi inventory mainly takes place in the troposphere where a maximum value of 0.079 Bq m^{-2} is reached after 8 days. Over the next 20 days it then declines rapidly (with a half-life of around 8 days). After around 16 days the tropospheric inventory falls below that of the stratosphere causing a reverse flux from the stratosphere. This becomes significant after around 50 days, slowing down the rate of decline in the troposphere and increasing the half-life of the remaining tropospheric inventory to around 15 days. The stratospheric inventory reaches a maximum value of 0.056 Bq m^{-2} at around 20 days. After around 40 days the decline settles down to a steady rate with a half-life of 15 days similar to that of the tropospheric inventory. Fallout from the atmosphere is 90% complete after around 30 days, and 99% complete after around 75 days.

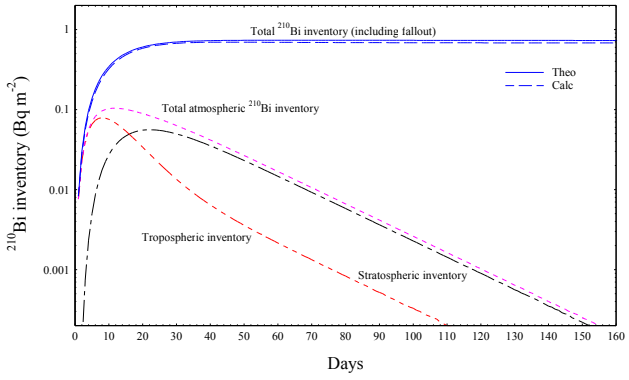

Figure 3.5: Evolution of the tropospheric, stratospheric and total ^{210}Bi inventories in a vertical column of air assuming a 5 day residence time, calculated from the numerically determined ^{210}Bi profiles following an impulsive input of ^{222}Rn at time $t = 0$. Also shown is the exact total inventory determined from the decay equations.

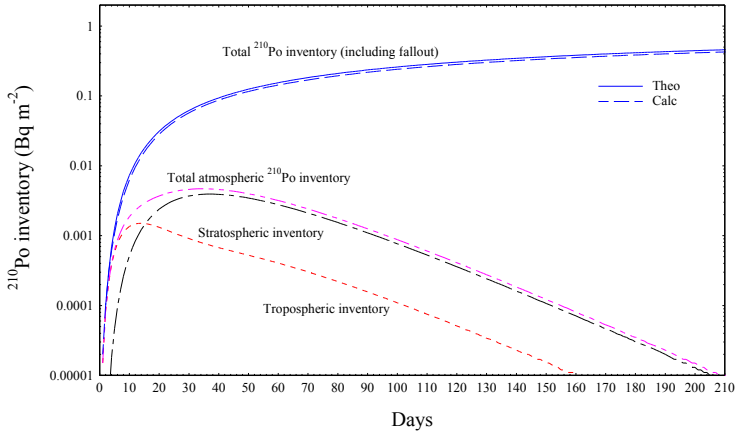

Figure 3.6: Evolution of the tropospheric, stratospheric and total ^{210}Po inventories in a vertical column of air assuming a 5 day residence time, calculated from the numerically determined ^{210}Po profiles following an impulsive input of ^{222}Rn at time $t = 0$. Also shown is the exact total inventory determined from the decay equations.

Because of its longer half-life ^{210}Po takes a significantly longer time to reach radioactive equilibrium with ^{210}Bi and ^{210}Pb, around 150 days to reach 50% equilibrium, and over 500 days to reach 90% equilibrium. The initial rapid increase in the ^{210}Po inventory again mainly takes place in the troposphere where a maximum value of 0.0015 Bq m^{-2} is reached after 13 days. The initial rate of decline (over the next 20 days) has a half-life of around 20 days, significantly slower than for ^{210}Bi, and not very different from the long-term value of around 17 days. The stratospheric inventory reaches a maximum value of 0.0039 Bq m^{-2} at around 35 days. Its subsequent decline has a long-term half-life of around 17 days. The atmosphere inventory has declined by 90% after around 110 days, and 99% after around 170 days. Further increases in the total inventory take place almost entirely in the cumulative fallout component on the earth's surface, due to ingrowth from the fallout ^{210}Bi.

Figure 3.7 plots values of the stratospheric, tropospheric, and total ^{210}Bi/^{210}Pb and ^{210}Po/^{210}Bi inventory ratios versus time calculated from the above results. The total inventory ratios (including fallout) are in good agreement with the theoretical values. The ^{210}Bi/^{210}Pb inventory ratios in all three compartments increase from around 10% in the first couple of days to 50% after around 10 days. Equilibrium is reached after around 45 days. Values in the troposphere are a consistently a little lower than in the stratosphere. The ^{210}Po/^{210}Bi inventory ratios are much lower and only reach 10% after

around 35 days. At the end of 170 days they are still just around 55%, well short of equilibrium.

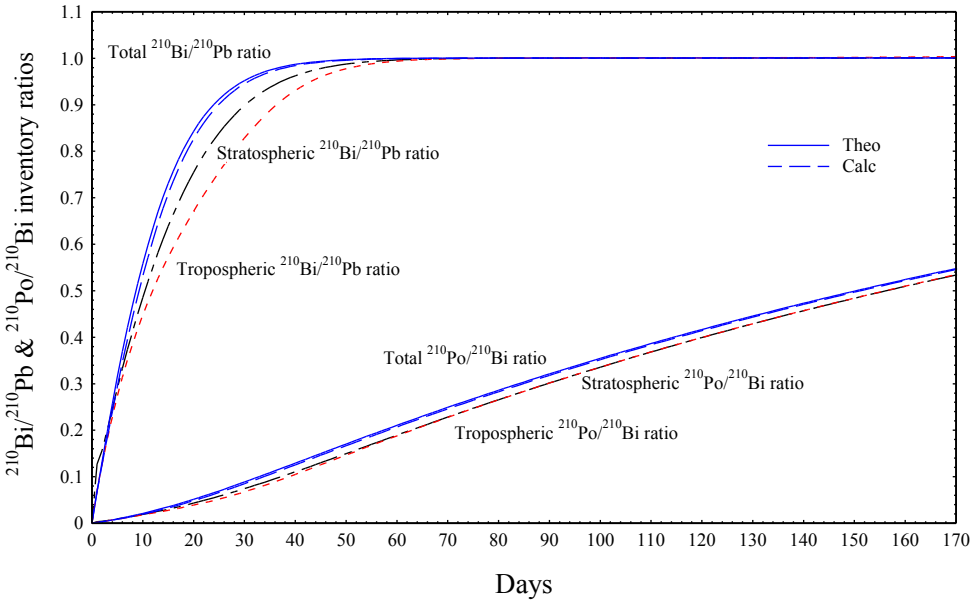

Figure 3.7: Evolution of the tropospheric, stratospheric and total ^{210}Bi/^{210}Pb and ^{210}Po/^{210}Bi inventory ratios in a vertical column of air assuming a 5 day residence time, following an impulsive input of ^{222}Rn at time $t = 0$. Also shown are the exact inventory ratios determined from the decay equations.

Qualitatively, similar results were obtained from ratios for values of the removal rate coefficient ranging varying from 0.1d^{-1} to 0.3 d^{-1}.

Solution for a prolonged input

Using the above results the solution for a prolonged ^{222}Rn flux $\mathcal{F}$ into the base of the column is readily achieved by discretising the problem and representing the input as a series of discrete inputs I_m at the beginning of each time interval $(m-1)h < t < mh$. The ^{222}Rn distribution in the column at time nh (the end of the nth time interval) due to input at the beginning of the m^{th} time interval (time $(m-1)h$) can be written

$$I_m G_{Rn}(z,(n-m+1)h), \tag{3.30}$$

where

$$G_{Rn}(z,t) = \frac{e^{-\lambda_{Rn}t}}{\sqrt{\pi D t}} e^{-\frac{z^2}{4Dt}} \tag{3.31}$$

is the ^{222}Rn distribution due to a unit impulsive input at time $t = 0$. Due to ^{222}Rn decay the ^{222}Rn inventory at end of the m^{th} time interval due to this input will be $I_m \, e^{-\lambda_{Rn} h}$. The input of ^{222}Rn is however a continuous process. Writing $\mathcal{F}_m$ for the mean flux during the time interval $(m-1)h < t < mh$ the ^{222}Rn inventory at time mh due to this input will be

$$\mathcal{F}_m \frac{1}{\lambda_{Rn}} (1 - e^{-\lambda_{Rn} h}) .$$

To generate the same inventory at times $t > mh$ the value of the discrete input needs to be

$$I_m = \phi_{Rn} \mathcal{F}_m \quad \text{where} \quad \phi_{Rn} = \frac{1}{\lambda_{Rn}} (e^{\lambda_{Rn} h} - 1) .$$

For values of $h < 1$ day we have

$$\phi_{Rn} \approx h(1 + h/10) . \tag{3.32}$$

If $h = 1$ day, the correction is ~10%. If $h = 0.1$ day it is just 1%.

Summing the contributions from all inputs during time intervals 1 through n the ^{222}Rn concentration in the column at time nh is

$$C_{Rn}(z, nh) = \sum_{m=1}^{n} I_m G_{Rn}(z, (n-m+1)h) = I_1 G_{Rn}(z, nh) + I_2 G_{Rn}(z, (n-1)h) + ... + I_n G_{Rn}(z, h) .$$

In the same way, writing

$$G_{Pb}(z, n) , \quad G_{Bi}(z, n) , \quad G_{Po}(z, n)$$

for the (numerically determined) ^{210}Pb, ^{210}Bi and ^{210}Po distributions at the end of day n due to a unit input of ^{222}Rn at time $t = 0$, the ^{210}Pb, ^{210}Bi and ^{210}Po distributions in the column at time nh are

$$C_{Pb}(z, nh) = \sum_{m=1}^{n} I_m G_{Pb}(z, (n-m+1)h) = I_1 G_{Pb}(z, nh) + I_2 G_{Pb}(z, (n-1)h) + ... + I_n G_{Pb}(z, h) \tag{3.33}$$

$$C_{Bi}(z, nh) = \sum_{m=1}^{n} I_m G_{Bi}(z, (n-m+1)h) = I_1 G_{Bi}(z, nh) + I_2 G_{Bi}(z, (n-1)h) + ... + I_n G_{Bi}(z, h) \tag{3.34}$$

$$C_{Po}(z,nh)=\sum_{m=1}^{n} I_m G_{Po}(z,(n-m+1)h)=I_1 G_{Po}(z,nh)+I_2 G_{Po}(z,(n-1)h)+\ldots+I_n G_{Po}(z,h) \quad (3.35)$$

Implementation

The above calculations can easily be carried out using either MATHEMATICA or FORTRAN. The four Green's functions need to be stored as arrays

GRN(31,N), GPB(31,N), GBI(31,N), GPO(31,N)

where N is the number of time steps. The height of the altitude is taken as 30 km, divided into steps of length z_0 = 1 km. The values of the array GRN are calculated using the formula

$$\mathrm{GRN}(i,j)=G_{Rn}(i,jh)=\mathrm{e}^{-\lambda_{rn} jh}\frac{1}{\sqrt{\pi Djh}}\mathrm{e}^{-\frac{i^2}{4Djh}},$$

where h is the length of the time step. The values of GPB, GBI, GPO determined are determined numerically using MATHEMATICA:

$$\mathrm{GPB}(i,j)=G_{Pb}(i,jh),\quad \mathrm{GBI}(i,j)=G_{Bi}(i,jh),\quad \mathrm{GPO}(i,j)=G_{Po}(i,jh).$$

The ^{222}Rn exhalation rates need to be stored as a vector array F(N) where F(j) is the input at the beginning of step j. The concentration profiles need to be stored in arrays

CRN(31,N), CPB(31,N), CBI(31,N), CPO(31,N)

where CRN(i,j), CPB(i,j), CBI(i,j), CPO(i,j) are the radionuclide concentrations at altitude $z=iz_0$ and time $t=jh$. The entries for these arrays are calculated using the formulae

$$\mathrm{CRN}(i,j)=\sum_{k=1}^{j}\mathrm{F}(k)\mathrm{GRN}(i,j-k+1)$$

$$\mathrm{CPB}(i,j)=\sum_{k=1}^{j}\mathrm{F}(k)\mathrm{GPB}(i,j-k+1)$$

$$\mathrm{CBI}(i,j)=\sum_{k=1}^{j}\mathrm{F}(k)\mathrm{GBI}(i,j-k+1)$$

$$\mathrm{CPO}(i,j)=\sum_{k=1}^{j}\mathrm{F}(k)\mathrm{GPO}(i,j-k+1)$$

Constant input for a finite time

Initially, the case of a constant ^{222}Rn flux $\mathcal{F}$ for a constant time $0 \leq t \leq T$ and then zero flux for all times $t > T$ is considered. Dividing the interval [0, T] into M time steps of length h it is assumed that there is a discrete input

$$I_0 = \phi_{Rn}\mathcal{F}$$

at the beginning of each of the time steps 1 through to M, and zero input thereafter. Using the stored value of the ^{222}Rn Green's function GRN(i, j) the ^{222}Rn distribution at time $t = nh$ for $n \leq M$ is

$$C_{Rn}(z,nh) = I_0\{\mathrm{G}_{Rn}(z,nh) + \mathrm{G}_{Rn}(z,(n-1)h) + ... + \mathrm{G}_{Rn}(z,h)\}$$

that is, the sum of the Green's functions for inputs at all time steps 1 through to n. For $n > M$

$$C_{Rn}(z,nh) = I_0\{\mathrm{G}_{Rn}(z,nh) + \mathrm{G}_{Rn}(z,(n-1)h) + ... + \mathrm{G}_{Rn}(z,(n-M)h\}$$

that is, the sum of the Green's functions for inputs at all time steps prior to and including the M^{th}. The distributions of the other radionuclides are calculated in the same way. The calculations are easily carried out using Excel.

Numerical results

In a test on the reliability of the procedures, distributions of ^{222}Rn were calculated assuming a constant ^{222}Rn input of 1570 Bq m^{-2} d^{-1} for the first 20 days followed by a period of 80 days with no input. This corresponds to a column of air spending 20 days over land and then moving out over an ocean. Results determined by a direct numerical solution of the PDE using MATHEMATICA were compared with those obtained by the Green's function method firstly using a 1-day time-step without correction and secondly using a 0.5 day time-step with correction.

Figure 3.8 plots atmospheric inventories versus time for ^{222}Rn inputs over a 20-day period. Values calculated using MATHEMATICA are in excellent agreement with the exact solution calculated from the decay equations up to around 40 days. After around 45 days (at which point the ^{222}Rn inventory falls below 1% of the 20-day maximum value) the errors become increasingly large, presumably due to errors in the MATHEMATICA program when handling very small numbers. Values calculated by

the Green's function method using a 1-day time-step without correction significantly overestimate the inventory during the first few days and slightly underestimate it after 20 days, though are generally in good agreement with the exact solution throughout the whole 100-day period. Using a 0.5 day time-step with correction for decay there is excellent agreement throughout the 100 day period.

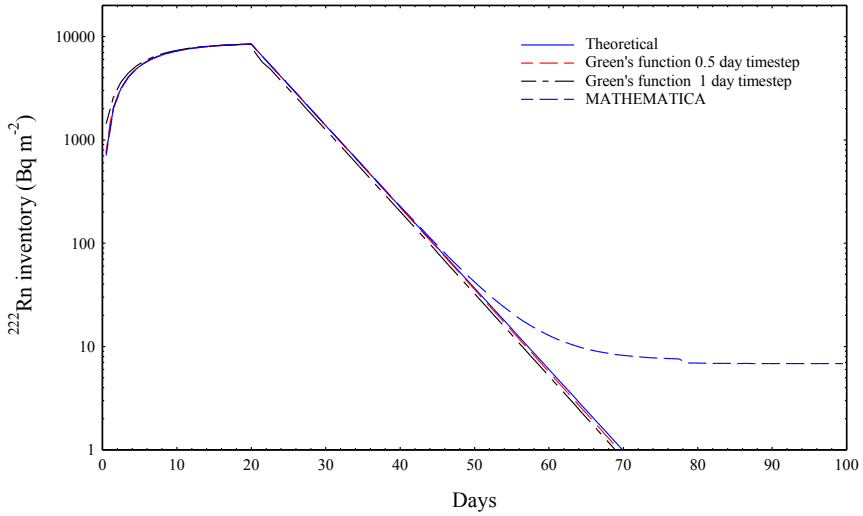

Figure 3.8: ^{222}Rn inventories versus day over a period of 100 days assuming a constant input of 1570 Bq m^{-2} d^{-1} for the first 20 days. The solid line shows the exact value calculated using the decay equations. The dashed lines show results calculated using the Green's function method, and direct numerical solution of the PDE.

Clearly, calculations carried out by using the Green's function method are in excellent agreement with the theoretical values.

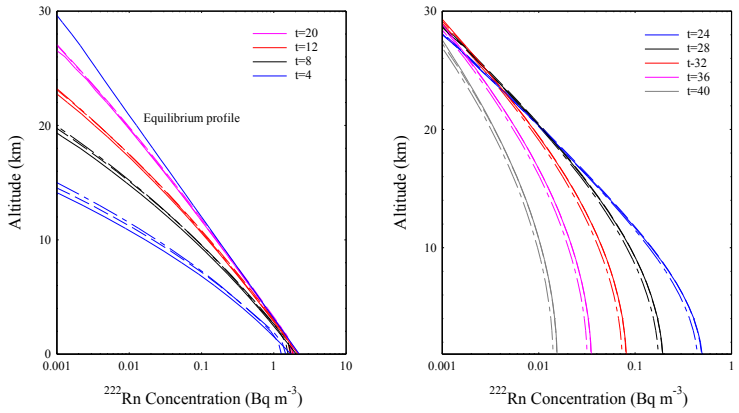

Figure 3.9: ^{222}Rn profiles at various times up to 40 days assuming a constant input of 1570 Bq m^{-2} d^{-1} for the first 20 days. The solid line shows the calculated by direct numerical solution of the PDE. The dashed lines show results calculated using the Green's function method.

Figure 3.9 plots vertical profiles of the ^{222}Rn concentration for times up to 40 days. The solid lines show results determined by numerical solution of the PDE. The dashed lines show results calculated using the Green's function method with a time-step of 0.5 days (long dashes) and 1 day (long and short dashes). The Green's function results appears to slightly underestimate the ground level concentrations during the input period, presumably due the difficulty in tracking the very rapid changes with time following the discrete inputs at the beginning of each time-step. There is also a small discrepancy at high altitude caused by the numerical solution setting a zero boundary condition at a height of 30 km. Excluding these small differences the two methods are in excellent agreement.

^{210}Pb, ^{210}Bi and ^{210}Po distributions

In a further test of the method, ^{210}Pb, ^{210}Bi and ^{210}Po distributions were calculated for a constant ^{222}Rn exhalation rate of 1570 Bq m^{-2} d^{-1} in the first case for a period of 11 days, and in the second for a period of 29 days. In each case it was assumed that there were no inputs for the remainder of the period. The fallout coefficient was assumed to be 0.2 d^{-1}. In both cases, results calculated by solving the PDEs numerically were reasonably accurate during the input period but following its cessation deviated significantly from the expected exponential decline after around 40 days.

^{210}Pb results

Figure 3.10 shows the ^{210}Pb inventories determined from the distributions for the case of an 11-day input. The dashed lines show values determined from the profiles calculated using the Green's function method. They include the tropospheric and stratospheric inventories, the total atmospheric inventory, and the total inventory (including fallout). The solid line shows the theoretical value of the total ^{210}Pb inventory (including fallout) calculated from the mass balance decay equation.

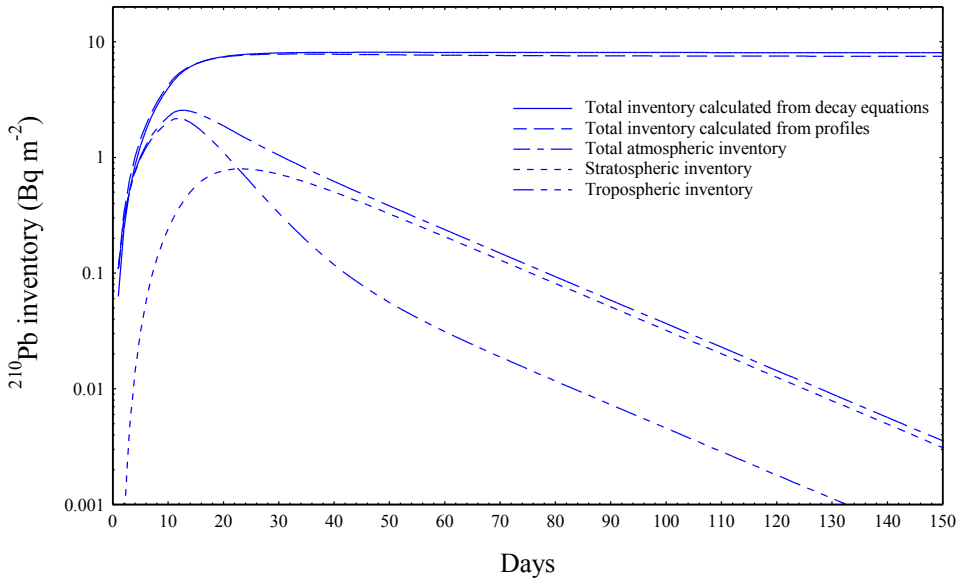

Figure 3.10: ^{210}Pb inventories over a period of 150 days assuming a constant input of 1570 Bq m^{-2} d^{-1} for the first 11 days. The dashed lines shows the exact values calculated from the decay equations. The solid line show inventories for the different compartment determined from profiles calculated using the Green's function method.

The total ^{210}Pb inventory (including fallout) should reach a maximum value of 8.09 Bq m^{-2} at around 40 days. After this time further production by ^{222}Rn decay is virtually zero and the inventory declines slowly with in accordance with the ^{210}Pb radioactive decay law. Values calculated from the Green's function results are in good agreement with the theoretical values. The initial rapid increase in the atmospheric ^{210}Pb inventory mainly takes place in the troposphere, reaching a maximum value of 2.18 Bq m^{-2} after 12 days. Over the next 24 days it then declines rapidly (with a half-life of around 6 days) due mainly to a combination of reduced creation by ^{222}Rn decay and loss by fallout. After around 23 days the tropospheric inventory falls below that of the stratosphere causing a reverse flux from the stratosphere. This becomes increasingly significant, slowing down the rate of decline. After around 60 days, the remaining tropospheric inventory declines exponentially with time with a half-life of around 15 days, significantly longer than the nominal 10-day residence time but similar to that for a single impulsive input. The stratospheric inventory peaks at around 0.80 Bq m^{-2} after 23 days. After around 45 days the remaining stratospheric inventory declines exponentially with time, again with a half-life of around 15 days.

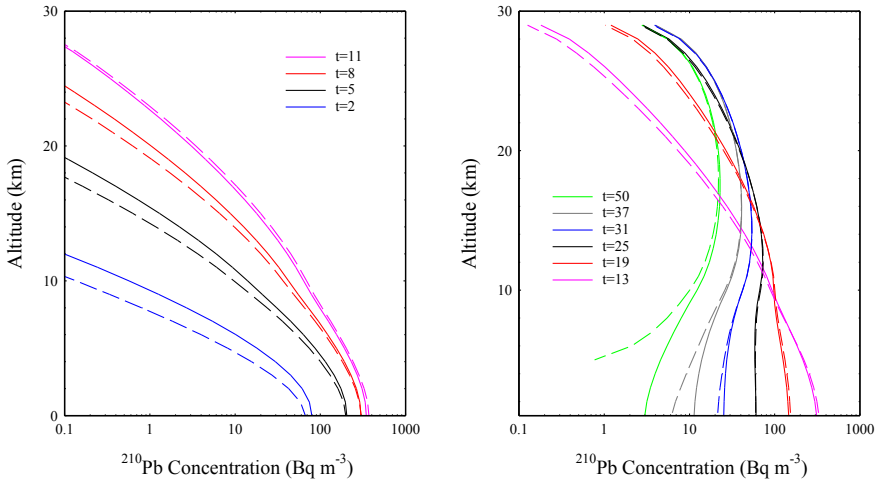

Figure 3.11: ^{210}Pb profiles at various times up to 40 days assuming a constant input of 1570 Bq m^{-2} d^{-1} for the first 11 days. The dashed lines show the results calculated by direct numerical solution of the PDE. The solid lines show results calculated using the Green's function method.

Figure 3.11 compares ^{210}Pb profiles calculated using the Green's function method (solid lines) and the numerical solution of the PDEs(dashed lines). During the exhalation stage the profiles are qualitatively similar though with a systematic discrepancy that diminishes as they develop. After exhalation ceases the agreement is initially very good. After around 35 days the near ground-level concentrations determined decrease much more rapidly than expected, even having negative values, almost certainly due to propagating errors in the numerical calculations.

Calculations were carried out for the case of a constant input spanning 29 days yielded qualitatively similar results. Results obtained by MATHEMATICA again became unstable after around 60 days when inventories fell to below 1% of their maximum values. In contrast, values calculated using the Green's function method appeared to remain stable for at least 150 days at which time inventories had fallen to less than 0.1% of their maximum values. The long-term rate of decline in the inventories (after around 50 days in the case of the stratosphere and 70 days in the case of the troposphere) again corresponded to a half-life of 15 days.

^{210}Bi and ^{210}Po results

Figures 3.11-3.14 show corresponding results for the ^{210}Pb daughters ^{210}Bi and ^{210}Po for the case of an 11-day input. The inventories follow a similar pattern to that for ^{210}Pb. During the initial period the inventory is predominantly in the troposphere, but falls relatively rapidly following the cessation of inputs. After around 20 days the

stratospheric inventory exceeds that of the troposphere and reaches a maximum value after around 35 days in the case of ^{210}Bi and 60 days in the case of ^{210}Po. The reversed flux from the stratosphere to the troposphere after 20 days results in the long-term in an apparent removal rate from the troposphere significantly slower than the nominal value. The calculations continued beyond 220 days without any sign of numerical instability even though values had declined by 3 orders of magnitude from the maximum values.

During the input phase ground level concentrations of ^{210}Bi increase from zero to around 100 Bq m^{-3} before falling back to around 2 Bq m^{-3} after 70 days. Changes to the ground level concentrations of ^{210}Po lagged behind those of ^{210}Bi. Figure 3.15 plots values of ground level ^{210}Bi/^{210}Pb and ^{210}Po/^{210}Bi activity ratios assuming ^{222}Rn inputs lasting 11 days (solid line) and 29 days (dashed line). Following the cessation of inputs, the ^{210}Bi/^{210}Pb activity ratio increase rapidly towards unity with radioactive equilibrium being reached after a period of around 80 days. In contrast, there is still a large disequilibrium between ^{210}Po and ^{210}Bi after 200 days.

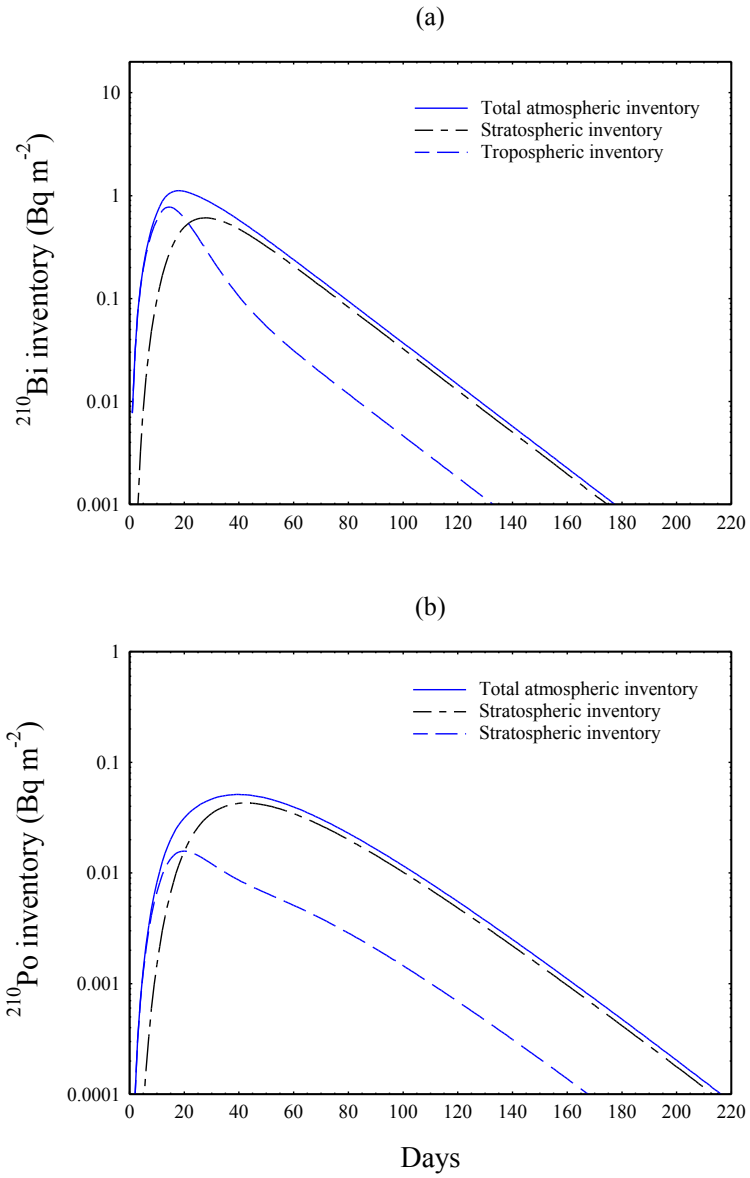

Figure 3.12: (a) ^{210}Bi and (b) ^{210}Pb inventories over a period of 220 days assuming a constant input of 1570 Bq m^{-2} d^{-1} for the first 11 days, calculated using the Green's function method.

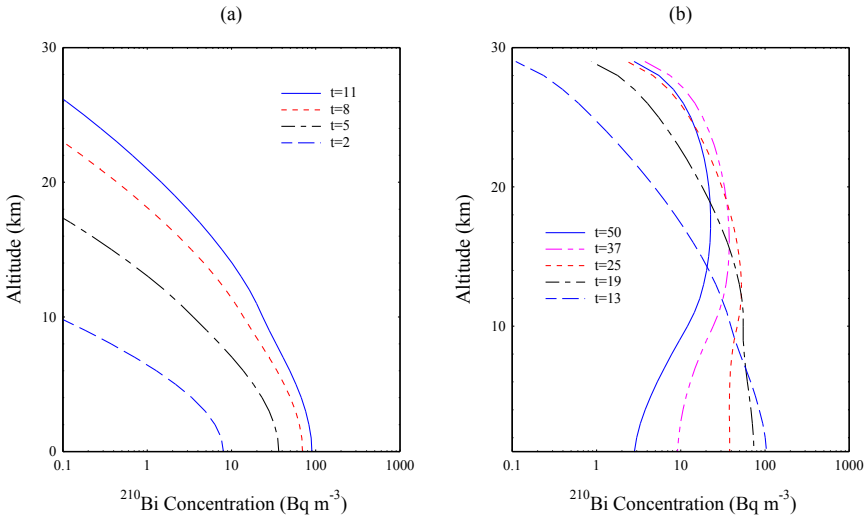

Figure 3.13: ^{210}Bi profiles assuming a constant input of 1570 Bq m^{-2} d^{-1} for the first 11 days (a) at times up to 11 days and (b) at times greater than 11 days.

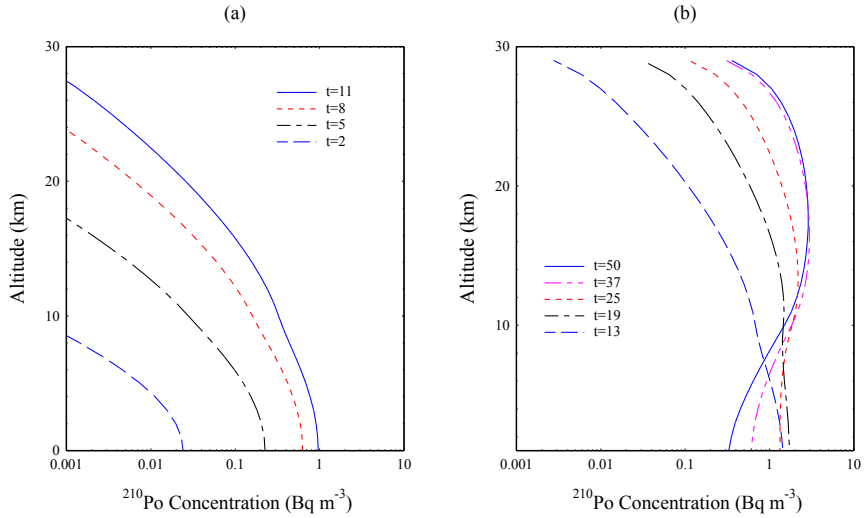

Figure 3.14 ^{210}Po profiles assuming a constant input of 1570 Bq m^{-2} d^{-1} for the first 11 days (a) at times up to 11 days and (b) at times greater than 11 days.

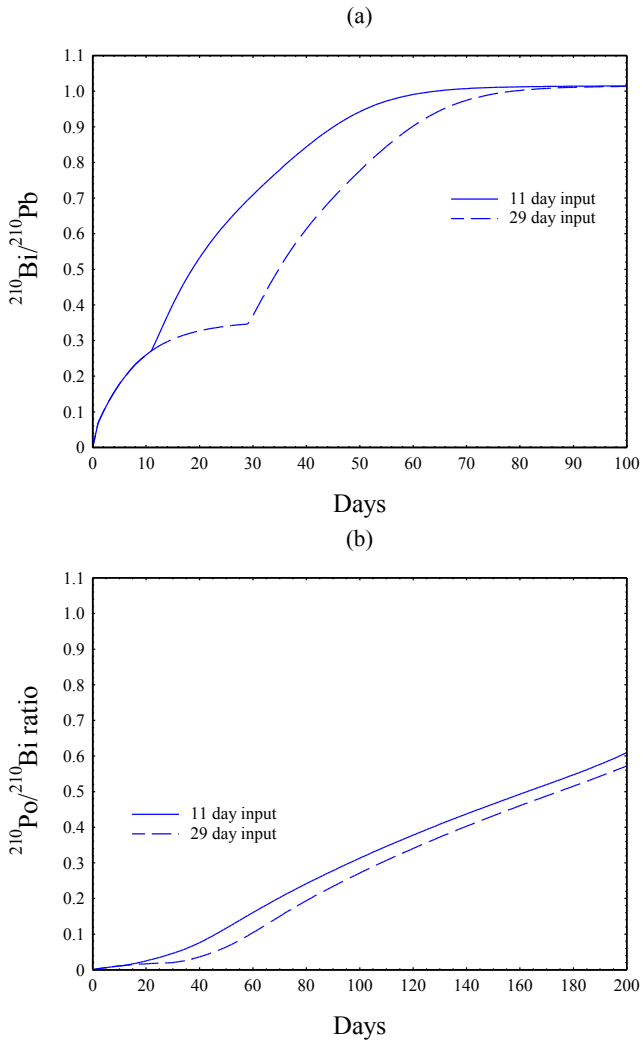

Figure 3.15: (a) ^{210}Bi/^{210}Pb and (b) ^{210}Po/^{210}Bi ground level activity ratios assuming a constant input of 1570 Bq m^{-2} d^{-1} for the first 11 days (solid lines) and 29 days (dashed lines).

Chapter 4. Global equilibrium distribution

4.1 Introduction

Figure 4.1 plots mean annual fallout of ^{210}Pb (per m of mean annual rainfall) versus longitude across the major land masses in the Northern Hemisphere from sites lying between 30^{o} – 65^{o} N. The results, based on data extracted from the literature and held in the ERRC data base, indicate a consistent increase in ^{210}Pb fallout from around 70 Bq m^{-2} y^{-1} at the western margins of each land mass to maximum values of more than 150 Bq m^{-2} y^{-1} near the eastern seaboard of North America and over 250 Bq m^{-2} y^{-1} in the far east of the Eurasian land mass. Greatly reduced values are observed at the three Oceanic sites in the Northern Pacific and North Atlantic, data from which are also shown in Figure 4.1. This distribution can be attributed to the prevailing west-east global circulation at northern mid-latitudes (30^{o} – 65^{o}). Air masses at these latitudes travelling from west to east over the North Pacific or North Atlantic will be highly depleted in ^{222}Rn and ^{210}Pb by the time they arrive at the western margin of North America or Europe. Concentrations will then build up again as the column moves over the land mass before declining again after it passes over the eastern seaboard.

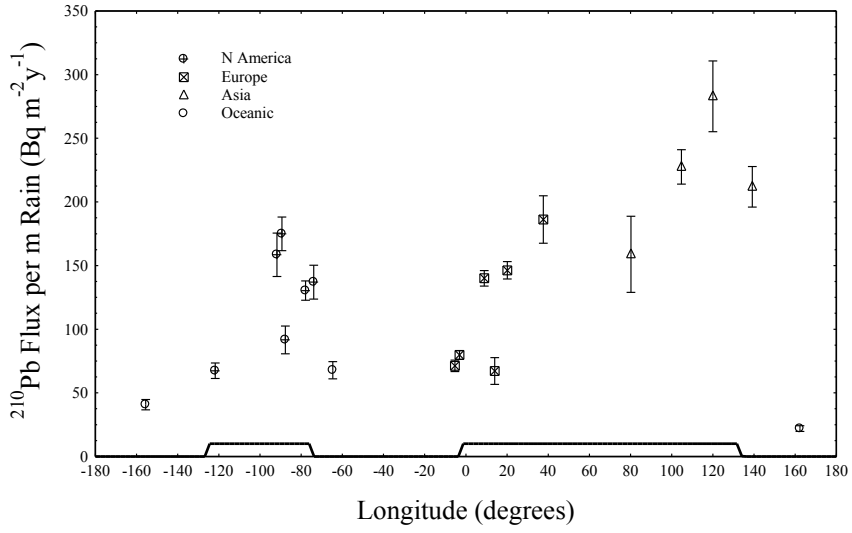

Figure 4.1: Mean annual fallout of ^{210}Pb (normalised against rain) at sites in North America, Europe and Asia. Each point represents the average value for all fallout data within a given geographical region. Also shown are data from three oceanic sites in the Northern Pacific and North Atlantic. The error bars are standard deviations in the datasets used to calculate each of these points.

The distribution shown in Figure 4.1 was broadly reproduced by Piliposian & Appleby (2003) using the simple model of an air column moving from west to east at northern mid-latitudes with a global circulation time of 78 days. The mean path of such a column is shown in Figure 4.2. Since 51% of the earth's surface at these latitudes is covered by land, the total travel time over land was estimated to be 40 days, 11 days over North America and 29 days over Eurasia. Transit times over the Atlantic and Pacific were estimated to be 16 days and 22 days respectively. The ^{222}Rn exhalation rate from land surfaces was assumed to be 1570 Bq m^{-2} d^{-1}. The mean ^{210}Pb residence time in the troposphere was assumed to be 5 days. Values of the residence time given in the literature vary widely, ranging from 5-17 days for calculations based on measured ^{210}Bi/^{210}Pb ratios and up to 40 days for those based on measured ^{210}Po/^{210}Pb ratios. The calculations were however based on the questionable assumption that the measured ratios were close to the mean global ratios. The main objective of this chapter will be to model the global distribution of ^{210}Bi and ^{210}Po at northern mid-latitudes and determine a best value of the ^{210}Pb residence time by comparing the modelled ratios to the available empirical data.

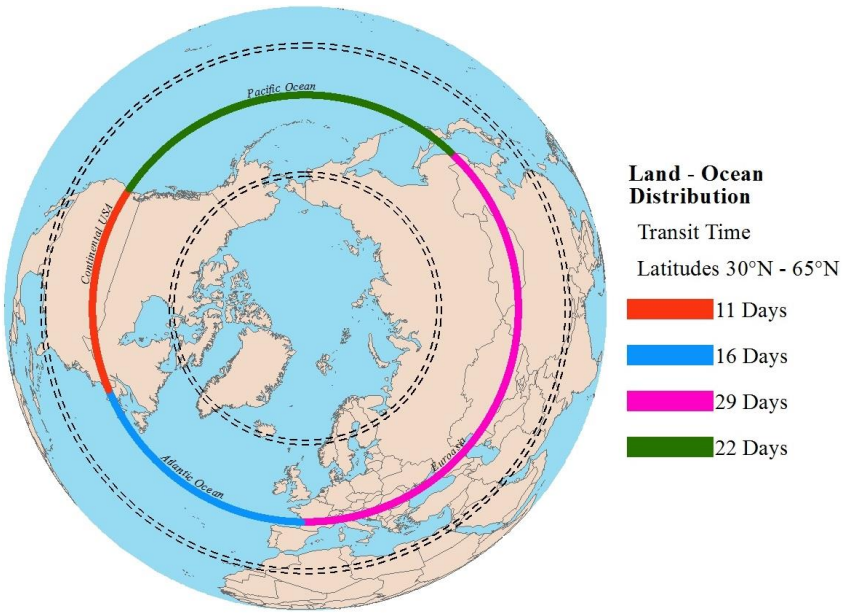

Figure 4.2: Map of the Earth's northern hemisphere showing the land lying between 30°–65° N. Also shown are the approximate transit times across the major land masses and oceans for a notional air column moving from west to east.

Latitudinal variations within the Westerlies Zone may be reduced by a transverse component of the circulation that carries surface air poleward and high altitude equatorward, the so called Ferrel cell (Figure 4.3). Although there is insufficient data to clearly support this inference, measurements of ^{210}Pb fallout along the western seaboard of Europe (ERRC data base) do show relatively small differences between sites ranging from Portugal (40^{o} N) to Norway (66^{o} N).

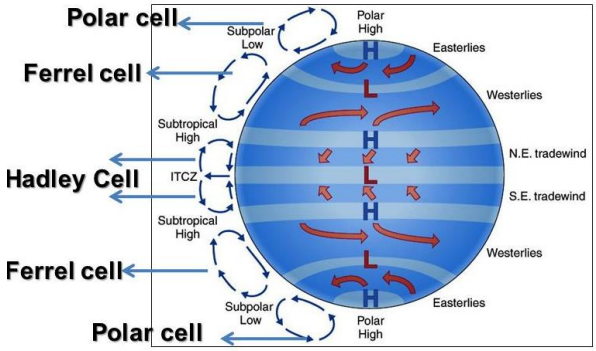

Figure 4.3: Sketch of global circulation of the atmosphere showing the Ferrel cell at northern mid-latitudes. Source: http://slideplayer.com/4981868/16/images/5/Sketch+of+the+global+circulation.jpg.

Although ^{222}Rn exhalation rates from land surfaces are subject to short-term seasonal and weather-related fluctuations, mean annual inputs to the atmosphere will be relatively constant on longer timescales of a year or more. Assuming a uniform ^{222}Rn exhalation rate from land surfaces of $\hat{\mathcal{F}} = 1570$ Bq m^{-2} d^{-1}, and negligible inputs from oceans, inputs at northern mid-latitudes can (on these time-scales) be represented as a function

$$\mathcal{F}(\theta) = \hat{\mathcal{F}}\{\mathrm{H}(\theta-\theta_0) - \mathrm{H}(\theta-\theta_1) + \mathrm{H}(\theta-\theta_2) - \mathrm{H}(\theta-\theta_3)\} \qquad (4.1)$$

of longitude θ, where θ_0 is the longitude of the western seaboard of North America, θ_1 the longitude of the eastern seaboard, is θ_2 the longitude of the western seaboard of Eurasia, and θ_3 the longitude of the eastern seaboard and H(θ) is again the Heaviside unit step function. Modelling global circulation at these latitudes as that of a notional column of air moving from west to east with a speed of 4.6^{o} longitude per day (Piliposian & Appleby 2003) ^{222}Rn inputs into the base of the column can be represented as a periodic function of time

$$\mathcal{F}(t) = \hat{\mathcal{F}}\{\mathrm{H}(t-t_0) - \mathrm{H}(t-t_1) + \mathrm{H}(t-t_2) - \mathrm{H}(t-t_3)\} \quad 0 \le t < T\,, \quad \mathcal{F}(t) = \mathcal{F}(t+T) \tag{4.2}$$

where t_0 is the time at which the column crosses the western seaboard of North America, t_1 the time at which it crosses the eastern seaboard, t_2 the time at which it crosses the western seaboard of Europe, and t_3 the time at which it crosses the eastern margin of the Eurasian land mass and $T = 78$ days is the global transit time. The ^{222}Rn distribution within the column can be obtained by solving equations (3.1) and (3.2) subject to this input function. Distributions of the daughter radionuclides can be obtained by solving linked equations (3.3)–(3.8). From equation (3.27), fallout of ^{210}Pb from the column when it is at longitude θ (at time $t = \frac{\theta}{360}T$) will be

$$\mathcal{P}(\theta) = \kappa A_{Pb}^{T}(\theta),$$

where κ is the tropospheric removal rate constant and A_{Pb}^{T} is the tropospheric inventory at longitude θ.

To a close approximation the Heaviside functions in equation (4.2) can be approximated by the differentiable function

$$\frac{1}{2}\left(1 + \tanh(\alpha t)\right),$$

where the value of the parameter a is chosen so as to give suitably small transition zones across seaboards, as shown in Figure (4.4).

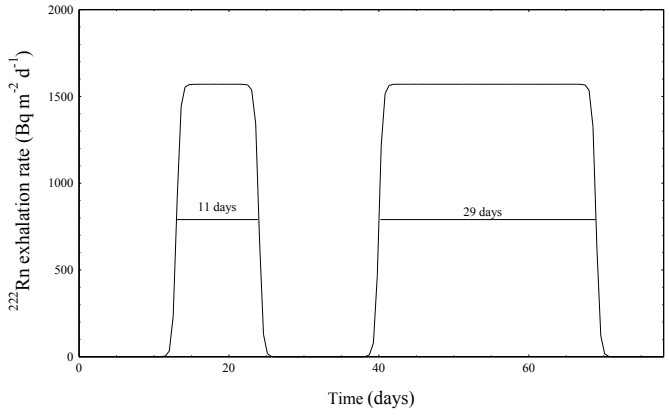

Figure 4.4 ^{222}Rn exhalation rate versus time into a notional column of air moving from west to east at northern mid-latitudes.

4.2 Global equilibrium distribution for northern mid-latitudes

Equilibrium Green's functions

Solving the governing partial differential equations starting from a zero initial condition, in order to determine the equilibrium (periodic) distribution it would be necessary to track the solution over several circuits of the globe. This approach can however result in the build-up of significant numerical errors. The process can be simplified, and made more accurate by introducing the notion of an equilibrium Green's function.

Each time the column passes a fixed point on the Earth's surface it will receive a brief impulsive input of ^{222}Rn from that point the strength of which we denote by I_0. Setting the time $t=0$ just as the column passes this point, the distribution of ^{222}Rn in the column at times $t>0$ due to the input from this location at time $t=0$ will be $I_0 G_{Rn}(z,t)$ (equation (3.30)). The distribution at time t due to the input from the same location on the previous circuit (at time $-T$) will be $I_0 G_{Rn}(z,t+T)$. Adding the contributions from inputs on all previous occasions (at times $-kT$, $k = 0,1,2,\ldots$), the distribution in the column at times $0<t<T$ due to present and past inputs from this location will be

$$I_0\{G_{Rn}(z,t) + G_{Rn}(z,t+T) + G_{Rn}(z,t+2T) + \cdots\cdots\} = I_0 G_{Rn}^{equ}(z,t) \qquad (4.3)$$

where

$$G_{Rn}^{equ}(z,t) = \sum_{k=0}^{\infty} G_{Rn}(z,t+kT) \qquad (4.4)$$

represents an equilibrium Green's function for the ^{222}Rn distribution. Since the distribution at time $t+T$ will be the same as the distribution at time t, this function will be a periodic function of period T. The solutions for the ^{222}Rn daughters can be similarly be written as periodic functions

$$\left.\begin{aligned} I_0 G_{Pb}^{equ}(z,t) &= I_0 \sum_{k=0}^{\infty} G_{Pb}(z,t+kT) \\ I_0 G_{Bi}^{equ}(z,t) &= I_0 \sum_{k=0}^{\infty} G_{Bi}(z,t+kT) \\ I_0 G_{Po}^{equ}(z,t) &= I_0 \sum_{k=0}^{\infty} G_{Po}(z,t+kT) \end{aligned}\right\}, \tag{4.5}$$

where $G_{Pb}(z,t)$, $G_{Bi}(z,t)$, $G_{Po}(z,t)$ are the corresponding Green's functions for a single impulsive input (section 3.3). The equilibrium Green's functions $G_{Pb}^{equ}(z,t)$, $G_{Bi}^{equ}(z,t)$, $G_{Po}^{equ}(z,t)$ are easily generated by continuing to add terms from previous circuits, up until the values are negligible. In practice it was found that 6 periods were sufficient for the longer-lived ^{222}Rn daughters, although because of its short half-life, one period (78 days) was sufficient for ^{222}Rn itself.

Global distributions

Using the above concept, the vertical distribution of ^{222}Rn in the atmosphere at longitude θ can be equated to the equilibrium distribution in the column as it passes over that point and will include equilibrium contributions from each point of the entire circuit of the globe. In particular the contribution due to emissions from that part of the circuit lying between longitudes ψ and $\psi - \delta\psi$ where $\theta - 360 < \psi \leq \theta$ will be

$$G_{Rn}^{equ}(z,s)\mathcal{F}(\psi)\,\delta s$$

where $\mathcal{F}(\psi)$ is the ^{222}Rn exhalation rate at longitude ψ, s is the travel-time in a west-to-east direction to reach longitude θ, and δs is the time taken for the column to traverse the incremental longitude $\delta\psi$. If V (= 360°/T) is the circulation velocity in degrees per day, so that $\psi = \theta - Vs$ and $\delta s = \delta\psi / V$, the equilibrium ^{222}Rn distribution at longitude θ will include all such contributions, and so be given by

$$C_{Rn}^{equ}(z,\theta) = \int_0^T G_{Rn}^{equ}(z,s)\mathcal{F}(\theta - Vs)\,\mathrm{d}s\,. \tag{4.6}$$

The equilibrium distributions of the daughter radionuclides can similarly be written

$$\left.\begin{aligned} C_{Pb}(z,\theta) &= \int_0^T G_{Pb}^{equ}(z,s)\mathcal{F}(\theta - Vs)\,\mathrm{d}s \\ C_{Bi}(z,\theta) &= \int_0^t G_{Bi}^{equ}(z,s)\mathcal{F}(\theta - Vs)\,\mathrm{d}s \\ C_{Po}(z,\theta) &= \int_0^t G_{Po}^{equ}(z,s)\mathcal{F}(\theta - Vs)\,\mathrm{d}s \end{aligned}\right\}. \tag{4.7}$$

Numerical procedure

The above solutions are readily calculated by discretising the problem and dividing the global circulation time T into N time steps $h = T/N$ (and the geographical location into N spatial steps 360/N). The ^{222}Rn input into the column during the m^{th} time step can be approximated by a source of strength $I_m = \phi_{Rn}\mathcal{F}_m$ where $\mathcal{F}_m$ is the value of the exhalation rate at time $s = (m-1)h$, the beginning of the m^{th} time step and ϕ is the ^{222}Rn decay correction factor for time step h (equation (3.32)). Noting that the equilibrium Green's function is periodic of period T, the contribution of exhalation from this geographical location to the equilibrium ^{222}Rn distribution in the column at time $t=nh$, the end of the n^{th} time step, can be written

$$I_m G_{Rn}^{equ}(z, t+T-s) = I_m G_{Rn}^{equ}(z, (n+N-m+1)h) .$$

The equilibrium ^{222}Rn distribution at time $t=nh$ due to inputs from all N steps is thus

$$C_{Rn}(z, nh) = \sum_{m=1}^{N} I_m G_{Rn}^{equ}(z, (n+N-m+1)h) . \qquad (4.8)$$

The distributions of the daughter radionuclides ^{210}Pb, ^{210}Bi and ^{210}Po can similarly be written

$$\left.\begin{aligned} C_{Pb}(z, nh) &= \sum_{m=1}^{N} I_m G_{Pb}^{equ}(z, (n+N-m+1)h) \\ C_{Bi}(z, nh) &= \sum_{m=1}^{N} I_m G_{Bi}^{equ}(z, (n+N-m+1)h) \\ C_{Po}(z, nh) &= \sum_{m=1}^{N} I_m G_{Po}^{equ}(z, (n+N-m+1)h) \end{aligned}\right\} . \qquad (4.9)$$

Implementation

The four equilibrium Green's functions were stored as arrays over two cycles EGRN(31,2N), EGPB(31,2N), EGBI(31,2N), EGPO(31,2N) where N is the number of time steps in each cycle,

$$\text{EG RN}(i, j) = G_{Rn}^{equ}(i, jh) ,$$

and

$$\text{EGPB}(i, j) = G_{Pb}^{equ}(i, jh) , \quad \text{EGBI}(i, j) = G_{Bi}^{equ}(i, jh) , \quad \text{EGPO}(i, j) = G_{Po}^{equ}(i, jh) .$$

The ^{222}Rn exhalation rates were stored as a vector array F(N) where F(j) is the input at the beginning of the j^{th} time interval. The equilibrium concentration profiles were stored in arrays

$$\text{ECRN}(31,N),\ \text{ECPB}(31,N),\ \text{ECBI}(31,N),\ \ \text{ECPO}(31,N)$$

where ECRN(i,j), ECPB(i,j), ECBI(i,j), ECPO(i,j) are the radionuclide concentrations at altitude $z=i$ at time j, the end of the j^{th} time interval. The entries for these arrays were calculated using the formulae

$$\text{ECRN}(i,j)=\sum_{k=1}^{N}\text{F}(k)\,\text{EGRN}(i,j+N-k+1)),$$

$$\text{ECPB}(i,j)=\sum_{k=1}^{N}\text{F}(k)\,\text{EGPB}(i,j+N-k+1)),$$

$$\text{ECBI}(i,j)=\sum_{k=1}^{N}\text{F}(k)\,\text{EGBI}(i,j+N-k+1)),$$

$$\text{ECPO}(i,j)=\sum_{k=1}^{N}\text{F}(k)\,\text{EGPO}(i,j+N-k+1)).$$

The results can be expressed in terms of time by setting $t=jh$ or geographical location by setting $\theta=j/N\times360^{o}$.

4.3 Results

Most measurements of the ^{210}Pb daughters ^{210}Bi and ^{210}Po were carried out either on ground-level air or rainwater samples. Values in rainwater can be regarded as representative of the mean tropospheric concentration, or equivalently, the tropospheric inventory. In this section we compare modelled values of the ^{210}Bi/^{210}Pb and ^{210}Po/^{210}Pb ground-level concentration ratios and tropospheric inventory ratios for different values of the removal rate constant with the available empirical data.

^{210}Bi/^{210}Pb and ^{210}Po/^{210}Pb concentration ratios in ground-level air

Figure 4.5 plots modelled values of the ^{210}Bi/^{210}Pb and ^{210}Po/^{210}Pb concentration ratios in ground-level air at mid-latitudes as functions of longitude θ for values of the tropospheric removal rate constant κ ranging from 0.08 d^{-1} to 0.2 d^{-1} calculated using equations (4.9). Also shown are mean empirical values calculated from all the

measurements of ^{210}Pb, ^{210}Bi and ^{210}Po in ground level air carried out at sites in Colorado (~105º W, Poet et al. 1972), Lisbon Portugal (~9º W, Carvalho 1995) and Hawaii (~156º W, Moore et al. 1974) and from ^{210}Pb and ^{210}Po measurements at Harwell UK (~1º W, Burton & Stewart 1960; Peirson et al. 1966).

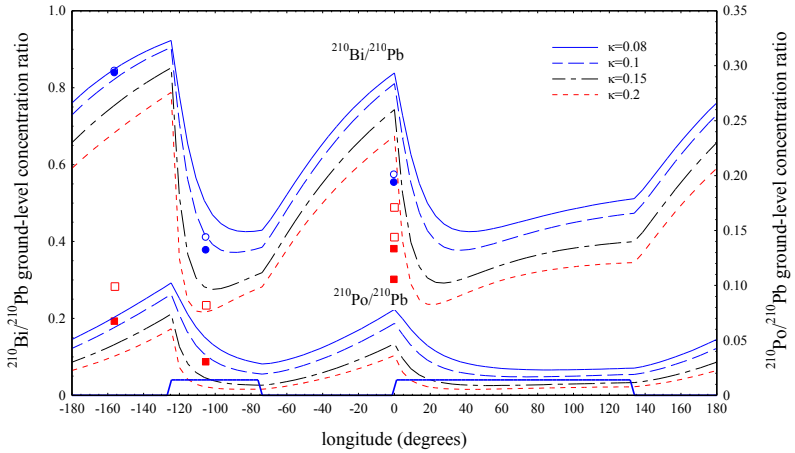

Figure 4.5: Modelled values of the ^{210}Bi/^{210}Pb (left-hand axis) and ^{210}Po/^{210}Pb (right-hand axis) activity ratios in ground-level air at northern mid-latitudes plotted versus longitude for values of the tropospheric removal rate constant ranging from 0.08 d^{-1} to 0.2 d^{-1}, showing also the major land masses. Mean activity ratios for Hawaii, the interior of the USA, and the western margin of Europe calculated from all the available empirical data are shown by the symbols ○ (^{210}Bi/^{210}Pb) and □ (^{210}Po/^{210}Pb). Unsupported activity ratios are represented by the solid symbols (●, ■).

It is evident from these results that for any given value of κ the theoretical ^{210}Bi/^{210}Pb and ^{210}Po/^{210}Pb concentration ratios vary considerably with longitude, the variations largely being governed by the position of the air column relative to major land masses. The ^{210}Bi/^{210}Pb ratio increases rapidly over large oceans to values close to unity (radioactive equilibrium). Renewed ^{210}Pb production at the western margins of the major land masses causes its value to fall dramatically, reaching a minimum value after approximately 4 days in the case of $\kappa = 0.2$ (minimum value 0.23) or 7 days in the case of $\kappa = 0.08$ (minimum value 0.43). As the column moves further into the land mass, increased ^{210}Bi production results in a gradual increase in the ^{210}Bi/^{210}Pb ratio. Reduced ^{210}Pb production once the column has crossed the eastern seaboard and moves out over the ocean causes a sharp acceleration in the rate of increase. The ^{210}Po/^{210}Pb ratios follow a similar pattern though values are an order of magnitude lower due to the longer ^{210}Po half-life.

Empirical values of the raw ^{210}Bi/^{210}Pb concentration ratio in surface air at the Colorado site ranged from 0.18-0.65 with a mean value of 0.41 ± 0.02. Those at Lisbon ranged from 0.12-1.33 with a mean value of 0.57 ± 0.10, whilst those at Hawaii at sea

level on the windward side of the island ranged from 0.81-0.97 with a mean value of 0.84 ± 0.03. The results from the Colorado and Hawaiian sites suggest that the value of κ lies between 0.08 and 0.1. Although measured results from Lisbon suggest a higher value of κ, its position on the western edge of Europe where values of the $^{210}Bi/^{210}Pb$ concentration ratio change rapidly with distance makes the use of data from this location highly problematic. Further, the mean value may well be significantly influenced by local prevailing factors. $^{210}Bi/^{210}Pb$ values at this site determined during times of westerly air flows will have much higher values than those determined during times of easterly conditions.

Empirical values of the $^{210}Po/^{210}Pb$ ratio are an order of magnitude lower than the $^{210}Bi/^{210}Pb$ ratios. Raw values at ground-level at the Colorado site ranged from 0.03-0.25 with a mean value of 0.082 ± 0.012. Those at Lisbon ranged from 0.03-0.78 with a mean value of 0.17 ± 0.05. The mean value at Harwell, also a problematic location, was 0.16 ± 0.05. At Hawaii the $^{210}Po/^{210}Pb$ ratio at sea level on the windward side of the island ranged from 0.08-0.18 with a mean value of 0.10 ± 0.01. Although these results appear to suggest a significantly lower value of κ than that suggested by the $^{210}Bi/^{210}Pb$ ratios, the most likely explanation for the discrepancy would appear to be contamination of samples by ground-level dust containing supported ^{210}Pb and its daughters in radioactive equilibrium (Poet et al. 1972; Baskaran 2011).

Atmospheric ^{210}Pb derived from ^{222}Rn decay will be unsupported activity, and measured by the difference between the total and supported activities. Writing p for the fraction of ^{210}Pb activity arising from the in-situ decay of ^{226}Ra, the unsupported activities will be $^{210}Pb - p^{210}Pb$, $^{210}Bi - p^{210}Pb$, $^{210}Po - p^{210}Pb$. The amount of supported activity can then be estimated by adjusting the value of p so that the unsupported $^{210}Bi/^{210}Pb$ and $^{210}Po/^{210}Pb$ activity ratios yield the same value of κ. The results of these calculations, shown in Table 4.1, suggest a relatively low amount of supported ^{210}Pb, varying from 3.4% to 5.3% of the total ^{210}Pb activity. This correction had a relatively insignificant effect on the $^{210}Bi/^{210}Pb$ ratio but a much greater effect on the $^{210}Po/^{210}Pb$ ratio due to the much lower ^{210}Po concentration. Excluding the data from the West-European seaboard (Lisbon and Harwell) the value of κ was calculated to be between $0.09 \pm 0.02\ d^{-1}$ (Hawaiian data) and $0.11 \pm 0.01\ d^{-1}$ (Colorado data).

^{210}Bi/^{210}Pb and ^{210}Po/^{210}Pb tropospheric inventory ratios

Figure 4.6 shows modelled values of the ^{210}Bi/^{210}Pb and ^{210}Po/^{210}Pb tropospheric inventory ratios calculated for values of the tropospheric removal rate constant κ ranging from 0.08 d^{-1} to 0.2 d^{-1}. The results follow a similar pattern to those for ground-level air. ^{210}Bi/^{210}Pb ratios increase rapidly over large oceans to values close to radioactive equilibrium, but then fall steeply as the column arrives at the western margins of the major land masses. Minimum values over the land masses are reached after around 6 days in the case κ= 0.2 d^{-1} (minimum value 0.32) or 10 days in the case κ= 0.08 d^{-1} (minimum value 0.53). ^{210}Po/^{210}Pb ratios are again an order of magnitude lower than the ^{210}Bi/^{210}Pb ratios.

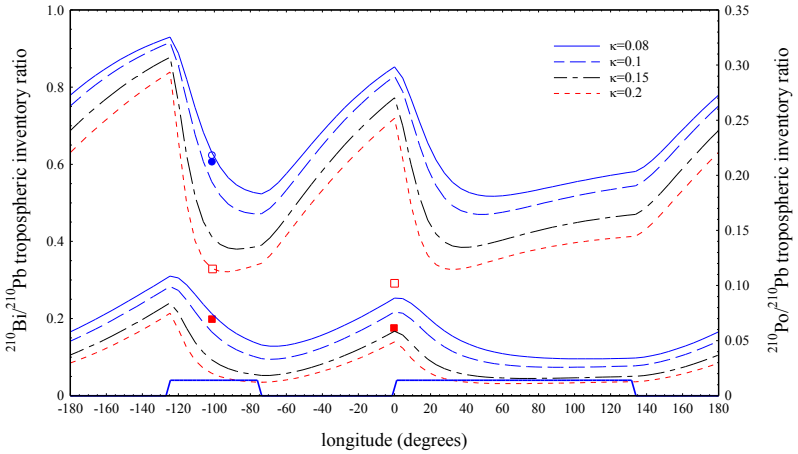

Figure 4.6: Modelled values of the ^{210}Bi/^{210}Pb (left-hand axis) and ^{210}Po/^{210}Pb (right-hand axis) tropospheric inventory ratios at northern mid-latitudes plotted versus longitude. Values of the tropospheric removal rate constant range from 0.08 d^{-1} to 0.3 d^{-1}, also showing the major land masses. Mean activity ratios for the interior of the USA and the western margin of Europe, calculated from all the available empirical data, are shown by the symbols ○ (^{210}Bi/^{210}Pb) and □ (^{210}Po/^{210}Pb). Unsupported activity ratios are represented by the solid symbols (●, ■).

Since the isotopic composition of the troposphere as a whole is likely to be reflected in the isotopic composition of rainwater, empirical measurements of the ^{210}Bi/^{210}Pb and ^{210}Po/^{210}Pb tropospheric inventory ratios are most readily made using rainwater samples. Measurements of ^{210}Pb, ^{210}Bi and ^{210}Po in rainwater were carried out at sites in Colorado (~105° W, Poet et al. 1972) and Arkansas (94° W, Gavini et al. 1974). Measurements of ^{210}Pb and ^{210}Po in rainwater were carried out at Harwell (Burton & Stewart 1960).

A more direct estimate of tropospheric inventory ratios can however be made using measured profiles of ^{210}Pb, ^{210}Bi and ^{210}Po in the atmosphere. Concentrations of

these radionuclides at altitudes ranging from ground-level up to 17 km were determined by Moore et al. (1973) at a number of sites in continental USA ranging from Utah (~112° W) to Kansas (~95° W). Many of the measurements were repeated on a number of separate occasions. Tropospheric inventories calculated by combining all the atmospheric profiles yielded a mean $^{210}Bi/^{210}Pb$ ratio of 0.52 ± 0.05. Values calculated from rainwater measurements at the Colorado site ranged from 0.48–0.84 with a mean value of 0.61 ± 0.01. Those from the Arkansas site ranged from 0.32–1.05 with a mean value of 0.74 ± 0.10. Averaging all these results, a best estimate of the mean $^{210}Bi/^{210}Pb$ tropospheric inventory ratio for the interior of continental USA is 0.62 ± 0.04. Similar calculations of the mean $^{210}Po/^{210}Pb$ tropospheric inventory ratio for the interior of continental USA yielded values of 0.14 ± 0.03 from the atmospheric profiles, 0.061 ± 0.005 from the Colorado rainwater measurements, and 0.13 ± 0.02 from the Arkansas rainwater measurements, with a mean value of 0.11 ± 0.02. The Harwell rainwater measurements had a mean $^{210}Po/^{210}Pb$ ratio of 0.10 ± 0.02.

Table 4.1: Mean values of the empirical ^{210}Pb, ^{210}Bi and ^{210}Po activity ratios, supported ^{210}Pb, corrected (unsupported) activity ratios, and the tropospheric removal rate determined by fitting the empirical data to the modelled values.

(a) Ground-level concentration ratios						
	Raw values		Supported	Corrected values		κ
Longitude	$^{210}Bi/^{210}Pb$	$^{210}Po/^{210}Pb$	^{210}Pb	$^{210}Bi/^{210}Pb$	$^{210}Po/^{210}Pb$	d^{-1}
-156	0.84 ± 0.03	0.10 ± 0.01	3.4%	0.84 ± 0.03	0.067	0.09 ± 0.02
-105	0.41 ± 0.02	0.082 ± 0.012	5.3%	0.38 ± 0.02	0.030	0.11 ± 0.01
0	0.57 ± 0.10	0.17 ± 0.05	4.4%	0.55 ± 0.10	0.13	
0		0.16 ± 0.05	4.4%		0.11	
(b) Tropospheric inventories ratios						
	Raw values		Supported	Corrected values		κ
Longitude	$^{210}Bi/^{210}Pb$	$^{210}Po/^{210}Pb$	^{210}Pb	$^{210}Bi/^{210}Pb$	$^{210}Po/^{210}Pb$	d^{-1}
-101	0.62 ± 0.04	0.11 ± 0.02	4.4%	0.61 ± 0.04	0.069	0.09 ± 0.01
0		0.10 ± 0.02	4.4%		0.061	
				Mean value		0.097 ± 0.012

NB: The standard errors given in this Table are standard deviations in the relevant datasets.

The raw tropospheric $^{210}Bi/^{210}Pb$ ratio from the continental USA suggests a value of κ comparable to that determined from the ground-level data. The raw $^{210}Po/^{210}Pb$ activity ratio again suggests a much lower value, presumably due to the disproportionate effect

of a small amount of supported activity estimated in this case to be just 4.4% of the total ^{210}Pb activity. The corrected unsupported activity ratios are shown in Figure 4.6. These results, also given in detail in Table 4.1, yielded a value of $\kappa = 0.09 \pm 0.01$ d^{-1}, similar to that determined from the ground-level data. Averaging the results from both data sets, a best estimate of the tropospheric removal rate constant is 0.097 ± 0.012 d^{-1}, corresponding to a residence time of 10.3 ± 1.2 days. In practice, these figures can be rounded to $\kappa = 0.10$ d^{-1} and the residence time to 10 days.

4.4 Reservoir effect of the stratosphere

Although the theoretical tropospheric residence time of ^{210}Pb and its daughters appears to be around 10 days, the practical residence time is significantly greater due to the reservoir effect of the stratosphere. ^{222}Rn and its daughters are transported from the troposphere to the stratosphere when concentrations are higher in the troposphere. This process is reversed once tropospheric concentrations fall below those in the stratosphere. Figure 4.7 plots the tropospheric, stratospheric and total ^{210}Pb inventories (including fallout) versus time resulting from an impulsive ground-level ^{222}Rn input of 1570 Bq m^{-2} at time $t = 0$, for the case $\kappa = 0.1$. The inventories were calculated by numerical integration of the ^{210}Pb profiles given by the Green's function $I_o G_{Pb}(z,t)$ with $I_o = 1570$ Bq m^{-2}. The good agreement of the total ^{210}Pb inventory with the theoretical values determined from the mass balance equation

$$A_{Pb}(t) = I_0 \frac{\lambda_{Pb}}{\lambda_{Rn} - \lambda_{Pb}} (e^{-\lambda_{Pb} t} - e^{-\lambda_{Rn} t}) ,$$

also plotted in Figure 4.7, demonstrates the accuracy of the numerical calculations. According to this equation the total ^{210}Pb inventory should reach a maximum value of 0.74 Bq m^{-2} after approximately 40 days, though 90% of this value is achieved after just 24 days. Production by ^{222}Rn is then effectively zero, and thereafter the ^{210}Pb inventory declines slowly in accordance with the ^{210}Pb radioactive decay law.

From the numerical calculations the ^{210}Pb inventory in the troposphere reaches a maximum value of 0.32 Bq m^{-2} after just 6 days. Up to around 40 days it then declines rapidly at a rate corresponding to an apparent residence time of around 13 days due mainly to a combination of reduced creation by ^{222}Rn decay and loss by fallout. After around 22 days the tropospheric inventory falls below that of the stratosphere causing a reverse flux from the stratosphere. This becomes significant after around 60 days,

slowing down the rate of decline in the troposphere and increasing the residence time of the remaining tropospheric inventory to around 25 days.

The stratospheric inventory reaches a maximum value of around 0.12 Bq m^{-2} after 19 days, at which point it is almost equal to that in the troposphere. It then begins a long slow decline due to depletion of the ^{222}Rn and the reverse flux to the troposphere. This decline has a residence time of 25 days, similar to that of the tropospheric inventory, with transport rates from the stratosphere to the troposphere then matching fallout rates from the troposphere. Fallout from the atmosphere has declined by 50% from its maximum value after around 18 days, 90% after around 40 days, and 99% after around 90 days. Given a mean global circulation velocity of around 360 km d^{-1} (4.6° d^{-1}, corresponding to the global circulation time of 78 days), these results show that fallout originating in ^{222}Rn inputs from a particular source reaches a maximum value after the column has travelled a distance of ~2,000 km. It then falls to around 50% of this value after ~6,500 km.

Assuming no stratospheric reservoir effect and that the removal constant κ applies to the atmosphere as a whole, the atmospheric inventory would be given by the equation

$$A_{Pb}(t) = I_0 \frac{\lambda_{Pb}}{\lambda_{Rn} - \lambda_{Pb} - \kappa}\left(e^{-(\lambda_{Pb}+\kappa)t} - e^{-\lambda_{Rn}t}\right).$$

This result, also plotted in Figure 4.7, shows that the reservoir effect only becomes significant after around 35 days.

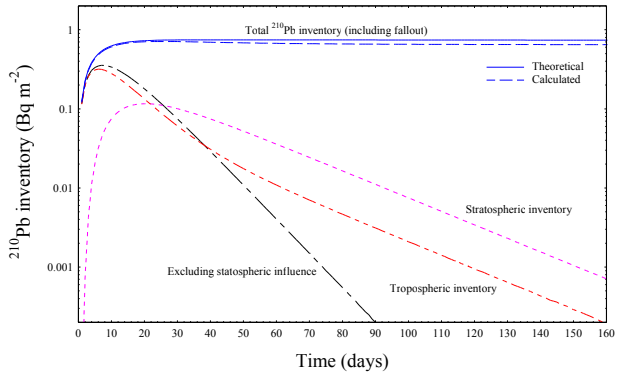

Figure 4.7: ^{210}Pb inventories in the troposphere and stratosphere versus time following the brief impulsive injection of 1570 Bq m^{-2} of ^{222}Rn into the base of an air column, calculated from the vertical distribution of the ^{210}Pb activity assuming a tropospheric removal rate coefficient of 0.1 d^{-1}. Also shown are the total ^{210}Pb inventories (including both the atmospheric and fallout components). Values are calculated from both the numerical solutions and the theoretical mass balance equation, assuming no stratospheric reservoir effect to the atmospheric inventory.

4.5 Discussion

The results presented here show that while the $^{210}Bi/^{210}Pb$ and $^{210}Po/^{210}Pb$ activity ratios can potentially provide important information on the ^{210}Pb atmospheric residence time, the sampling location plays an important role. The $^{210}Bi/^{210}Pb$ ratios are probably more reliable, being less influenced by traces of supported activity. Discrepancies between the $^{210}Bi/^{210}Pb$ and $^{210}Po/^{210}Pb$ ratios can be used to make small corrections for the supported activity. Although the $^{210}Bi/^{210}Pb$ ratios have their highest values in air masses approaching western continental margins, the rapid decline in values (especially at ground-level) as the column moves into the land mass makes the use of such locations highly problematic for model validation. The most suitable locations would appear to be the interiors of large land masses.

The most extensive and reliable ^{210}Pb, ^{210}Bi, ^{210}Po datasets are those obtained from sites in the interior of continental USA. They include measurements carried out on atmospheric samples from a range of different altitudes, and rainwater. Comparisons between the empirical data and model values suggest that the tropospheric removal rate constant has a value between 0.09-0.11 d^{-1}. Much higher $^{210}Bi/^{210}Pb$ ratios from the oceanic site were also consistent with the model predictions. The corresponding mean tropospheric residence time of 10 days is significantly longer than the value of between 4–7 days suggested by Poet et al. (1972) and less than 7 days suggested by Moore et al. (1973). These values were however based on the assumption that ^{222}Rn and its daughters were locally in a state of radioactive equilibrium, governed by equations (1.7) – (1.9). It is also significantly longer than the value suggested by Piliposian and Appleby (2003) though that was largely based on a review of earlier estimates.

The results presented here also highlight the role played by the stratosphere in extending the practical residence time of ^{210}Pb in the atmosphere. The reservoir effect of the stratosphere, capturing ^{210}Pb when tropospheric concentrations are high and releasing it when they are low, significantly enhances the long-range transport of ^{210}Pb from its source locations. Figure 4.8 plots the modelled ^{210}Pb flux versus longitude at northern mid-latitudes assuming a tropospheric removal rate of 0.1 d^{-1} and a 78-day global transit time. The relatively high fluxes at the western margins of Europe and the USA are largely due to long-range transport across the Atlantic and Pacific oceans

respectively. The model values for these western margins (~60 Bq m^{-2} y^{-1} for Europe and ~55 Bq m^{-2} y^{-1} for the USA) are comparable to the empirical values for southern England reported by Burton and Stewart (1960) and Peirson et al. (1966), and for coastal regions of western USA reported by Monaghan et al. (1989). Atmospheric fluxes at specific localities within a given region will however be strongly influenced by local factors such as the mean annual rainfall.

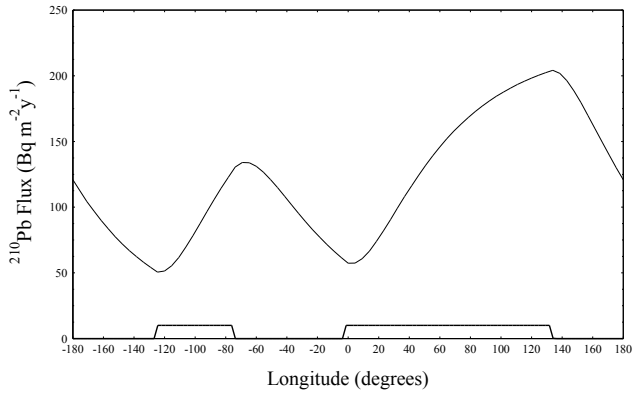

Figure 4.8: ^{210}Pb flux at northern mid-latitudes versus longitude assuming a tropospheric removal rate coefficient of 0.1 d^{-1} and global circulation transit time of 78 days.

PART B: MODELLING CATCHMENT LAKE TRANSPORT PROCESSES IN BROTHERSWATER

Chapter 5. Modelling Catchment/Lake transport

5.1 Introduction

Fallout ^{210}Pb deposited on the landscape has two main applications, as a chronometer for dating environmental records stored in natural archives such as lake sediments and peat bogs, and as a tracer for studying the long-term fate of pollutants deposited on the landscape. Since ^{210}Pb is strongly attached to particulates, the principle mechanisms controlling its redistribution following deposition on the landscape will be soil erosion within catchments (Appleby 1997a) and sediment transport within water bodies. Simple models of transport processes within the water column of a lake (Appleby 1997b) indicate that a substantial fraction of ^{210}Pb entering the water column either by direct deposition from the atmosphere or indirectly by erosive transport from the catchment accumulates in the bottom sediments. The sediments deposited in earlier times can then be dated by comparing their present ^{210}Pb activity to modelled values of their original ^{210}Pb activity (Appleby 2001).

Although the ^{210}Pb method has been used in numerous studies since its initial development in the late 1960s and early 1970s for dating environmental records stored in natural archives such as lake sediments and peat bogs, the processes by which ^{210}Pb itself accumulates in these archives is not well understood. Two simple models developed in the late 1970s (Appleby & Oldfield 1978, Robbins 1978) assumed either a constant rate of supply of fallout ^{210}Pb to the sampling site (CRS model) or a constant initial concentration (CIC model) in newly deposited sediments. Experience has however shown that there are many cases where neither of these highly simplified models is valid. Changes in local and regional environmental conditions often result in changing sedimentation rates and also changes to ^{210}Pb concentrations in freshly deposited sediments. The CRS model assumes that the ^{210}Pb supply rate is governed by the constant atmospheric flux (when averaged over timescales of a year or more) and that changes to ^{210}Pb concentrations are inversely proportional to changes to the sedimentation rate. Although this model has proved to be the more reliable (Appleby 2013), ^{210}Pb supply rates at particular locations within the lake can vary due factors

such as changes in the pattern of sediment focussing, or changes in the erosive input of ^{210}Pb from the catchment. Sensitivity to the influence of catchment inputs will be particularly important at sites where there is a substantial fraction of total inputs. There are however relatively few mass-balance studies of catchment/lake systems capable of identifying the extent of these inputs and their implications for ^{210}Pb dating. A study of the transport and mass balance of fallout radionuclides in Blelham Tarn, Cumbria (Appleby et al. 2003) showed that around 47% of ^{210}Pb in the sediments of that lake derived from erosive inputs from the catchment. These inputs were however concentrated near one of the major input streams. Away from this part of the lake, the sediment record was dominated by direct atmospheric fallout, though the detailed pattern was influenced by sediment focussing.

The purpose of the present work is to study the transport processes controlling the fate of ^{210}Pb deposited on the catchment of Brotherswater in the English Lake District, and in particular the impact of these processes on the supply of ^{210}Pb to the sediment record in the lake. This site is unique in that it has been the subject of a number of multi-core studies of fallout ^{210}Pb (and also the artificial radionuclide ^{137}Cs) since the early 1970s. The information gained by comparing and combining results from the present study with those from earlier studies offers the possibility of yielding not only a better understanding of the long-term fate of fallout radionuclides in the Brotherswater catchment but also evidence as to the long-term stability of lake sediment records as natural environmental archives. Given the widespread use of these archives for reconstructing the history of environmental change, this issue is of fundamental importance to this whole area of environmental research.

This chapter will present a brief summary of mass balance models used for characterising the transport of fallout radionuclides through catchment/lake systems. Chapter 6 will be concerned with obtaining a best estimate of atmospheric fallout of ^{210}Pb and ^{137}Cs at Brotherswater. Chapter 7 will present the results of measurements of the fluxes of ^{210}Pb and ^{137}Cs through the water column of Brotherswater, and Chapter 8 presents measurements of the inventories of fallout ^{210}Pb and ^{137}Cs in the sediment record. Finally, Chapter 9 will utilise data from this and earlier studies to present a model of the transport of fallout ^{210}Pb and ^{137}Cs through the case study of Brotherswater catchment lake system. Appendix 2 includes a paper recently submitted for publication in which ^{210}Pb and ^{137}Cs records in sediment cores collected recently

are compared with those collected in earlier studies, and the results used to make an assessment as to the long-term stability of these records and their reliability for determining historical sedimentation rates."

5.2 Mass-balance model

Figure 5.1 shows a mass-balance model of the transport processes governing the fate of fallout radionuclides deposited onto a lake and its catchment. Writing $\Phi(t)$ for the flux (Bq m^{-2} y^{-1}) at time t, the catchment inventory $Q_C(t)$ will be controlled by inputs via the direct atmospheric flux $A_C\Phi(t)$, and losses $\lambda Q_C(t)$ via radioactive decay and $\Psi_C(t)$ via transport to the lake, where A_C is the catchment area, and λ the radioactive decay constant. The overall impact of these processes may be represented by the mass-balance equation

$$\dot{Q}_C = A_C\Phi - \Psi_C - \lambda Q_C . \tag{5.1}$$

The water column inventory $Q_L(t)$ is controlled by inputs via the direct atmospheric flux $A_L\Phi(t)$ plus transport $\Psi_C(t)$ from the catchment, and losses $\lambda Q_L(t)$ via radioactive decay, $\Psi_O(t)$ via the outflow, and $A_L\ \Phi_S(t)$ via deposition on the bed of the lake where A_L is the area of the lake and $\Phi_S(t)$ (Bq m^{-2} y^{-1}) the mean rate of supply to the sediment record per unit area of the lake. The overall impact may be represented by the mass-balance equation

$$\dot{Q}_L = A_L\Phi + \Psi_C - A_L\Phi_S - \Psi_O - \lambda Q_L . \tag{5.2}$$

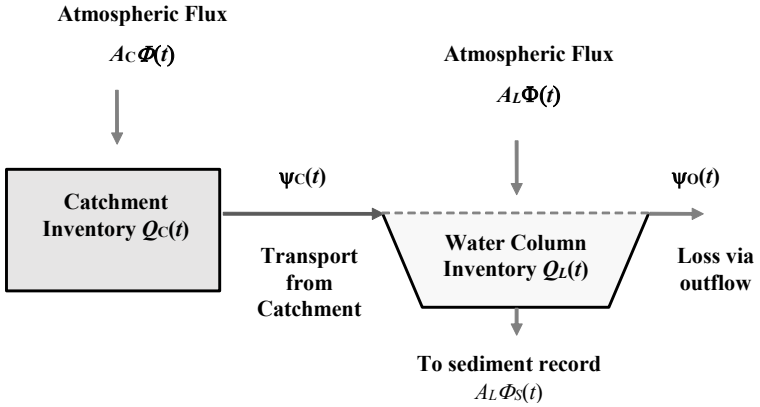

Figure 5.1: Representation of the catchment/lake mass balance model.

The atmospheric flux can be measured directly via bulk deposition collectors and indirectly through soil cores at selected sites. The rate of supply to the sediment record

can be measured via sediment cores collected from a representative set of sites in the lake. Transport rates from the catchment and loss rates via the outflow can be estimated using a combination of mass balance arguments and simple models of transport processes from the catchment and through the water column.

5.3 Catchment model

Following Appleby et al. (2003) it is suggested that the decay corrected transport rate at time t due to a unit amount of fallout onto the catchment at time $t = 0$ can be represented by a unit response function h(t). Using this approach, since the amount of fallout s years ago during the short time increment δs will be $A_C \Phi(t-s)\delta s$ its contribution to the transport rate at time t will thus be $A_C \Phi(t-s)\,\mathrm{h}(s)\,\mathrm{e}^{-\lambda s}\,\delta s$. The transport rate at time t due to fallout at all times t–s ($0 \leq s < \infty$) can then be written

$$\Psi_C(t) = A_C \int_0^\infty \Phi(t-s)\,\mathrm{h}(s)\,\mathrm{e}^{-\lambda s}\,\mathrm{d}s = A_L \alpha \int_0^\infty \Phi(t-s)\,\mathrm{h}(s)\,\mathrm{e}^{-\lambda s}\,\mathrm{d}s\,, \qquad (5.3)$$

where $\alpha = A_C / A_L$ is the catchment/lake area ratio. For ^{210}Pb, where there is a constant atmospheric flux $\mathcal{P}$, the transport rate has a constant value

$$\Psi_C = A_L \alpha \eta_{Pb} \mathcal{P}\,, \qquad (5.4)$$

where

$$\eta_{Pb} = \int_0^\infty \mathrm{h}(s)\,\mathrm{e}^{-\lambda s}\,\mathrm{d}s \qquad (5.5)$$

is the decay weighted area under the response function, or alternatively, the fraction of annual fallout onto the catchment delivered to the lake. Assuming a single impulsive flux I at time t = 0 (such as that due to Chernobyl) the total amount of fallout on the catchment will be $A_C I = A_L \alpha I$. Taking radioactive decay into account the transport rate at a later time t will therefore be

$$\Psi_C(t) = A_L \alpha I\,\mathrm{h}(t)\,\mathrm{e}^{-\lambda t}\,. \qquad (5.6)$$

Fallout transported from the catchment at time t will include both freshly deposited material and older material deposited in previous years. Since surface soils are more readily available for erosion than sub-surface material, the transport rate will be more strongly related to surface concentrations. If we consider in particular the

response to a discrete amount of fallout Q_0 at time $t = 0$, simple diffusion models suggest that the surface concentration at time t can be written

$$C_0(t) = \frac{Q_0}{\sqrt{\pi D t}} e^{-\lambda t}$$

and hence that the resulting transport rate will reduce inversely with the square root of time. If we further assume that it is proportional to the residual inventory $Q(t)$, it follows that the transport rate at time t due to the fallout amount Q_0 can be modelled by an equation of the form

$$\hat{\Psi}(t) = kQ(t)/\sqrt{t}$$

(Appleby et al. 2003) where k is an empirical transport coefficient that can loosely be related to the quantity $1/\sqrt{\pi D}$. The value of the residual inventory $Q(t)$ will thus be governed by the mass balance equation

$$\dot{Q} = -\lambda Q - kQ/\sqrt{t}, \qquad Q(0) = Q_0.$$

Integrating we obtain

$$Q(t) = Q_0 \, \mathrm{e}^{-(\lambda t + 2k\sqrt{t})},$$

whence

$$\hat{\Psi}(t) = \frac{k}{\sqrt{t}} Q_0 \, \mathrm{e}^{-(\lambda t + 2k\sqrt{t})}.$$

It follows that the unit response function can in this case be written

$$\mathrm{h}(s) = \frac{k}{\sqrt{s}} \mathrm{e}^{-2k\sqrt{s}}. \tag{5.7}$$

For ^{210}Pb in particular

$$\eta_{Pb} = \int_0^\infty \mathrm{h}(s) \mathrm{e}^{-\lambda s} \mathrm{d}s = \int_0^\infty \frac{k}{\sqrt{s}} \mathrm{e}^{-(\lambda s + 2k\sqrt{s})} \mathrm{d}s. \tag{5.8}$$

By measuring η_{Pb} this equation can be solved to find a value for k. Noting that equation (5.8) can be integrated to give

$$\eta_{Pb} = \sqrt{\pi} \frac{k}{\sqrt{\lambda}} \mathrm{e}^{k^2/\lambda} \operatorname{erfc}\left\{\frac{k}{\sqrt{\lambda}}\right\} = 2\frac{k}{\sqrt{\lambda}} \mathrm{e}^{k^2/\lambda} \int_{k/\sqrt{\lambda}}^\infty \mathrm{e}^{-s^2} \mathrm{d}s,$$

since the ^{210}Pb decay constant λ has the value 0.03114 y^{-1}, and k is typically of the order of 0.001, the parameter $k/\sqrt{\lambda}$ will always be small and to a first approximation this relationship can be written

$$\eta_{Pb} \approx 2\frac{k}{\sqrt{\lambda}}\int_0^{\infty} \mathrm{e}^{-u^2}\,\mathrm{d}u = k\sqrt{\frac{\pi}{\lambda}} \approx 10.04\times k$$

From this first approximation equation (5.8) can quickly be used to obtain a more exact value. For a single impulsive input I (per unit area) at time t =0, the transport rate at a later time t will be

$$\Psi_C(t) = A_L \alpha I \frac{k}{\sqrt{t}} \mathrm{e}^{-(\lambda t + 2k\sqrt{t})} \tag{5.9}$$

5.4 Water column model

The fate of radionuclides entering the water column of a lake will be controlled by a number of different factors, including the water residence time, the fraction of the radionuclide attached to particulates, the particulate settling velocity and the water depth.

Water residence time

Assuming the mean annual volume V of water in a lake to be relatively constant from year to year, losses via the outflow will on these longer timescales be balanced by fresh inputs via direct precipitation or runoff from the catchment. The mean water residence time for the lake is defined as the time taken for the throughput of water to completely replace the existing volume and is given by the formula

$$T_W = \frac{V}{q_0}, \tag{5.10}$$

where q_0 is the mean net annual loss via the outflow. It may be regarded as the nominal time taken for fresh inputs to reach the outflow. The value of the water residence time can be estimated directly by monitoring the outflow, or indirectly by using a mass balance approach. Fresh inputs will include runoff from the catchment and direct rainfall onto the lake. Assuming the mean annual volume of water stored in the catchment to be relatively constant from year to year, mean annual runoff will be equal to the mean net amount of water deposited onto the catchment from the atmosphere. Writing R_C and R_L for the mean net annual atmospheric flux (precipitation less evaporation) over the catchment and onto the lake, the mean annual input of water to the lake may be written

$$q_i = R_C A c + R_L A_L .$$

Since fresh inputs will on average balance losses via the outflow, the water residence time can be estimated using the formula

$$T_W = \frac{V}{R_C A_C + R_L A_L}. \tag{5.11}$$

Assuming net precipitation rates over the catchment to be similar to those over the lake this simplifies to

$$T_W = \frac{V}{R_L A_L (1+\alpha)}, \tag{5.12}$$

where α is the catchment/lake area ratio.

Transport of particulates within the water column

Fallout radionuclides in the water column may include both a dissolved fraction and a fraction associated with suspended particulates. The fate of the particulate fraction will largely be determined by the fate of the associated particulates. These may include both mineral and organic particles, ranging in size from medium silts down to colloidal material. Their fate will largely be determined by the particle size. Drag forces ensure that the horizontal component of their motion is for all practical purposes that of the lake water. The action of gravity may however result in a significant steady vertical motion through the water in which the downwards gravitational force is balanced by an upwards hydrostatic buoyancy force and an upwards drag force opposing the motion. Assuming the particle to be spherical of diameter D μm, and of mass density ρ_s g/cm^3, the gravitational force will be

$$F_G = \frac{1}{6}\pi D^3 \rho_s g,$$

where g is the gravitational acceleration, and the buoyancy force (from Archimedes Law)

$$F_B = -\frac{1}{6}\pi D^3 \rho_w g,$$

where ρ_w is the density of water. Assuming slow laminar flow the drag force will be

$$F_D = -3\pi\eta D v_p,$$

where v_p is the settling velocity and η is the viscosity of water. At the terminal velocity, these forces will balance whence

$$\frac{1}{6}\pi D^3(\rho_s - \rho_w)g - 3\pi\eta D v_p = 0\,.$$

Rearranging, the velocity v_p will be given by the well-known Stoke's formula

$$v_p = \frac{D^2 g(\rho_s - \rho_W)}{18\mu}\,.$$

Since drag forces quickly eliminate any deviation from the terminal velocity, this will essentially be the settling velocity. Measuring D in μm, and using the values $\mu = 1.3\times10^{-3}$ kg s^{-1} m^{-1} (at 10°C), g = 9.81 ms^{-2} and $\rho_S - \rho_W = 1.6\times10^3$ kg m^{-3}, this reduces to

$$v_p = \frac{9.81\times1.6\times10^3}{18\times1.3\times10^{-3}}\times(10^{-6})^2\times86400\times D^2 = 0.058\,D^2 \text{ m d}^{-1}$$

Calculations show that this equation is valid for particles up to 20 μm in diameter (medium silts) and a good approximation for particles up to 50 μm in diameter.

Particles larger than 20 μm settle at over 20 m d^{-1} and will normally be deposited close to the mouth of the inflow stream. Colloidal size particle (< 0.4 μm) settle at less than 1 cm d^{-1} (at least 100 days to settle 1 m) and are essentially transported with aqueous phase. Fine (2 – 6 μm) and medium (6 – 20 μm) silts have settling velocities in the ranges 0.2 – 2 m d^{-1} and 2 – 20 m d^{-1} respectively (op. cit.). The extent to which these fractions settle out or are lost from the lake via the outflow depend on lake parameters such as the mean water depth and water residence time.

The mean settling time can be defined as the time taken for particles to settle a distance equal to the mean water depth of the lake. Denoting the mean water depth by d, the mean settling time for particles of diameter D with settling velocity v will be

$$T_S = \frac{d}{v}\,. \tag{5.13}$$

Writing s for the mean suspended sediment concentration, the mean sediment flux through the water column can be written $r = sv$. If A_L is the area of the lake and $Q_S = A_L sd$ the total mass of suspended sediments in the water column, the total rate at which sediments accumulate on the bed of the lake can then be written

$$A_L r = A_L sv = A_L sd / T_S = Q_S / T_S\,. \tag{5.14}$$

Writing $\mathcal{F}_S$ for the fraction of sediment entering the water column that settles out on the bed of the lake the suspended sediment concentration in lake water at the outflow

will be $(1-\mathcal{F}_S)s$. If q_O is the water discharge through the outflow, the rate of loss of sediment from the lake through the outflow is then

$$q_O(1-\mathcal{F}_S)s = V_L(1-\mathcal{F}_S)s/T_W = (1-\mathcal{F}_S)Q_S/T_W .$$

Total losses from the water column can thus be written

$$\frac{Q_S}{T_S} + \frac{(1-\mathcal{F}_S)Q_S}{T_W} = \frac{Q_S}{T_{SL}} , \tag{5.15}$$

where T_{SL} is a measure of the residence time of sediments in the water column, given by

$$\frac{1}{T_{SL}} = \frac{1}{T_S} + \frac{(1-\mathcal{F}_S)}{T_W} . \tag{5.16}$$

The fraction of sediments entering the lake that accumulate in the bottom sediments is therefore

$$\mathcal{F}_S = \frac{T_{SL}}{T_S} . \tag{5.17}$$

and the fraction lost via the outflow

$$1-\mathcal{F}_S = \frac{T_{SL}}{T_W} . \tag{5.18}$$

For given values of the water residence time and particle settling time equations (5.16) and (5.17) can be solved for the sediment residence time T_{SL} and settling fraction $\mathcal{F}_S$. This will vary from values close to 1 for coarse sediments and zero for colloidal size particles. Thus although evidently quite simplistic, this modelling does give some useful "ball-park" figures as to the fate of particulates entering the water column.

5.5 Transport of radionuclides through the water column

One of the key parameters controlling the fate of fallout radionuclides entering the water column of a lake is the fraction f_D attached to settling particulates. The soluble fraction or fraction attached to colloidal sized particles will exit the lake via the outflow with the same residence time as that of the lake waters. Although a proportion of the particulate fraction will exit the lake via the outflow, a significant part of this fraction will accumulate on the bed of the lake and become incorporated in

the sediment record. Writing Q_L for the total inventory of the radionuclide in the water column, and C_L for the mean concentration, the rate of loss via the outflow will be

$$\Psi_O = q_0 C_L = \frac{q_0 Q_L}{V} = \frac{Q_L}{T_W}, \tag{5.19}$$

where V is the volume of water in the lake and T_W is the water residence time (equation 5.10). Writing C_S for the mean concentration of the radionuclide of settling particulates it follows from equation (5.14) that the rate of loss to the bottom sediments will be

$$A_L \Phi_S = A_L r C_S = \frac{Q_S C_S}{T_S} = \frac{f_D Q_L}{T_S}, \tag{5.20}$$

where A_L (m^2) is the lake area, r (kg m^{-2} y^{-1}) the mean sedimentation rate, Q_S (kg) the total mass of suspended sediments and T_S (y) the mean particulate settling time. Substituting equations (5.19) and (5.20) into the mass balance equation (5.2) and dividing by the lake volume, the mean radionuclide concentration in the lake will satisfy the equation

$$\dot{C}_L = \frac{1}{d}\left(1+\alpha\mathcal{T}\right)\Phi - \left(\frac{1}{T_L}+\lambda\right)C_L, \tag{5.21}$$

where T_L is a measure of the mean residence time of the radionuclide in the water column of the lake, given by

$$\frac{1}{T_L} = \frac{f_D}{T_S} + \frac{1}{T_W}, \tag{5.22}$$

and from (5.3)

$$\mathcal{T}\Phi = \alpha \int_0^\infty \Phi(t-s)\,\mathrm{h}(s)\,\mathrm{e}^{-\lambda s}\,\mathrm{d}s\,. \tag{5.23}$$

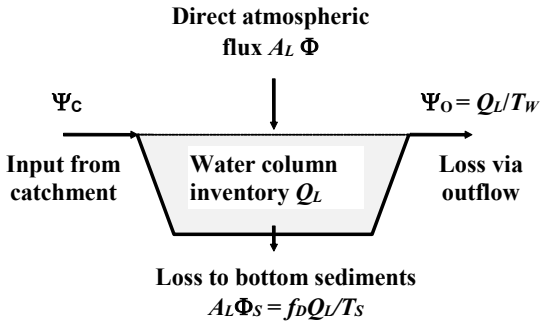

Figure 5.2: Representation of the water column model

.

It follows from equations (5.19) and (5.20) that the fraction of the radionuclide accumulating in the bottom sediments will be (Appleby et al. 2003)

$$\mathcal{F} = \frac{f_D / T_S}{f_D / T_S + 1/T_W} = \frac{f_D T_L}{T_S}. \tag{5.24}$$

Given that the residence time T_L will usually be measured at most in a few months, the radioactive decay constant for the fallout radionuclides ^{210}Pb and ^{137}Cs will be negligible compared to the reciprocal of T_L; equation (5.21) governing the radionuclide concentration in the water column can to a good approximation be simplified to

$$\dot{C}_L = \frac{1}{d}\left(1+\alpha\mathcal{T}\right)\Phi - \left(\frac{1}{T_L}+\lambda\right)C_L. \tag{5.25}$$

Application to ^{210}Pb

Assuming a constant (on annual timescales) atmospheric flux $\mathcal{P}$ the ^{210}Pb transfer function for may be written

$$\mathcal{T}\Phi = \eta_{Pb} P,$$

where from (5.8)

$$\eta_{Pb} = \int_0^\infty \mathrm{h}(s)\mathrm{e}^{-\lambda s}\mathrm{d}s \;= \int_0^\infty \frac{k}{\sqrt{s}}\mathrm{e}^{-\lambda(s+2k\sqrt{s})}\mathrm{d}s.$$

Since the mean concentration of ^{210}Pb in the water column can also be assumed constant (on annual timescales) it follows from equation (5.24) that the mean ^{210}Pb concentration is

$$C_{Pb} = \frac{T_L}{d}(1+\alpha\eta_{Pb})P. \tag{5.26}$$

Further, the mean flux of ^{210}Pb to the sediment record will be

$$P_S = \frac{f_D}{T_S}C_{Pb} = \mathcal{F}_{Pb}(1+\alpha\eta_{Pb})P, \tag{5.27}$$

where

$$\mathcal{F}_{Pb} = \frac{f_D T_L}{T_S} \tag{5.28}$$

is the ^{210}Pb water column to sediment record transfer fraction.

Application to ^{137}Cs

Fallout from the Chernobyl accident was delivered over a very short period of time and can be represented as a Dirac impulse function of strength I_{Ch}. Inputs to the lake will include an initial direct input $A_L I_{Ch}$ and continued inputs from the catchment

$$\Psi_C(t) = A_L \alpha I_{Ch}\, \mathrm{h}(t)\, \mathrm{e}^{-\lambda_{Cs} t} = A_L \alpha I_{Ch} \frac{k}{\sqrt{t}} \mathrm{e}^{-(\lambda_{Cs} t + 2k\sqrt{t})}.$$

Decay correcting all inputs to the fallout date, the cumulative inputs up to time t will be

$$A_L I_{Ch} \left(1 + \alpha \int_0^t \frac{k}{\sqrt{s}} \mathrm{e}^{-\lambda_{Cs} 2k\sqrt{s}}\, \mathrm{d}s \right).$$

Noting that

$$\frac{\mathrm{d}}{\mathrm{d}t} \mathrm{e}^{-2k\sqrt{t}} = -\frac{k}{\sqrt{t}} \mathrm{e}^{-2k\sqrt{t}}$$

it follows that cumulative inputs at time t are

$$A_L I_{Ch} \left\{ 1 + \alpha \left(1 - \mathrm{e}^{-2k\lambda_{Cs}\sqrt{t}} \right) \right\}.$$

Cumulative decay corrected inputs per unit area to the sediment record will thus be

$$I_S(t) = \mathcal{F}_{Cs} I_{Ch} \left\{ 1 + \alpha \left(1 - \mathrm{e}^{-2k\lambda_{Cs}\sqrt{t}} \right) \right\} \tag{5.29}$$

Letting f_D be the fraction of ^{137}Cs in the water column attached to settling particulates and T_L the ^{137}Cs residence time,

$$\mathcal{F}_{Cs} = \frac{f_D T_L}{T_S} \tag{5.30}$$

is the ^{137}Cs water column to sediment record transfer fraction.

Chapter 6. Atmospheric deposition of ^{210}Pb and ^{137}Cs at Brotherswater

6.1 The study site

Brotherswater is a small (0.18 km^2), upland (altitude 158 m) lake in the Hartsop valley, in Cumbria, N.W.England, about 13 kilometres north of Windermere (Figure 6.1). It has a large catchment (13 km^2) and large catchment-to-lake area ratio (72). Catchment measurements were carried out using the relevant Hydrology toolset from the ArcGIS software package, while the topographic data used as input were supplied by Ordnance Survey, which are licensed for academic use.

The catchment drains northwards by way of a several small becks that merge to form a single input stream (Kirkstone beck) near the south-western corner of Brotherswater. The outlet stream, Goldrill Beck, is located at the north-western corner of the lake and drains northwards into Ullswater. The bathymetry of the lake (Figure 6.2) is dominated by a central flat profundal zone with a maximum depth of 17 m. The basic physiographic parameters of the catchment and its lake are summarised in Table 6.1.

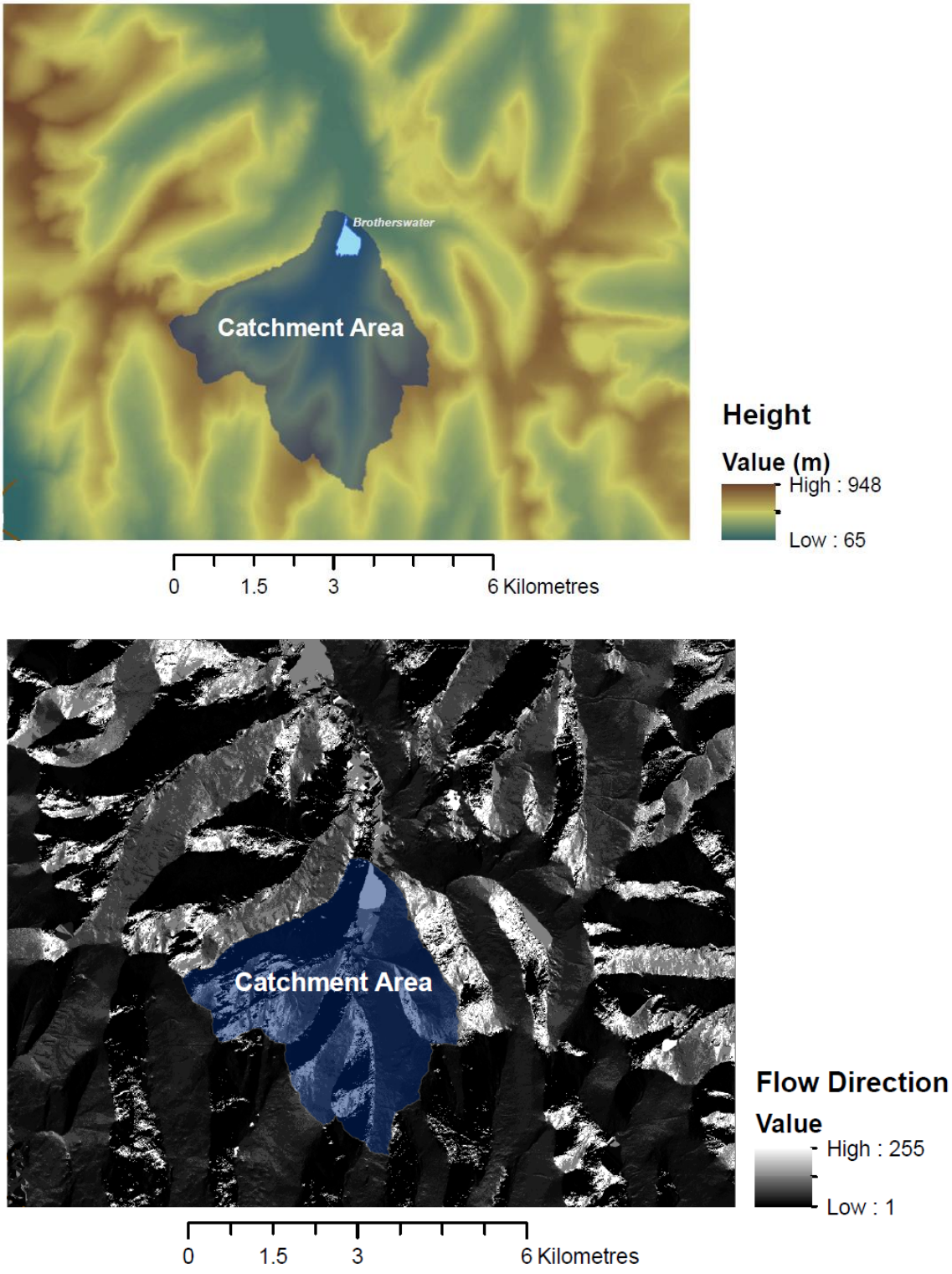

Figure 6.1: Top: Catchment area of Brotherswater, superimposed over the local topography. The catchment area, approximated to be 13.054 km, has been derived based on the flow direction (bottom) and flow accumulation in the water basin as specified by the Brotherswater outlet point (pour point). Calculations were carried out using the ArcGIS software.

Table 6.1: Brotherswater Catchment-Lake parameters (source: Ordnance Survey).

Catchment area:	13 km^2
Location:	54.5°N, 2.9°W
Altitude range:	158-800 m
Rainfall:	2594 mm
Lake area	1.8×10^5 m^2
Lake volume:	1.33×10^6 m^3
Maximum depth:	17 m
Mean depth:	7.4 m
Catchment Area to Lake ratio	72.3

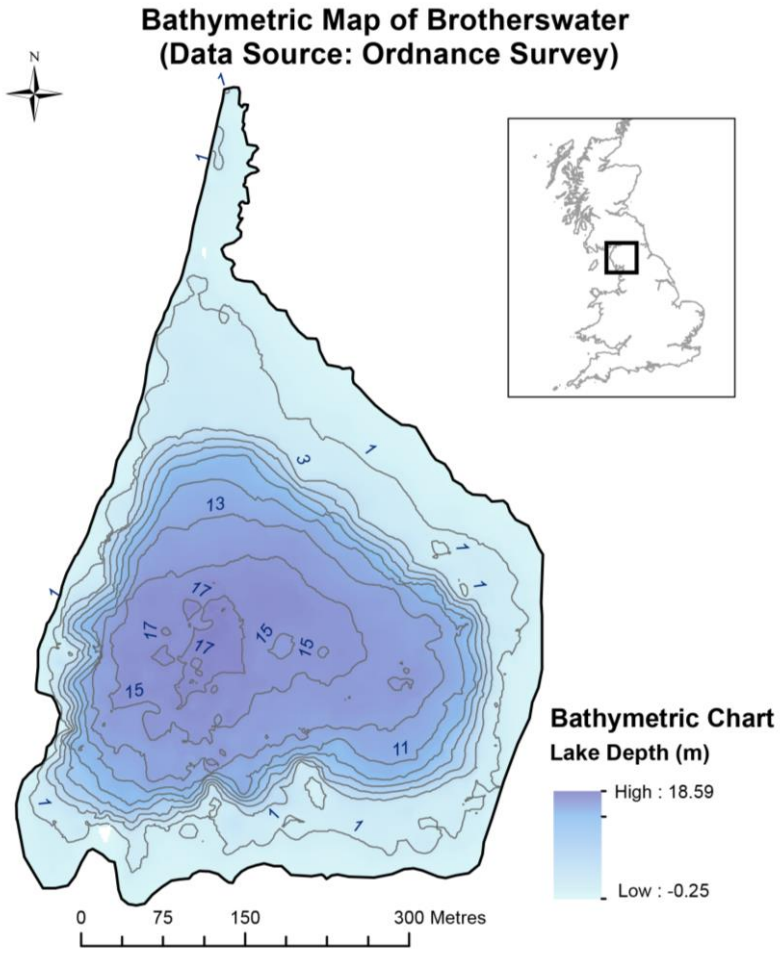

Figure 6.2: Bathymetric map of Brotherswater.

6.2 Historical studies

The earliest reported study of fallout radionuclides in Brotherswater was carried out in the early 1970s by Winifred Pennington (Freshwater Biological Association, Ambleside, Cumbria). In this study two cores were collected from

Brotherswater and analysed for weapons fallout ^{137}Cs by Roger Cambray at AERE Harwell. The first, Core BW1, was collected in 1974 from a site close to the present inflow. The second, Core BRW, was collected in 1975 from site on the western side of the lake. The results from BW1 were published in Pennington (1981).

A more detailed investigation into the transfer of fallout radionuclides in Brotherswater and its catchment was carried out by John Eakins and Roger Cambray (AERE Harwell) in 1976/7. Sediment cores collected from five locations in the lake were analysed at Harwell for ^{210}Pb, ^{226}Ra (John Eakins) and ^{137}Cs (Roger Cambray). Atmospheric deposition was measured directly via rainwater samples collected monthly from a site near the lake and indirectly via soil cores collected from five different locations in the catchment. Lake water samples collected on five occasions during the study period and stream water samples collected on three occasions were analysed for ^{210}Pb, ^{210}Po and ^{137}Cs. The results of this study were published in Eakins et al. (1981) and Eakins et al. (1984). The authors concluded that over 90% of total inputs of ^{210}Pb to the lake were transported to the lake from the catchment with less than 10% coming from direct atmospheric fallout. They also concluded that only 14% of the total inputs were retained in the sediments; the remaining 86% leaving via the outflow. Their calculations further suggested that around 80% of sediments entering the lake from the catchment are lost via the outflow. These results are however open to argument. Although 90% of sediments entering the lake do so during brief rising flood conditions, measurements of ^{210}Pb on these sediments were only made during normal flow conditions. Since increased suspended sediment loads during floods may well derive largely from accelerated bank erosion of old sediments with lower ^{210}Pb concentrations, their results may significantly overestimate catchment inputs.

A further investigation was carried out in 1988/9 under a DOE contract PECD 7/9/385, the focus of which was a study of fallout from the 1986 Chernobyl accident. A total of six lake sediment cores were collected from sites similar to those sampled in the 1976/7 study and analysed in the Liverpool University ERL for ^{210}Pb, ^{226}Ra, ^{137}Cs, ^{134}Cs and ^{241}Am. Soil cores collected from six different locations were used to quantify atmospheric fallout. The results have been published by Bonnett et al. (1992) in a DOE report DOE/RAS/92.004, and by Hilton et al. (1992) in a DOE report DOE/RW/92.005. A further suite of six soil cores were collected in November 1991

from a flat site adjacent to the lake (Smith et al. 1997) as part of a study of ^{210}Pb and ^{137}Cs fallout in Cumbria.

6.3 Rainfall data for Brotherswater

Since the principle mechanism for removing ^{210}Pb from the atmosphere is wet deposition, the amount of fallout in any given locality is strongly related to mean annual rainfall. Table 6.2 gives estimates of rainfall at Brotherswater from direct measurement at a number of sites close to the lake for the period 1974-2010. A weighted average of all the data is 2,609 mm y^{-1}.

Table 6.2: Rainfall data for sites adjacent to Brotherswater Lake.

Site	Altitude (m)	Rain (mm y^{-1})	Date	Source
Grisedale Bridge	146	2614	1974-2010	Schillereff (pers. comm.)
Brotherswater Inn	183	2442	1976-1980	NW Water
Hartsop Hall	200	2640	1981-1988	NW Water
Hartsop Hall	200	2108	1976/7	AEA
Hartsop Village	200	2942	1990	AEA
Weighted mean		2609		

Precipitation at upland areas of the catchment is likely to be significantly higher than at low lying sites close to the lake. One method for determining mean precipitation over the catchment as a whole is from the volume V of rain deposited annually on the catchment. Writing A_C for the area of the catchment the mean annual rainfall will be

$$R = V / A_C . \tag{6.1}$$

Neglecting losses by evapotranspiration a first approximation to V can be made from measurements of the mean annual flow of water into the lake via inflow streams. Measurements of weekly discharge through the main Brotherswater inflow made by Chambers (1978) over a two-year period from 25th September 1975 through to 25th September 1977 suggested a mean inflow rate during that time of 24.8×10^6 m^3 y^{-1}. Flood events not recorded by the routine monitoring were estimated to contribute an additional 19×10^6 m^3 y^{-1}. Since discharge measurements through the outflow carried out over the same period suggest that ground water flow may contribute a further 3.1×10^6 m^3 y^{-1}, total inputs could amount to as much as 46.9×10^6 m^3 y^{-1}. Given that the

catchment area is 13×10^6 m^2, these results suggest a mean annual rainfall over the catchment of 3,605 mm y^{-1}, 40% higher than at the lake. Although higher rainfall on the fells is to be expected, a significant cause of the discrepancy may be uncertainties in the discharge measurements, particularly during flood events. In the absence of better information, we take the average and assume a mean annual rainfall over the catchment as a whole of 3,108 mm y^{-1}.

6.4 Direct fallout measurements

Direct measurements of fallout of ^{210}Pb and ^{137}Cs Brotherwater were carried out by Eakins et al. (1981, 1984) during a 12-month period from November 1976 to October 1977. Monthly rainwater samples collected from Hartsop Hall (~1 km from the lake) were analysed for ^{210}Pb and ^{137}Cs. The total amount of ^{210}Pb fallout during that period was 148 Bq m^{-2}. Total rainfall was 2,108 mm, significantly lower than the long-term average of 2,609 mm y^{-1} for sites adjacent to the lake.

Figure 6.3 compares ^{210}Pb deposition at Brotherswater with corresponding data from Esthwaite Water, 10 miles to the south west (Appleby et al. 2003). At both sites the relationship between monthly ^{210}Pb deposition and monthly rainfall is broadly linear. Further, values from Brotherwater are broadly similar to those from Esthwaite Water. Assuming the mean annual fallout to be proportional to the mean annual rainfall, correcting the Eakins et al. result for the rainfall deficiency during their study period the mean long term atmospheric ^{210}Pb flux is calculated to be 183 Bq m^{-2} y^{-1}. Fitting a regression line to the Brotherswater data shows that the relationship between monthly fallout and monthly rainfall is not quite proportional but more accurately represented by the linear equation

$$^{210}\text{Pb flux} = 0.059 \times \text{rainfall (mm y}^{-1}) + 24.0 \text{ (Bq m}^{-2}\text{ y}^{-1}). \quad (6.2)$$

Fitting a regression line to all the data yields the relationship

$$^{210}\text{Pb flux} = 0.053 \times \text{rainfall (mm y}^{-1}) + 49.8 \text{ (Bq m}^{-2}\text{ y}^{-1}). \quad (6.3)$$

Calculated values of the mean annual ^{210}Pb flux at Brotherswater using these two relationships range from 177-188 Bq m^{-2} y^{-1}. The mean value by all three methods of 183 ± 5 Bq m^{-2} y^{-1} represents a best estimate of the atmospheric ^{210}Pb flux at Brotherswater via direct fallout measurements.

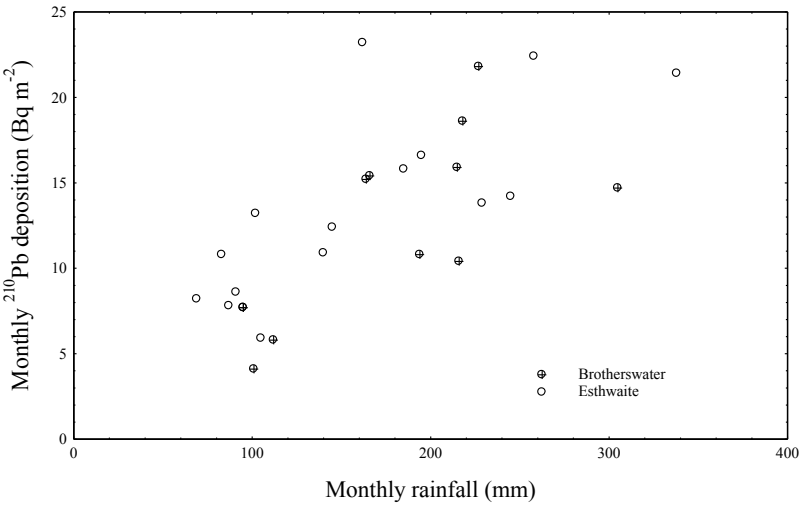

Figure 6.3: Monthly ^{210}Pb deposition over rainfall.

6.5 Fallout measurements using soil cores

Measurements of the cumulative long-term fallout can be made using soil cores collected from sites within the catchment selected according to the criteria:

- there should have been no major soil disturbance for at least 30 years.
- soil types should be of a type that inhibits radionuclide migration through the soil column,
- they should be on open level ground not subject to erosion or flooding by surface waters,
- the soils should be relatively compact and saturated (to minimise in situ ^{222}Rn escape),
- the soil depth should be sufficient to contain the entire fallout inventory.

The mean ^{210}Pb supply rate to such a core is calculated using the equation

$$P = \lambda A_0 ,$$

where A_o is the unsupported ^{210}Pb inventory of the core and λ the ^{210}Pb radioactive decay constant. Although individual cores may not be perfect collectors, the average value from a number of such cores should be a good measure of the mean long-term atmospheric flux. The ^{137}Cs inventory in pre-1986 cores can be used to reconstruct the flux of weapons fallout ^{137}Cs using historical records of weapons test fallout such as those given in Cambray et al. (1989). Post-1986 cores will also contain fallout ^{137}Cs from the 1986 Chernobyl accident.

In the 1976/7 study soil cores were collected on three separate occasions from four different locations within the Brotherswater catchment:

- Brotherswater Delta A and B,
- Hartsop Hall Farm,
- Junction of Kirkstone and Caiston Becks,
- Upper Kirkstone Beck (~1 mile north of Kirkstone Inn).

The first sampling took place during July 1976 when single cores were collected from each site apart from Hartsop Hall. A second sampling was carried out in September 1976 when four cores were collected from each site and corresponding sections amalgamated to form a single composite core for each site. These cores were all analysed for ^{137}Cs at AERE Harwell. A third sampling took place in May 1977 when pairs of cores were collected from the Upper Kirkstone and Delta sites. These cores were also analysed for ^{210}Pb and ^{226}Ra. The ^{137}Cs results are recorded in detail in Roger Cambray's logbook and, together with the ^{210}Pb results, published in Eakins et al. (1981) and Eakins et al. (1984).

In the 1989 study (Bonnett et al. 1992) pairs of cores were collected from each of the above locations plus one near Caudalebeck Farm. Duplicates were collected from the Delta, Hartsop Hall and Kirkstone/Caiston Beck sites. Corresponding sections from each pair were amalgamated and all nine composite cores analysed for ^{137}Cs and ^{134}Cs at AERE Harwell. In the 1991 study (Smith et al. 1997), six cores were taken on a 10 m ×10 m grid within a large flat field at the head of the lake. These cores were sectioned at 2 cm intervals and dried sub-samples analysed for fallout ^{210}Pb and ^{137}Cs by gamma spectrometry in the Liverpool University Environmental Radiometric Laboratory.

Present study

Four soil cores were collected in 2015 from two locations in the Brotherswater catchment, the first from a moraine site near Caudalebeck Farm and the second from a field near the head of the lake, as shown in Figure 6.4. At each site, two cores were extracted using a 6.35 cm diameter corer. Each core was sectioned at 5 cm intervals and dried sub-samples analysed for fallout radionuclides by gamma spectrometry in the Liverpool University Environmental Radiometric Laboratory. Three further cores

were extracted from each of these two sites in August 2016 and analysed in a similar way.

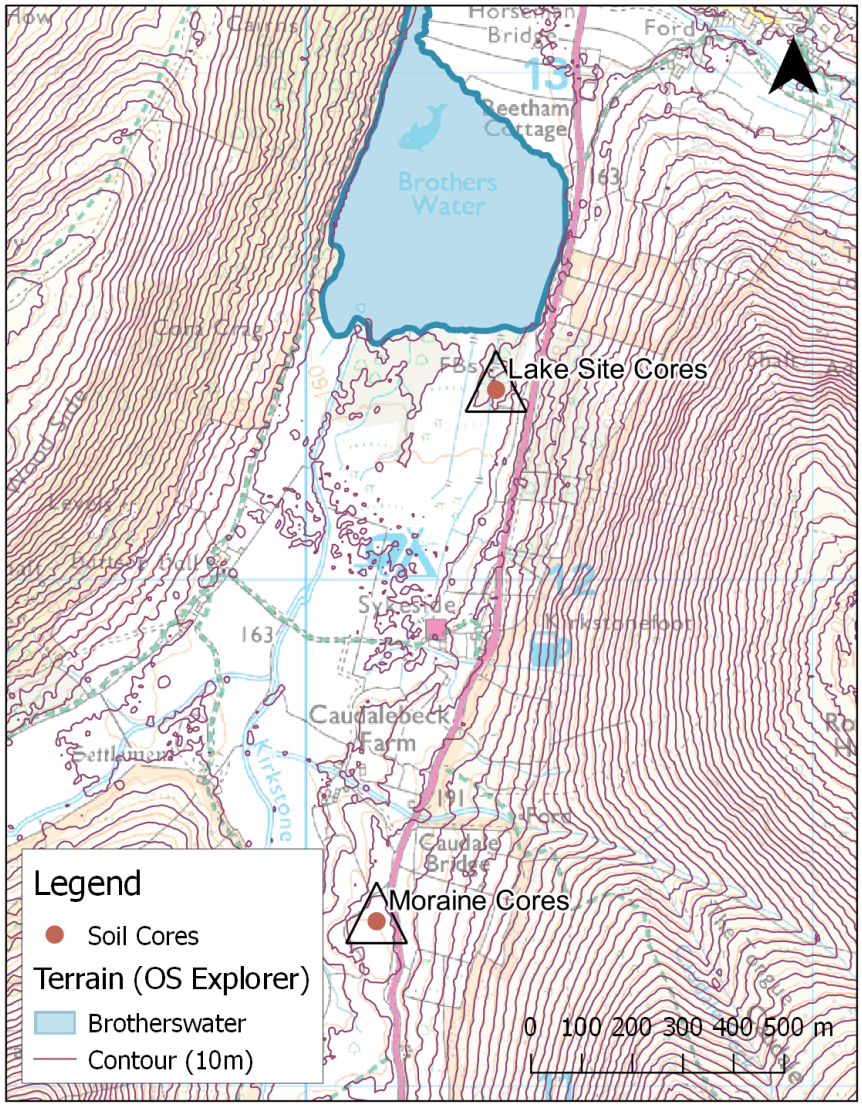

Figure 6.4: Map with the locations of soil cores (present study).

6.6 Results

^{210}Pb inventories and fluxes

Table 6.3 summarises the results of measurements of ^{210}Pb inventories and fluxes from soil cores in each of the above studies. Those from the 1976/77 study have been taken directly from Eakins et al. (1981,1984). Results from the 1991 study are slightly different to those published in Smith et al. (1997), following a revision of the original data.

Table 6.3: ^{210}Pb Inventory and Flux.

(a) 1976/77 study

Location	^{210}Pb Inventory Bq m^{-2}	^{210}Pb Flux Bq m^{-2}y^{-1}
Brotherswater Delta	5291	165
Upper Kirkstone	5117	159
	5204	162

(b) 1991 Study

Core	^{210}Pb Inventory Bq m^{-2}	^{210}Pb Flux Bq m^{-2} y^{-1}
BRS1	5512	172
BRS2	5632	175
BRS3	5304	165
BRS4	8354	260
BRS5	4105	128
BRS6	3753	117
Mean	5430	169

(c) 2015/16 Study

Location	Core	^{210}Pb Inventory Bq m^{-2}	±	^{210}Pb Flux Bq m^{-2} y^{-1}	±
Caudalebeck Farm	BWSC15/1	8309	219	258	7
	BWSC15/2	7116	165	226	5
	BWSC16/1	5108	132	159	4
	BWSC16/2	6376	143	199	4
	BWSC16/3	5089	80	158	3
	Mean	6399		200	
Lake side	BWSC15/3	6788	137	207	4
	BWSC15/4	5589	131	171	4
	BWSC16/4	6733	112	210	3
	BWSC16/5	6323	99	197	3
	BWSC16/6	7289	94	227	3
	Mean	6544		202	

The mean value of the ^{210}Pb flux from the results of all three studies of 185 Bq m^{-2} y^{1} is very similar to the mean value of 182 Bq m^{-2} y^{-1} determined from the precipitation

data. Combining the two approaches, a best estimate of the ^{210}Pb flux at Brotherswater is 183 Bq m^{-2} y^{-1}.

^{137}Cs inventories

Results of the ^{137}Cs measurements are summarised in Table 6.4. They include both raw inventories (where available) and values decay corrected to 1986. The raw inventories from the 1976/77 study are essentially those published in Eakins et al. (1981,1984) though for the two Delta sites only the mean value has been given. The decay corrected inventories include a small adjustment for the fact that weapons test fallout at the time of 1976/77 study results was incomplete. Weapons test fallout data (Cambray et al. 1989) suggest that post-1977 fallout would have contributed a further 3.25% to the total inventory.

Pre-1986 soil cores contained ^{137}Cs that derived solely from weapons fallout. This essentially ended in 1986. Results from the 1976/7 cores indicated that total fallout from this source at Brotherswater decay corrected to 1986 amounted to 7,886 Bq m^{-2}. This is in good agreement with the estimated value determined from the results of a detailed survey of weapons fallout in the UK published by Cawse (1983). Using an OLS fit to the data presented in that survey, the cumulative weapons fallout inventory at any site (decay corrected to 1986) can be estimated using the relation

$$I_{Cs} = 2.49R + 825 \qquad (6.4)$$

where R is the mean annual rainfall in mm y^{-1}. From this formula, the Brotherswater weapons ^{137}Cs fallout inventory (mean annual rainfall 2609 mm y^{-1}) is calculated to be 7,332 Bq m^{-2}. The average value by these two methods, 7,609 Bq m^{-2}, represents a best estimate of the cumulative fallout of nuclear weapons test fallout at Brotherswater, decay corrected to 1986. The historical record (decay corrected to 1986) can be reconstructed by an appropriate scaling of the history of weapons test fallout in the northern hemisphere given e.g. in Cambray et al. (1989). The results, shown in Figure 6.4, indicate that by the time of the 1976/7 study fallout had declined to around 50 Bq m^{-2}. This is consistent with the empirical value of 61 Bq m^{-2} obtained by Eakins & Cambray.

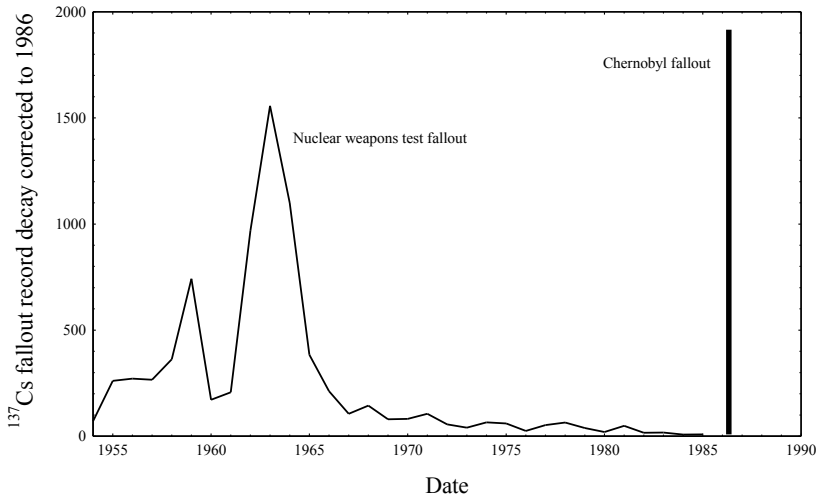

Figure 6.5: ^{137}Cs fallout record at Brotherswater versus time decay corrected to 1986.

The much higher ^{137}Cs inventories in the post-1986 soil cores other than those from the 1989 study are attributable to fallout from the Chernobyl accident in April/May 1986. The contribution from this source, also shown in Figure 6.4, is not to scale. Results from the 1989 study were clearly flawed in that they yielded ^{137}Cs inventories significantly lower than those determined from the 1976/7 study. The results from the present study are in good agreement with those from the 1991 study. Excluding the values from cores BWSC16/1 and BWSC16/2 where the records were evidently not complete, the mean value from both these studies is 11,611 Bq m^{-2}. Subtracting the 1986 weapons fallout inventory, fallout of ^{137}Cs at Brotherswater due to Chernobyl is calculated to be 4,020 Bq m^{-2}. This is consistent with the estimate made by Smith and Clarke (1989) that levels of Chernobyl ^{137}Cs deposition in the Brotherswater catchment were between 2000-5000 Bq m^{-2}.

Table 6.4: ^{137}Cs soil core inventories.

(a) 1976/77 Study

Location	^{137}Cs Inventory	
	Raw	Decay corrected to 1986
	Bq m^{-2}	Bq m^{-2}
Lake Delta	8801	7842
Hartsop Hall	8813	7852
Caiston Beck	9624	8574
Kirkstone Pass	8168	7277
Mean	8851	7886

(b) 1989 study

Location	^{137}Cs Inventory			^{134}Cs Inventory
	Decay corrected to 1986			
	Total	Weapons	Chernobyl	Chernobyl
	Bq m^{-2}	Bq m^{-2}	Bq m^{-2}	Bq m^{-2}
Lake Delta	5505	4026	1479	888
Hartsop Hall	3330	2905	425	255
Caudalebeck Farm	5060	3527	1533	920
Caiston Beck	4320	3324	996	598
Kirkstone Pass	5420	4137	1283	770
Middle Dodd	13340	10585	2755	1653
Mean	6163	4751	1412	847

(c) 1991 Study

Lakeside	^{137}Cs Inventory			
	Raw		Decay corrected to 1986	
	Bq m^{-2}	±	Bq m^{-2}	±
BRS1	8747	191	9926	216
BRS2	10380	539	11780	612
BRS3	10902	1020	12371	1157
BRS4	11326	451	12853	512
BRS5	9818	317	11141	359
BRS6	10673	367	12111	416
Mean	10308		11697	

(d) 2015/16 Study

Location	Core	^{137}Cs Inventory Raw Bq m^{-2}	±	Decay corrected to 1986 Bq m^{-2}	±
Caudalebeck Farm	BWSC15/1	7470	89	14637	174
	BWSC15/2	6194	74	12137	145
	BWSC16/1	1222*	69	2453*	139
	BWSC16/2	2351*	399	4720*	801
	BWSC16/3	4312	1134	8654	2276
	Mean	5992		11809	
Lake edge	BWSC15/3	5431		10642	150
	BWSC15/4	3780		7407	102
	BWSC16/4	7251		14554	176
	BWSC16/5	5609		11259	150
	BWSC16/6	6443		12933	148
	Mean	5703		11359	

* The records in these cores were evidently not complete and have been excluded from the mean.

Chapter 7. Fluxes of ^{210}Pb and ^{137}Cs through the water column of Brotherswater

7.1 Introduction

Sediment trap samples collected during an earlier investigation (Schillereff et al., 2016) were analysed for ^{210}Pb and ^{137}Cs in order to measure the concentrations and fluxes of fallout radionuclides through the water column of Brotherswater. The sediment traps consisted of pairs of 11 cm diameter cylindrical PVC tubes with a 1:8 (width:depth) aspect ratio and removable basal sampling cups (Bloesch and Bums 1980). They were deployed at two different locations in the lake (Figure 7.1):

- site A near the delta (75 m from the inflow) in ~12 m water depth,
- site B near the central area of the lake in ~17 m water depth,

at three different levels, 25%, 75% and 100% of water depth. Samples were collected at near-monthly intervals.

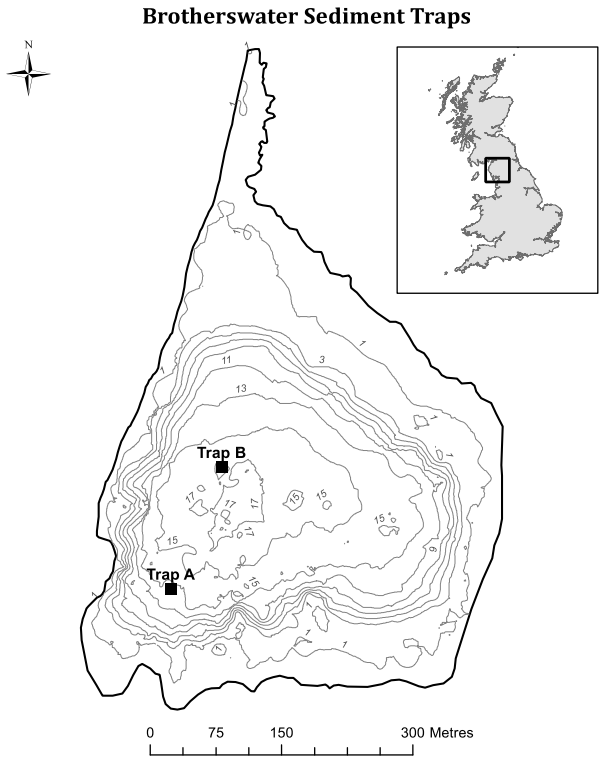

Figure 7.1: Map of Brotherswater showing the locations of the sediment traps.

7.2 Sediment fluxes

Table 7.1 shows the amounts of dry sediment collected in each sampling tube during each sampling period (Schillereff, Pers. Comm.). At Trap A, for each pair of tubes the amounts collected in each tube are reasonably comparable. Comparing the amounts collected at the different levels (although there are some differences for particular collection periods) the total amounts collected at the upper and mid-levels levels appear to be very similar. Amounts collected at the lower level were however significantly higher.

Table 7.1: Dry masses of sediment collected in each sampling tube.

(a) Trap A

Collection period		Dry Mass (g)					
Start	Finish	Top (1)	Top (2)	Mid (1)	Mid (2)	Base (1)	Base (2)
15-Aug-12	10-Oct-12	2.4435	2.4051	1.8647	2.1373	3.4616	4.0241
10-Oct-12	09-Jan-13	2.9652	3.0650	2.0751	2.7748	2.7798	2.4414
09-Jan-13	15-Feb-13	Lost	Lost	1.6303	1.3382	3.1928	1.2794†
15-Feb-13	24-Apr-13	Lost	Lost	1.0403	Lost	3.3043	5.1612
24-Apr-13	06-Jun-13	0.3857	0.4697	Lost	Lost	2.9714	2.8738
06-Jun-13	10-Jul-13	0.1528	0.1159	0.2660*	0.2737*	1.5727	1.1744
10-Jul-13	10-Aug-13	1.6301	1.5281	2.1165	1.9953	2.4994	2.7051
10-Aug-13	10-Dec-13	1.6842	1.7370	1.6146	2.2170	2.6613	Lost

† Beaker contained a fish.
* Include an additional 0.1674 g shared between the two mid-level collectors.

(b) Trap B

Collection period		Dry Mass (g)					
Start	Finish	Top (1)	Top (2)	Mid (1)	Mid (2)	Base (1)	Base (2)
15-Aug-12	10-Oct-12	0.3728	1.0208	1.1950	Lost	5.5437‡	3.4428
10-Oct-12	09-Jan-13	Lost					
09-Jan-13	15-Feb-13	0.5266	0.5652	0.6843	0.5560	1.0728	1.0583
15-Feb-13	24-Apr-13	0.7412	0.7732	0.7692	0.9211	1.2996	1.1858
24-Apr-13	06-Jun-13	0.4062	0.3395	0.3086	0.4296	3.0485	22.7565
06-Jun-13	10-Jul-13	0.1549	0.1541	0.2660	0.1634	1.4525	13.3288
10-Jul-13	10-Aug-13	1.0863	1.2151	0.7464	0.7996	Lost	Lost
10-Aug-13	10-Dec-13	1.5699	1.3577	1.7663	1.9023	2.4597	6.7546

‡ Includes an additional 0.3102 g placed in a separate bag.

At Trap B, for each pair of upper-level and mid-level tubes the amounts collected in each tube are again reasonably comparable, apart from the first collection period (Aug-Oct 2012) where there appears to be a significant deficiency in the amount

recorded by the Top (1) tube. Excluding this sample, the total amounts collected in the upper and mid-level tubes are also very similar, though significantly lower than at Trap A. The amounts collected in the base-level tubes were again significantly higher than in the upper two levels. There were also significant differences between the tubes, particularly for the second half of year when the amounts collected in the Base (2) tube were up to an order of magnitude greater than in the Base (1) tube.

Table 7.2 shows the mean sediment fluxes at the top, middle and bottom levels of the sediment traps for each collection period, the average values for the top and middle traps, and the mean sediment fluxes for the entire collection period.

Table 7.2: Water column sediment fluxes.

(a) Trap A

Collection period		Sediment fluxes (g cm^{-2} y^{-1})			
Start	Finish	Top	Middle	Top+Middle	Base
15-Aug-12	10-Oct-12	0.166	0.137	0.152	0.257
10-Oct-12	09-Jan-13	0.127	0.102	0.115	0.110
09-Jan-13	15-Feb-13	Lost	0.154	0.154	0.332†
15-Feb-13	24-Apr-13	Lost	0.059	0.059	0.239
24-Apr-13	06-Jun-13	0.038	Lost	0.038	0.261
06-Jun-13	10-Jul-13	0.015	0.030	0.023	0.155
10-Jul-13	10-Aug-13	0.196	0.255	0.225	0.323
10-Aug-13	10-Dec-13	0.054	0.060	0.057	0.084
	Mean			0.093	0.186

† Excludes data from beaker with fish

(b) Trap B

Collection period		Sediment fluxes (g cm^{-2} y^{-1})			
Start	Finish	Top	Middle	Top+Middle	Base
15-Aug-12	10-Oct-12	0.070*	0.082	0.076	0.308
09-Jan-13	15-Feb-13	0.057	0.064	0.061	0.111
15-Feb-13	24-Apr-13	0.043	0.048	0.045	0.070
24-Apr-13	06-Jun-13	0.033	0.033	0.033	0.272‡
06-Jun-13	10-Jul-13	0.017	0.024	0.021	0.164‡
10-Jul-13	10-Aug-13	0.143	0.096	0.119	Lost
10-Aug-13	10-Dec-13	0.046	0.058	0.052	0.077‡
	Mean			0.056	0.147

* Excludes anomalous data from Top (1) tube
‡ Exclude anomalous data from Base (2) tubes

Figure 7.2 plots mean sediment fluxes from the top and middle levels for each collection period against the mean collection date. The vertical dashed lines show the end of each collection period. Sediment fluxes through the upper and middle levels of Trap A have a mean annual value of 0.093 g cm^{-2} y^{-1}. The significantly lower value at Trap B (0.056 g cm^{-2} y^{-1}) presumably reflects its greater distance from the mouth of the inflow stream. Figure 7.2 also shows the 4-day average discharge data from the Patterdale gauging station, approximately 3 km downstream from Brotherswater. Although discharge through this station includes additional inputs from the Deepdale catchment, flood events are almost certainly common to both catchments. High sediment fluxes at Trap A during the collection periods from 15th August 2012 through to 15th February 2013 and 10th July to 10th August presumably record the impact of major flood events during each of those periods. The reduced impacts at Trap B are due to much of the relatively coarse material transport by these events settling out before reaching the centre of the lake. Much lower sediment fluxes were recorded during the low flow conditions spanning the collection periods from 24th April through to 10th July. The small difference between trap sites during this period can be attributed to the fact that catchment inputs during low flow conditions will consist of much finer material. Slower settling velocities will allow these sediments to be delivered much deeper into the lake.

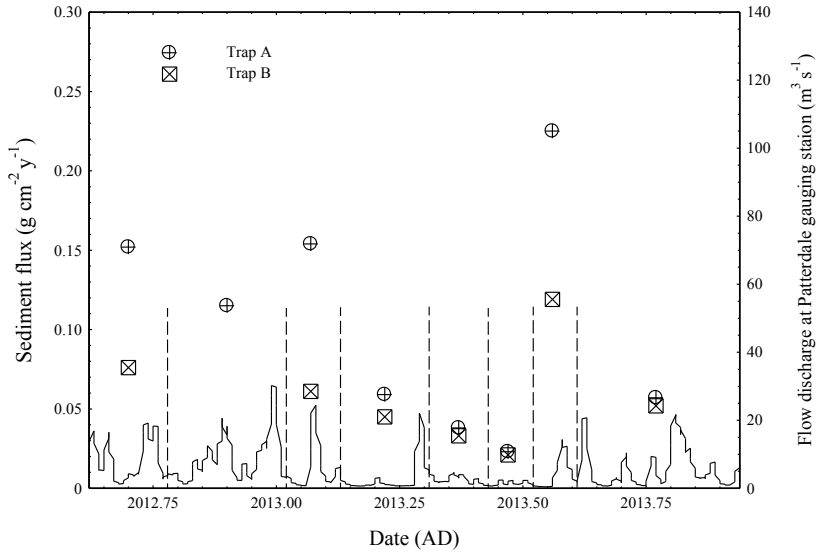

Figure 7.2: Sediment fluxes through the water column of Brotherswater determined from the upper and middle level sediment traps at site A (near the inflow stream) and site B (near the centre of the lake). The dashed vertical lines show the dates of the ends of the collection periods. Also shown is the discharge data through the Patterdale gauging station.

At both sites there was a much higher rate of accumulation of sediment in the bottom level traps. Since these were placed very close to the bed of the lake, and the difference (compared to the top and mid-level traps) was greater at site B, the most likely cause would appear to be sediment focussing.

7.3 ^{210}Pb and ^{137}Cs activities

Table 7.3 shows ^{210}Pb, ^{226}Ra and ^{137}Cs activities in samples collected from (a) Trap A and (b) Trap B at each of the three levels. The radiometric analyses were carried out by direct gamma assay in the Liverpool University Environmental Radioactivity Laboratory. Figure 7.3 plots values of (a) unsupported ^{210}Pb concentrations and (b) ^{137}Cs concentrations in the top and mid-level traps against the corresponding sediment fluxes through the water column. The results indicate a strong inverse relationship between ^{210}Pb concentrations and the sediment flux with high ^{210}Pb concentrations at times of low sediment flux and low concentrations at times of high sediment flux. Samples from Trap B follow the same relationship as those from Trap A. Excluding a small number of outliers, one associated with an anomalously small sample and two others with large uncertainties in the ^{210}Pb measurements, using a least squares fit procedure the ^{210}Pb concentration C_{Pb} (Bq kg^{-1}) and sediment flux r (g cm^{-2} y^{-1}) to a good approximation satisfy the power law relationship

$$C_{Pb} = 102 r^{-0.525}.$$

Since low sediment fluxes are associated with low flow regimes, these results suggest that fallout ^{210}Pb is strongly associated with fine particulates. High flow rates transport relatively more coarse material that effectively dilutes the ^{210}Pb. This inference is supported by the fact that the mean ^{210}Pb concentration in top and mid-level samples from Trap B (506 Bq kg^{-1}) is significantly higher than the mean concentration in samples from Trap A (355 Bq kg^{-1}).

In contrast, ^{137}Cs concentrations are much lower and have only a weak inverse relationship with the sedimentation rate. This suggests that since there has been no significant ^{137}Cs fallout for more than 30 years, the remaining catchment inventory is attached to a wider range of particle sizes. The mean values are 48 Bq kg^{-1} at Trap A and 60 Bq kg^{-1} at Trap B.

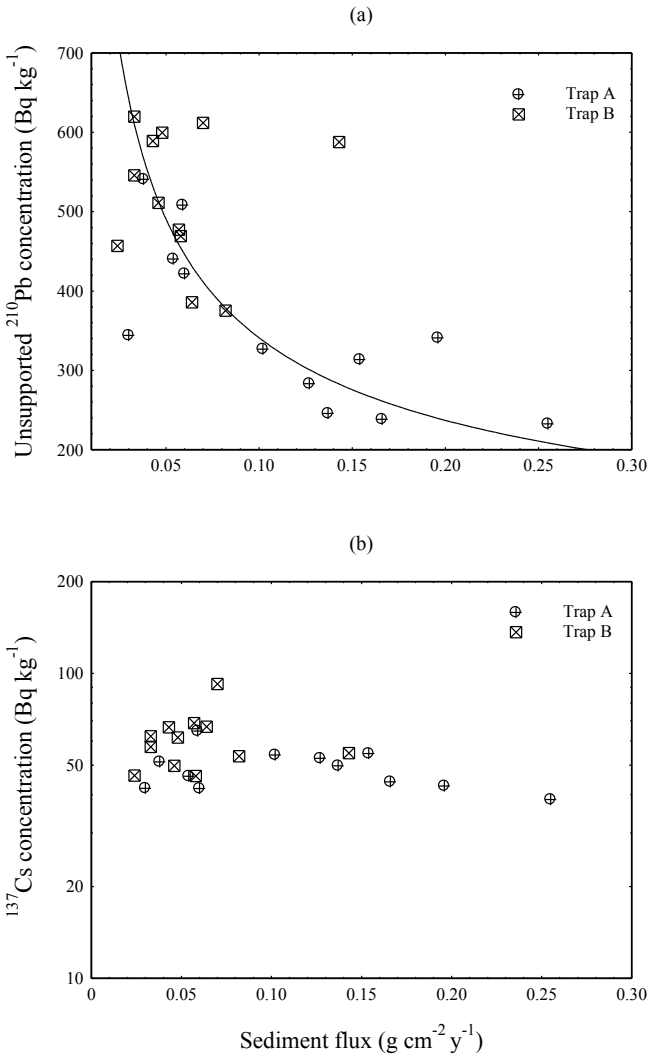

Figure 7.3: (a) ^{210}Pb and (b) ^{137}Cs concentrations in Brotherswater sediment trap samples versus sediment flux through the water column.

7.4 ^{210}Pb and ^{137}Cs fluxes

Fluxes of fallout ^{210}Pb and ^{137}Cs through the water column (Bq m^{-2} y^{-1}) were calculated by multiplying the radionuclide concentrations (Bq kg^{-1}) by the sediment fluxes (kg m^{-2} y^{-1}). The results for (a) Trap A and (b) Trap B are shown in Tables 7.4 and 7.5. Fluxes at the top and mid-level collectors are reasonably comparable, apart from Trap B during July and August 2013 when there is a threefold difference in the ^{210}Pb values. The role of catchment inputs is evidenced by the fact that mean annual fluxes of both ^{210}Pb and ^{137}Cs are significantly higher at Trap A (nearer to the inlet stream) than at the more distant Trap B. Since there has been no significant ^{137}Cs fallout since 1986, catchment inputs can be the only source for this radionuclide. The mean annual ^{210}Pb fluxes (336 Bq m^{-2} y^{-1} at Trap A, 278 Bq m^{-2} y^{-1} at Trap B) suggest that catchment inputs of ^{210}Pb in this part of the lake are comparable to the

atmospheric flux (183 Bq m^{-2} y^{-1}). The apparently higher fluxes recorded in the base-level collectors are entirely due to the higher rates of sediment accumulation. Radionuclide concentrations are similar to those in sediments from the upper levels. The high base-level accumulation rates are most probably due to interactions between the collectors and bottom level currents.

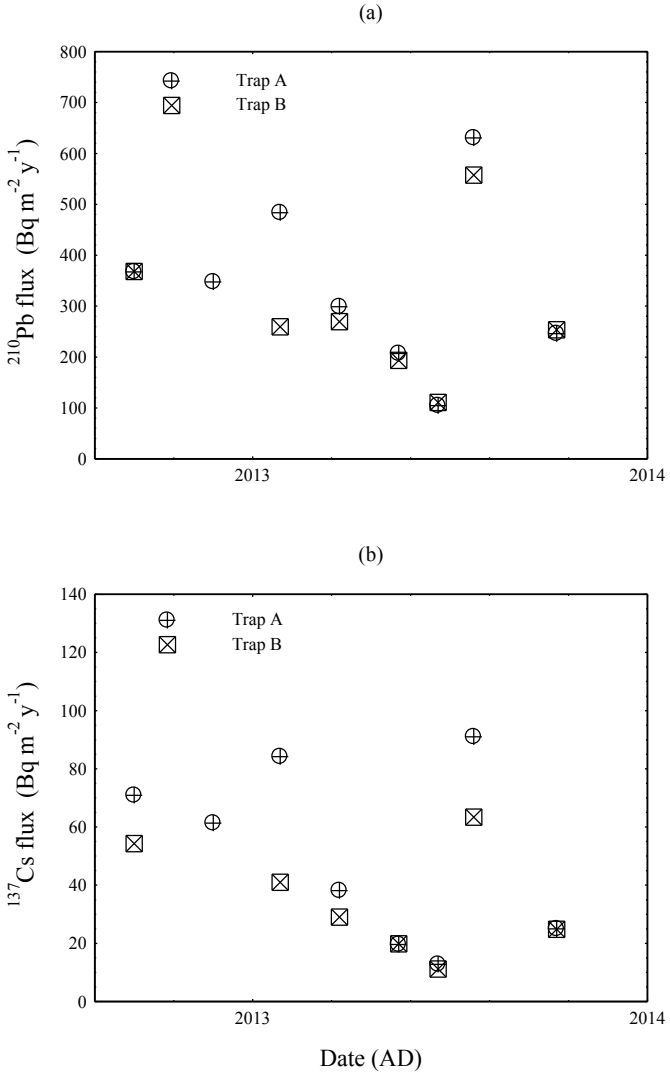

Figure 7.4 Fluxes of (a) ^{210}Pb and (b) ^{137}Cs through the water column of Brotherswater versus time.

Figure 7.4 plots mean values of (a) ^{210}Pb and (b) ^{137}Cs fluxes versus time from the top and mid-level collectors. Although at both sites ^{210}Pb fluxes are generally lower during periods of low flow and higher during periods where there have been significant flood events, the fact that even during flood events differences between traps A and B are in most cases relatively small (Figure 7.4(a)) provides further evidence that ^{210}Pb is transported on fine particulates that have relatively long residence times in the water column.

Table 7.3: ^{210}Pb, ^{226}Ra and ^{137}Cs activities in sediment trap samples.

(a) Trap A

Collection period		Level	Total ^{210}Pb		Unsupp ^{210}Pb		^{226}Ra		^{137}Cs	
Start date	End date		Bq kg^{-1}	±	Bq kg^{-1}	±	Bq kg^{-1}	±	Bq kg^{-1}	±
15-Aug-12	10-Oct-12	Top	270.8	14.5	238.4	14.7	32.4	2.6	44.1	2.4
		Mid	281.0	15.9	245.7	16.1	35.3	3.0	49.8	3.0
		Base	278.7	16.1	237.2	16.4	41.5	3.2	48.1	2.8
10-Oct-12	09-Jan-13	Top	313.4	10.8	283.2	11.0	30.2	2.0	52.7	2.1
		Mid	353.1	8.6	326.7	8.6	26.4	1.2	54.0	1.6
		Base	396.7	10.6	367.0	10.7	29.7	1.7	63.8	1.9
09-Jan-13	15-Feb-13	Top	Sample lost							
		Mid	343.6	12.2	313.5	12.4	30.1	1.9	54.6	2.1
		Base	530.3	12.5	491.6	12.6	38.7	2.0	79.7	2.2
15-Feb-13	24-Apr-13	Top	Sample lost							
		Mid	541.7	28.7	508.2	29.2	33.5	5.4	64.7	5.3
		Base	489.4	12.2	460.2	12.3	29.2	1.8	47.9	1.7
24-Apr-13	06-Jun-13	Top	579.4	24.6	540.8	25.1	38.6	4.9	51.3	4.2
		Mid	Sample lost							
		Base	426.6	10.6	395.5	10.7	31.2	1.5	54.8	1.7
06-Jun-13	10-Jul-13	Top	Too little material							
		Mid†	373.3	57.1	344.0	57.3	29.3	4.74	42.0	22.3
		Base	487.1	13.4	453.9	13.5	33.2	2.1	51.1	2.0
10-Jul-13	10-Aug-13	Top	368.0	18.6	341.0	19.0	27.0	3.5	42.7	3.4
		Mid	255.0	16.3	232.6	16.6	22.4	3.2	38.6	3.1
		Base	329.6	11.3	300.0	11.5	29.6	1.8	38.7	1.7
10-Aug-13	10-Dec-13	Top	468.6	10.9	440.3	11.0	28.3	1.7	46.0	1.7
		Mid	450.0	9.2	421.7	9.3	28.3	1.3	41.9	1.4
		Base	385.2	15.7	363.3	15.8	21.9	2.2	36.0	2.2
	Means	Top	400.1		368.8		31.3		47.4	
		Mid	371.1		341.8		29.3		49.4	
		Base	415.4		383.6		31.9		52.5	

† The large standard errors for these measurements are due to the small sample size. The ^{226}Ra activity is the estimated from mean value for other mid-level samples.

(b) Trap B

Collection period		Level	Total ^{210}Pb		Unsupp ^{210}Pb		^{226}Ra		^{137}Cs	
Start date	End date		Bq kg^{-1}	±	Bq kg^{-1}	±	Bq kg^{-1}	±	Bq kg^{-1}	±
15-Aug-12	10-Oct-12	Top	685.8	26.6	611.8	27.1	74.0	5.3	92.3	5.0
		Mid	419.5	30.2	375.3	30.7	44.2	5.3	53.5	4.7
		Base	417.0	20.0	380.9	20.2	36.1	3.1	51.2	2.9
10-Oct-12	09-Jan-13	Top	Sample lost							
		Mid	Sample lost							
		Base	Sample lost							
09-Jan-13	15-Feb-13	Top	513.2	34.4	477.4	34.8	35.7	5.7	68.7	5.5
		Mid	431.2	26.2	385.8	26.6	45.5	5.1	66.9	5.1
		Base	522.3	27.4	477.7	27.7	44.7	4.4	68.6	4.2
15-Feb-13	24-Apr-13	Top	619.9	21.5	589.0	21.8	31.0	3.7	66.6	4.0
		Mid	644.3	27.8	599.6	28.2	44.7	4.5	61.6	4.1
		Base	546.4	16.6	513.9	16.7	32.5	2.3	59.3	2.8
24-Apr-13	06-Jun-13	Top	661.5	25.3	619.7	25.8	41.8	5.0	57.4	4.3
		Mid	581.5	21.0	545.8	21.3	35.8	3.9	62.2	3.8
		Base	467.0	10.0	440.6	10.1	26.3	1.4	62.8	1.5
06-Jun-13	10-Jul-13	Top	Too little material							
		Mid‡	495.4	57.7	456.9	58.2	38.5	7.3	46.2	22.2
		Base	370.7	12.5	350.1	12.6	20.6	2.0	56.0	2.1
10-Jul-13	10-Aug-13	Top	617.2	16.3	587.6	16.5	29.5	2.4	54.8	2.4
		Mid	321.4	15.8	288.9	16.2	32.5	3.3	50.6	3.2
		Base	Sample lost							
10-Aug-13	10-Dec-13	Top	540.4	13.5	511.1	13.7	29.4	2.3	49.8	2.1
		Mid	497.4	10.2	469.1	10.3	28.3	1.4	46.1	1.5
		Base	398.8	8.1	377.2	8.2	21.5	1.2	60.1	1.5
	Means	Top	606.3		566.1		40.2		64.9	
		Mid	484.4		445.9		38.5		55.3	
		Base	453.7		423.4		30.3		59.6	

‡ The large standard errors for these measurements are due to the small sample size. The ^{226}Ra activity is the estimated from mean value for other mid-level samples.

Table 7.4: Water column fluxes of fallout ^{210}Pb.

(a) Trap A

Collection period		^{210}Pb fluxes (Bq m^{-2} y^{-1})			
Start	Finish	Top	Middle	Top+Middle	Base
15-Aug-12	10-Oct-12	396.7	337.5	367.1	609.4
10-Oct-12	09-Jan-13	360.7	334.6	347.6	404.7
09-Jan-13	15-Feb-13		483.4	483.4	1630.5
15-Feb-13	24-Apr-13		298.8	298.8	1101.0
24-Apr-13	06-Jun-13	206.8		206.8	1033.0
06-Jun-13	10-Jul-13		104.7	104.7	704.8
10-Jul-13	10-Aug-13	667.7	592.9	630.3	968.0
10-Aug-13	10-Dec-13	237.3	254.5	245.9	304.6
	Mean			336.1	708.9

(b) Trap B

Collection period		Sediment fluxes (Bq m^{-2} y^{-1})			
Start	Finish	Top	Middle	Top+Middle	Base
15-Aug-12	10-Oct-12	428.6	307.8	368.2	1174.5
09-Jan-13	15-Feb-13	270.7	248.5	259.6	528.7
15-Feb-13	24-Apr-13	252.1	286.4	269.3	360.9
24-Apr-13	06-Jun-13	206.5	180.1	193.3	1200.7
06-Jun-13	10-Jul-13		110.9	110.9	574.8
10-Jul-13	10-Aug-13	838.4	276.9	557.6	
10-Aug-13	10-Dec-13	235.7	271.1	253.4	292.3
	Mean			278.3	602.0

Table 7.5: Water column fluxes of fallout ^{137}Cs.

(a) Trap A

Collection period		137Cs fluxes (Bq m-2 y-1)			
Start	Finish	Top	Middle	Top+Middle	Base
15-Aug-12	10-Oct-12	73.4	68.4	70.9	123.6
10-Oct-12	09-Jan-13	67.2	55.3	61.3	70.3
09-Jan-13	15-Feb-13		84.2	84.2	264.2
15-Feb-13	24-Apr-13		38.1	38.1	114.5
24-Apr-13	06-Jun-13	19.6		19.6	143.1
06-Jun-13	10-Jul-13		12.8	12.8	79.3
10-Jul-13	10-Aug-13	83.6	98.4	91.0	124.8
10-Aug-13	10-Dec-13	24.8	25.3	25.0	30.2
Mean				46.5	98.1

(b) Trap B

Collection period		137Cs fluxes (Bq m-2 y-1)			
Start	Finish	Top	Middle	Top+Middle	Base
15-Aug-12	10-Oct-12	64.7	43.9	54.3	158.0
09-Jan-13	15-Feb-13	38.9	43.1	41.0	75.9
15-Feb-13	24-Apr-13	28.5	29.4	29.0	41.6
24-Apr-13	06-Jun-13	19.1	20.5	19.8	171.0
06-Jun-13	10-Jul-13		11.2	11.2	91.9
10-Jul-13	10-Aug-13	78.2	48.5	63.4	
10-Aug-13	10-Dec-13	23.0	26.6	24.8	46.6
Mean				32.6	85.1

Chapter 8. Fallout ^{210}Pb and ^{137}Cs supply rates to the sediments of Brotherswater

8.1 Introduction

Earlier chapters have considered the inputs of fallout ^{210}Pb and ^{137}Cs to Brotherswater directly via fallout onto the surface of the lake and indirectly via transport from the catchment, and their transport through the water column. The purpose of this chapter is to quantify the extent to which these radionuclides accumulate on the bed of the lake and become embedded in the sediment record. Their distribution over the bed of the lake will be used to highlight the relative contribution of catchment inputs as opposed to direct fallout. Results from the present study will be compared with those from earlier studies carried out in the 1970s and 1980s with the objective of determining any long-term changes.

Core dates, depths and locations

Earlier studies

The initial investigation by Pennington into sediment records of fallout radionuclides in Brotherswater collected cores from two sites near the south-western part of the lake, BW1 (1974, near the mouth of the inflow stream), and BRW (1975, from the western side of the lake), both of which were analysed for ^{137}Cs. In the more detailed studies carried out by Eakins and Cambray (1976/7) and Bonnett et al. (1988/9) a total of 11 cores were collected from five different locations broadly covering the whole of the lake:

- Site 1 from the southern end close to the present inflow,
- Site 2 on the western side of the lake,
- Site 3 in the central basin at a depth,
- Site 4 on the eastern side of the lake,
- Site 5 from the northern end of the lake close to the present outflow.

These cores, listed in Table 8.1, were all analysed for ^{210}Pb and ^{137}Cs, those from the 1976/7 study at AERE Harwell and those from the 1988/9 study in the Liverpool University ERL.

Table 8.1: List of historical Brotherswater cores analysed for ^{210}Pb and ^{137}Cs.

	1976/7 study		1988/9 study	
Site	Core	Depth	Core	Depth
Inlet	BW1/76	8.5 m	BW89/1	8.5 m
Western	BWW	7.5 m	BW88/2	11 m
″			BW89/2	5 m
Central	BWC	17 m	BW89/3	17 m
Eastern	BWE	7.5 m	BW89/4	8.5 m
Northern	BWN	4 m	BW89/5	4.5 m

Present study

Two sediment cores were collected from Brotherswater in 2011/12 as part of a study of metal and sediment fluxes in the lake (Schillereff et al., 2016) using a short 8 cm diameter gravity corer designed to capture an intact sediment water–interface (Boyle 1995). The first (BW11-2) was from the western side of the lake (Site 2) in 15.1 m water depth. The second (BW12-9) was from the central profundal zone (Site 3) in 16.3 m water depth. A further four cores were collected in 2014 specifically for this study, BW14/E1 and BW14/E2 from the eastern side of the lake (Site 4), and BW14/N1 and BW14/N2 from the northern end (Site 5). The southwestern corner near the inlet stream (Site 1) was not resampled due to the very rapid and irregular inputs of sediment from the catchment.

Following retrieval, cores were wrapped, sealed and stored in a refrigerator until ready for subsampling. This was done by extruding and slicing the sediment at 0.5 cm intervals with care being taken to preserve all of the material. Each slice was then weighed wet, freeze dried, and weighed again dry to determine the water content and wet and dry bulk densities. Dried sediment samples from each core were analysed for ^{210}Pb, ^{226}Ra, ^{137}Cs and ^{241}Am by direct gamma assay in the Liverpool University ERL using Ortec HPGe GWL series well-type coaxial low background intrinsic germanium detectors (Appleby et al. 1986). Samples were placed in 5 cm long by 1 cm diameter nylon sample tubes sealed with flanged rubber Suba-Seals dipped in paraffin wax to prevent ^{222}Rn escape.

^{210}Pb was determined via its gamma emissions at 46.5 keV, and ^{226}Ra by the 295 keV and 352 keV γ-rays emitted by its daughter isotope ^{214}Pb following 3 weeks

storage to allow $^{214}Pb/^{226}Ra$ radioactive equilibration. ^{137}Cs and ^{241}Am were measured by their emissions at 661.7 keV and 59.5 keV respectively. The absolute efficiencies of the detectors were determined using calibrated sources and sediment samples of known activity. Corrections were made for the effect of self-absorption of low energy γ-rays within the sample (Appleby et al., 1992), and for background radiation from the detectors themselves. The background counts of 60-hour duration were carried out on each detector at regular intervals. Mean background count-rates were typically around 0.5 cph (counts per hour) for the 46.5 keV peak and 1 cph for the 661.7 keV.

In order to get a better coverage of the lake, four more cores were collected in 2016, two from the south-eastern corner and two from the northern end. They were analysed following the same protocol, though since the main objective was to determine the radionuclide inventories, these cores were sectioned more coarsely, at 2 cm intervals. A list of the 2011-2016 cores, their locations and water depths is given in Table 8.2.

Table 8.2: List of 2011-2016 Brotherswater cores analysed for ^{210}Pb and ^{137}Cs.

Core	Date	Depth (m)	Map coordinates	
			North	East
BW11/2	2011	16.3	512678	340127
BW12/9	2012	15.1	512763	340206
BW14/E1	2014	12.5	512706	340423
BW14/E2	2014	13.5	512697	340404
BW14/N1	2014	11.5	512851	340215
BW14/N2	2014	13.5	512809	340232
BW16/SE1	2016	5.2	512565	340315
BW16/SE2	2016	10.3	512593	340349
BW16/NO1	2016	5.6	512883	340176
BW16/NO2	2016	10.2	512853	340163

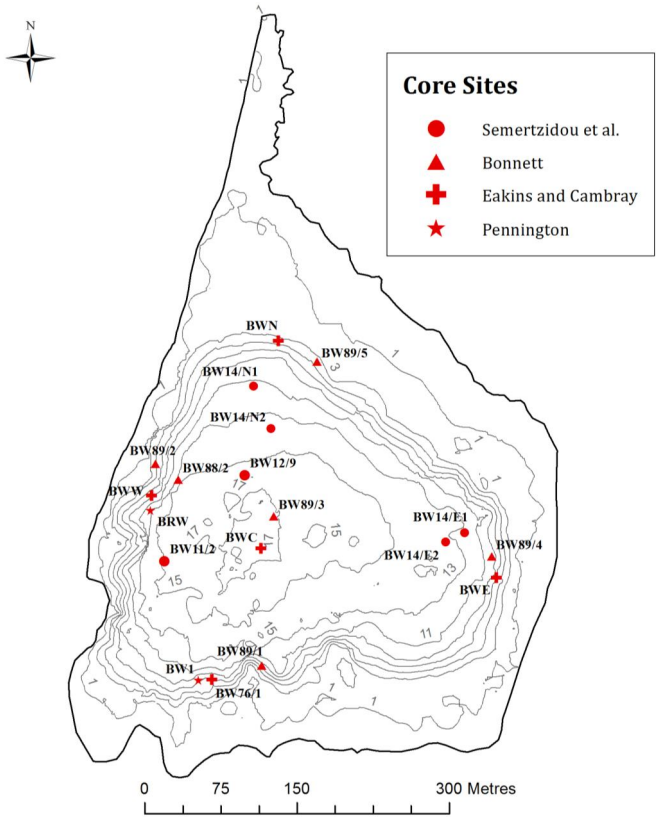

Figure 8.1: Locations of the Brotherswater core sites from all four studies.

8.2 Radionuclide inventories

Radionuclide inventories (Bq m^{-2}) for each core have been calculated by numerically integrating the activity versus depth records. The mean ^{210}Pb supply rate P (Bq m^{-2} y^{-1}) required to support the measured ^{210}Pb inventory $A(0)$ has been calculated using the formula

$$P = \lambda A(0)$$

where λ is the ^{210}Pb radioactive decay constant. The results of these calculations are summarised in Table 8.3. Mean inventories and fluxes for each series of cores are compared with estimated values due to direct fallout.

1974/7 cores

Results for the 1974/7 cores are shown in Table 8.3(a). The values shown are essentially those published in Pennington (1981) and Eakins et al. (1981 & 1984), apart from those for BRW. Results from this core do not appear to have been previously published and have been calculated from the original data recorded in Roger Cambray's logbook, a copy of which is held in the ERRC. A small correction to the

published ^{210}Pb inventories has been made for the unmeasured ^{210}Pb below the lowest data point using the methods summarised in Appleby (2001). The table also shows ^{137}Cs inventories decay corrected to 1986 in order to facilitate comparison with data collected at other times.

The mean ^{210}Pb supply rate of 326 Bq m^{-2} y^{-1} is around 80% higher than the estimated atmospheric flux. Although these results do suggest significant catchment inputs, the mean value does appear to be inflated by anomalously high values at the northern (outlet) and eastern sites BWN and BWE. The mean ^{210}Pb supply rate to these two cores (400 Bq m^{-2} y^{-1}) is significantly higher than for the BW76/1, BWW and BWC cores which are much closer to the inlet stream (mean value 277 Bq m^{-2} y^{-1}), most probably due to reworking of sediments from the margins of the lake. In contrast, the mean ^{137}Cs inventory of 5,132 Bq m^{-2} is 32% lower than the estimated fallout value, suggesting that catchment inputs of this radionuclide have been more than balanced by significant losses from the lake via the outflow. The ^{137}Cs/^{210}Pb inventory ratio (~1.3 in fallout) declines from ~0.7 at the inlet end and western side of the lake to ~0.5 at the centre and ~0.4 at the eastern side and outlet end.

1988/9 cores

Results for the 1988/9 cores, shown in Table 8.3(b), differ slightly from those published in Bonnett et al. (1992) following a re-evaluation of the raw data, the original values of which are stored in the ERRC data base. Whereas the sole source of ^{137}Cs in the 1974/7 cores was fallout from the atmospheric testing of nuclear weapons, records in the 1988/9 cores included a significant additional contribution arising from fallout from the 1986 Chernobyl reactor fire. Total ^{137}Cs activities for these cores have been decay corrected to 1986 and partitioned into their weapons test and Chernobyl components using measured values of the short-lived radionuclide ^{134}Cs and the established ^{134}Cs/^{137}Cs activity ratio (0.61) in Chernobyl fallout. The weapons test and Chernobyl inventories, also shown in Table 8.3(b), were then calculated by numerically integrating their respective activity versus depth records.

The mean ^{210}Pb supply rate of 219 Bq m^{-2} y^{-1} is around 20% higher than the estimated atmospheric flux. Values are a little higher in cores nearer to the mouth of the inlet stream. The mean ^{137}Cs inventory (decay corrected to 1986) is 5,656 Bq m^{-2}, of which 5,007 Bq m^{-2} (88%) derives from nuclear weapons test fallout and 649 Bq m^{-}

^{2} (12%) from Chernobyl fallout. The ^{137}Cs inventories are significantly lower than the fallout values, again suggesting significant losses from the lake via the outflow. The weapons ^{137}Cs/^{210}Pb inventory ratios are similar to those in the 1970s cores, with a value of ~0.74 in cores nearer to the inlet and 0.65 in cores further from the inlet. The Chernobyl ^{137}Cs/^{210}Pb inventory ratio is approximately 0.10.

2011/16 cores

Results for the 2011/16 cores are shown in Table 8.3(c). Since ^{134}Cs activities were below the level of detection, partitioning was carried out by linear extrapolation of the weapons ^{137}Cs record from the minimum point between the weapons and Chernobyl peaks up to the surface of the core. It was assumed that concentrations in the uppermost sample were equally divided between weapons test and Chernobyl ^{137}Cs. In spite of the significant uncertainties, the results do suggest that in cores more distant from the inlet stream the percentage of the ^{137}Cs inventory due to Chernobyl fallout had a relatively consistent value of 13%. This value was used to partition the ^{137}Cs inventories in the 2016 cores where the coarser resolution did not allow separation of the weapons test and Chernobyl records. The high ^{210}Pb inventory in BW11/2 (from the western side of the lake nearest the inflow) reflects the much greater influence of catchment inputs in this part of the lake.

The 2016 core BW16/NO2 appears to be incomplete, possibly due to a hiatus. Although relatively close to the 2014 core BW14/N1, the 2016 core has a much shorter record and significantly lower radionuclide inventories. Excluding this core, the mean ^{210}Pb supply rate to this suite of cores is 217 Bq m^{-2} y^{-1}, around 21% higher than the estimated atmospheric flux and similar to that in the 1980s cores. Excluding the anomalously high value in core BW11/2 the mean value in the remaining more distant cores (169 Bq m^{-2} y^{-1}) is comparable to the estimated atmospheric flux. This suggests although there are significant catchment inputs, in many parts of the lake the ^{210}Pb supply rate is dominated by the direct atmospheric flux. The mean ^{137}Cs inventory is 6,456 Bq m^{-2}, of which 5,381 Bq m^{-2} (83%) derives from nuclear weapons test fallout and 1,084 Bq m^{-2} (17%) from Chernobyl fallout.

Although uncertainties in the partitioning of the ^{137}Cs between its weapons test and Chernobyl components makes them less reliable than the 1980s cores, the weapons

$^{137}Cs/^{210}Pb$ inventory ratio is similar to that in the earlier cores, with a mean value of 0.77. The mean Chernobyl $^{137}Cs/^{210}Pb$ inventory ratio is 0.16.

Summary

The above results appear to provide clear evidence of significant inputs of fallout ^{210}Pb from the catchment. Mean ^{210}Pb supply rates at the inlet and western sites consistently exceeded the estimated atmospheric flux by more than 20%. The average value for these sites (315 Bq m^{-2} y^{-1}) was comparable to the mean annual ^{210}Pb flux through the water column determined from the upper and mid-levels sediment collectors at Trap A (336 Bq m^{-2} y^{-1}). The ^{210}Pb flux through the water column at the more centrally placed Trap B (278 Bq m^{-2} y^{-1}) was a little higher than at the central core sites, possibly due to its location a little further to the west. Anomalously high ^{210}Pb supply rates at the eastern (BWE) and northern (BWN) 1977 core sites are almost certainly due to local factors, most probably reworking of sediments from the shallower margins of the lake.

Since the processes transporting ^{210}Pb from the catchment will also transport ^{137}Cs, the fact that ^{137}Cs inventories are generally lower that the estimated atmospheric flux suggests significant higher losses from the sediment record, presumably due to its greater solubility compared to ^{210}Pb (Appleby 1997, Appleby et al. 2002). In the post-1986 studies, weapons ^{137}Cs inventory appears to represent ~83-88% of the total fallout inventory. The weapons $^{137}Cs/^{210}Pb$ inventory ratio is relatively consistent at around 70%.

The Chernobyl ^{137}Cs inventory is somewhat lower than expected and suggests that a very substantial fraction of direct fallout from this source was lost via the outflow. Although the method for partitioning ^{137}Cs into its weapons and Chernobyl components in the 2011/16 cores is fairly simplistic, there does appear to have been a significant increase in the Chernobyl inventory since 1988, presumably due to catchment inputs.

Table 8.3: Radionuclide inventories and fluxes in the Brotherswater lake sediment cores.

(a) 1974/7 cores

	^{210}Pb				Weapons ^{137}Cs			
	Inventory		Flux				Decay corrected to 1986	
	Bq m^{-2}	±	Bq m^{-2} y^{-1}	±	Bq m^{-2}	±	Bq m^{-2}	±
BW1/74					5916	123	4491	94
BRW/75					6464	159	5021	121
BW1/76	8911	383	277	12	8272	140	6574	106
BWW	9990	384	311	12	8280	316	6733	240
BWC	7772	350	242	11	5013	156	4077	119
BWE	10360	392	323	12	5164	237	4200	180
BWN	15354	498	478	15	7532	195	6125	148
mean	10477		326		6435		5162	
Fallout	5889		183				7609	

(b) 1988/9 cores

	^{210}Pb				^{137}Cs Decay corrected to 1986					
	Inventory		Flux		Total		Weapons		Chernobyl	
	Bq m^{-2}	±	Bq m^{-2} y^{-1}	±	Bq m^{-2}	±	Bq m^{-2}	±	Bq m^{-2}	±
BW89/1	8051	298	251	9	6368	136	6032	139	337	38
BW88/2	7998	280	249	9	7288	145	5829	147	1458	87
BW89/2	6298	240	196	7	4951	100	4478	104	473	40
BW89/3	7195	223	224	7	6109	127	5533	129	576	40
BW89/4	6222	192	194	6	4697	98	4042	110	655	66
BW89/5	6507	233	203	7	4985	121	4272	127	713	61
mean	7025		219		5656		5007		649	
Fallout	5889		183		11611		7609		4002	

(c) 2011/16 cores

	^{210}Pb				^{137}Cs Decay corrected to 1986					
	Inventory		Flux		Total		Weapons		Chernobyl	
	Bq m^{-2}	±	Bq m^{-2} y^{-1}	±	Bq m^{-2}	±	Bq m^{-2}	±	Bq m^{-2}	±
BW11/2	19450	458	606	14	19702	302	15452	492	4250	451
BW12/9Bs	5542	175	173	5	5697	100	4582	159	1115	142
BW14/E1	6048	128	188	4	4996	69	4422	96	575	81
BW14/E2	4634	116	144	4	4209	60	3664	88	545	81
BW14/N1	6884	136	214	4	5983	79	5086	99	897	81
BW14/N2	5606	134	175	4	5064	72	4364	99	701	87
BW16/SE1	4220	195	131	6	3293	83	2854	72	439	11
BW16/SE2	3683	149	115	5	3479	87	3016	76	464	12
BW16/NO1	6773	208	211	6	5760	116	4993	100	767	15
BW16/NO2	3440	146	107	5	2558	73	2217	63	341	10
mean	6962		217		6456		5381		1084	
Fallout	5889		183		11611		7609		4002	

8.3 Total ^{210}Pb inventory mean supply rate to the bed of the lake

In order to carry out a mass balance calculation for ^{210}Pb in Brotherswater it is necessary to determine the whole basin inventory and the mean supply rate needed to support it, or equivalently their mean values per unit area. The simplest way of doing this is from the arithmetical mean of the measured inventories or supply rates for a suite of cores providing a reasonable coverage of the entire bed of the lake. Since the atmospheric flux can be assumed relatively constant from year to year, such a calculation can include cores collected at different times. Applying this approach to the 21 sites listed in Table 8.3 the mean inventory is calculated to be 7,664 Bq m^{-2}. Alternatively, placing the sites into 6 different groups by locality (Inlet, West, Central, South East, East, North) and averaging the mean of each group, the inventory is calculated to be 7,408 Bq m^{-2}. Averaging the above approximations, a first estimate of the mean inventory for the whole basin is thus 7,536 Bq m^{-2}, and the mean supply rate 233 Bq m^{-2} y^{-1}.

A third, more accurate approach is to calculate the mean inventory via spatial interpolation. This usually involves employing some kind of weighted average interpolation; methods include inverse distance weighting, kriging or natural neighbours interpolation. The latter was preferred since sample points are distributed with uneven density. This method also has the advantage of not having to specify parameters such as radius or power function.

The method uses a geometric estimation technique (Delauney Triangulation) that divides the area into regions represented as a set of Voronoi cells or polygons. The mean value for each cell is calculated as a weighted average in which the weighting factor is the proportionate area of the lake that can be associated with each data point. The implementation of the method was carried out using the ArcGIS software. Figure 8.2 shows the value of the ^{210}Pb supply rate (or inventory) at each of the sites listed in Table 8.3.

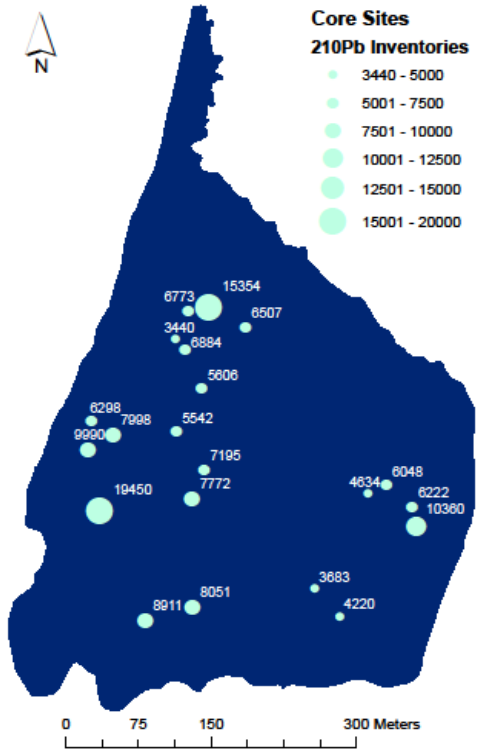

Figure 8.2: Mean ^{210}Pb supply rates (or inventories) at each of the Brotherswater core sites. The value at each site is indicated by the size of the marker.

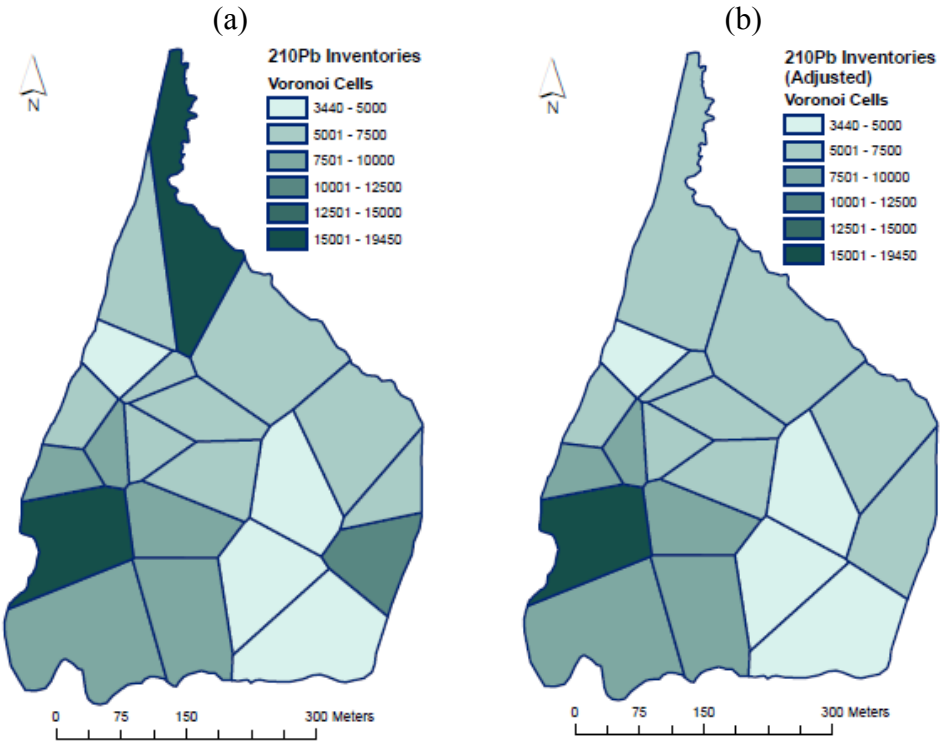

Figure 8.3: Voronoi diagrams for ^{210}Pb supply rates (or inventories) in Brotherswater (a) using all the data and (b) excluding the anomalous values from BWN and BWE.

Figure 8.3 shows the Voronoi diagrams for ^{210}Pb supply rates (or inventories) in Brotherswater (a) using all the data in Table 8.3 and (b) excluding the anomalous values from BWN and BWE. Table 8.4 summarises mean values determined from the simple arithmetic mean and the two Voronoi diagrams. In view of the uncertainties associated with each of these approaches a best estimate of the mean whole basin ^{210}Pb inventory in the sediments of Brotherswater is the average value of 7,600 Bq m^{-2}. A best estimate of the mean ^{210}Pb supply rate is 237 Bq m^{-2} y^{-1}.

Table 8.4: Mean whole basin ^{210}Pb inventories and supply rates in Brotherswater sediments.

	Mean ^{210}Pb Inventory	Mean ^{210}Pb supply rates
Simple mean	7536 Bq m^{-2}	233 Bq m^{-2} y^{-1}
Voronoi (a)	8054 Bq m^{-2}	251 Bq m^{-2} y^{-1}
Voronoi (b)	7212 Bq m^{-2}	225 Bq m^{-2} y^{-1}
Mean value	7600 Bq m^{-2}	237 Bq m^{-2} y^{-1}

Chapter 9. Mass balance calculations and residence times for ^{210}Pb in Brotherswater

9.1 Introduction

In a study of the transfer of natural and artificial radionuclides to Brotherswater from its catchment carried out by Eakins et al. (1984) in the late 1970s, it was estimated that the annual supply of fallout ^{210}Pb to the water column of the Brotherswater, including direct input by rain, was approximately 15 mCi y^{-1}. This is equivalent to a supply rate per unit area of 2275 Bq m^{-2} y^{-1}. Since their measurements indicated that direct fallout onto the surface of the lake contributed no more than around 170 Bq m^{-2} y^{-1}, it was concluded that the main source of ^{210}Pb (93%) was indirect inputs via transport from the catchment. Further, since the sediment core results suggested that just 14% of inputs (325 Bq m^{-2} y^{-1}) were delivered to the sediment record, it was also concluded that 86% of ^{210}Pb (12.9 mCi y^{-1}) entering the water column was lost from the lake via the outflow.

These results are however inconsistent with an alternative estimate based on the outflow data. ^{210}Pb concentrations in samples collected from the outlet stream during July 1976 through to November 1977 had a mean value of 48.6 fCi L^{-1} (1.8 Bq kL^{-1}). Given that the discharge through the outflow was estimated to be 48.9×10^6 m^3 y^{-1}, this implies an outflow loss of just 2.4 mCi y^{-1}. The discrepancy is almost certainly due to an assumption that the ^{210}Pb concentration on all sediments entering the lake via the inflow would be similar to that on fine particulates in the water column (~380 Bq kg^{-1}). Stream sediments, particularly during flood events (>90% of the annual total), include large amount of coarse material much of which contains relatively little ^{210}Pb. Here the calculations are revisited, taking into account results from more recent studies.

Although the bulk of fallout ^{210}Pb in the water column of a lake will normally be attached to sedimenting particulates, a significant fraction may be present either in solution or attached to colloidal size particle (< 0.4 μm). The soluble and colloidal fractions are essentially transported with the aqueous phase. The fate of the particulate fraction, and in particular the extent to which it is deposited on the bed of the lake or lost via the outflow, is largely determined by factors controlling the transport of

suspended sediments through the lake. These include the particle size distribution, water depth, and water residence time.

9.2 Water residence time

Chambers (1978) carried out weekly measurements of the discharge through streams flowing into and out of Brotherswater over a two-year period from 25th September 1975 to 25th September 1977. Estimates of the mean annual discharge rates based on a simple numerical procedure for integrating the individual measurements yielded values of 24.75×10^6 m^3 y^{-1} and 28.35×10^6 m^3 y^{-1} for the mean inflow rate and outflow rates respectively. The difference between the two can be attributed to additional inputs via direct rainfall onto the lake (0.47×10^6 m^3 y^{-1}) and groundwater flow (3.13×10^6 m^3 y^{-1}). The calculations necessarily underestimated the impact of flood events that took place between flow measurements. Although it was estimated that these might have accounted for an additional inflow of 19.05×10^6 m^3 y^{-1}, the procedure was acknowledged by Chambers to be highly uncertain and give no better than an order of magnitude of the true figure. Calculations based on the rainfall estimates given in Chapter 6 (2,609 mm y^{-1} near the lake, 3,108 mm y^{-1} over the catchment) give values of 37.3×10^6 m^3 y^{-1} for the mean inflow rate and 40.9×10^6 m^3 y^{-1} for the mean outflow rates. These figures are consistent with estimates based on daily precipitation data from the nearby Grisedale Bridge monitoring station (Schillereff, pers. comm.) which indicate that 36% of rainfall during the period monitored by Chambers fell on days with 25 mm of rain or more. Assuming this to be representative of the fraction of discharge taking place during flood events, the mean inflow rate for that period is calculated to be 38.5×10^6 m^3 y^{-1}. Table 9.1 gives estimated values of water inputs and outputs for Brotherswater based on Chambers results and the rainfall estimates. Given the total discharge (42.1×10^6 m^3 y^{-1}) and lake volume (1.33×10^6 m^3) it follows from equation (5.10) that the mean water residence time for Brotherswater is 12 days. Other estimates in the literature range from 7 days (Eakins et. al., 1984) to 21 days (Maberly et al. 2006). This range of values will at least in part reflect the fact that the residence time will be considerably less than 12 days during flood events and considerable longer during periods of low flow.

Table 9.1: Water balance estimates for Brotherswater.

Inputs		10^6 m^3 y^{-1}
Input stream	Normal flow	24.75
	Flood conditions	12.55
	Total	37.30
Direct rainfall onto the lake		0.47
Groundwater flow		3.13
	Total inputs	40.90
Outputs		
Outlet stream	Normal flow	28.35
	Flood conditions	12.55
	Total outputs	40.90

9.3 Sediment transport

The input of suspended sediments, the main vector for transporting fallout ^{210}Pb through the water column of a lake, were also monitored weekly by Chambers over a period of about one year, from 11th October 1976 to 25th November 1977. The calculated discharge based on these measurements, 81×10^3 kg y^{-1}, was however thought to greatly underestimate the total discharge. Particle concentrations were found to be up to three orders of magnitude higher during flood events, most of which were not picked up by the weekly monitoring. Total inputs including flood discharge peaks during the monitoring period were estimated by Chambers to be $1{,}300 \times 10^3$ kg, or $1{,}356 \times 10^3$ kg y^{-1}, though since the procedure for determining this figure was again highly uncertain, it can probably be regarded as no more than an educated guess.

The extent to which sediments entering the water column of Brotherswater accumulate in the sediment record can be determined using ^{210}Pb records from the suite of cores collected during this and earlier studies, shown in Figure 8.1. Sedimentation rates determined from the ^{210}Pb records were consistent with chronostratigraphic dates determined from the ^{137}Cs records (Appendix 2, Semertzidou et al. submitted for publication). A good estimate of the mean long-term accumulation rate at any individual site is given by the 90% ^{210}Pb equilibrium depth, corresponding to 75 years accumulation. Mean sedimentation rates determined in this way ranged from 0.173 g cm^{-2} y^{-1} at BW11/2 (relatively near the mouth of the main inlet stream) to 0.026 g cm^{-2} y^{-1} at BW16/SE2 (towards the south-eastern corner of the lake) and are consistent

with the sediment trap data (Chapter 7) which suggest sediment fluxes through the water column of 0.093 g cm^{-2} y^{-1} at Site A near the inflow stream and 0.056 g cm^{-2} y^{-1} at Site B near the centre of the lake. Integrating over all the data, the mean accumulation rate was calculated to be 0.059 g cm^{-2} y^{-1} giving a mean whole basin accumulation rate of 106×10^3 kg y^{-1}.

Although Eakins et al. (1984) appear to suggest that the discrepancy between this figure and the estimated catchment inputs can be accounted for by sediments exiting the lake via the outflow, this is not supported or by Chambers' field work. Because of the buffering effect of the lake, particle concentrations at the outflow will be much more uniform than at the inflow. Suspended sediment concentrations in samples collected from the outflow during weekly monitoring had a mean value of 1.1 mg L^{-1}. Assuming this to be typical of the total discharge through the outflow (40.9×10^6 m^3 y^{-1}), the total sediment loss via the outflow is calculated to be 46×10^3 kg y^{-1}. The combined total (152×10^3 kg y^{-1}) of losses via sedimentation and outflow is nearly double the measured inputs during normal flow conditions and probably a good measure of the total input of relatively fine sediments from the catchment. The balance is almost certainly relatively coarse material (sand and gravel) mobilised during flood events and deposited in a delta relatively close to the point of entry to the lake.

Table 9.2 shows a typical particle size classification for lake sediments. Colloidal size particles (< 0.4 μm) settle at less than 1 cm d^{-1} and are essentially transported with aqueous phase. From equation (5.17) the fraction retained in the sediment record (as opposed to exiting the lake via the outflow) is less than 1%. Excluding the delta region, particles accumulating on the bed of the lake will predominantly be fine (2 – 6 μm) or medium (6 – 20 μm) silts. These have settling velocities in the ranges 0.2 – 2 m d^{-1} and 2 – 20 m d^{-1} respectively. Their retention fraction rises from 27% for 2 μm particles to 77% for 6 μm particles and is greater than 90% for particles larger than 10 μm. For particles larger than a coarse silt (>20 μm) the retention fraction is virtually 100%. Further, with settling velocities in excess of 20 m d^{-1} they can only be transported beyond the lake delta within turbidity currents.

Table 9.2: Particle size classification.

Colloids	< 0.4 μm
Clay	0.4-2 μm
Fine silt	2-6 μm
Medium silt	6-20 μm
Coarse silt	20-60 μm
Fine sand	60-200 μm
Medium sand	200-600 μm
Coarse sand	600-2000 μm

9.4 ^{210}Pb mass balance

Using the estimated value of the atmospheric flux of 183 Bq m^{-2} y^{-1} (Chapter 6) the total amount of ^{210}Pb entering Brotherswater via direct fallout onto the surface of the lake is calculated to be 3.30×10^7 Bq y^{-1} (0.89 mCi y^{-1}). Given that the mean ^{210}Pb supply rate to the sediment record (Chapter 8) is 237 Bq m^{-2} y^{-1}, or 4.26×10^7 Bq y^{-1} (1.15 mCi y^{-1}), it is evident that a significant fraction is due to inputs from the catchment. The difference between these figures, 0.96×10^7 Bq y^{-1} (0.24 mCi y^{-1}) is a measure of the extent to which inputs from the catchment exceed losses via the outflow.

Losses via the outflow

Eakins et al. (1984) carried out measurements of ^{210}Pb in water samples collected from the Brotherswater outflow stream on five occasions during July 1976 to November 1977 under both low flow conditions and following heavy rain. Concentrations ranged from 0.9–3.2 Bq kL^{-1} (23–87 fCi L^{-1}) with a mean value of 1.8 Bq kL^{-1} (49 fCi L^{-1}). Multiplying by the estimated mean outflow rate (40.9×10^6 m^3 y^{-1}), one estimate of the annual rate of loss of ^{210}Pb from the lake via the outflow is calculated to be 7.36×10^7 Bq y^{-1}. Because of the relative sparsity of the measurements and their wide range of values this figure does however have a large uncertainty.

An alternative estimate can be made using measured values of the ^{210}Pb concentrations on suspended particulates in the water column (Chapter 7). Unsupported ^{210}Pb concentrations on samples from sediment Trap B near the centre of the lake were significantly higher than those in samples from Trap A, closer to the

inflow, presumably due to the progressive settling out of coarser particles with lower concentrations. Mean concentrations in Trap B samples (Table 7.3(b)) ranged from 423 Bq kg^{-1} in the base-level collector to 566 Bq kg^{-1} in the top-level collector. Assuming the latter value to be more typical of suspended sediments reaching the outflow, multiplying by the estimated sediment load (46×10^3 kg y^{-1}), and also allowing for the estimated 25% of ^{210}Pb on fine material that is essentially transported with the aqueous phase (Eakins et al. 1984), this method gives a lower value of 3.44×10^7 Bq y^{-1} for the ^{210}Pb loss rate. In view of the uncertainty surrounding both figures, the mean value of 5.4×10^7 Bq y^{-1} (1.46 mCi y^{-1}) provides a best estimate for the rate of discharge of ^{210}Pb through the outflow.

Inputs from the catchment

Direct estimates of ^{210}Pb inputs from the catchment are highly problematic due to the large uncertainties associated with inputs during flood events. In the study carried out by Eakins et al. it was supposed that ^{210}Pb concentrations on all sediments entering the lake (including those during storm events) were similar to those on suspended sediments in the water column, estimated to be 10.3 pCi g^{-1} (381 Bq kg^{-1}). Using Chambers' estimate for the sediment load (1356×10^3 kg y^{-1}), the annual supply of ^{210}Pb from the catchment was calculated to be around 14 mCi y^{-1} (51.7×10^7 Bq y^{-1}). The assumptions used in this calculation are however contradicted by recent measurements of fallout ^{210}Pb and ^{137}Cs in sediment samples from traps placed in the inflow stream close to its mouth, summarised in Table 9.3. Unsupported ^{210}Pb concentrations varied widely from as little as 13 Bq kg^{-1} to more than 200 Bq kg^{-1}. The mean concentrations of around 80 Bq kg^{-1} is just 20% of the value assumed by Eakins et al. The samples referred to in this table mainly consisted of sediments collected during periods of relatively normal flow. Sediments transported during flood events include large quantities of relatively coarse material containing relatively little ^{210}Pb, exemplified by the October 2016b and October 2017b sample. Excluding these, the mean unsupported ^{210}Pb concentration on the remaining mainly fine-grained material was around 106 Bq kg^{-1}. Assuming this to be typical of the estimated 152×10^3 kg y^{-1} of fine sediments entering the lake via the main inflow, and again supposing that that 25% of ^{210}Pb was on fine material that is effectively in solution, the amount of catchment derived ^{210}Pb entering the lake via this pathway is calculated to be 2.15×10^7 Bq y^{-1}. Assuming further that the coarse sediments transported during flood events

(~1200×10^3 kg y^{-1}) had a minimal unsupported ^{210}Pb concentration of 15 Bq kg-1 (the mean value of the two October b samples), total inputs of catchment derived ^{210}Pb are calculated to be 4.59×10^7 Bq y^{-1}.

Table 9.3: ^{210}Pb and ^{137}Cs concentrations on sediment samples from traps placed in the main Brotherswater inflow stream.

Date	Total ^{210}Pb		Unsupp ^{210}Pb		^{226}Ra		^{137}Cs	
	Bq kg^{-1}	±	Bq kg^{-1}	±	Bq kg^{-1}	±	Bq kg^{-1}	±
Jul-16	131.5	15.0	104.7	16.9	26.9	3.1	37.4	4.4
Aug-16	86.4	14.4	62.4	14.9	24.0	1.2	19.4	3.9
Oct-16a	104.3	18.0	76.8	20.4	27.5	2.8	25.7	5.1
Oct-16b	37.9	4.7	12.7	4.8	25.2	0.8	12.0	0.6
Jul-17	98.0	38.1	72.2	33.9	25.8	4.4	25.1	3.8
Oct-17a	245.6	53.7	215.0	52.9	30.6	2.2	41.5	7.3
Oct-17b	41.1	2.4	17.8	2.4	23.3	0.5	12.2	0.4
Mean	106.4		80.2		26.2		24.7	
			106.2*					

* Excluding the two coarse-grained samples from October 2016b and October 2017b

An alternative estimate can be made using the measurements carried out by Eakins et al. (1984) on water samples from the Brotherswater inlet stream. Concentrations on samples collected on five occasions during July 1976 to November 1977 under both low flow conditions and following heavy rain ranged from 0.5-2.6 Bq kL^{-1} (14-60 fCi L^{-1}) with a mean value of 1.5 Bq kL^{-1} (41 fCi L^{-1}). Multiplying by the estimated discharge rate through the inflow of 37.3×10^6 m^3 y^{-1}, this calculation suggests an annual rate of supply of ^{210}Pb from the catchment of 5.69×10^7 Bq y^{-1}. The mean value from both methods is 5.14×10^7 Bq y^{-1}.

9.5 Modelling the transport of ^{210}Pb through the water column

In spite of the large uncertainties surrounding the above estimates there is a reasonable consensus that the total supply of ^{210}Pb to Brotherswater lies between 8.44×10^7 Bq y^{-1} (based on input values) and 9.66×10^7 Bq y^{-1} (based on output values). The mean value of 9.05×10^7 Bq y^{-1} implies catchment inputs of 5.75×10^7 Bq y^{-1} and losses via the outflow of 4.76×10^7 Bq y^{-1}. These results suggest that 47% of ^{210}Pb entering the water column of Brotherswater is transferred to the sediment record, and 53% lost via the outflow.

A check on the consistency of these figures can be made using the model of the transport of ^{210}Pb through the water column outlined in Chapter 5. Whereas the supply of ^{210}Pb is controlled by external factors, its fate once in the water column is controlled by internal factors such as the water residence time T_W, the fraction of the ^{210}Pb in the water column attached to particulates f_D, the settling velocity of the particulates v, and the mean water depth d. From equation (5.27) the fraction of ^{210}Pb inputs transferred to the sediment record is given by the equation

$$\mathcal{F}_{Pb} = \frac{f_D T_L}{T_S},$$

where $T_S = d/v$ is the settling time and T_L the ^{210}Pb residence time, given by

$$\frac{1}{T_L} = \frac{f_D}{T_S} + \frac{1}{T_W}.$$

Noting from equations (5.19) and (5.20) that the ratio of losses to the sediment record to losses to the outflow can be written

$$\frac{\mathcal{F}_{Pb}}{1-\mathcal{F}_{Pb}} = \frac{f_D Q_L / T_S}{Q_L / T_W} = \frac{f_D T_W}{T_S} = \frac{f_D v T_W}{d},$$

it follows that the mean water column concentration C_L, mean supply rate to the sediments Φ_S, and ^{210}Pb retention fraction $\mathcal{F}_{Pb}$ are related by the equation

$$\Phi_S = v f_D C_L = \frac{\mathcal{F}_{Pb}}{1-\mathcal{F}_{Pb}} \frac{d}{T_W} C_L.$$

Eakins et al. (1984) carried out measurements of ^{210}Pb in samples collected from the water column of Brotherswater on eight occasions during July 1976 to January 1978 under both low flow conditions and following heavy rain. Concentrations ranged from 0.4–5.2 Bq kL^{-1} (14–60 fCi L^{-1}) with a mean value of 1.8 Bq kL^{-1} (41 fCi L^{-1}). Using the values 7.4 m for the mean depth of Brotherswater, 12 days for the water residence time, and 237 Bq m^{-2} y^{-1} for the mean rate of supply of ^{210}Pb to the sediments, solving the above equation gives a lower but comparable value of 0.37 for the fraction of ^{210}Pb transferred to the sediment record and implies catchment inputs of 8.20×10^7 Bq y^{-1} and losses via the outflow of 7.21×10^7 Bq y^{-1}.

The best estimates of the ^{210}Pb budget for the water column of Brotherswater based on the present data are summarized in Table 9.4 and Figure 9.1.

Table 9.4: Inputs of ^{210}Pb to and outputs of ^{210}Pb from the water column of Brotherswater.

Inputs		Outputs	
Direct fallout	3.30×10^7 Bq y^{-1}	To sediment record	4.29×10^7 Bq y^{-1}
From catchment	$5.75–8.20 \times 10^7$ Bq y^{-1}	Through outflow	$4.76–7.21 \times 10^7$ Bq y^{-1}
Total	$9.05–11.5 \times 10^7$ Bq y^{-1}	Total	$9.05–11.5 \times 10^7$ Bq y^{-1}

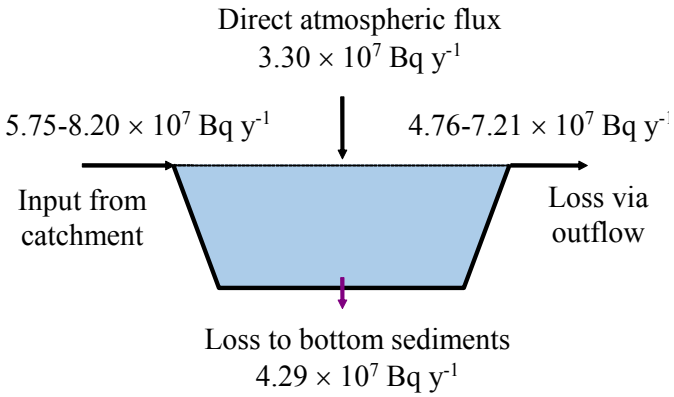

Figure 9.1: Mass balance for ^{210}Pb in Brotherswater.

Mean particle size

The relatively high fraction of ^{210}Pb lost via the outflow is surprising, given that particle size analyses carried out on sediment trap samples (Schillerreff, 2016) showed a substantial fraction in excess of 10 μm. Retention rates for particles in this size range should be in excess of 90%. From Stoke's law the settling velocity for particles of diameter D μm (Chapter 5) reduces to

$$v = 0.058\, D^2 \text{ m d}^{-1}.$$

(This equation is valid for particles up to 20 μm, and a good approximation for particles up to 50 μm.) Substituting into the expression for the particle settling time T_S (equation 5.13), the expression for the retention fraction (equation 5.17) can be rearranged to give an explicit relation

$$\mathcal{F}_{Pb} = \frac{1}{1 + \dfrac{d}{0.058 D^2 f_D T_W}}$$

between the retention fraction and particle size. Figure 9.2 plots values of $\mathcal{F}_{Pb}$ against particle diameter for values of the particulate fraction f_D in the range 0.75–0.85, assuming a mean water depth of 7.4 m and a mean water residence time of 12 days. The results show that the value of $\mathcal{F}_{Pb}$ is relative insensitive to the precise value of f_D but strongly dependent on particle size. The fraction of ^{210}Pb transported to the sediment record is less than 10% for particles less than 1 μm and over 90% for particle larger than 10 μm. For particle between 2–6 μm, it increases rapidly from around 25% to 75%. Since the empirically determined values of $\mathcal{F}_{Pb}$ are in the range of 0.37-0.47, it appears that the bulk of ^{210}Pb in the water column of Brotherswater is transported on particulates with a mean size of around 3 μm.

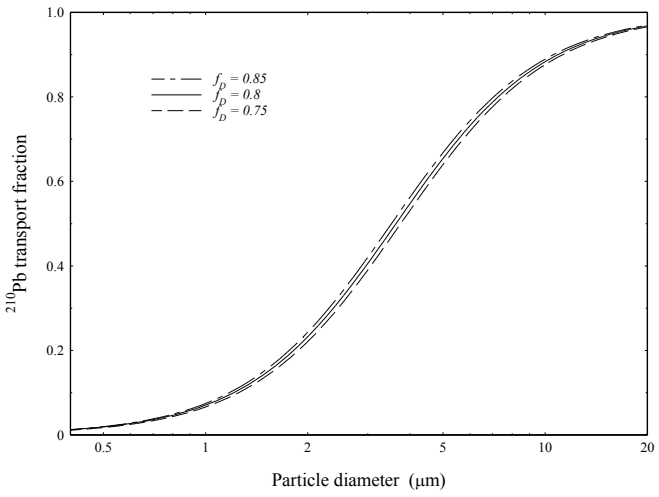

Figure 9.2: ^{210}Pb sediment record transfer fractions in Brotherswater versus particle size.

9.6 Catchment/lake transport parameter

The above results illustrate the extent to which catchment inputs may be significant source of ^{210}Pb in lakes with large catchment/lake area ratios. Between 64-71% of ^{210}Pb entering the water column of Brotherswater is catchment derived. Further, between 53-63% is then lost from the lake through the outflow. From equation (5.4) the catchment/lake transport rate can be written

$$\Psi_C(t) = A_L \alpha \eta_{Pb} \mathcal{P},$$

where $\mathcal{P}$ is the atmospheric flux, A_L the area of the lake, α the catchment/lake area ratio, and η_{Pb} the fraction of annual fallout on the catchment delivered to the lake. Substituting the values

$$\mathcal{P} = 183 \text{ Bq m}^{-2} \text{ y}^{-1},\ A_L = 0.18 \text{ km}^2,\ \alpha = 72,\ \Psi_C = 5.70 \times 10^7 \text{ Bq y}^{-1}$$

the parameter η_{Pb} is calculated to lie within the range of 0.024-0.034, that is, between 2.4-3.4% of annual fallout onto the catchment. Further, solving equation (5.8)

$$\eta_{Pb} = \int_0^\infty \frac{k}{\sqrt{s}} \mathrm{e}^{-(\lambda s + 2k\sqrt{s})} \mathrm{d}s$$

the catchment/lake transport coefficient k (section 5.3) lies between 0.0024-0.0033. The corresponding value for Blelham Tarn (Appleby et al. 2003) was 0.0022.

Chapter 10: Conclusions

Further advances in the use of ^{210}Pb as a tool for dating environmental records in natural archives such as lake sediments demand a better understanding of the origins of fallout ^{210}Pb and the extent to which the rate at which it is delivered to the archive is been influenced by mediating transport processes. Although early applications assumed that a constant atmospheric flux (on yearly timescales) was the dominant factor and would result in a fairly constant rate of delivery to the archive, it is now clear that the processes involved are much more complex and that the ^{210}Pb supply rate may be significantly influenced by other factors such as delayed inputs from the catchment, and sediment transport processes within the lake. In order to determine the possible impact of these processes it is essential to be able to make reasonable estimates of the atmospheric flux at the study site, and the relative importance of indirect inputs from the catchment. Since lakes used for these studies now amount to many thousands, often from remote (polar, alpine, wetland) sites chosen for the potential environmental records they may contain, detailed site studies of the kind presented here are in most cases quite impractical and estimates of the atmospheric flux and the impact of catchment inputs must be made using a relatively small number of parameters such as the geographical location, lake area and volume, and catchment area.

Although there is a reasonable amount of information on ^{210}Pb fallout in Western Europe and continental USA, there are large areas of the world where such data are virtually non-existent. Estimates of fallout at such sites depends on having good information on how fallout varies from place to place over the Earth's surface. The results obtained in the first part of this thesis were primarily concerned with obtaining a better estimate of the residence time of ^{210}Pb in the atmosphere, one of the key parameters controlling its fallout. Although the relationships between ^{210}Pb and its daughter radionuclides were quite early on seen as an ideal means for estimating the residence time, large discrepancies between results based on the ^{210}Bi/^{210}Pb and ^{210}Po/^{210}Pb ratios appeared to discredit this approach. One reason for the discrepancies was a failure to recognise the extent to which the values of these ratios depended on geographical location. As shown in Figures 4.5 and 4.6, ^{210}Bi/^{210}Pb ratios varied widely from around 0.4-0.9, whilst ^{210}Po/^{210}Pb ratio varied from around 0.1-0.12. A second reason was a failure to correct for supported activities of these radionuclides.

The model results also showed that because of sharp spatial gradient in the values of these ratios near the western margins of large land masses, data from such sites particularly unsuitable for estimating residence times. As shown in Table 4.1, once account is taken of these factors discrepancies between the two methods were effectively resolved, yielding a best estimate for the tropospheric residence time of 10 days.

The model presented here was based on a relatively simple model of global circulation only applicable to northern mid-latitudes. Although reasonably consistent with the empirical data shown in Figure 4.1, more reliable estimates do require a more complex model. One possibility for future research is to apply the concept of a notional column to two dimensional models of mean atmospheric circulation. Such models can be developed on a regional scale and as such are easier to validate than the more complex global three-dimensional models,

In spite of many large uncertainties. mainly associated with the difficulty in determining the precise impact of large flood events, the mass balance calculations presented in Chapter 9 show that although catchment inputs provide a significant proportion of ^{210}Pb entering the water column of Brotherswater, their contribution is significantly less than the 94% suggested in the earlier study by Eakins el al (1984). Although amounting to no more than between 2.4-3.4% of annual fallout onto the catchment, they have a disproportionate effect on Brotherswater due to the very large catchment/lake area ratio. This is comparable to the result obtained from a similar mass balance study carried out at Blelham Tarn (Appleby et al. 2003) where it was shown that catchment inputs to the lake amounted to 2.2% of annual fallout onto the catchment. Because of the smaller catchment/lake area at Blelham Tarn ($\alpha = 42$ compared to 72 at Brotherswater) they represented a smaller fraction of total inputs (47% compared to around 67% at Brotherswater).

Table 10.1 ^{210}Pb Transport parameters and coefficients for various catchments

Catchment	^{210}Pb transport parameter η_{Pb} (y^{-1})	Transport coefficient k ($y^{-0.5}$)	Reference
Susquehanna	0.016	0.0016	Lewis (1977)
Mississipi	0.012	0.0012	Scott et al. (1985)
Alpine Rhone	0.023	0.0023	Dominik et al. (1987)
Blelham	0.022	0.0022	Appleby et al. (2003)
Brotherswater	0.024-0.034	0.0024-0.0033	This study

Other studies using quite different methods carried out on catchments varying in scale from a European Alpine lake to the Mississipi River Basin yielded surprisingly similar values, summarised in Table 10.1. Also shown are corresponding values of the transport coefficient k, defined in equation (5.8). This parameter is not related to a particular fallout record and can be used to calculate transport rates for species that are chemically similar to ^{210}Pb regardless of their fallout history. These results suggest that values of the ^{210}Pb transport parameter of around 2% can provide a reasonable first estimate of the contribution of catchment inputs to the water column. Total inputs of ^{210}Pb to a lake would then be $(1+0.02\alpha)\mathcal{P}$ where a is the catchment/lake area ratio and $\mathcal{P}$ the direct atmospheric flux.

A distinctive feature of Brotherswater is the relatively large fraction of ^{210}Pb entering the water column that is then lost via the outflow, estimated to amount to between 53%-63% of total inputs. Outflow losses for Blelham Tarn were calculated to be around 25%, less than half those for Brotherswater. Values for other Cumbrian lakes in the ERRC database ranged between 10% - 30%, with a mean value of under 20%. The much greater losses from Brotherswater are attributable to its relatively short water residence time (12 days compared to 32 days at Blelham Tarn. Figure 10.1 compares values of the ^{210}Pb transport fraction (to the bottom sediments) versus particle size for values of the particulate fraction f_D in the range 0.75-0.85 for Blelham Tarn with the corresponding values for Brotherswater. It shows that for any given particle size the fraction retained in the bottom sediments of Blelham Tarn is significantly greater than the fraction retained in Brotherswater. It also shows that the empirically determined value of $\mathcal{F}_{Pb}$ for Blelham Tarn (0.75) corresponds to a mean particle size of between 3-4 μm, similar to that for Brotherswater. Given that ^{210}Pb

becomes attached to micron size particles in the atmosphere the inference that it remains attached to fine particulates in the water column is not unreasonable. Their relatively slow removal from the water column allows them to be transported relatively uniformly throughout the lake, one of the key factors supporting their use as a dating tool.

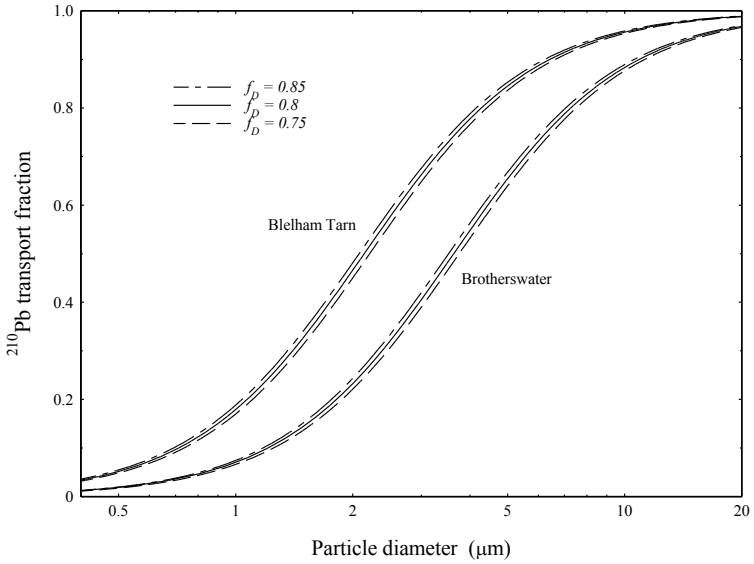

Figure 10.1 ^{210}Pb sediment record transfer fractions in Belham versus particle diameter compared to those for Brotherswater

Although this thesis is primarily concerned with ^{210}Pb, the fact that the samples were analysed by gamma spectrometry has also yielded some interesting data on the transport of fallout ^{137}Cs through Brotherswater and its catchment. The sediment trap results in particular highlight the extent to which significant quantities of ^{137}Cs deposited on the catchment of Brotherswater continue to be transported to the lake 30 years after the last fallout event. Because of the episodic nature of the ^{137}Cs fallout record an analysis of these data is significantly more complicated, particularly in view of the fact that the distinction between Chernobyl ^{137}Cs and weapons test ^{137}Cs at Brotherswater is less clear than at Blelham Tarn. Because of its relative solubility compared to ^{210}Pb, catchment transport rates for ^{137}Cs are expected to be higher than those for ^{210}Pb and this is supported by the fact that the ^{137}Cs catchment/lake transport coefficient at Blelham Tarn was calculated to be 0.0060 $y^{-0.5}$ (Appleby et al. 2003), nearly three times higher than its value for ^{210}Pb. A higher dissolved fraction in the water column will also result in greater losses through the outflow (Appleby 1997). Although an analysis of these data is outside the scope of the present thesis, future

work is intended to model and quantify ^{137}Cs transport processes in Brotherswater and its catchment.

References

Appleby PG, (1997a). The use of 210Pb and 137Cs as tracers in modelling transport processes in lake catchment systems. In: G.Desmet, R.J.Blust et al. (eds.), Freshwater and Estuarine Radioecology, Proceedings of an International Seminar, Lisbon, March 1994, Elsevier, pp.441-448.

Appleby PG, (1997b). Sediment records of fallout radionuclides and their application to studies of sediment-water interactions. Water, Air & Soil Pollution 99, 573-586.

Appleby PG, (2001). Chronostratigraphic techniques in recent sediments, in Tracking Environmental Change Using Lake Sediments Volume 1: Basin Analysis, Coring, and Chronological Techniques, (eds W M Last & J P Smol), Kluwer Academic, pp171-203.

Appleby PG (2013). ^{210}Pb Dating - Thirty Five Years On. J Paleolimnol 49:697-702.

Appleby PG, Oldfield F (1978) The calculation of lead-210 dates assuming a constant rate of supply of unsupported 210Pb to the sediment. Catena 5: 1-8

Appleby P.G., Haworth E.Y., Michel H., Short D.B., Laptev G. and Piliposian G.T., 2003. The transport and mass balance of fallout radionuclides in Blelham Tarn, Cumbria (UK). J. Paleolimnology 29, 459-473.

Appleby PG, Koulikov AO, Camarero L & Ventura M, 2002. The input and transmission of fallout radionuclides through Redó, a high mountain lake in the Spanish Pyrenees. Water, Air & Soil Pollution: Focus 2:19-31.

Appleby.P.G., Nolan, P.J., Gifford, D.W., Godfrey, M.J., Oldfield, F., Anderson, N.J. & Battarbee, R.W., 1986. 210Pb dating by low-background gamma counting. Hydrobiologia, 143:21-27.

Appleby PG, Richardson N. Nolan PJ, (1991) 241Am dating of lake sediments. Hydrobiologia, 214: 35-42.

Appleby, P.G., Piliposian, G.T., 2010. The origins of 210Pb in the atmosphere and its deposition on and transport through catchment lake systems. In: Hanrahan, G. (Ed.), Advanced Topics in Environmental Science Volume II: Modelling of Pollutants in Complex Environmental Systems, pp.381-404. ILM Publications, St Albans.

Anderson R.V. & R.E, Larson, 1974. Atmosphere Electric and Radon Profiles Over a Closed Basin and the Open Ocean. J Geophys. Res. 79:3432-3435.

Balkanski, Y. J., Jacob, D. J., Gardner, G. M., 1993. Transport and residence times of tropospheric aerosols from a global three-dimensional simulation of 210Pb. J Geophys. Res. 98D, 20573–20586.

Baskaran, M., 2011. Po-210 and Pb-210 as atmospheric tracers and global atmospheric Pb-210 fallout: a Review. J. Environ. Radioact, 102, 500-513.

Bloesch J, Burns N., 1980. A critical review of sedimentation trap technique. Schweizerische Zeitschrift fur Hydrol42:15–55.

Bradley,W. E., Pearson, J. E., 1970. Aircraft measurements of the vertical distribution of radon in the lower atmosphere. J Geophys. Res. 75, 5890–5894.

Bonnett PJP, Appleby PG, Haworth EY, Hilton J, Davison W, Oldfield F (1992). Environmental behaviour of radioactivity from Chernobyl: Brotherswater study. DOE Report No. DOE/RAS/92.004, 55pp.

Boyle JF (1995) A simple closure mechanism for a compact, large-diameter, gravity corer. Journal of Paleolimnology 13: 85–87.

Burton,W.M. & N.G.Stewart, 1960. Use of long-lived natural radioactivity as an atmospheric tracer. Nature, 186:584-589.

Carvalho, F.P., 1995. Origins and concentrations of 222Rn, 210Pb, 210Bi and 210Po in surface air at Lisbon, Portugal, at the Atlantic edge of the European continental landmass. Atmospheric Environment 29, 1809-1819.

Cambray,R.S., K.Playford, G.N.J.Lewis & R.C.Carpenter, 1989. Radioactive fallout in air and rain: results to the end of 1987. AERE-R 13226, Harwell.

Cawse, P., 1983. The accumulation of ^{137}Cs and $^{239+240}Pu$ in soils of Great Britain, and transfer to vegetation. In P. J. Coughtrey, (ed.), Ecological aspects of radionuclide release. Blackwell, Oxford, 47–61.

Chambers KC, 1978. Source-sediment relationship in the Cumbrian lakes. PhD thesis, University of Reading, 222 pp.

Dibb JE, Meeker LD, Finkel RC, Southon JR & Caffee, 1994. Estimation of Stratospheric input to the Arctic troposphere: 7Be and 10Be in aerosols at Alert, Canada. J Geophys Res 99(D6):12855-12864.

Dibb JE, Talbot RW, Klemm KI, Gregory GL, Singh HB, Bradshaw JD & Sandholm ST, 1996. Asian influence over the western North Pacific during the fall season: Inferences from lead 210, soluble ionic species and ozone. J Geophys Res 101(D1):1779-1792.

Dibb JE, Talbot RW, Lefer BL, Scheuer E, Gregory GL, Browell EV, Bradshaw JD Sandholm ST & Singh HB, 1997. Distributions of beryllium and lead 210, and soluble aerosol-associated ionic species over the western Pacific: PEM West B, February – March 1994. J Geophys Res 102(D23):28287-28302.

Dibb JE, Talbot RW, Meeker LD, Scheuer E, Blake NJ, Blake DR, Gregory GL & Sachse GW, 1999. Constraints on the age and dilution of Pacific Exploratory Mission – Tropics biomass burning plumes from the natural radionuclide tracer 210Pb. J Geophys Res 104(D13):16233-16241.

Eakins, J.D., Cambray, R.S., Chambers, K.C.& Lally, A.E., 1981. The transfer of natural and artificial radionuclides to Brotherswater from its catchment. AERE-R 10375, Harwell, 26pp.

Eakins, J.D., Cambray, R.S., Chambers, K.C.& Lally, A.E., 1984. The transfer of natural and artificial radionuclides to Brotherswater from its catchment. In: E.Y. Haworth and J.G.Lund (eds.), Lake Sediments and Environmental History, 125-144. Leicester Univ. Press.

Feely, H.W., Larson, R.J. & Sanderson, C.G., 1988. Factors that cause seasonal variations in 7Be concentrations in surface air. Annual Report of the Surface Air Sampling Program, Rep. EML-497, pp.91-165, U.S. Dept of Energy, Washington D.C.

Feichter, J., Brost, R.A., Heimann, M., 1991. Three-dimensional modelling of the concentration and deposition of 210Pb aerosols. J. Geophys. Res. 96 (D12), 22447-22460.

Gavini M.B., J.J.Beck & P.K. Kuroda, 1974. Mean Residence Times of the Long-lived Radon Daughters in the Atmosphere. J Geophys Res 79:4447-4452

Garcia-Leon M & Garcia-Tenorio R (1994). Low-level Measurements of Radioactivity in the Environment: Techniques and Applications - Proceedings of the Third International Summer School 20 Sep-2 Oct 1993. World Scientific, 584 pp.

Gillette DA, Blifford IH & Fenster CR, (1972). Measurements of aerosol size distributions and vertical fluxes of aerosols on land subject to wind erosion. J. Appl. Meteorol., 11:977-987.

Guelle, W., Balkanski, Y. J., Dibb, J. E., Schulz, M., Dulac, F., 1998a: Wet deposition in a global size-dependent aerosol transport model. 1. Comparison of a 1 year simulation with ground measurements. J Geophys. Res. 103D, 11,429–11,445.

Guelle W, Balkanski YJ, Dibb JE, Schulz M & Dulac F., 1998b. Wet deposition in a global size-dependent aerosol transport model. 2. Influence of the scavenging scheme on 210Pb vertical profiles, surface concentrations, and deposition. J Geophys Res 103(D22):28875-28891.

Hilton,J., E.Y.Haworth, W.Davison, M.Kelly, J.Hamilton-Taylor & P.G.Appleby, 1992. Transport processes of 137Cs in the aquatic environment. DOE Report for contract PECD 7/9/385. 97pp.

Israël, H., 1951. Radioactivity of the atmosphere. In Compendium of Meteorology, ed. T.F. Malone, Amer. Meteor. Soc., Boston, 155-161.

Jacobi, W., André, K., 1963. The vertical distribution of radon 222, radon 220 and their decay products in the atmosphere. J. Geophys. Res. 68(13), 3799–3814

Jonassen N. & M.H. Wilkening, 1970. Airborne measurements of radon 222 daughter ions in the atmosphere. J Geophys. Res. 75:1745-1752.

Junge CE, (1962). Note on the exchange rate between the northern and southern atmosphere. Tellus XIV, 242-246.

Junge CE, (1963). Air Chemistry and Radioactivity. Academic, New York.

Kirichenko LV (1970). Radon exhalation from vast areas according to vertical distribution of its short-lived decay products. J Geophys. Res. 75:3639-3649.

Krishnaswami S, Lal D, Martin JM & Meybeck M, (1971). Geochronology of lake sediments. Earth Planet. Sci. Lett., 11, 407–414.

Krishnaswami,S. & D.E.Seidmann, 1988. Comparative study of 222Rn, 40Ar, 39Ar, 37Ar leakage from rocks and minerals: Implications for the role of nanopores in gas transport through natural silicates. Geochim. Cosmochim. Acta, 52: 655-658.

Kritz M.A., 1990. The China Clipper – fast advective transport of radon-rich air from the Asian boundary layer to the upper troposphere near California. Tellus 42B:46-61.

Larson R.E., and Hoppel W.A., 1973. Radon 222 measurements below 4 km as related to atmospheric convection. Pure and Applied Geophysics 105:900-906.

Larson R.E., 1974. Radon profiles over Kilauea, the Hawaiian islands and Yukon Valley snow cover. Pure and Applied Geophysics 112:204-208.

Lauer NE, Hower JC, Hsu-Kim H, Taggart RK & Avner V, (2015). Naturally occurring Radioactive Materials in Coals and Coal Combustion Residuals in the United States. Environ. Sci. Technol.49 (18), pp 11227–11233 DOI: 10.1021/acs.est.5b01978

Liu, H., Jacob, D.J., Bey, I., Yantosca, R.M., 2001. Constraints from ^{210}Pb and ^{7}Be on wet deposition and transport in a global three-dimensional chemical tracer driven model driven ny assimilated meteorological fields. J. Geophys. Res.79, 4447-4452

Maberly SC, MM De Ville, SJ Thackeray, G Aimsworth, F Carse, JM Fletcher, R Groben, P Hodgson, JB James, JL Kelly, CD Vincent, DR Wilson, 2006. "A survey of the lakes of the English Lake District: The Lakes Tour 2005". Report to: Environment Agency, North West Region Date: April 2006 CEH Ref: LA/C02714/1, 87pp.

Maberly S, De Ville M, Thackeray S, Feuchtmayr H, Fletcher JM, James JB, Kelly JL, Vincent CD, Winfield IJ, Newton A, Atkinson D, Croft A, Drew H, Saag M, Taylor S, Titterington H (2011) A survey of the lakes of the English Lake District: The Lakes Tour 2010. Final report to the Environment Agency, Northwest region.

Monaghan, M.C., 1989. Lead-210 in surface air and soils from California: Implications for the behaviour of trace constituents in the planetary boundary layer. J. Geophys. Res. 94D, 6449-6456.

Moore H.E., S.E. Poet & E.A. Martell, 1973. 222Rn, 210Pb, 210Bi and 210Po profiles and aerosol residence times versus altitude. J Geophys. Res. 78:7065-7075.

Moore H.E., S.E. Poet E.A. Martell & MH Wilkening, 1974. Origin of 222Rn and its Long-lived Daughters in Air over Hawaii. J Geophys. Res. 79:5019-5024.

Nazarov LE, Kuzenkov AF, Malakhov SG, Volokitina LA, Gaziyev Ya I, Vasil'yev AS (1970). Radioactive aerosol distribution in the middle and upper troposphere over the USSR in 1963-1968. J Geophys. Res. 75:3575-3588.

Peirson, D.H., R.S.Cambray & G.S.Spicer, 1966. 210Pb and 210Po in the atmosphere. Tellus, 18:427-433.

Pennington, W., 1981. Records of a lake's life in time: the sediments. Hydrobiologia 79, 197-219.

Piliposian, G.T., Appleby, P.G., 2003. A simple model of the origin and transport of 222Rn and 210Pb in the atmosphere. Continuum Mech. Thermodyn., 15, 503-518.

Poet S.E., Moore H.E. and Martell E.A., 1972. Lead 210, Bismuth 210 and Polonium 210 in the atmosphere: accurate ratio measurement and application to aerosol residence time determination. J. Geophysical Research 77, 6515-6527.

Rasch, P.J., Feichter, J., Law, K., et al., 2000. A comparison of scavenging and deposition processes in global models: results from the WCRP Cambridge Workshop of 1995. Tellus 52B, 1025-1056.

Rehfeld, S., Heiman, M., 1995. Three dimensional atmospheric transport simulation of the radioactive tracers 210Pb, 7Be, 10Be, and 90Sr. J. Geophys. Res. 100, 26141-26161.

Robbins, J. A., 1978. Geochemical and geophysical applications of radioactive lead. In: Biogeochemistry of Lead in the Environment, ed. J. O. Nriagu. Elsevier Scientific, Amsterdam, 285-393.

Schillereff DN, Chiverrell RC, Macdonald N, Hooke JM, 2016. Hydrological thresholds and basin control over paleoflood records in lakes. Geology, 44; p. 43–46, doi:10.1130/G37261.1

Smith, F.B. & Clarke, M.J., 1989. The transport and deposition of airborne debris from the Chernobyl nuclear power plant accident with special emphasis on the consequences to the United Kingdom. Meteorological Office Scientific Paper 42, 56pp.

Smith, J.T., Appleby, P.G, Hilton, J. & Richardson, N., 1997. Inventories and fluxes of 210Pb, 137Cs and 241Am determined from the soils of three small catchments in Cumbria, UK. J. Environ. Radioact. 37:127-142.

Turekian, K.K., Nozaki, Y., Benninger, L.K., 1977. Geochemistry of atmospheric radon and radon products. Ann. Rev. Earth. Planet. Sci. 5, 227-255.

Turekian KK & JK Cochran, 1981. 210Pb in surface air at Enewetak and the Asian dust flux to the Pacific. Nature 292:522-523.

Warneck, P., 2000. Chemistry of the Natural Atmosphere. Academic Press, 927 pages.

Wilkening MH (1970). Radon 222 concentration in the convective patterns of a mountain environment. J. Geophys. Res. 75:1733-1740.

Wilkening, MH & Clements WE, (1975). Radon 222 from the ocean surface. J Geophys. Res. 80:3828-3830.

Wilkening ML, Clements WE & Stanley D (1975). Radon-222 flux in widely separated regions. In (ed. J.A.S. Stanley): The Natural Radiation Environment 2, Ch.38, pp.717-730. U.S. Energy and Research Development Administration, Oak Ridge, Tenn.

Wójcik M & Zuzel G, (2013). ^{226}Ra, ^{210}Pb, ^{210}Bi and ^{210}Po deposition and removal from surfaces and liquids. J Radioanal Nucl Chem. 296(2):639–645. doi:10.1007/s10967-012-2180-5

Appendices

Appendix 1.

P. Semertzidou, G.T. Piliposian, P.G. Appleby, *Atmospheric residence time of ^{210}Pb determined from the activity ratios with its daughter radionuclides ^{210}Bi and ^{210}Po,* Journal of Environmental Radioactivity, Vol. 160, August 2016, Pages 42-53.

Atmospheric residence time of ^{210}Pb determined from the activity ratios with its daughter radionuclides ^{210}Bi and ^{210}Po

Abstract. The residence time of ^{210}Pb created in the atmosphere by the decay of gaseous ^{222}Rn is a key parameter controlling its distribution and fallout onto the landscape. These in turn are key parameters governing the use of this natural radionuclide for dating and interpreting environmental records stored in natural archives such as lake sediments. One of the principal methods for estimating the atmospheric residence time is through measurements of the activities of the daughter radionuclides ^{210}Bi and ^{210}Po, and in particular the ^{210}Bi/^{210}Pb and ^{210}Po/^{210}Pb activity ratios. Calculations used in early empirical studies assumed that these were governed by a simple series of equilibrium equations. This approach does however have two failings; it takes no account of the effect of global circulation on spatial variations in the activity ratios, and no allowance is made for the impact of transport processes across the tropopause. This paper presents a simple model for calculating the distributions of ^{210}Pb, ^{210}Bi and ^{210}Po at northern mid-latitudes (30^{o}–65^{o}N), a region containing almost all the available empirical data. By comparing modelled ^{210}Bi/^{210}Pb activity ratios with empirical data a best estimate for the tropospheric residence time of around 10 days is obtained. This is significantly longer than earlier estimates of between 4–7 days. The process whereby ^{210}Pb is transported into the stratosphere when tropospheric concentrations are high and returned from it when they are low, significantly increases the effective residence time in the atmosphere as a whole. The effect of this is to significantly enhance the long range transport of ^{210}Pb from its source locations. The impact is illustrated by calculations showing the distribution of ^{210}Pb fallout versus longitude at northern mid-latitudes.

1. Introduction

The natural radionuclide ^{210}Pb is widely used for dating and interpreting environmental records stored in natural archives such as lake or marine sediments and peat bogs. Since the source of the ^{210}Pb is atmospheric fallout, models of the processes controlling its distribution in the atmosphere and subsequent deposition onto the Earth's surface are of considerable importance to this work. Outputs from the atmospheric model become inputs to models of the transport processes by which fallout deposited on the landscape accumulates in the sediment record. These terrestrial and aquatic models are of fundamental importance to the ^{210}Pb dating methodology. They are also essential to the use of sediment records for reconstructing historical levels of atmospheric pollution by e.g. heavy metals (lead and mercury) and persistent organic pollutants (POPs). Use of ^{210}Pb as a tracer for establishing the validity of these models requires good estimates of the atmospheric ^{210}Pb flux. Good estimates of the ^{210}Pb flux are also necessary to a reliable interpretation of ^{210}Pb dating calculations. Atmospheric models of ^{210}Pb are also of considerable interest to studies of global circulation and the long-range transport of atmospheric pollutants. The source of ^{210}Pb is well-known and relatively constant on timescales of a year or more. It is thus an ideal tracer for studying atmospheric processes on these longer timescales (Baskaran 2011; Rehfeld & Heimann, 1995).

One of the key parameters controlling the distribution of ^{210}Pb over the Earth's surface is its residence time in the atmosphere. This has been estimated using a number of different methods. One of the earliest estimates (Burton & Stewart, 1960) used two different approaches. The first, based on mass balance arguments for the ^{210}Pb inventory of a vertical column of air at Harwell in the UK, suggested a tropospheric residence time of around 17 days. The second, based on the activity ratios of ^{210}Pb and its grand-daughter radionuclide ^{210}Po, suggested values of 36 days from measurements in surface air at Harwell and 22-29 days from measurements on rainwater samples. Further measurements of the ^{210}Po/^{210}Pb activity ratio in surface air at Harwell carried out by Peirson et al. (1966) yielded a residence time of around 40 days. Since the measured values or ratios on which these calculations were based are unlikely to be representative of the atmosphere as a whole, and the equilibrium assumptions on which they were based unlikely to be realised, the validity of these results is highly uncertain.

Similar calculations were carried out by Poet et al. (1972) using the ^{210}Bi/^{210}Pb and ^{210}Po/^{210}Pb activity ratios in surface air and precipitation at Boulder, Colorado, and by Moore et al. (1973) using the ^{222}Rn, ^{210}Pb, ^{210}Bi and ^{210}Po activity ratios in tropospheric and lower stratospheric air at a range of continental sites over the United States. Residence times were calculated by assuming that the measured activities of ^{210}Pb and its daughters arise from the decay of ^{222}Rn in the atmosphere, and that their production and removal from the atmosphere are in steady state equilibrium. The parent/daughter relationship in the decay series was expressed by the equation

$$\dot{N}_2 = \lambda_1 N_1 - \lambda_2 N_2 - k N_2 = 0$$

where N_1 and N_2 are the numbers of atoms of the parent and daughter, λ_1 and λ_2 their radioactive decay constants, and k a first order rate constant for the removal of aerosols from the atmosphere. ^{210}Pb atoms are highly reactive and quickly attached to aerosol particles. It is reasonable therefore to suppose that the daughters are similarly attached and subject to the same removal rates.

Radionuclides are usually measured in terms of their activities (disintegrations per unit time), defined by $A_1 = \lambda_1 N_1$, $A_2 = \lambda_2 N_2$. In these terms the above equation becomes

$$\dot{A}_2 = \lambda_2 \dot{N}_2 = \lambda_2(\lambda_1 N_1 - \lambda_2 N_2 - k N_2) = \lambda_2(A_1 - A_2) - k A_2 = 0 \ .$$

Applying this to ^{210}Pb and its daughters, the relationships between them will be governed by the equations

$$\left.\begin{aligned} \lambda_{Bi}(A_{Pb} - A_{Bi}) - k A_{Bi} = 0 \\ \lambda_{Po}(A_{Bi} - A_{Po}) - k A_{Po} = 0 \end{aligned}\right\} \qquad (1)$$

where A_{Pb}, A_{Bi} and A_{Po} are the activities and λ_{Pb}, λ_{Bi}, λ_{Po} their radioactive decay constants. Rearranging, the activity ratios will satisfy the equations (c.f. Moore et al. 1973):

$$\frac{A_{Bi}}{A_{Pb}} = \frac{\lambda_{Bi}}{\lambda_{Bi} + k}, \qquad \frac{A_{Po}}{A_{Pb}} = \frac{\lambda_{Po}\lambda_{Bi}}{(\lambda_{Po} + k)(\lambda_{Bi} + k)} \qquad (2)$$

Given the activity ratios, each of these equations can be solved to yield a value for the removal rate k. The ^{210}Pb residence time will be $T = 1/k$ (or $\ln 2/k$ depending on the preferred convention). A similar approach was adopted by Gavini et al. (1974) who measured ^{210}Pb, ^{210}Bi and ^{210}Po activity ratios in rain samples from Fayetteville, Arkansas, and by Carvalho (1995) who measured their concentrations in surface air at Lisbon, Portugal.

Table 1 summarises mean values of the ^{210}Pb residence time calculated from the ^{210}Bi/^{210}Pb and ^{210}Po/^{210}Pb activity ratios in surface air and rainwater from the above studies. Possible causes of the large discrepancy between residence times calculated from ^{210}Bi/^{210}Pb ratios and those calculated from ^{210}Po/^{210}Pb ratios were thought to be inputs of older stratospheric air, or contamination by dust particles containing ^{210}Pb, ^{210}Bi and ^{210}Po in secular equilibrium (Poet et al. 1972; Gavini et al. 1974). Assuming the main cause to be dust contamination, Poet et al. (1972) corrected their estimates of the mean atmospheric residence time to ~4 days for particles in the lower troposphere and ~7 days for particles in precipitation. Using various arguments, Gavini et al. (1974) suggested mean residence times of ~30 days for aerosols in the troposphere and ~1 year for the stratosphere. While some of the reasons advanced may be factors, the main cause of error is almost certainly failure of the ^{210}Pb, ^{210}Bi and ^{210}Po activities in the samples to satisfy the equilibrium conditions implicit in equations (1). Since the concentrations of these radionuclides vary considerably with both geographical location and altitude, it is likely that their ratios will show similar variations. The main objective of this research is to model these variations and match the results to empirical data. This will provide a more accurate estimate of the ^{210}Pb atmospheric residence time, while also producing a simple yet reliable model of the distribution of fallout ^{210}Pb over the landscape.

Table 1

Atmospheric residence times calculated from ^{210}Pb, ^{210}Bi and ^{210}Po activity ratios in surface air and rainwater.

	Residence time from			
	^{210}Bi/^{210}Pb	^{210}Po/^{210}Pb	Location	Reference
Surface air	5 d	24 d	Boulder, Co	Poet et al. 1972
	9 d	24 d	Continental USA	Moore et al. 1973
	6 d	33 d	Lisbon, Portugal	Carvalho 1995
		36 d	Chilton, UK	Burton & Stewart 1960
		40 d	Chilton, UK	Peirson et al. 1966
Rainwater	8 d	19 d	Boulder, Co	Poet et al. 1972
	17 d	32 d	Fayetteville, Ark	Gavini et al. 1974
		22-29 d	Chilton, UK	Burton & Stewart 1960

2. Model equations and assumptions

The radioactive gas ^{222}Rn enters the atmosphere via exhalation from the land surface. Its subsequent distribution in the atmosphere is controlled by processes of advection,

115 diffusion, and radioactive decay. The distributions of the ^{222}Rn daughters ^{210}Pb, ^{210}Bi
116 and ^{210}Po are also influenced by the process of fallout. On short time-scales (hours or
117 days), these processes can only be accurately described by using detailed 3-
118 dimensional models (e.g. Feichter et al. 1991, Liu et al. 2001). Such models suffer
119 from two major disadvantages, they are very computationally intensive, and over
120 many parts of the world there is very little empirical data against which they can be
121 validated. They are also highly dependent on the extent to which the processes and
122 parameterizations on which they are based are accurate representations of real world
123 processes. An international workshop (Rasch et al. 2000) comparing different global
124 models found that they produced significantly different results for the atmospheric
125 distribution of ^{210}Pb.

126 On longer time-scales (time-averaged over a year or more), some of the
127 essential features of the available empirical data have been captured using simpler
128 models in which conservation principles are applied to a notional vertical column of
129 air moving horizontally over the Earth's surface, with little net transfer between
130 adjacent columns (Jacobi & André 1963, Turekian et al. 1977). Piliposian and
131 Appleby (2003) presented a more detailed model that took account of the vertical
132 distribution of ^{222}Rn and ^{210}Pb in the atmosphere. Here we extend that work to
133 include distributions of the ^{210}Pb daughters ^{210}Bi and ^{210}Po, and the ^{210}Bi/^{210}Pb and
134 ^{210}Po/^{210}Pb ratios used in studies of atmospheric residence times.

135 *2.1 Mass balance equations and models*

136 In view of the potential complexity in solving these simplified equations, it
137 will be useful to consider first the associated mass balance equations. Apart from
138 providing some justification of the validity of the simplified model, they can also be
139 used as a means for checking the validity of the numerical solutions.

140 If $\mathcal{F}$ denotes the mean global flux (per unit area) of ^{222}Rn from the Earth's land
141 surfaces, the mean supply rate to the atmosphere as a whole will be $A_L\mathcal{F}$ where A_L is
142 the effective area of the Earth's land surface contributing to this flux. The global
143 ^{222}Rn inventory in the atmosphere with activity denoted by Q_{Rn} will satisfy the balance
144 equation

145 $$\dot{Q}_{Rn} = A_E\mathcal{F} - \lambda_{Rn}Q_{Rn} \ . \qquad (3)$$

146 The global inventory of the ^{222}Rn daughter ^{210}Pb, the activity of which is denoted by
147 Q_{Pb}, will similarly satisfy the balance equation

$$\dot{Q}_{Pb} = \lambda_{Pb} Q_{Rn} - \lambda_{Pb} Q_{Pb} - A_E \mathcal{P} \quad (4)$$

(c.f. equations (1)) where $\mathcal{P}$ is the mean ^{210}Pb fallout rate from the atmosphere and A_E the area of the Earth's surface over which it is distributed. These equations exclude any supported ^{210}Pb, normally a small fraction, present on atmospheric dust particles. ^{210}Pb dating is concerned only with the unsupported component.

It is reasonable to suppose that on timescales of a year or more the global inventories are in a state of near equilibrium, that is, $\dot{Q}_{Rn} = \dot{Q}_{Pb} = 0$. Assuming further that the mean ^{210}Pb fallout rate is proportional to the global ^{210}Pb inventory we can write

$$A_E \mathcal{P} = k_g Q_{Pb} \quad (5)$$

where k_g is a mean global loss-rate coefficient. It then follows that the global ^{222}Rn inventory can be written

$$Q_{Rn} = \frac{A_L \mathcal{F}}{\lambda_{Rn}}$$

and the mean ^{210}Pb fallout rate

$$\mathcal{P} = \frac{k_g}{\lambda_{Pb} + k_g} \frac{\lambda_{Pb}}{\lambda_{Rn}} \frac{A_L}{A_E} \mathcal{F} .$$

Estimates of the ^{210}Pb atmospheric residence time suggest that it is measured in days or at most weeks, and so is negligible compared to the radioactive ^{210}Pb half-life (22.26 years). The radioactive decay constant λ_{Pb} will accordingly be negligible compared to the loss rate k_g. It follows that to a close approximation the above equation can be written

$$\mathcal{P} = \frac{\lambda_{Pb}}{\lambda_{Rn}} \frac{A_L}{A_E} \mathcal{F} . \quad (6)$$

If the ^{222}Rn emanation rate and decay constant are measured in Bq m^{-2} d^{-1} and d^{-1} and the ^{210}Pb decay constant measured in y^{-1}, from dimensional arguments this equation will give the ^{210}Pb flux in Bq m^{-2} y^{-1}.

Although applicable to the atmosphere as a whole, since there is relatively little exchange between the Northern and Southern Hemispheres these equations are to a good approximation also applicable to the two hemispheres separately. Whereas inter-hemispheric exchanges take place on timescales of a few years (Junge 1962), the atmospheric residence times of these radionuclides are measured in days or weeks. Estimates of the mean ^{222}Rn exhalation rate from land surfaces vary from ~0.7 atom

178 $cm^{-2}\ s^{-1}$ (Israël 1951) to ~1.2 atom $cm^{-2}\ s^{-1}$ (Turekian et al. 1977). Although the rate
179 will be highly variable on small spatio-temporal scales, it is reasonable to suppose that
180 mean values on longer time-scales of a year or more will be relatively constant (c.f.
181 Feichter et al. 1991, Liu et al. 2001). Here we assume a value of 1570 Bq $m^{-2}\ d^{-1}$
182 (0.87 atom $cm^{-2}\ s^{-1}$) determined from the atmospheric inventories at continental sites
183 where the vertical distribution is close to the equilibrium state (Piliposian, & Appleby
184 2003). This approach does in principle integrate inputs from all sources over large
185 geographical areas. Global balances have been calculated by applying the above figure
186 to the c.74% of Earth's continental land surface free of ice sheets, permafrost and
187 fresh water bodies (~1.1×10^8 km^2). We have also assumed an exhalation rate of ~10
188 Bq $m^{-2}\ d^{-1}$ (Wilkening & Clements 1975) from the oceans (~3.62×10^8 km^2). Given
189 that ~70% of the ice-free land is in the Northern Hemisphere, the mean ^{210}Pb flux
190 from the atmosphere is calculated to be ~80 Bq $m^{-2}\ y^{-1}$ in the Northern Hemisphere
191 and ~38 Bq $m^{-2}\ y^{-1}$ in the Southern Hemisphere. Considering the fact that information
192 on ^{210}Pb fallout over much of the Earth's surface (and particularly the oceans) is very
193 sparse, these figures are relatively consistent with values determined from the
194 Liverpool University ERRC (Environmental Radioactivity Research Centre) global
195 database on ^{210}Pb fallout. The ERRC holds one of the world's most comprehensive
196 collection of ^{210}Pb fallout data, accumulated over a period of more than 30 years as
197 part of the program of ^{210}Pb dating. These data suggest a mean ^{210}Pb flux of ~73 Bq
198 $m^{-2}\ y^{-1}$ in the Northern Hemisphere and ~39 Bq $m^{-2}\ y^{-1}$ in the Southern Hemisphere
199 (Appleby & Piliposian, 2010).
200 Data from sites in continental USA, Europe and Asia lying within the largely
201 ice-free northern mid-latitudes (30^o-65^oN) suggest that the ^{222}Rn-^{210}Pb cycle
202 (measured on long time-scales) is largely self-contained in this zone. Since dry land
203 occupies around 51% of this total area it follows from equation (6) that ^{222}Rn
204 exhalation would if contained generate a mean ^{210}Pb flux of 139 Bq $m^{-2}\ y^{-1}$. The mean
205 empirical value from our database is ~136 Bq $m^{-2}\ y^{-1}$. Given that intrahemispheric
206 mixing is thought to take place on timescales of a few months (Warneck 2000), this
207 approximate balance (though once again keeping in mind the sparsity of the data) is
208 again consistent with the notion that ^{210}Pb has a relatively short tropospheric residence
209 time. The distribution of fallout within this zone is however strongly influenced by
210 the major continental land masses. Driven by the predominantly west-to-east global
211 circulation, air masses arriving at the western margins of North America and Eurasia

212 are depleted in ^{222}Rn and ^{210}Pb during their passage over the Pacific and Atlantic
213 oceans but replenished by ^{222}Rn exhalation during their passage over the land masses.
214 This is demonstrated by the regional data on mean annual fallout of ^{210}Pb in North
215 America and Eurasia shown in Figure 1. Fallout data from the Liverpool University
216 ERRC database (encompassing data from around 250 sites) has been grouped together
217 on a regional basis and mean values calculated for each region. ^{210}Pb fallout has its
218 highest values near the eastern margins of the continental land masses where the flux
219 can exceed 200 Bq m^{-2} y^{-1} (per meter of rainfall).

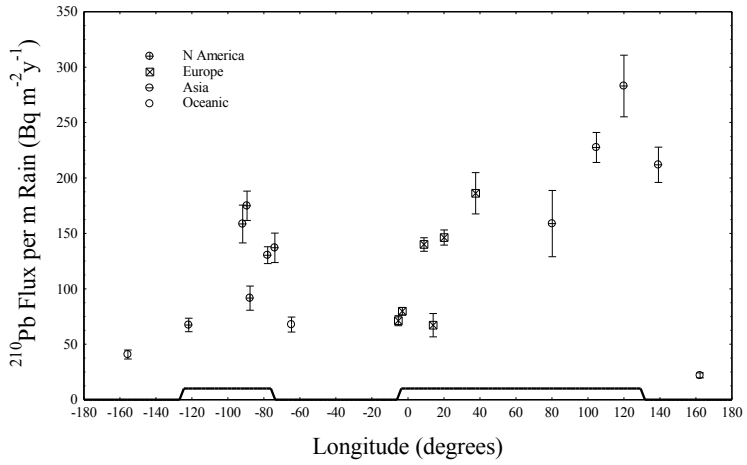

220

221 **Figure 1.** Mean annual fallout of ^{210}Pb (normalised against rain) at sites in North America and Eurasia
222 extracted from the Liverpool University ERRC global database. Each point represents the average
223 value for all fallout data within a given geographical region.
224

225 A similar distribution was obtained theoretically by Turekian et al. (1977) by
226 applying mass balance principles to a notional vertical column of air moving over the
227 Earth's surface at northern mid latitudes. The model assumed a predominately west-
228 to-east global circulation, a steady circulation velocity, a uniform ^{222}Rn exhalation rate
229 from land surfaces and negligible emissions from the oceans. It also assumed a mean
230 ^{210}Pb residence time of 5 days. Writing Q_{Rn} and Q_{Pb} for the radionuclide inventories
231 of the column per unit area the calculations in effect solved equations (3)–(5) to
232 determine variations in the ^{210}Pb flux $\mathcal{P}$ with longitude.

233 *2.2 Transport processes within the air column*

234 A major limitation of mass balance models is that they give no information
235 about the vertical distribution of the radionuclides within the column. Nor do they
236 take into account the reservoir effect of the stratosphere. The fallout equation (5) is
237 only applicable to that component of the ^{210}Pb distribution lying within the
238 troposphere. A significant stratospheric component built up during passage over major

land masses is slowly released to the troposphere as the air column moves out over large water bodies and the troposphere becomes depleted by fallout. The principal mechanism controlling the vertical distribution of ^{222}Rn and its daughters within an air column will be turbulent diffusion (Jacobi & André 1963). Since ^{222}Rn (half-life 3.825 days) is an inert gas it is removed from the column only by radioactive decay. Assuming a Lagrangian coordinate system imbedded in the column, its distribution will thus satisfy the partial differential equation

$$\frac{\partial C_{Rn}}{\partial t} = \frac{\partial}{\partial z}\left(D \frac{\partial C_{Rn}}{\partial z} \right) - \lambda_{Rn} C_{Rn} \tag{7}$$

where $C_{Rn}(z,t)$ denotes the ^{222}Rn concentration (in Bq m^{-3}) at altitude z and time t, D is an effective vertical diffusivity, and λ_{Rn} is the ^{222}Rn radioactive decay constant. The boundary conditions are

$$-D \left. \frac{\partial C_{Rn}}{\partial z} \right|_{(0,t)} = \mathcal{F}, \qquad C_{Rn}(z,t) \to 0 \text{ as } z \to \infty \tag{8}$$

where $\mathcal{F}$ denotes the ^{222}Rn flux (in Bq m^{-2}) by emanation from the Earth's surface into the base of the column. In contrast to ^{222}Rn, ^{210}Pb atoms are highly reactive and readily adsorbed onto dust particles, and may be removed from the atmosphere by wet and dry deposition, as well as by radioactive decay to its daughter radionuclides ^{210}Bi (half-life 5.013 d) and ^{210}Po (half-life 138.4 d). Adding terms for this process, the ^{210}Pb concentration $C_{Pb}(z,t)$ (in Bq m^{-3}) will be governed by the partial differential equation

$$\frac{\partial C_{Pb}}{\partial t} = \frac{\partial}{\partial z}\left(D \frac{\partial C_{Pb}}{\partial z} \right) + \lambda_{Pb}(C_{Rn} - C_{Pb}) - \Lambda(C_{Pb}) \tag{9}$$

and boundary conditions

$$\left. \frac{\partial C_{Pb}}{\partial z} \right|_{(0,t)} = 0, \qquad C_{Pb}(z,t) \to 0 \text{ as } z \to \infty \tag{10}$$

where $\Lambda(C_{Pb})$ is a term characterizing the rate at which ^{210}Pb condenses from the aerosol state dominated by turbulent diffusion to incipient precipitation dominated by gravity. In Piliposian and Appleby (2003) equations (7)–(10) were solved numerically, assuming a constant diffusivity $D = 2.7\ \text{km}^2\ \text{d}^{-1}$ ($3.1 \times 10^5\ \text{cm}^2\ \text{s}^{-1}$) and a mean ^{222}Rn flux from land surfaces of $1570\ \text{Bq m}^{-2}\ \text{d}^{-1}$. The values of these parameters were determined from vertical ^{222}Rn distributions at sites where this radionuclide appeared to have reached equilibrium. The fact that the mean empirical profiles at

these sites could be represented by an exponential relation suggests that the assumption of a constant diffusivity is a reasonable first approximation. We follow Piliposian and Appleby (2003) in supposing that droplet formation occurs only in the troposphere. The value of the term $\Lambda(C_{Pb})$ characterizing the rate at which ^{210}Pb condenses from the aerosol state is thus effectively zero in the stratosphere. Its value in the troposphere was assumed to be proportional to the ^{210}Pb concentration and so could be written

$$\Lambda(C_{Pb}) = \kappa C_{Pb} \{1–\mathrm{H}(z–z_1)\}$$

where κ is a tropospheric removal rate constant, $\mathrm{H}(z)$ the Heaviside function defined by

$$\mathrm{H}(z) = \begin{cases} 0 & z \le 0 \\ 1 & z > 0 \end{cases},$$

and z_1 the height of the tropopause. The reciprocal of κ is a measure of the tropospheric residence time. It is again important to emphasise that these equations and concepts are only meaningful when applied to quantities time-averaged over sufficiently long time-scales to smooth out short-term fluctuations. For numerical calculations it was more practical, both from a mathematical and physical point of view, to replace the Heaviside function by the differentiable function

$$\tfrac{1}{2}(1 + \tanh(\beta z)) ,$$

whence

$$\Lambda(C_{Pb}) = \kappa C_{Pb} \left\{ \tfrac{1}{2}(1 - \tanh(\beta z)) \right\}.$$

This will give a transition zone at the tropopause of thickness δ across which the value of the term

$$\tfrac{1}{2}(1 - \tanh(\beta z))$$

in the condensation function declines from 0.95 to 0.05 provided β is chosen so that $\beta > 3/\delta$.

The transport processes for ^{210}Bi and ^{210}Po can reasonably be presumed to follow those of ^{210}Pb. Much of their production will take place after ^{210}Pb atoms have become attached to dust or aerosol particles. The atmospheric concentrations of ^{210}Bi and ^{210}Po (in Bq m^{-3}) can thus be assumed to satisfy the partial differential equations

$$\frac{\partial C_{Bi}}{\partial t} = \frac{\partial}{\partial z}\left(D \frac{\partial C_{Bi}}{\partial z} \right) + \lambda_{Bi}(C_{Bi} - C_{Pb}) - \Lambda(C_{Bi}) \qquad (11)$$

$$\frac{\partial C_{Po}}{\partial t} = \frac{\partial}{\partial z}\left(D\frac{\partial C_{Po}}{\partial z} \right) + \lambda_{Po}(C_{Po} - C_{Bi}) - \Lambda(C_{Po}) \tag{12}$$

together with the boundary conditions

$$\left.\frac{\partial C_{Bi}}{\partial z}\right|_{(0,t)} = 0, \qquad C_{Bi}(z,t) \to 0 \text{ as } z \to \infty, \tag{13}$$

$$\left.\frac{\partial C_{Po}}{\partial z}\right|_{(0,t)} = 0, \qquad C_{Po}(z,t) \to 0 \text{ as } z \to \infty. \tag{14}$$

Here we solve these equations numerically and use the results to calculate the distributions of the isotope ratios ^{210}Bi/^{210}Pb and ^{210}Po/^{210}Pb for different values of the tropospheric removal rate constant κ. The results are compared with the available empirical data in order to determine the extent to which these data can be used to provide a good estimate of the tropospheric residence time.

3. Numerical approach

The value of the ^{222}Rn flux $\mathcal{F}$ in the boundary condition (8) for equation (7) will depend mainly on whether the column is moving over land or water. Exhalation rates from oceans are estimated to be two orders of magnitude less than those from ice-free land surfaces. Although the distributions of ^{222}Rn and its daughter radionuclides ^{210}Pb, ^{210}Bi and ^{210}Po for the case of a prolonged ^{222}Rn flux $\mathcal{F}$ into the base of the column can be obtained by using the MATHEMATICA software to solve *ab initio* the system of partial differential equations and boundary conditions (7)–(14), a numerically more stable solution is obtained by using a Green's function approach, whereby we first consider the response of the system to a brief impulsive input of ^{222}Rn

$$\mathcal{F}(t) = I_0\delta(t) \tag{15}$$

where $\delta(t)$ is the Dirac delta function. The response to a prolonged ^{222}Rn input can then be constructed by representing it as a series of discrete inputs and superimposing the responses to different inputs at different times.

Under conditions of a constant diffusivity the ^{222}Rn distribution for a brief impulsive input has the exact analytical solution

$$C_{Rn}(z,t) = I_0\, \mathrm{e}^{-\lambda_{Rn}t}\, \frac{1}{\sqrt{\pi D t}}\, \mathrm{e}^{-\frac{z^2}{4Dt}} = I_0 G_{Rn}(z,t) \tag{16}$$

where

$$G_{Rn}(z,t) = \frac{\mathrm{e}^{-\lambda_{Rn} t}}{\sqrt{\pi D t}} \mathrm{e}^{-\frac{z^2}{4Dt}} \tag{17}$$

is the response to a unit input at time $t = 0$ (Piliposian &Appleby 2001). Substituting this function into equation (9) the three partial differential equations for ^{210}Pb, ^{210}Bi and ^{210}Po were solved in turn numerically to give three Green's functions

$$G_{Pb}(z,t), \quad G_{Bi}(z,t), \quad G_{Po}(z,t) \tag{18}$$

characterising the further responses of the system to an impulsive ^{222}Rn input. Numerical calculations of these functions have been carried out for values of the tropospheric removal rate constant κ ranging from 0.08 d^{-1} (12.5 days residence time) to 0.3 d^{-1} (3.3 days residence time).

For a prolonged ^{222}Rn flux $\mathcal{F}(s)$ $(0 < s < t)$, noting that the contribution of the amount of ^{222}Rn injected into the atmosphere at time τ during the time interval $\mathrm{d}\tau$ to the ^{222}Rn distribution at time t will be

$$G_{Rn}(z, t-\tau)\mathcal{F}(\tau)\,\mathrm{d}\tau = G_{Rn}(z,s)\mathcal{F}(t-s)\,\mathrm{d}s \quad \text{where } s = t-\tau$$

the ^{222}Rn distribution has an exact analytical form

$$C_{Rn}(z,t) = \int_0^t \frac{\mathrm{e}^{-\lambda_{Rn} s}}{\sqrt{\pi D s}} \mathrm{e}^{-\frac{z^2}{4Ds}} \mathcal{F}(t-s)\,\mathrm{d}s = \int_0^t G_{Rn}(z,s)\mathcal{F}(t-s)\,\mathrm{d}s \ . \tag{19}$$

The distributions of the daughter radionuclides can similarly be written

$$\left.\begin{aligned} C_{Pb}(z,t) &= \int_0^t G_{Pb}(z,s)\mathcal{F}(t-s)\,\mathrm{d}s \\ C_{Bi}(z,t) &= \int_0^t G_{Bi}(z,s)\mathcal{F}(t-s)\,\mathrm{d}s \\ C_{Po}(z,t) &= \int_0^t G_{Po}(z,s)\mathcal{F}(t-s)\,\mathrm{d}s \end{aligned}\right\} \tag{20}$$

though these must be determined numerically. The procedure used for carrying out these calculations is given in the Appendix A. The validity of the solutions has been checked very carefully using mass balance arguments, by comparison with the equilibrium ^{222}Rn distribution for a constant ^{222}Rn flux over a long period of time, and also by comparison with standard numerical solutions of the governing equations using MATHEMATICA. Although the two methods were in good agreement over short to medium time-scales, the Green's function method was numerically much more stable over long time-scales, where ^{222}Rn concentrations had decayed to very low values.

4. Global equilibrium distribution for northern mid-latitudes

The above approach is used here to model the mean annual distribution of the ^{222}Rn daughters ^{210}Pb, ^{210}Bi, and ^{210}Po in the atmosphere at northern mid-latitudes. The results are fitted to the available empirical data in order to determine a best value for the removal rate constant κ. From a model validation point of view these regions, defined as 30°–65° N spanning continental USA and Western Europe as far north as central Scandinavia (Fig. 2), have the advantage of a relatively good coverage of data on the distribution and fallout of ^{210}Pb (Fig.1). They also cover virtually all the available empirical data on the daughter products ^{210}Bi and ^{210}Po (Table 1).

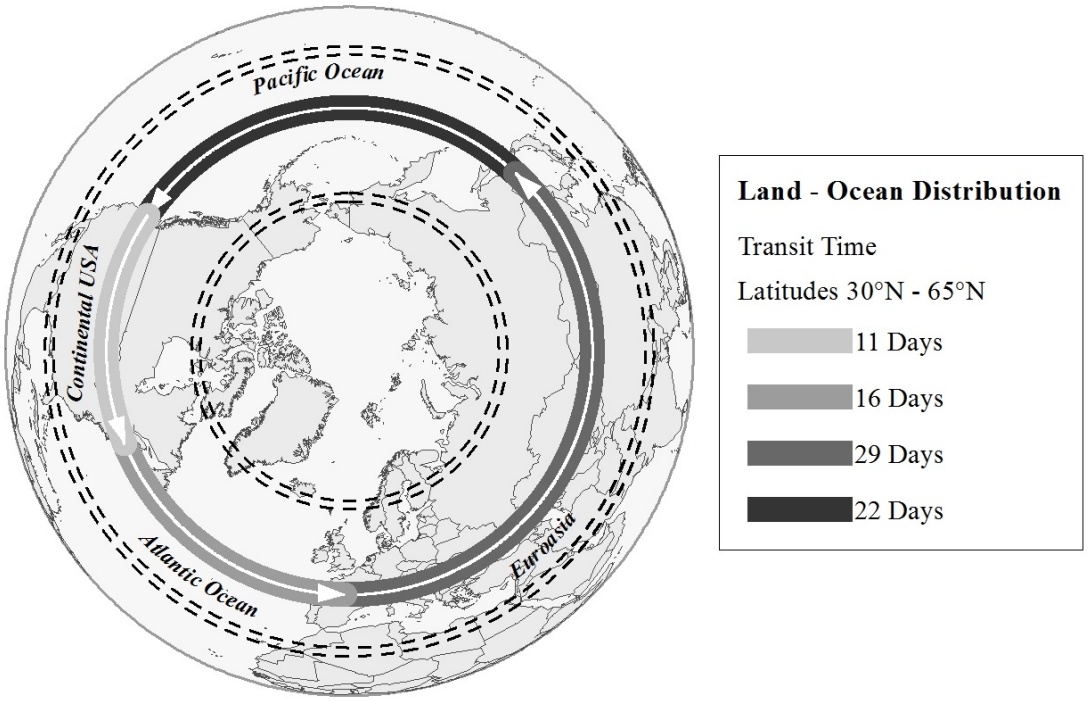

Figure 2. Map of the Earth's northern hemisphere showing the land lying between 30°–65° N. Also shown are the approximate transit times across the major land masses and oceans for a notional air column moving from west to east.

Although ^{222}Rn exhalation rates from land surfaces are subject to short-term seasonal and weather-related fluctuations, mean annual inputs to the atmosphere will be relatively constant on longer timescales of a year or more. On these timescales the mean annual spatial distributions of the ^{222}Rn daughters ^{210}Pb, ^{210}Bi, and ^{210}Po will also be similar from year to year. The distribution within a notional column moving from west to east may thus be assumed to be a periodic function of longitude θ (period

360^o), or equivalently, of the time t with a period equal to the global transit time T. Using estimates from a range of different sources, Piliposian and Appleby (2003) estimated the mean annual global transit time to be around 78 days. Since the largely ice-free land within these northern mid-latitudes occupies roughly 51% of the total area, on each circuit and the column would spend 40 days over land and 38 days over the ocean. To a reasonable approximation, this can be divided into 11 days over North America, 16 days over the Atlantic, 29 days over Eurasia, and 22 days over the Pacific. Assuming a ^{222}Rn exhalation rate over land of $\mathcal{F} = 1570$ Bq m^{-2} d^{-1}, and negligible inputs from the oceans, the ^{222}Rn exhalation rate into the base of the column will be

$$\mathcal{F}(t) = \mathcal{F}\{\mathrm{H}(t-t_0) - \mathrm{H}(t-t_1) + \mathrm{H}(t-t_2) - \mathrm{H}(t-t_3)\} \qquad (21)$$

where t_0 is the time at which the column crosses the western seaboard of North America, t_1 the time at which it crosses the eastern seaboard, t_2 the time at which it crosses the western seaboard of Europe, and t_3 the time at which it crosses the eastern margin of the Eurasian land mass. For numerical calculations the Heaviside function H(t) can be approximated by the differentiable function

$$\tfrac{1}{2}(1 + \tanh(\alpha t))$$

where the value of the parameter α is chosen so as to give suitably small transition zones across seaboards.

4.1 Equilibrium Green's functions

Solving the governing partial differential equations (7)–(14) starting from a zero initial condition, in order to determine the equilibrium (periodic) distribution it would be necessary to track the solution over several circuits of the globe. This approach can however result in the build up of significant numerical errors. The process can be simplified, and made more accurate by introducing the notion of an equilibrium Green's function.

Each time the column passes a fixed point on the Earth's surface it will receive a brief impulsive input of ^{222}Rn from that point the strength of which we denote by I_0. Setting the time $t = 0$ just as the column passes this point, the distribution of ^{222}Rn in the column at times $t > 0$ due to the input from this location at time $t = 0$ will be $I_0 G_{Rn}(z,t)$ (equation (16)). The distribution at time t due to the input from the same

location on the previous circuit (at time $-T$) will be $I_0 G_{Rn}(z,t+T)$. Adding the contributions from inputs on all previous occasions (at times $-kT$, $k = 0,1,2,\ldots$), the distribution in the column at times $0 < t < T$ due to present and past inputs from this location will be

$$I_0\{G_{Rn}(z,t) + G_{Rn}(z,t+T) + G_{Rn}(z,t+2T) + \cdots\cdots\} = I_0 G_{Rn}^{equ}(z,t) \qquad (22)$$

where

$$G_{Rn}^{equ}(z,t) = \sum_{k=0}^{\infty} G_{Rn}(z,t+kT) \qquad (23)$$

represents an equilibrium Green's function for the ^{222}Rn distribution. Since the distribution at time $t+T$ will be the same as the distribution at time t, this function will be a periodic function of period T.

The solutions for the ^{222}Rn daughters due to this impulse can be similarly written as periodic functions

$$\left.\begin{aligned} I_0 G_{Pb}^{equ}(z,t) &= I_0 \sum_{k=0}^{\infty} G_{Pb}(z,t+kT) \\ I_0 G_{Bi}^{equ}(z,t) &= I_0 \sum_{k=0}^{\infty} G_{Bi}(z,t+kT) \\ I_0 G_{Po}^{equ}(z,t) &= I_0 \sum_{k=0}^{\infty} G_{Po}(z,t+kT) \end{aligned}\right\} \qquad (24)$$

where $G_{Pb}(z,t)$, $G_{Bi}(z,t)$, $G_{Po}(z,t)$ are the corresponding Green's functions for a single impulsive input. The equilibrium Green's functions $G_{Pb}^{equ}(z,t)$, $G_{Bi}^{equ}(z,t)$, $G_{Po}^{equ}(z,t)$ are easily generated by continuing to add terms from previous circuits, up until the values are negligible. In practice we found that 6 periods were sufficient for the longer-lived ^{222}Rn daughters, although because of its short half-life, one period (78 days) was sufficient for ^{222}Rn itself.

Using this concept, the contribution to the equilibrium of ^{222}Rn distribution at longitude θ due to ^{222}Rn emissions from the Earth's surface lying between longitudes ϕ and $\phi - \delta\phi$ will be

$$G_{Rn}^{equ}(z,s)\mathcal{F}(\phi)\,\delta s$$

where $\mathcal{F}(\phi)$ is the ^{222}Rn exhalation rate at longitude ϕ, s is the travel-time in a west-to-east direction to reach longitude θ, and δs is the time taken for the column to traverse the incremental longitude $\delta\phi$. If V (= $360^o/T$) is the circulation velocity, so that $\phi = \theta - Vs$ and $\delta s = \delta\phi / V$, the equilibrium ^{222}Rn distribution at longitude θ will include all such contributions, and will thus be

$$C_{Rn}^{equ}(z,\theta) = \int_0^T G_{Rn}^{equ}(z,s)F(\theta - Vs)\,\mathrm{d}s \quad . \tag{25}$$

The equilibrium distributions of the daughter radionuclides can similarly be written

$$\left.\begin{aligned} C_{Pb}(z,t) &= \int_0^T G_{Pb}^{equ}(z,s)F(\theta - Vs)\,\mathrm{d}s \\ C_{Bi}(z,t) &= \int_0^t G_{Bi}^{equ}(z,s)F(\theta - Vs)\,\mathrm{d}s \\ C_{Po}(z,t) &= \int_0^t G_{Po}^{equ}(z,s)F(\theta - Vs)\,\mathrm{d}s \end{aligned}\right\} . \tag{26}$$

The numerical procedure for carrying out these calculations is given in Appendix A.

5. Results

5.1 ^{210}Bi/^{210}Pb and ^{210}Po/^{210}Pb concentration ratios in ground-level air

Figure 3 plots modelled values of the ^{210}Bi/^{210}Pb and ^{210}Po/^{210}Pb concentration ratios in ground-level air at mid-latitudes as functions of longitude θ for values of the tropospheric removal rate constant κ ranging from 0.08 d^{-1} to 0.2 d^{-1} calculated using equations (26). Also shown are mean empirical values calculated from all the measurements of ^{210}Pb, ^{210}Bi and ^{210}Po in ground level air carried out at sites in Colorado (~105^{o} W, Poet et al. 1972), Lisbon Portugal (~9^{o} W, Carvalho 1995) and Hawaii (~156^{o} W, Moore et al. 1974) and from ^{210}Pb and ^{210}Po measurements at Harwell UK (~1^{o} W, Burton & Stewart 1960; Peirson et al. 1966).

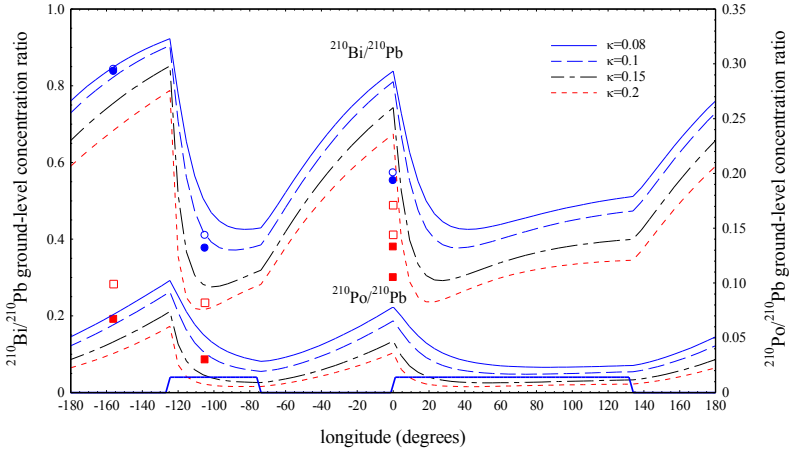

Figure 3. Modelled values of the ^{210}Bi/^{210}Pb (left-hand axis) and ^{210}Po/^{210}Pb (right-hand axis) activity ratios in ground-level air at northern mid-latitudes plotted versus longitude for values of the tropospheric removal rate constant ranging from 0.08 d^{-1} to 0.2 d^{-1}, showing also the major land masses. Mean activity ratios for Hawaii, the interior of the USA, and the western margin of Europe calculated from all the available empirical data are shown by the symbols ○ (^{210}Bi/^{210}Pb) and □ (^{210}Po/^{210}Pb). Unsupported activity ratios are represented by the solid symbols (●, ■).

It is evident from these results that for any given value of κ the theoretical ^{210}Bi/^{210}Pb and ^{210}Po/^{210}Pb concentration ratios vary considerably, the variations

largely being governed by the position of the air column relative to major land masses. The $^{210}Bi/^{210}Pb$ ratio increases rapidly over large oceans to values close to unity (radioactive equilibrium). Renewed ^{210}Pb production at the western margins of the major land masses causes its value to fall dramatically, reaching a minimum value after approximately 4 days in the case of $\kappa = 0.2$ (minimum value 0.23) or 7 days in the case of $\kappa = 0.08$ (minimum value 0.43). As the column moves further into the land mass, increased ^{210}Bi production results in a gradual increase in the $^{210}Bi/^{210}Pb$ ratio. Reduced ^{210}Pb production once the column has crossed the eastern seaboard and moves out over the ocean causes a sharp acceleration in the rate of increase. The $^{210}Po/^{210}Pb$ ratios follow a similar pattern though values are an order of magnitude lower due to the longer ^{210}Po half-life.

Empirical values of the raw $^{210}Bi/^{210}Pb$ concentration ratio in surface air at the Colorado site ranged from 0.18-0.65 with a mean value of 0.41 ± 0.02. Those at Lisbon ranged from 0.12-1.33 with a mean value of 0.57 ± 0.10, whilst those at Hawaii at sea level on the windward side of the island ranged from 0.81-0.97 with a mean value of 0.84 ± 0.03. The results from the Colorado and Hawaiian sites suggest that the value of κ lies between 0.08 and 0.1. Although measured results from Lisbon suggest a higher value of κ, its position on the western edge of Europe where values of the $^{210}Bi/^{210}Pb$ concentration ratio change rapidly with distance makes the use of data from this location highly problematic. Further, the mean value may well be significantly influenced by local prevailing factors. $^{210}Bi/^{210}Pb$ values at this site determined during times of westerly air flows will have much higher values than those determined during times of easterly conditions.

$^{210}Po/^{210}Pb$ ratios are an order of magnitude lower than the $^{210}Bi/^{210}Pb$ ratios. Raw values at ground-level at the Colorado site ranged from 0.03-0.25 with a mean value of 0.082 ± 0.012. Those at Lisbon ranged from 0.03-0.78 with a mean value of 0.17 ± 0.05. The mean value at Harwell, also a problematic location, was 0.16 ± 0.05. At Hawaii the $^{210}Po/^{210}Pb$ ratio at sea level on the windward side of the island ranged from 0.08-0.18 with a mean value of 0.10 ± 0.01. Although these results appear to suggest a significantly lower value of κ, the most likely explanation for the discrepancy would appear to be contamination of samples by ground-level dust containing supported ^{210}Pb and its daughters in radioactive equilibrium (Poet et al. 1972; Baskaran 2011). Writing $p = {}^{226}Ra/^{210}Pb$ for the supported ^{210}Pb fraction the

unsupported activities will be $(1-p)^{210}$Pb, ^{210}Bi$-p^{210}$Pb, ^{210}Po$-p^{210}$Pb. The amount of supported activity can then be estimated by adjusting the value of p so that the unsupported ^{210}Bi/^{210}Pb and ^{210}Po/^{210}Pb activity ratios yield the same value of κ. The results of these calculations, shown in Table 2, suggest a relatively low amount of supported ^{210}Pb, varying from 3.4% to 5.3% of the total ^{210}Pb activity. Because of the low ^{210}Po activities this correction has a disproportionate effect on the ^{210}Po/^{210}Pb ratio, as shown in Figure 3. The effect on the much higher ^{210}Bi/^{210}Pb ratio was relatively insignificant. Excluding the data from the West-European seaboard (Lisbon and Harwell) the value of κ was calculated to be between 0.09 ± 0.02 d^{-1} (Hawaiian data) and 0.11 ± 0.01 d^{-1} (Colorado data).

5.2 ^{210}Bi/^{210}Pb and ^{210}Po/^{210}Pb tropospheric inventory ratios

Figure 4 shows modelled values of the ^{210}Bi/^{210}Pb and ^{210}Po/^{210}Pb tropospheric inventory ratios calculated for values of the tropospheric removal rate constant κ ranging from 0.08 d^{-1} to 0.2 d^{-1}. The results follow a similar pattern to those for ground-level air. ^{210}Bi/^{210}Pb ratios increase rapidly over large oceans to values close to radioactive equilibrium, but then fall steeply as the column arrives at the western margins of the major land masses. Minimum values over the land masses are reached after around 6 days in the case $\kappa = 0.2$ d^{-1} (minimum value 0.32) or 10 days in the case $\kappa = 0.08$ d^{-1} (minimum value 0.53). ^{210}Po/^{210}Pb ratios are again an order of magnitude lower than the ^{210}Bi/^{210}Pb ratios.

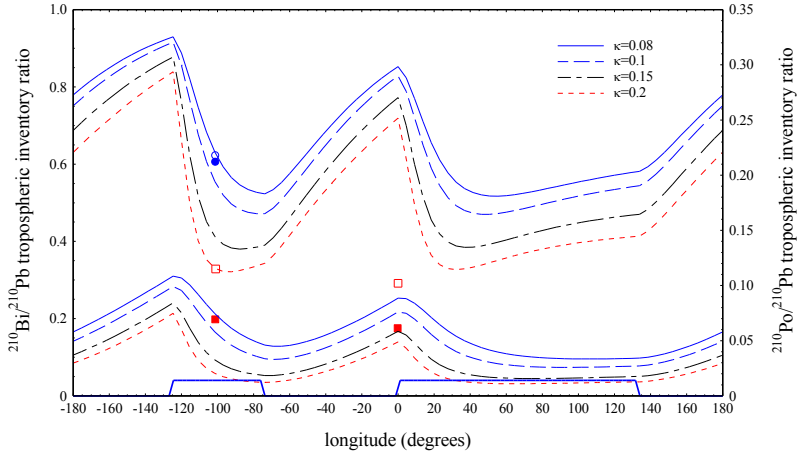

Figure 4. Modelled values of the ^{210}Bi/^{210}Pb (left-hand axis) and ^{210}Po/^{210}Pb (right-hand axis) tropospheric inventory ratios at northern mid-latitudes plotted versus longitude. Values of the tropospheric removal rate constant range from 0.08 d^{-1} to 0.3 d^{-1}, also showing the major land masses. Mean activity ratios for the interior of the USA and the western margin of Europe, calculated from all the available empirical data, are shown by the symbols ○ (^{210}Bi/^{210}Pb) and □ (^{210}Po/^{210}Pb). Unsupported activity ratios are represented by the solid symbols (●, ■).

Since the isotopic composition of the troposphere as a whole is likely to be reflected in the isotopic composition of rainwater, empirical measurements of the $^{210}Bi/^{210}Pb$ and $^{210}Po/^{210}Pb$ tropospheric inventory ratios are most readily made using rainwater samples. Measurements of ^{210}Pb, ^{210}Bi and ^{210}Po in rainwater were carried out at sites in Colorado (~105° W, Poet et al. 1972) and Arkansas (94° W, Gavini et al. 1974). Measurements of ^{210}Pb and ^{210}Po in rainwater were carried out at Harwell (Burton & Stewart 1960). A more direct estimate of tropospheric inventory ratios can be made using measured profiles of ^{210}Pb, ^{210}Bi and ^{210}Po in the atmosphere. Concentrations of these radionuclides at altitudes ranging from ground-level up to 17 km were determined by Moore et al. (1973) at a number of sites in continental USA ranging from Utah (~112° W) to Kansas (~95° W). Many of the measurements were repeated on a number of separate occasions. Tropospheric inventories calculated by combining all the atmospheric profiles yielded a mean $^{210}Bi/^{210}Pb$ ratio of 0.52 ± 0.05. Values calculated from rainwater measurements at the Colorado site ranged from 0.48–0.84 with a mean value of 0.61 ± 0.01. Those from the Arkansas site ranged from 0.32–1.05 with a mean value of 0.74 ± 0.10. Averaging all these results, a best estimate of the mean $^{210}Bi/^{210}Pb$ tropospheric inventory ratio for the interior of continental USA is 0.62 ± 0.04. Similar calculations of the mean $^{210}Po/^{210}Pb$ tropospheric inventory ratio for the interior of continental USA yielded values of 0.14 ± 0.03 from the atmospheric profiles, 0.061 ± 0.005 from the Colorado rainwater measurements, and 0.13 ± 0.02 from the Arkansas rainwater measurements, with a mean value of 0.11 ± 0.02. The Harwell rainwater measurements had a mean $^{210}Po/^{210}Pb$ ratio of 0.10 ± 0.02.

The raw tropospheric $^{210}Bi/^{210}Pb$ ratio from the continental USA suggests a value of κ comparable to that determined from the ground-level data. The raw $^{210}Po/^{210}Pb$ activity ratio again suggests a much lower value, presumably due to the disproportionate effect of a small amount of supported activity estimated in this case to be just 4.4% of the total ^{210}Pb activity. The corrected unsupported activity ratios are shown in Figure 4. These results, also given in detail in Table 2, yielded a value of $\kappa = 0.09 \pm 0.01\ d^{-1}$ similar to that determined from the ground-level data. Averaging the results from both data sets, a best estimate of the tropospheric removal rate constant is $0.097 \pm 0.012\ d^{-1}$, corresponding to a residence time of 10.3 ± 1.2 days. In practice we round these figures to $\kappa = 0.10\ d^{-1}$ and the residence time to 10 days.

548 **Table 2**

549 Mean values of the empirical ^{210}Pb, ^{210}Bi and ^{210}Po activity ratios, supported ^{210}Pb, corrected
550 (unsupported) activity ratios, and the tropospheric removal rate determined by fitting the
551 empirical data to the modelled values.

(a) Ground-level concentration ratios						
	Raw values		Supported	Corrected values		κ
Longitude	^{210}Bi/^{210}Pb	^{210}Po/^{210}Pb	^{210}Pb	^{210}Bi/^{210}Pb	^{210}Po/^{210}Pb	d^{-1}
-156	0.84 ± 0.03	0.10 ± 0.01	3.4%	0.84 ± 0.03	0.067	0.09 ± 0.02
-105	0.41± 0.02	0.082 ± 0.012	5.3%	0.38 ± 0.02	0.030	0.11 ± 0.01
0	0.57± 0.10	0.17 ± 0.05	4.4%	0.55 ± 0.10	0.13	
0		0.16 ± 0.05	4.4%		0.11	
(b) Tropospheric inventories ratios						
	Raw values		Supported	Corrected values		κ
Longitude	^{210}Bi/^{210}Pb	^{210}Po/^{210}Pb	^{210}Pb	^{210}Bi/^{210}Pb	^{210}Po/^{210}Pb	d^{-1}
-101	0.62 ± 0.04	0.11 ± 0.02	4.4%	0.61 ± 0.04	0.069	0.09 ± 0.01
0		0.10 ± 0.02	4.4%		0.061	
				Mean value		0.097 ± 0.012

552 NB: The standard errors given in this Table are based on the 1σ counting errors reported in
553 the original publications (Table 1).

554

555 **6. Reservoir effect of the stratosphere**

556 Although the theoretical tropospheric residence time of ^{210}Pb and its daughters
557 appears to be around 10 days, the practical residence time is significantly greater due
558 to the reservoir effect of the stratosphere. ^{222}Rn and its daughters are transported from
559 the troposphere to the stratosphere when concentrations are higher in the troposphere.
560 This process is reversed once tropospheric concentrations fall below those in the
561 stratosphere. Figure 5 plots the tropospheric, stratospheric and total ^{210}Pb inventories
562 (including fallout) versus time, resulting from an impulsive ground-level ^{222}Rn input
563 of 1570 Bq m^{-2} at time $t = 0$, for the case $\kappa = 0.1$. The inventories were calculated by
564 numerical integration of the ^{210}Pb profiles given by the Green's function $I_o G_{Pb}(z,t)$
565 (equation (18)) with $I_o = 1570$ Bq m^{-2}. The good agreement of the total ^{210}Pb inventory
566 with the theoretical values determined from the mass balance equation

567 $$A_{Pb}(t) = I_0 \frac{\lambda_{Pb}}{\lambda_{Rn} - \lambda_{Pb}} (e^{-\lambda_{Pb} t} - e^{-\lambda_{Rn} t}), \qquad (27)$$

568 also plotted in Figure 5, demonstrates the accuracy of the numerical calculations.
569 According to equation (27) the total ^{210}Pb inventory should reach a maximum value of
570 0.74 Bq m^{-2} after approximately 40 days, though 90% of this value is achieved after

just 24 days. Production by ^{222}Rn is then effectively zero, and thereafter the ^{210}Pb inventory declines slowly in accordance with the ^{210}Pb radioactive decay law.

From the numerical calculations the ^{210}Pb inventory in the troposphere reaches a maximum value of 0.32 Bq m^{-2} after just 6 days. Up to around 40 days it then declines rapidly at a rate corresponding to an apparent residence time of around 13 days due mainly to a combination of reduced creation by ^{222}Rn decay and loss by fallout. After around 22 days the tropospheric inventory falls below that of the stratosphere causing a reverse flux from the stratosphere. This becomes significant after around 60 days, slowing down the rate of decline in the troposphere and increasing the residence time of the remaining tropospheric inventory to around 25 days.

The stratospheric inventory reaches a maximum value of around 0.12 Bq m^{-2} after 19 days, at which point it is almost equal to that in the troposphere. It then begins a long slow decline due to depletion of the ^{222}Rn and the reverse flux to the troposphere. This decline has a residence time of 25 days, similar to that of the tropospheric inventory, transport rates from the stratosphere to the troposphere then matching fallout rates from the troposphere. Fallout from the atmosphere has declined by 50% from its maximum value after around 18 days, 90% after around 40 days, and 99% after around 90 days. Given a mean global circulation velocity of around 360 km d^{-1} (corresponding to the global circulation time of 78 days), these results show that fallout originating in ^{222}Rn inputs from a particular source reaches a maximum value after the column has travelled a distance of ~2000 km. It then falls to around 50% of this value after ~6500 km.

Assuming no stratospheric reservoir effect and that the removal constant κ applies to the atmosphere as a whole, the atmospheric inventory would be given by the equation

$$A_{Pb}(t) = I_0 \frac{\lambda_{Pb}}{\lambda_{Rn} - \lambda_{Pb} - \kappa} (\mathrm{e}^{-(\lambda_{Pb}+\kappa)t} - \mathrm{e}^{-\lambda_{Rn}t}) . \quad (28)$$

This result, also plotted in Figure 5, shows that the reservoir effect only becomes significant after around 35 days.

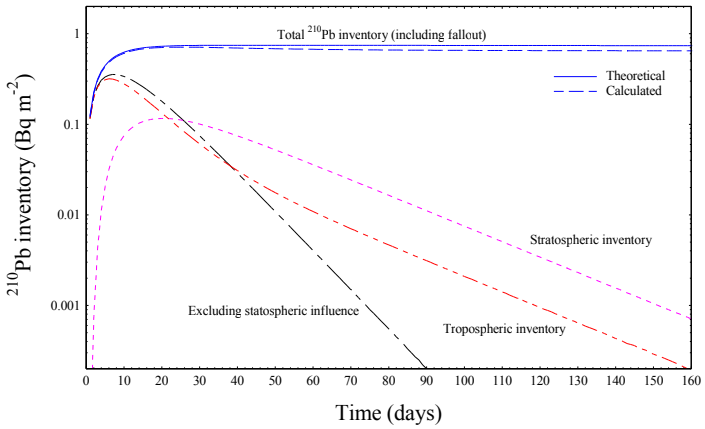

Figure 5. ^{210}Pb inventories in the troposphere and stratosphere versus time following the brief impulsive injection of 1570 Bq m^{-2} of ^{222}Rn into the base of an air column, calculated from the vertical distribution of the ^{210}Pb activity assuming a tropospheric removal rate coefficient of 0.1 d^{-1}. Also shown are the total ^{210}Pb inventories (including both the atmospheric and fallout components). Values are calculated from both the numerical solutions and the theoretical mass balance equation, assuming no stratospheric reservoir effect to the atmospheric inventory

7 Discussion

The results presented in this paper show that while the ^{210}Bi/^{210}Pb and ^{210}Po/^{210}Pb activity ratios can potentially provide important information on the ^{210}Pb atmospheric residence time, the sampling location plays an imporatant role that must be taken into account. The ^{210}Bi/^{210}Pb ratios are probably the more reliable, being less influenced by traces of supported activity. Discrepancies between the ^{210}Bi/^{210}Pb and ^{210}Po/^{210}Pb ratios can be used to make small corrections for the supported activity. Although the ^{210}Bi/^{210}Pb ratios have their highest values in air masses approaching western continental margins, the rapid decline in values (especially at ground-level) as the column moves into the land mass makes the use of such locations highly problematic for model validation. The most suitable locations would appear to be the interiors of large land masses.

The most extensive and reliable ^{210}Pb, ^{210}Bi, ^{210}Po datasets are those obtained from sites in the interior of continental USA. They include measurements carried out on atmospheric samples from a range of different altitudes, and rainwater. Comparisons between the empirical data and model values suggest that the tropospheric removal rate constant has a value between 0.09-0.11 d^{-1}. Much higher ^{210}Bi/^{210}Pb ratios from the oceanic site were also consistent with the model predictions. The corresponding mean tropospheric residence time of 10 days is significantly longer than the value of between 4–7 days suggested by Poet et al. (1972) and less than 7 days suggested by Moore et al. (1973). These values were however based on the assumption that ^{222}Rn

629 and its daughters were locally in a state of radioactive equilibrium, governed by
630 equations (1). It is also significantly longer than the value suggested by Piliposian and
631 Appleby (2003) though that was largely based on a review of earlier estimates.
632 The results presented here also highlight the role played by the stratosphere in
633 extending the practical residence time of ^{210}Pb in the atmosphere. The reservoir effect
634 of the stratosphere, capturing ^{210}Pb when tropospheric concentrations are high and
635 releasing it when they are low, significantly enhances the long range transport of ^{210}Pb
636 from its source locations. Figure 6 plots the modelled ^{210}Pb flux versus longitude at
637 northern mid-latitudes assuming a tropospheric removal rate of 0.1 d^{-1} and a 78 day
638 global transit time. The relatively high fluxes at the western margins of Europe and
639 the USA are largely due to long range transport across the Atlantic and Pacific oceans
640 respectively. The model values for these western margins (~60 Bq m^{-2} y^{-1} for Europe
641 and ~55 Bq m^{-2} y^{-1} for the USA) are comparable to the empirical values for southern
642 England reported by Burton and Stewart (1960) and Peirson et al. (1966), and for
643 coastal regions of western USA reported by Monaghan et al. (1989). Atmospheric
644 fluxes at specific localities within a given region will however be strongly influenced
645 by local factors such as the mean annual rainfall.
646

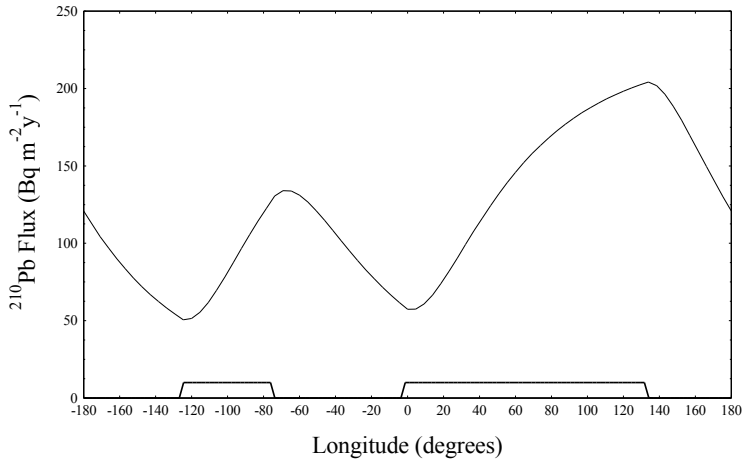

647

648 **Figure 6.** ^{210}Pb flux at northern mid-latitudes versus longitude assuming a tropospheric removal rate
649 coefficient of 0.1 d^{-1} and global circulation transit time of 78 days.
650

651 ## References

652 Appleby, P.G., Piliposian, G.T., 2010. The origins of ^{210}Pb in the atmosphere and its
653 deposition on and transport through catchment lake systems. In: Hanrahan, G. (Ed.),
654 Advanced Topics in Environmental Science Volume II: Modelling of Pollutants in Complex
655 Environmental Systems, pp.381-404. ILM Publications, St Albans.

656 Baskaran, M., 2011. Po-210 and Pb-210 as atmospheric tracers and global atmospheric Pb-
657 210 fallout: a Review. J. Environ. Radioact, 102, 500-513.
658 Burton, W.M., Stewart, N.G., 1960. Use of long-lived natural radioactivity as an atmospheric
659 tracer. Nature 186, 584-589.
660 Carvalho, F.P., 1995. Origins and concentrations of ^{222}Rn, ^{210}Pb, ^{210}Bi and ^{210}Po in surface air
661 at Lisbon, Portugal, at the Atlantic edge of the European continental landmass. Atmospheric
662 Environment 29, 1809-1819.
663 Feichter, J., Brost, R.A., Heimann, M., 1991. Three-dimensional modelling of the
664 concentration and deposition of ^{210}Pb aerosols. J. Geophys. Res. 96 (D12), 22447-22460.
665 Gavini, M.B., Beck, J.N., Kuroda, P.K., 1974. Mean residence times of the long-lived radon
666 daughters in the atmosphere. J. Geophys. Res. 79, 4447-4452
667 Israël, H., 1951. Radioactivity of the atmosphere. In Compendium of Meteorology, ed. T.F.
668 Malone, Amer. Meteor. Soc., Boston, 155-161.
669 Jacobi, W., André, K., 1963. The vertical distribution of radon 222, radon 220 and their decay
670 products in the atmosphere. J. Geophys. Res. 68(13), 3799–3814
671 Junge, C.E., 1962. Note on the exchange rate between the northern and southern atmosphere.
672 Tellus XIV, 242-246.
673 Liu, H., Jacob, D.J., Bey, I., Yantosca, R.M., 2001. Constraints from ^{210}Pb and ^{7}Be on wet
674 deposition and transport in a global three-dimensional chemical tracer driven model driven ny
675 assimilated meteorological fields. J. Geophys. Res.79, 4447-4452
676 Monaghan, M.C., 1989. Lead-210 in surface air and soils from California: Implications for
677 the behaviour of trace constituents in the planetary boundary layer. J. Geophys. Res. 94D,
678 6449-6456.
679 Moore, H.E., Poet, S.E., Martell, E.A., 1973. ^{222}Rn, ^{210}Pb, ^{210}Bi and ^{210}Po profiles and aerosol
680 residence times versus altitude. J. Geophys. Res.78, 7065-7075.
681 Moore, H.E., Poet, S.E., Martell, E.A., Wilkening, M.H., 1974. Origin of ^{222}Rn and its long-
682 lived daughters in air over Hawaii. J. Geophys. Res. 79, 5019-5024.
683 Peirson, D.H., Cambray, R.S., Spicer, G.S., 1966. Lead-210 and polonium-210 in the
684 atmosphere. Tellus 18, 427-433.
685 Piliposian, G.T., Appleby, P.G., 2003. A simple model of the origin and transport of ^{222}Rn and
686 ^{210}Pb in the atmosphere. Continuum Mech. Thermodyn., 15, 503-518.
687 Poet, S.E., Moore, H.E., Martell, E.A., 1972. Lead 210, Bismuth 210 and Polonium 210 in
688 the atmosphere: accurate ratio measurement and application to aerosol residence time
689 determination. J. Geophys. Res. 77, 6515-6527.
690 Rasch, P.J., Feichter, J., Law, K., et al., 2000. A comparison of scavenging and deposition
691 processes in global models: results from the WCRP Cambridge Workshop of 1995. Tellus
692 52B, 1025-1056.
693 Rehfeld, S., Heiman, M., 1995. Three dimensional atmospheric transport simulation of the
694 radioactive tracers ^{210}Pb, ^{7}Be, ^{10}Be, and ^{90}Sr. J. Geophys. Res. 100, 26141-26161.
695 Turekian, K.K., Nozaki, Y., Benninger, L.K., 1977. Geochemistry of atmospheric radon and
696 radon products. Ann. Rev. Earth. Planet. Sci. 5, 227-255.
697 Warneck, P., 2000. Chemistry of the Natural Atmosphere. Academic Press, 927 pages
698 Wilkening, M.H., Clements, W.E., 1975. Radon 222 from the ocean surface. J Geophys.
699 Res. 80:3828-3830.
700
701
702

Appendix A: Numerical Algorithms

Calculation of the radionuclide distributions for a prolonged ^{222}Rn flux

In the case of a prolonged ^{222}Rn flux $\mathcal{F}$(t) into the base of the column, assuming a constant diffusivity the distributions of ^{222}Rn and its daughter radionuclides ^{210}Pb, ^{210}Bi, ^{210}Po, are given in terms of their respective Green's functions by equations (19) and (20). In this section we develop a simple algorithm for evaluating these integrals using the numerically determined Green's functions. Discretising the problem and using a time step h (in days), to a good approximation the case of a continuous input can be solved by representing the ^{222}Rn flux as a series of discrete inputs $I_m = \phi \mathcal{F}_m h$ at the beginning of each time interval $(m-1)h < t < mh$ where $\mathcal{F}_m$ is the mean flux during that time interval and ϕ a small correction factor to compensate for any errors in the inventory at time $t = mh$ due to radioactive decay during the time step. From equation (16), the ^{222}Rn distribution in the column at time $t = nh$ (the end of the n^{th} time interval) due to input at the beginning of the m^{th} time interval (time $t = (m-1)h$) is then

$$I_m \, \mathrm{e}^{-\lambda_{Rn}(n-m+1)h} \frac{1}{\sqrt{\pi D(n-m+1)h}} \mathrm{e}^{-\frac{z^2}{4D(n-m+1)h}} = I_m G_{Rn}(z,(n-m+1)h). \qquad \text{(A1)}$$

Assuming a constant flux during each time step the correction factor will be

$$\phi = \frac{1}{\lambda_{Rn} h}(\mathrm{e}^{-\lambda_{Rn} h} - 1) \approx 1 + \tfrac{1}{2}\lambda_{Rn} h \quad \text{for values of } h < 1 \text{ day} \qquad \text{(A2)}$$

The correction is ~10% if $h = 1$ d and ~1% if $h = 0.1$ d. Summing the contributions from all inputs during time intervals 1 through n the ^{222}Rn concentration in the column at time $t = nh$ is

$$\begin{aligned} C_{Rn}(z,nh) &= \sum_{m=1}^{n} I_m G_{Rn}(z,(n-m+1)h) \\ &= I_1 G_{Rn}(z,nh) + I_2 G_{Rn}(z,(n-1)h) + .. + I_n G_{Rn}(z,h) \end{aligned} \quad . \qquad \text{(A3)}$$

In the same way, the ^{210}Pb, ^{210}Bi and ^{210}Po distributions at time $t = nh$ are

$$\begin{aligned} C_{Pb}(z,nh) &= \sum_{m=1}^{n} I_m G_{Pb}(z,(n-m+1)h) \\ &= I_1 G_{Pb}(z,nh) + I_2 G_{Pb}(z,(n-1)h) + ... + I_n G_{Pb}(z,h) \end{aligned} \quad , \qquad \text{(A4)}$$

$$\begin{aligned} C_{Bi}(z,nh) &= \sum_{m=1}^{n} I_m G_{Bi}(z,(n-m+1)h) \\ &= I_1 G_{Bi}(z,nh) + I_2 G_{Bi}(z,(n-1)h) + ... + I_n G_{Bi}(z,h) \end{aligned} \quad , \qquad \text{(A5)}$$

$$C_{Po}(z,nh) = \sum_{m=1}^{n} I_m G_{Po}(z,(n-m+1)h) = I_1 G_{Po}(z,nh) + I_2 G_{Po}(z,(n-1)h) + \ldots + I_n G_{Po}(z,h) \quad , \tag{A6}$$

where $G_{Pb}(z,s)$, $G_{Bi}(z,s)$, $G_{Po}(z,s)$ are the (numerically determined) ^{210}Pb, ^{210}Bi and ^{210}Po Green's functions.

Implementation

Calculations were carried using the MATHEMATICA software package. Assuming that the atmosphere has a vertical height of 30 km divided into 1 km steps, the four Green's functions were stored as arrays

GRN(31,N), GPB(31,N), GBI(31,N), GPO(31,N),

where N is the total number of time steps in the calculation. The values of GRN were calculated exactly using the formula

$$\mathrm{GRN}(i,j) = G_{Rn}(i,jh) = \mathrm{e}^{-\lambda_{rn} jh} \frac{1}{\sqrt{\pi D j h}} \mathrm{e}^{-\frac{i^2}{4Djh}} . \tag{A7}$$

The values of GPB, GBI, GPO were evaluated from the numerically determined Green's functions

$$\mathrm{GPB}(i,j) = G_{Pb}(i,jh), \quad \mathrm{GBI}(i,j) = G_{Bi}(i,jh), \quad \mathrm{GPO}(i,j) = G_{Po}(i,jh). \tag{A8}$$

The ^{222}Rn exhalation rates were stored as a vector array F(N), where F(j) is the input at the beginning of the j^{th} time step. The concentration profiles were stored in arrays

CRN(31,N), CPB(31,N), CBI(31,N), CPO(31,N)

where CRN(i,j), CPB(i,j), CBI(i,j), CPO(i,j) are the radionuclide concentrations at altitude $z=i$ at the end of the j^{th} time step. The entries for these arrays were calculated using the formulae

$$\left.\begin{aligned} \mathrm{CRN}(i,j) &= \sum_{k=1}^{j} \mathrm{F}(k)\,\mathrm{GRN}(i,j-k+1) \\ \mathrm{C\,PB}(i,j) &= \sum_{k=1}^{j} \mathrm{F}(k)\,\mathrm{G\,PB}(i,j-k+1) \\ \mathrm{C\,BI}(i,j) &= \sum_{k=1}^{j} \mathrm{F}(k)\,\mathrm{G\,BI}(i,j-k+1) \\ \mathrm{C\,PO}(i,j) &= \sum_{k=1}^{j} \mathrm{F}(k)\,\mathrm{G\,PO}(i,j-k+1) \end{aligned}\right\} . \tag{A9}$$

Using these equations, a numerical solution can be constructed for any given distribution of the ^{222}Rn exhalation rate $\mathcal{F}$(t), any given value of the removal rate constant κ, and any desired number of time steps N.

Global equilibrium distributions

The steady state distribution in a column moving from west to east will include steady state contributions from each part of the Earth's surface it passes over. In particular, dividing the global circulation time T into N time steps $h = T/N$, the input during the m^{th} time step can be approximated by a source of strength $I_m = \phi \mathcal{F}_m h$ where $\mathcal{F}_m$ is the value of the exhalation rate at time $s = (m-1)h$, the beginning of the m^{th} time step. Noting that the equilibrium Green's function is periodic of period T the contribution of exhalation from this geographical location to the equilibrium ^{222}Rn distribution in the column at time $t=nh$, the end of the n^{th} time step, can be written

$$I_m G_{Rn}^{equ}(z, t+T-s) = I_m G_{Rn}^{equ}(z, (n+N-m+1)h)$$

The equilibrium ^{222}Rn distribution at time $t=nh$ due to inputs from all N steps is thus

$$C_{Rn}(z, nh) = \sum_{m=1}^{N} I_m G_{Rn}^{equ}(z, (n+N-m+1)h)\,. \qquad \text{(A10)}$$

The distributions of the daughter radionuclides ^{210}Pb, ^{210}Bi and ^{210}Po can similarly be written

$$\left.\begin{aligned} C_{Pb}(z, nh) &= \sum_{m=1}^{N} I_m G_{Pb}^{equ}(z, (n+N-m+1)h) \\ C_{Bi}(z, nh) &= \sum_{m=1}^{N} I_m G_{Bi}^{equ}(z, (n+N-m+1)h) \\ C_{Po}(z, nh) &= \sum_{m=1}^{N} I_m G_{Po}^{equ}(z, (n+N-m+1)h) \end{aligned}\right\}\,. \qquad \text{(A11)}$$

Implementation

The four equilibrium Green's functions were stored as arrays over two cycles

EGRN(31,2N), EGPB(31,2N), EGBI(31,2N), EGPO(31,2N)

where N is the number of time steps in each cycle,

$$\text{EG RN}(i, j) = G_{Rn}^{equ}(i, jh)\,,$$

and

$$\text{EGPB}(i, j) = G_{Pb}^{equ}(i, jh), \quad \text{EGBI}(i, j) = G_{Bi}^{equ}(i, jh), \quad \text{EGPO}(i, j) = G_{Po}^{equ}(i, jh)\,.$$

775 The ^{222}Rn exhalation rates were stored as a vector array F(N) where F(j) is the input at
776 the beginning of the j^{th} time interval. The equilibrium concentration profiles were
777 stored in arrays

778 $$\mathrm{ECRN}(31,N),\ \mathrm{ECPB}(31,N),\ \mathrm{ECBI}(31,N),\quad \mathrm{ECPO}(31,N)$$

779 where ECRN(i,j), ECPB(i,j), ECBI(i,j), ECPO(i,j) are the radionuclide concentrations
780 at altitude $z=i$ at time j, the end of the j^{th} time interval. The entries for these arrays
781 were calculated using the formulae

782 $$\mathrm{ECRN}(i,j)=\sum_{k=1}^{N}\mathrm{F}(k)\,\mathrm{EGRN}(i,j+N-k+1)),$$

783 $$\mathrm{ECPB}(i,j)=\sum_{k=1}^{N}\mathrm{F}(k)\,\mathrm{EGPB}(i,j+N-k+1)),$$

784 $$\mathrm{ECBI}(i,j)=\sum_{k=1}^{N}\mathrm{F}(k)\,\mathrm{EGBI}(i,j+N-k+1)),$$

785 $$\mathrm{ECPO}(i,j)=\sum_{k=1}^{N}\mathrm{F}(k)\,\mathrm{EGPO}(i,j+N-k+1)).$$

786 **Author Contributions**

787 The manuscript was written through contributions from all authors. All authors have
788 given approval to the final version of the manuscript. All authors contributed equally.

789 **Graphical Abstract**

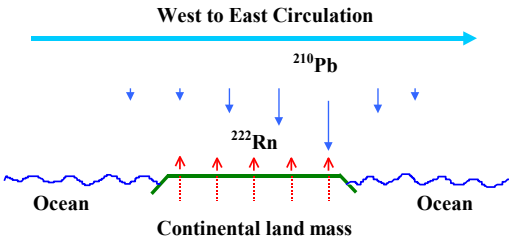

790

Appendix 2.

Long-term stability of records of fallout radionuclides in the sediments of Brotherswater, Cumbria (UK)

P. Semertzidou[*a], G.T. Piliposian[a], R.C. Chiverrell[b], P.G. Appleby[a]

[a] *Environmental Radioactivity Research Centre, Department of Mathematical Sciences University of Liverpool, Liverpool, UK*

[b] *School of Environmental Sciences, Roxby Building, University of Liverpool, Liverpool, UK*

[*]Corresponding author: semergt@liv.ac.uk

Key words: ^{210}Pb, ^{137}Cs, Brotherswater, Lake sediments, Radiometric dating

Abstract

Results from a recent multi-core study of ^{137}Cs and ^{210}Pb in Brotherswater, Cumbria, are compared with those from two similar multi-core studies carried out at the same lake in 1976/7 and 1988/9. The purpose of this new study was to assess of the long-term stability of fallout records of these radionuclides in the sediments of Brotherswater and their reliability as tools for dating the sediments. Six cores were taken from four different areas of the lake, similar to those used in the earlier studies. Dried sediment samples from each core were analysed by gamma spectrometry for ^{210}Pb, ^{226}Ra, ^{137}Cs and ^{241}Am following a similar protocol to that used in the 1988/9 study. The ^{137}Cs results graphically illustrate the progressive burial of a peak in concentrations recording the 1963 fallout maximum from the atmospheric testing of nuclear weapons, and its subsequent reduction due to radioactive decay. The post-1986 cores are characterised by the appearance and burial of a second peak recording fallout from the 1986 Chernobyl accident. Identification of the 1963 ^{137}Cs peak in post-1986 cores was confirmed by the co-presence of traces of ^{241}Am, also a product of nuclear weapons test fallout. In both the 1988/9 study and the present study, ^{210}Pb dates calculated using the CRS model for the most part placed 1963 and 1986 at depths very similar to those determined from the ^{137}Cs records. The maintenance of this agreement over a period of more than two decades provides evidence of the reliability of sediment records in this lake and the validity of models used to interpret them. The ^{137}Cs records were too indistinct and 1963 too recent to make similar comparisons in the case of the 1976/7 cores. Agreement between ^{210}Pb and ^{137}Cs dates was best at sites where the net rate of supply of ^{210}Pb to the sediment record was comparable to the atmospheric flux. Small but significant discrepancies were observed at sites where the ^{210}Pb supply rate greatly exceeded the atmospheric flux, most probably due to additional time-dependent inputs from the catchment, or post-depositional sediment redistribution within the lake.

Introduction

Measurements of fallout ^{137}Cs and ^{210}Pb in sediment cores from Brotherswater, Cumbria, have been made during the course of a number of different studies, dating back to the early 1970s. The first reported study was carried out by Winifred Pennington (Freshwater Biological Association, Ambleside, Cumbria). Two cores collected in 1974/5 were analysed for weapons fallout ^{137}Cs. The first, BW1, was from a site close to the present inflow. The second, BRW, was from a site on the western side of the lake. The results from BW1 were published in Pennington (1981). A more detailed investigation was carried out in 1976/7 by John Eakins and Roger Cambray (AERE Harwell). Sediment cores from five different locations in the lake were analysed for ^{210}Pb, ^{226}Ra and ^{137}Cs as part of a study of the transfer of radionuclides from the catchment to the lake (Eakins et al. 1981; Eakins et al. 1984). A further multi-core study was carried out in 1988/9 during an investigation into the impact of fallout from the 1986 Chernobyl accident. In this case a total of six cores were collected from the same areas of the lake as those sampled in 1976/7 and analysed for ^{210}Pb, ^{226}Ra, ^{137}Cs, ^{134}Cs and ^{241}Am in the Liverpool University Environmental Radioactivity Research Centre. The results were reported in Bonnett et al. (1992) and Hilton et al. (1992).

The techniques for dating recent sediments developed in those years have now been used in literally thousands of studies for measuring lake sediment accumulation rates and reconstructing histories of environmental change from the environmental records stored in these natural archives. Dating by ^{137}Cs assumes that particular events such as the 1963 fallout maximum from the atmospheric testing of nuclear weapons or the 1986 Chernobyl reactor fire leave identifiable chronostratigraphic features at the 1963 or 1986 depths in the sediment record. Dating by ^{210}Pb assumes that changes to the initial concentrations of sediment samples deposited on the bed of the lake are predominantly due to radioactive decay. The amount of time since deposition can then be calculated by comparing the current (measured) ^{210}Pb activity to the initial (estimated) activity. There are two simple models for calculating the initial concentrations, the CRS (Constant Rate of ^{210}Pb Supply) and CIC (Constant Initial ^{210}Pb Concentration) models (Appleby and Oldfield 1978; Robbins 1978). Since in many cases neither of these assumption is fully satisfied throughout the ^{210}Pb time-

span (~130 years) these models will often need to be applied in a piecewise way to different parts of the record (Appleby 2001).

One of the central assumptions of paleolimnology is that sediment records formed at the sediment/water interface and buried beneath successive layers of sediment are preserved relatively intact and not subject to significant degradation by diagenesis or post-depositional mobility. Although this is evidently not the case for more soluble species such as ^{137}Cs, traces of which are often found in sediments predating by many decades the 1950s introduction of this artificial radionuclide into the global environment, it is thought to be valid for less soluble species such as ^{210}Pb. Where species are subject to post-depositional mobility a key issue is the extent to which these processes affect particular features in the record. The existence of the above two earlier multi-core studies at Brotherswater spanning a period of four decades offers a unique opportunity to assess the long-term stability of sediment records, and in particular the reliability of their dating by ^{210}Pb and ^{137}Cs. With this objective in mind, further cores were recovered from Brotherswater during 2011-2014 at similar locations to those sampled in the earlier studies and their ^{210}Pb and ^{137}Cs records determined and compared with those from the 1970s and 1980s.

The study site

Brotherswater is a small (0.18 km^2), upland (altitude 158 m) lake in the Hartsop valley, in Cumbria, N.W.England, about 13 kilometres north of Windermere. It has a large catchment (13 km^2) and large catchment-to-lake area ratio (72). The catchment drains northwards by way of a several small becks that merge to form a single input stream (Kirkstone beck) near the south-western corner of Brotherswater. The outlet stream, Goldrill Beck, leaves the lake at the north-western corner and drains northwards into Ullswater. The basic physiographic parameters of the catchment and its lake are given in Table 1. Sediments mainly enter through the single inflow. The bathymetry of the lake is dominated by a central flat profundal zone with a maximum depth of 17 m. Brotherswater is classified on the meso/oligo-trophic boundary (Maberly et al. 2010) and develops weak summer thermal stratification.

Historical studies

The 1970s and 1980s Brotherswater sediment cores were collected from 5 different sites in the lake:

- Site 1 at the southern end of the lake near the inflow, at depths of around 8 m,
- Site 2 half way up on the western side of the lake, at depths of between 5-11 m,
- Site 3 in the central basin at a depth of around 15 m,
- Site 4 on the eastern side of the lake, at depths of between 7-10 m,
- Site 5 at the northern end of the lake near the outflow, at depths of around 4 m,

The original ^{137}Cs data for the 1970s cores are recorded in Roger Cambray's logbook, a copy of which is held in the ERRC. Since there are a number of issues concerning the data that are relevant to an understanding of the results, we give here a brief description of the original data and the way in which it has been collected and processed. Core BW1, collected in 1974 from site 1, was actually an amalgamation of three adjacent cores, obtained by combining corresponding 1 cm slices from each core. In the case of core BRW, collected a year later in 1975, the analyses were carried out on samples from a single core sliced a 1 cm intervals. In both cases Cambray's logbook reports the sample weight (gDW), total activity (pCi) and volumetric specific activity (pCi cm^{-2}) of each slice. To facilitate comparison with other studies mass specific activities (Bq kg^{-1}) and dry bulk densities (g cm^{-3}) have been calculated from the sample weights and total activities. The calculations have been corrected for the fact that the internal diameter of the core tube was 5.08 cm, not 5.3 cm as originally reported.

Cambray's logbook also records the original ^{137}Cs data for the 1976/7 cores. For BW1/76 (collected in September 1976), BWC and BWN, it gives the ^{137}Cs activity (pCi) and volumetric specific activity (pCi cm^{-2}) for each 1 cm slice. Mass specific activities as Bq kg^{-1} were determined using estimated values of the dry bulk density. For the uppermost 12 cm of the core these were given in graphical form in Eakins et al. (1981). At greater depths they were estimated from corresponding data for other nearby cores, scaled so as to yield the same radionuclide inventories as those given by Cambray. For cores BWW and BWE the logbook included dry weights, ^{137}Cs activities (pCi) and specific activities (pCi g^{-1}, pCi cm^{-2}), from which ^{137}Cs activities Bq kg^{-1} and dry bulk densities as g cm^{-3} could be calculated directly. ^{210}Pb and ^{226}Ra

analysis on the 1976/7 cores were carried out by John Eakins at Harwell using alpha spectrometry. Although the original data are not available, the results are given in graphical form in Eakins et al. (1981) and Eakins et al. (1984). It is not clear whether these analyses were carried out on the same cores as those used for the ^{137}Cs analysis or on adjacent parallel cores.

In the 1988/9 study a total of six cores were collected using a 1 m mini-Mackereth corer, BW88/2 in 1988 from site 2, and BW89/1-5 in August 1989 from sites 1-5. The cores were sectioned at 1 cm intervals, and analysed for fallout radionuclides in the Liverpool University ERL following its standard protocol (see below). The results have been published in UK Department of the Environment Research Reports (Bonnett et al. 1992; Hilton et al. 1992). Table 2 gives a list of cores collected during the 1976/7 and 1988/9 studies, dated by ^{210}Pb and ^{137}Cs. The 1974/75 cores BW1 and BRW were presumably collected from sites close to BW1/76 and BWW.

Present study

Two sediment cores were collected from Brotherswater in 2011/12 as part of a study of metal and sediment fluxes in the lake (Schillereff et al., 2016) using a short 8 cm diameter gravity corer designed to capture an intact sediment water–interface (Boyle 1995). The first (BW11-2) was from the western side of the lake (site 2) in 15.1 m water depth. The second (BW12-9) was from the central profundal zone (site 3) in 16.3 m water depth. A further four cores were collected in 2014 specifically for this study, BW14/E1 and BW14/E2 from the eastern side of the lake (site 4), and BW14/N1 and BW14/N2 from the northern end (site 5). The southwestern corner near the inlet stream (site 1) was not resampled due to the very rapid and irregular inputs of sediment from the catchment. Table 3 gives the water depths of each core and map coordinates (UK National Grid Reference). Following retrieval cores were wrapped and sealed and stored in a refrigerator until ready for subsampling. This was done by extruding and slicing the sediment at 0.5 cm intervals with care being taken to preserve all of the material. Each slice was then weighed wet, freeze dried, and weighed again dry to determine the water content and wet and dry bulk densities. The locations of all six core sites, together with those for the earlier studies, are shown in Figure 1.

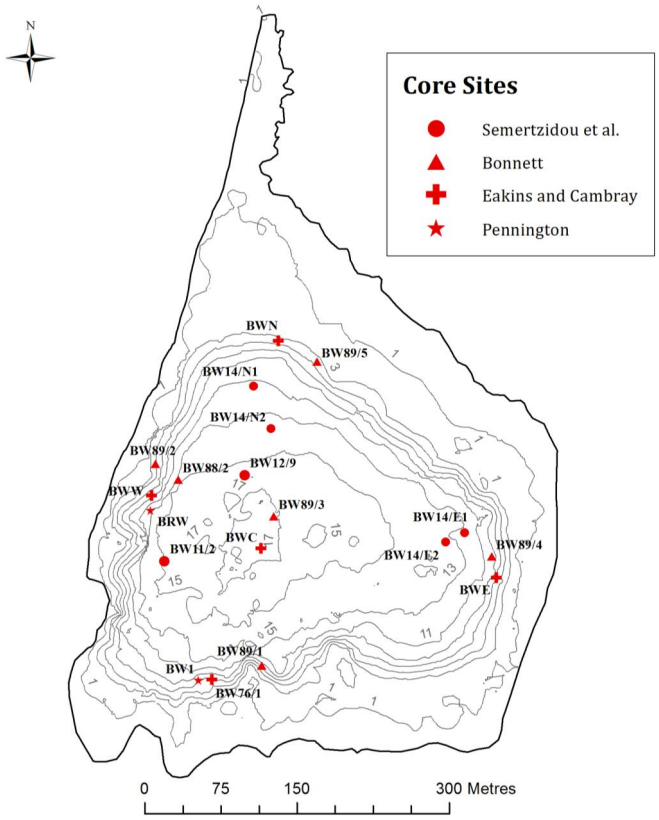

Fig 1. Locations of the 2010s core sites together with those from earlier studies.

Radiometric analyses

Dried sediment samples from each core were analysed for ^{210}Pb, ^{226}Ra, ^{137}Cs and ^{241}Am by direct gamma assay in the Liverpool University ERL (Environmental Radioactivity Laboratory) using Ortec HPGe GWL series well-type coaxial low background intrinsic germanium detectors (Appleby et al. 1986). Samples were placed in 5 cm long by 1 cm diameter nylon sample tubes sealed with flanged rubber Suba-Seals dipped in paraffin wax to prevent ^{222}Rn escape. ^{210}Pb was determined via its gamma emissions at 46.5 keV, and ^{226}Ra by the 295 keV and 352 keV γ-rays emitted by its daughter isotope ^{214}Pb following 3 weeks storage to allow ^{214}Pb/^{226}Ra radioactive equilibration. ^{137}Cs and ^{241}Am were measured by their emissions at 661.7 keV and 59.5 keV respectively. The absolute efficiencies of the detectors were determined using calibrated sources and sediment samples of known activity. Corrections were made for the effect of self-absorption of low energy γ-rays within the sample (Appleby et al. 1992), and for background radiation from the detectors themselves. The background counts of 60-hour duration were carried out on each

detector at regular intervals. Mean background count-rates were typically around 0.5 cph (counts per hour) for the 46.5 keV peak and 1 cph for the 661.7 keV.

X-ray fluorescence (XRF) analyses

Element analyses were conducted using a Bruker S2 ranger energy dispersive *X*-ray fluorescence (XRF) system, with XRF calibration and quality control based on a set of 14 certified reference materials including soil, sediment, rock and plant tissue. Samples were presented as homogenized loose powders pressed into sample cups lined with 6 μm polypropylene film, measured under a helium atmosphere at three *X*-ray intensity settings and measurements were corrected for variable organic matter concentrations. Organic content data were derived either as loss-on-ignition (LOI, 105–550°C) or thermogravimetric mass loss (150°-530°C) under an N atmosphere (PerkinElmer STA6000).

Results

Fallout ^{137}Cs and ^{210}Pb records for each study are given in the Electronic Supplementary Material, those for the 1976/7 cores in Table ESM1, those for the 1988/9 cores in Table ESM2, and those for the present study in Table ESM3.

Chronostratigraphic records

^{137}Cs records

Figure 2 shows ^{137}Cs records in four cores from the western side of Brotherswater (Site 2), BRW collected in 1975, BW88/2 collected in 1988, BW89/1 collected in 1989, and BW11/2 collected in 2011. At the time of the 1975 study the only significant source of ^{137}Cs was fallout from the atmospheric testing of nuclear weapons. Fallout from this source, which began on a global scale in 1954, reached a maximum value in 1963 before declining rapidly following the implementation of a global test ban treaty during that year. The ^{137}Cs record in BRW (Figure 2(a)), has a distinct peak in the 4-5 cm sample that can reasonably be assumed to record the 1963 weapons fallout maximum. This implies a mean sediment accumulation rate during the 12-year period 1963-75

that is similar to the value of 0.4 ± 0.2 cm y^{-1} inferred by Eakins et al. (1984) from the ^{137}Cs record in the nearby 1977 core BWW. The indistinct nature of the 1977 record suggests however that that core may have been taken from a disturbed site.

The 1988 core BW88/2, from a site around 30 metres to the north-west of BWW in slightly deeper water (~11 m compared to 7.5 m), was collected just two years after the area had been impacted by fallout from the 1986 Chernobyl accident. The ^{137}Cs record in this core, shown in Figure 3(b), has two distinct peaks. The most recent, in the 1-2 cm slice, records fallout from Chernobyl. This inference was supported by the presence at the same depth of traces of the short-lived Chernobyl isotope ^{134}Cs (half-life 2.2 years). The second older peak, between 7-10 cm, is almost certainly a record of the 1963 nuclear weapons fallout maximum. The reduced concentration in the 1963 peak in the 1988 core compared to its value in the 1975 core is largely attributable to radioactive decay. The 1989 core (BW89/2), from ~5 m water depth at a site around 30 meters directly north of BWW, had a very similar record to the 1988 core, with high concentrations of Chernobyl ^{137}Cs in the uppermost 3 cm and a well-defined weapons ^{137}Cs peak in the 7-8 cm sample. Differences in detail are likely to be due, at least in part, to the sub-sampling procedure.

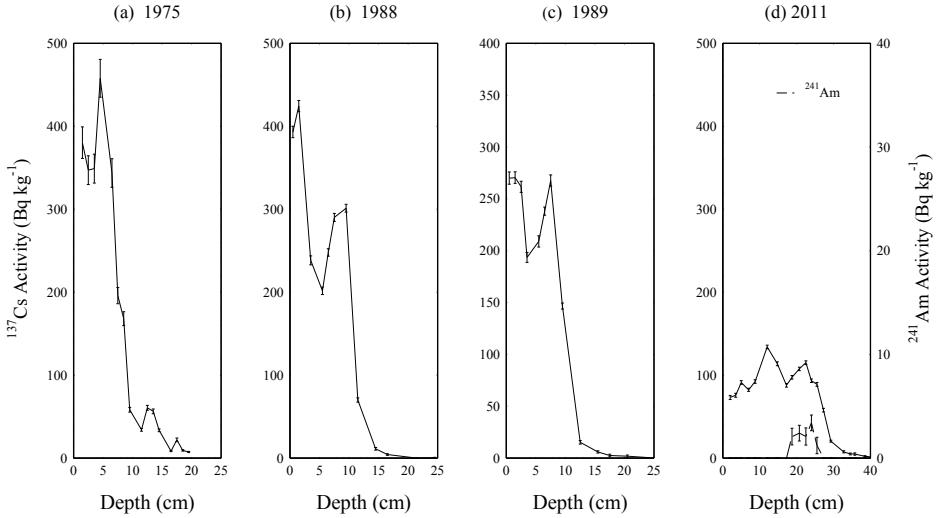

Fig 2. ^{137}Cs records in cores from the western side of Brotherswater collected in (a) 1975, (b) 1988, (c) 1989, (d) 2011.

The 2011 core (BW11/2) was also from the western side of the lake but around 75 m nearer to the inlet stream in 15 m water depth. Both ^{137}Cs peaks are clearly visible

(Figure 3(c)) though at significantly greater depths due to progressive burial under more recent sediments. Peak concentrations are somewhat reduced, again reflecting the influence of radioactive decay. A small but distinct peak in ^{241}Am concentrations at the same depth shows that the older peak records the 1963 weapons fallout maximum (Appleby et al. 1991).

Similar results were obtained from cores in other parts of the lake. Figure 3 shows the effects of progressive burial and radioactive decay on ^{137}Cs records in three cores from the central area, the 1977 core (BWC), 1989 core (BW89/3) and 2012 core (BW12/9). Evidence that the deeper peak in the 2012 core records the 1963 weapons ^{137}Cs fallout maximum is again provided by the co-presence of traces of ^{241}Am.

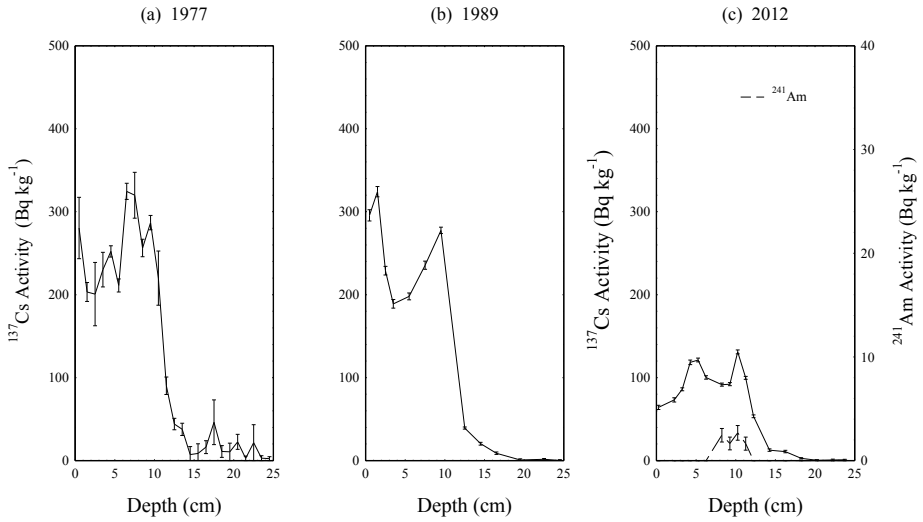

Fig 3. ^{137}Cs records in cores from the central area of Brotherswater collected in (a) 1977, (b) 1989, (c) 2012.

Records from the eastern side of the lake are shown in Figure 4, and from the northern (outlet) end in Figure 5. In both cases the 1977 records lack clarity compared to those from the 1989 cores. There also appears to have been a significant degradation of the ^{137}Cs records in the 2014 cores from the eastern side of the lake. Possible causes include slow diffusion of ^{137}Cs away from the peaks, localized sediment disturbances, or problems arising from sampling or instrumental procedures. Traces of ^{241}Am do however give some indication as to the 1963 depth in these cores. The 1986 and 1963 features do appear to be reasonably well preserved in the 2014 cores from the northern end of the lake.

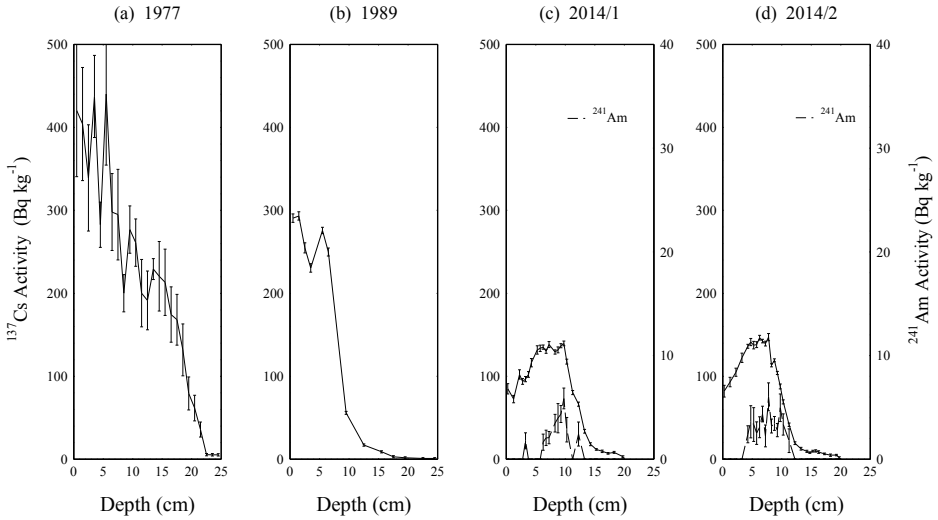

Fig 4. ^{137}Cs records in cores from the eastern side of Brotherswater collected in (a) 1977, (b) 1989, (c) & (d) 2014.

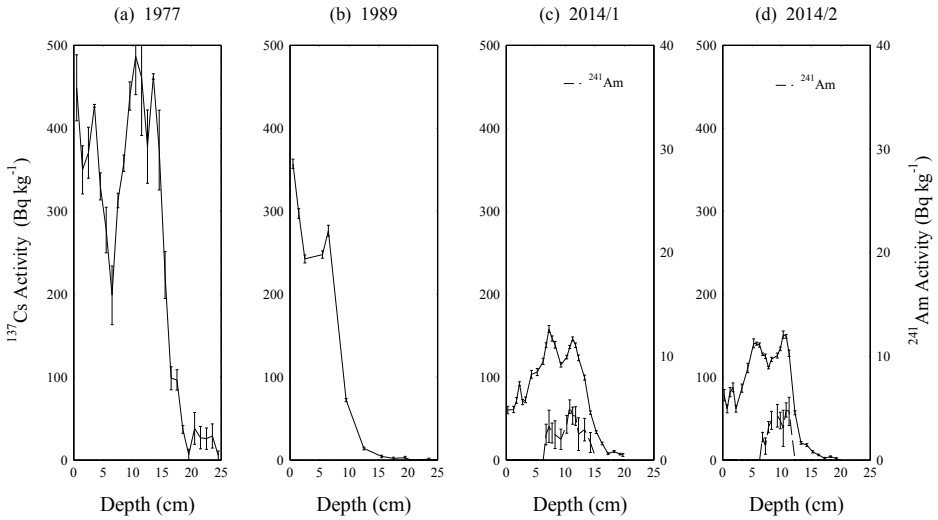

Fig 5. ^{137}Cs records in cores from the northern (outlet) end of Brotherswater collected in (a) 1977, (b) 1989, (c) & (d) 2014.

Mining Pb records

The sediments of Brotherswater contain a record of pollution in the lake by lead mining in the catchment, an activity that has been carried out since at least the late 17th century. Figure 6 shows stable Pb records in cores BW11/2 and BW12/9 from the western and central parts of the lake (Schillereff et al. 2016), BW14/E1 and BW14/E2 from the eastern areas, and BW14/N1 and BW14/N from the northern areas. The most notable feature of these records is a clearly identifiable peak in Pb concentrations due to a very

rapid, intense but short-lived increase in lead pollution associated with the introduction of water-powered milling at the Hartsop Hall mine during 1863-71 (Schillereff et al. 2016). The depths at which this clearly identifiable chronostratigraphic feature occurs range from a little over 50 cm in core BW11/2 nearest the inflow to around 20 cm in the more distant cores. Maximum Pb concentrations vary from more than 12000 ppm in BW11/2 to less than 5000 ppm at the more distant sites.

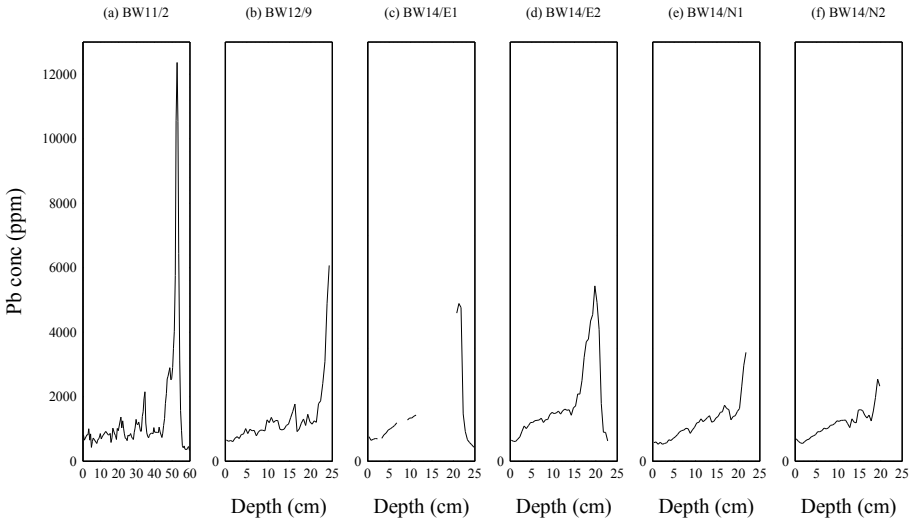

Fig 6. Stable Pb records in the Brotherswater cores collected for the present study

Chronostratigraphic dates

Table 4 summarises chronostratigraphic dates determined from the ^{137}Cs and stable Pb records for cores collected during 2011-2014. Sediments containing the mining Pb peak can reasonably be assumed to date from 1867 ± 4 years. The 1963 and 1986 dates are determined from the depths of peaks in the ^{137}Cs activity identified as recording the 1986 and 1963 peak fallout events. This assumes that time lags between the fallout record and sediment record are less than a year. Uncertainties in these dates can however arise from a number of causes. These include:

- Subsampling. Each core slice may include sediments from more than one year. Further, sediments from a given year may be spread over two or more slices.
- Fallout reaching the core site at any given time will include both direct inputs via atmospheric deposition onto the surface of the lake, and indirect inputs via transport from the catchment. The latter component may include significant amounts of fallout from earlier years.

- Degradation of the sediment record by horizontal or vertical post-depositional transport, e.g. displacement by chemical migration, physical mixing of the surficial sediments, sediment focussing and slump events.

The results given in Table 4 reflect these uncertainties.

The 1988/9 cores have just two chronostratigraphic dates, the 1963 nuclear weapons fallout maximum and the 1986 Chernobyl accident. These are shown in Table 5. Since these cores weren't analysed in the same detail and were sectioned more coarsely (1 cm intervals rather than 0.5 cm intervals) the depths of sediments recording these events have a greater uncertainty. Further, the 1986 event is too recent to provide much information apart from demonstrating the integrity of the core.

^{210}Pb records

The ^{210}Pb concentration in sediment samples deposited on the bed of the lake has two components, a supported component derived from the *in situ* decay of ^{226}Ra contained within the sample, and an unsupported component derived principally from atmospheric fallout of ^{210}Pb onto the lake and its catchment. The supported component is essentially constant over timescales relevant to ^{210}Pb dating and is determined by measuring the activity of the parent radionuclide ^{226}Ra. The unsupported (or fallout) component is determined by subtracting the measured supported activity from the measured total ^{210}Pb activity. Measured values of the ^{226}Ra (supported ^{210}Pb) activity in the Brotherswater sediments were relatively uniform over the bed of the lake, with a mean value of 38 ± 3 Bq kg^{-1}.

The supply of fallout ^{210}Pb to lake sediments can include both direct atmospheric inputs onto the surface of the lake itself and indirect inputs deposited onto the catchment and then transported to the lake by runoff or erosion. The distribution of ^{210}Pb over the bed of the lake can be affected both by the pattern of sedimentation and post-depositional transport processes such as sediment slumps from the margins of the lake. The initial concentrations $C_o(t)$ (Bq kg^{-1}) in sediments presently of age t are governed by the equation

$$C_0(t) = \frac{P(t)}{r(t)} \qquad (1)$$

where $P(t)$, $r(t)$ are the rates of supply of ^{210}Pb (Bq m^{-2} y^{-1}) and sediment (kg m^{-2} y^{-1}) at the time the sediments were laid down. These will diminish over time, principally by

the effects of radioactive decay but possibly also by other causes such as physical mixing of the near surface sediments or chemical diffusion within the pore waters. Where radioactive decay is dominant the present concentration in sediments of depth *z* and age *t* will be

$$C(z) = \frac{P(t)}{r(t)} \mathrm{e}^{-\lambda t}. \quad (2)$$

This equation shows that although the decline in ^{210}Pb activity with depth in a core is likely to be dominated by exponential decay, deviations from a simple exponential function may occur due to variations in the initial activity caused by changes in the rates of supply of ^{210}Pb and sediment at the core site.

Table 6 summarises a number of key parameters associated with each core including

- the measured unsupported ^{210}Pb activity in the surficial sediments of each core,
- the unsupported inventory calculated by numerical integration of the activity versus depth record:

$$A_0 = \int_0^{m_{equ}} C(z(m))\,\mathrm{d}m \quad (3)$$

where *m* is depth in the core measured in terms of cumulative dry mass (g cm^{-2}) and m_{equ} the ^{210}Pb equilibrium depth, and

- the mean ^{210}Pb supply rate required to sustain the inventory, calculated using the formula

$$P = \lambda A_0 . \quad (4)$$

The atmospheric flux of ^{210}Pb at Brotherswater is estimated to be around 179 Bq m^{-2} y^{-1}. At eight sites, mainly in the northern and eastern areas of the lake remote from the main inflow, the ^{210}Pb supply rates are close to the atmospheric flux. Much higher values at sites near the inflow clearly include significant inputs from the catchment. Anomalously high values in the 1977 cores BWE (near the eastern shore) and BWN (northern area) are most probably due to reworked inputs of sediment from the margins of the lake. Generally higher surface concentrations in sediments from the northern and eastern areas are presumably due to the fact that only the finer components of allochthonous inputs from the catchment will travel that far.

Figure 7 compares unsupported ^{210}Pb activity versus depth records in cores from the western side of Brotherswater collected in 1977, 1988, 1989 and 2011. To eliminate the influence of compaction the results have been plotted against depth as cumulative dry mass. The 1977 and 1988/9 cores have very similar surficial concentrations, with

a mean value of 393 Bq kg^{-1}. Although a significantly lower surficial concentration (286 Bq kg^{-1}) was recorded in the 2011 core, the maximum concentration (336 Bq kg^{-1}) in sediments at 5 cm depth was comparable to that in the surficial sediments of the earlier cores, particularly when account is taken of radioactive decay. There do however appear to have been significant variations in the overall sedimentation rates at these sites. Defining the ^{210}Pb dating horizon as the point at which unsupported ^{210}Pb activity declines to values close to the limit of detection, typically around 6 ^{210}Pb half-lives (~130 years), the depth at which this is reached varies from around 20 cm (6 g cm^{-2}) in the 1988/9 cores to 45 cm (19 g cm^{-2}) in the 2011 core. Deviations from a simple exponential decline are somewhat more pronounced in the 2011 core though this may in part be due to better resolution as a result of being sampled at 0.5 cm intervals compared to 1 cm intervals for the 1988/89 cores.

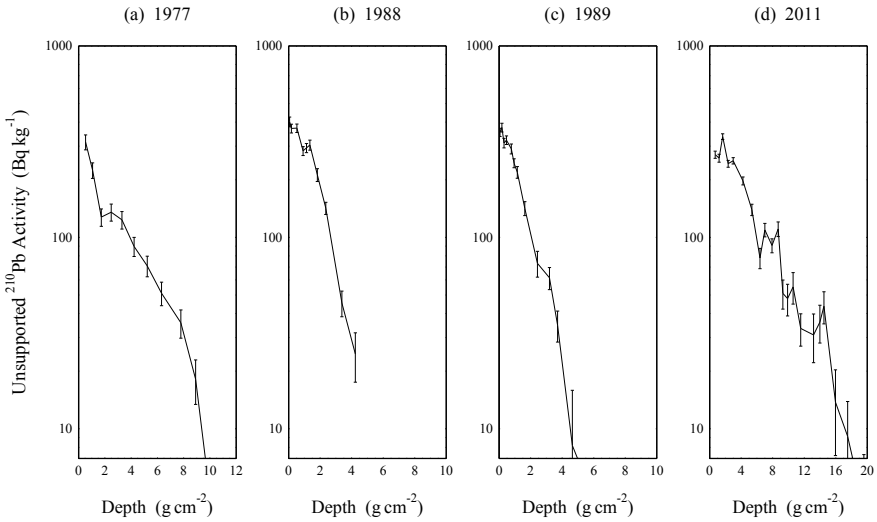

Fig 7. ^{210}Pb records in four cores from the western side of Brotherswater collected in (a) 1977, (b) 1988, (c) 1989, (d) 2011

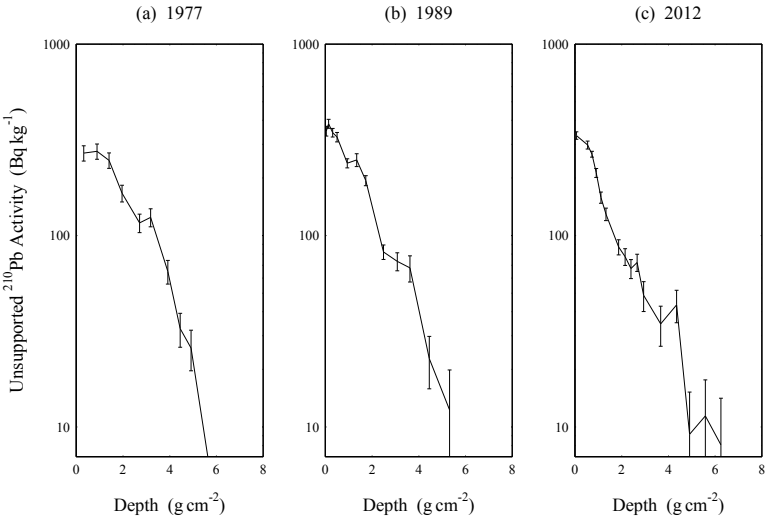

Fig 8. ^{210}Pb records in three cores from the central area of Brotherswater collected in (a) 1977, (b) 1989, (d) 2012

Unsupported ^{210}Pb records in cores from the central area of Brotherswater, collected in 1977, 1989 and 2012, are all quite similar (Figure 8). Although there are again a number of small irregularities that may reflect minor short time-scale differences over small spatial scales, these cores have similar surface concentrations and the ^{210}Pb dating horizons lie at similar depths (23-26 cm or 5.6-6.5 g cm^{-2} y^{-1}). Their records are also similar to those in the 1988/89 cores located in more northerly locations on the western side of the lake, which are less impacted by stream inputs from the catchment. Figure 9 compares unsupported ^{210}Pb records in cores from the eastern side of the lake collected in 1977, 1989 and 2014. Concentrations in the surficial sediments of these cores range from 452 Bq kg^{-1} to 579 Bq kg^{-1} with a mean value of 532 Bq kg^{-1}, significantly higher than in cores from the western and central areas of the lake. The 1989 and 2014 cores also had significantly lower overall sedimentation rates as measured by the depths of the ^{210}Pb dating horizon; in all three cores these were between 18-19 cm (3.5-4.25 g cm^{-2}). A higher sedimentation rate at the site of the 1977 core, indicated by the significantly deeper record, may be due to remobilisation of sediment from the margins of the lake. This core was from 7.5 m water depth compared to ~9 m for the 1989 core and more than 11 m for the 2014 cores. The 2014/2 core appears to have two small but significant irregularities, one at the middle of the record and the other near the base.

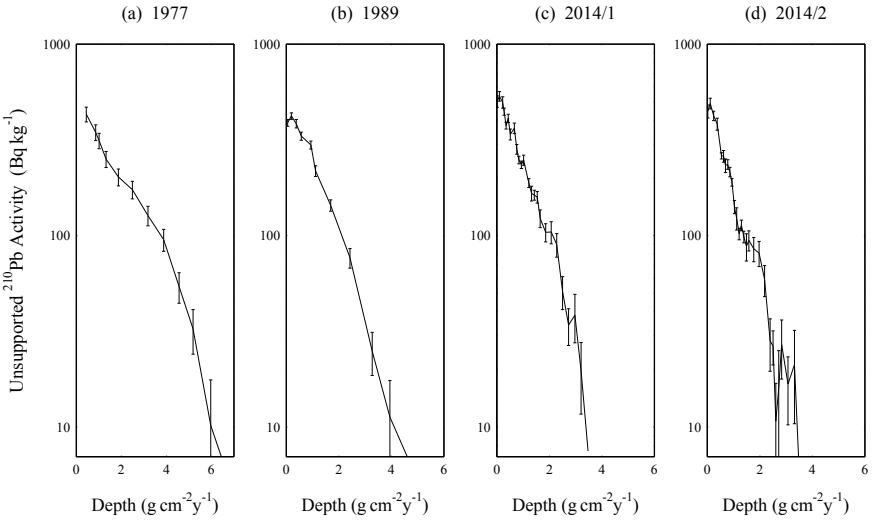

Fig 9. ^{210}Pb records in cores from the eastern side of Brotherswater collected in (a) 1977, (b) 1989, (c) & (d) 2014

Figure 10 plots records from a similar suite of cores from the northern part of the lake. Surface concentrations in these cores have a mean value (427 Bq kg^{-1}) intermediate between those from the western and central areas of the lake, and those from the eastern areas. The depths of the ^{210}Pb dating horizon in the 1989 and 2014 cores are similar to though slightly greater than those in the corresponding cores from the eastern area. A significantly higher sedimentation rate in the 1977 core (from 4 m water depth) may again be due to remobilisation of sediment from the margins of the lake.

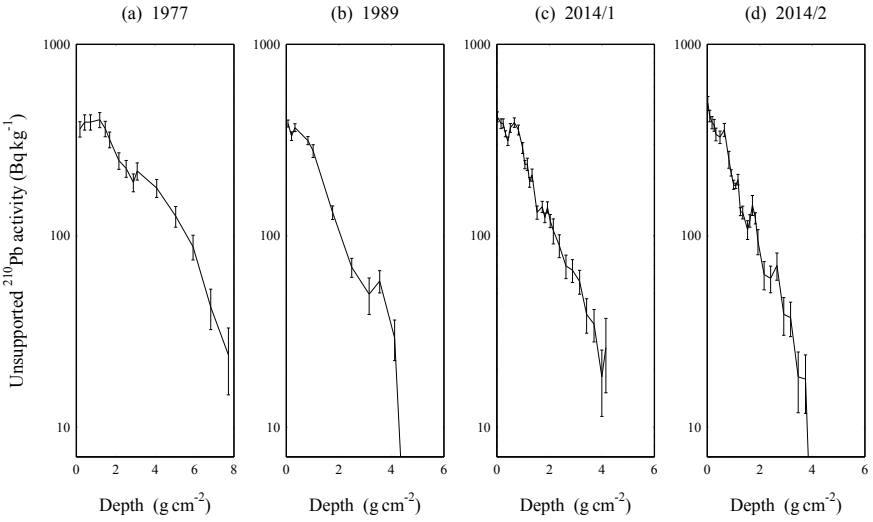

Fig 10. ^{210}Pb records in cores from the northern end of Brotherswater collected in (a) 1977, (b) 1989, (c) & (d) 2014

^{210}Pb dates and sedimentation rates

Most calculations of ^{210}Pb dates assume that the measured present day concentration $C(t)$ in sediments of age t is related to the original concentration $C_0(t)$ by the radioactive decay law

$$C(t) = C_0(t)\,\mathrm{e}^{-\lambda t} \tag{5}$$

where λ the ^{210}Pb radioactive decay constant. In order to calculate the age t it is first necessary to estimate the initial concentration $C_0(t)$. The two most common models used for making this estimate (Appleby & Oldfield 1978) are:

1. The CIC (Constant Initial Concentration model), which assumes that the initial concentration has a constant value C_0.
2. The CRS (Constant Rate of ^{210}Pb Supply), which assumes that initial concentration is governed by a constant rate of supply of fallout ^{210}Pb to the core site.

These assumptions greatly simplify the complexity of the processes by which fallout ^{210}Pb accumulates in lake sediments. Here we use the well-established chrono-stratigraphic dates determined from the ^{137}Cs and mining Pb records to investigate the reliability of ^{210}Pb as a dating tool, and in particular the extent to which either of the above assumptions provides a reasonably accurate approximation to the actual processes by which ^{210}Pb records are formed. Any discrepancies between raw dates calculated using either of the above simple models will be due to deviations of the actual processes from the model assumptions. The raw dates may however be corrected by applying the models in a piecewise way using the methods described in Appleby (2001). Using the results from all three studies, comparisons are made not only between records from different parts of the lake but also between records from different times.

Comparison between ^{210}Pb and chronostratigraphic dates

In most cases there was a relatively good level of agreement between the raw CRS ^{210}Pb model dates and those determined from the 1986 and 1963 ^{137}Cs/^{241}Am records. Cores showing a high level of agreement were mainly from sites more distant from the main inlet and included BW89/2 (western side of lake), BW12/9 (central area), BW14/E1, BW14/E2, BW89/4 (eastern side), and BW14/N2, BW89/5 (northern end).

At all these sites the ^{210}Pb supply rate appears to have been relatively constant and comparable to the atmospheric flux. Values ranged from 144-203 Bq m^{-2} y^{-1}, with a mean value of 180 Bq m^{-2} y^{-1}.

Sites where there were significant discrepancies between the ^{210}Pb and ^{137}Cs dates all had ^{210}Pb supply rates that significantly exceeded the atmospheric flux. They included BW11/2, BW88/2 (western side) BW89/3 (central) and BW14/N1 (northern). At BW11/2 the ^{210}Pb calculations placed 1963 at a depth of 20 cm, 2.5 cm above the 1963 depth determined from the ^{137}Cs record. The very high ^{210}Pb supply rate to this part of the lake can be attributed to substantial inputs of catchment ^{210}Pb via the main inlet stream. Calculations using the ^{137}Cs dates as reference points show the cause of the dating discrepancy to be a substantial increase in inputs of ^{210}Pb in recent decades. Net ^{210}Pb supply rates have risen from 482 Bq m^{-2} y^{-1} before 1963 to a post-1963 value of 648 Bq m^{-2} y^{-1}. Although less impacted by catchment inputs, there were similar increases at BW88/2 and BW89/3. At both sites the ^{210}Pb supply rates increased from pre-1963 values comparable to the atmospheric flux to post-1963 values of between 270-295 Bq m^{-2} y^{-1}.

At the northerly site BW14/N1 the ^{210}Pb 1963 depth was 1 cm below the weapons ^{137}Cs peak. In this case the discrepancy was due to a reduction in the ^{210}Pb supply rate, from 230 Bq m^{-2} y^{-1} before 1963 to a near atmospheric value (180 Bq m^{-2} y^{-1}) during 1963-86.

In the 2011-14 cores, additional 19th century chronostratigraphic information was provided by the stable Pb records. The ^{210}Pb dating horizon for these cores, measured by a 99% reduction in activity, was between 1863-1866. This coincides almost exactly with the 1863-71 period of intensive mining linked to the episodes of Pb pollution seen in the sediment records. Although calculations of the 99% equilibrium depths have a degree of uncertainty, at most sites they were relatively close to the depth of the Pb concentration peaks. This provides independent evidence of the origin of the Pb records. The Pb peaks can be thus be used as reliable chronostratigraphic markers.

In the 1977 cores, the ^{137}Cs records were too indistinct and 1963 too recent to make reliable comparisons between the ^{210}Pb and ^{137}Cs dates. ^{210}Pb dates for these cores, particularly those with high ^{210}Pb supply rates, need to be regarded with some caution.

Sedimentation rate records

At those sites were there were discrepancies between the raw ^{210}Pb dates and well-established chronological markers, corrections to the ^{210}Pb dates were calculated by applying the CRS model in a piecewise way. Detailed results including sedimentation rates versus time are given in the Electronic Supplementary Material Table ESM4 (1976/7 cores), Table ESM5, (1988/9 cores) and Table ESM6 (present study). Although there are differences in detail, a number of broad features do emerge.

- At most sites sedimentation rates were relatively constant during the first half of the 20th century but did show significant increases during the second half of the century.
- The largest increases were at sites along the western side of the lake nearer the main inlet, mainly driven by erosive inputs from the catchment and associated with substantial inputs of allochthonous fallout ^{210}Pb.
- The increases were relatively modest at sites in the central, eastern and northern areas of the lake, away from the main inlet. The supply of ^{210}Pb to these sites was dominated by the direct atmospheric flux.

Although the mean pre-1963, 1963-86 and post-1986 sedimentation rates determined from the ^{210}Pb records will be similar to those determined from the chronostratigraphic dates, the ^{210}Pb calculations do give more detail as to the timing of any changes. Results for cores from the western side of the lake, shown in Figure 11(a), highlight dramatic differences between the impacts of allochthonous inputs on cores separated by less than 100 m. The mean pre-1950 sedimentation rate at BW11/2 (0.14 g cm^{-2} y^{-1}) is 4 times higher than at BW88/2 and BW89/2 (0.032 g cm^{-2} y^{-1} and 0.043 g cm^{-2} y^{-1} respectively). The post-1950 increases at BW11/2, evidenced by the ^{137}Cs record, began late 1950s or early 1960s and reached a maximum value in the mid-1970s. Increased catchment inputs driving these changes appear to have had a significant impact at BW88/2. The ^{137}Cs record shows that the mean post-1963 sedimentation rate at this site is twice as high as the pre-1950 value. The ^{210}Pb calculations date the increase to around 1970 and suggest that it was relatively abrupt. A corresponding increase in the ^{210}Pb supply rate may indicate that the increase was due to sediment remobilization and downslope transport from the western margins. This core was from 11 m water depth, near the base of the slope. The more marginal core BW89/2 (5 m

water depth) appears to have experienced little impact. The results for this site indicate no more than a relatively minor increase in the 1980s.

The central cores BW12/9 and BW89/3 had very similar pre-1950 sedimentation rates (0.047 g cm^{-2} y^{-1} and 0.042 g cm^{-2} y^{-1} respectively), as shown in Figure 11(b). At BW12/9 there was an episode of increased sedimentation (independently supported by the ^{137}Cs dates) lasting from the 1950s through to the 1980s. This appears to have been a relatively localized event. At BW89/3 sedimentation rates remain relatively constant until around 1970 when there were abrupt increases in both the sediment and ^{210}Pb supply rates similar to those at BW88/2.

The eastern cores BW14/E1, BW14/E2 and BW89/4 also had very similar pre-1950 sedimentation rates, though significantly lower than in the central area. Mean values were 0.029 g cm^{-2} y^{-1}, 0.024 g cm^{-2} y^{-1} and 0.030 g cm^{-2} y^{-1} respectively. All three sites recorded small but significant increases during the second half of the 20th century, though there were differences in timing and duration (Figure 11(c)).

In the northern area of the lake the onset of increased sedimentation appears to have begun as early as the late 1920s or early 1930s (Figure 11(d)), though this was from a very low base. Pre-1920 sedimentation rates were just 0.027 g cm^{-2} y^{-1} at BW14/N1 and 0.022 g cm^{-2} y^{-1} at BW14/N2. Later results from these two sites follow a very similar pattern, apart from an episode of accelerated sedimentation at BW14/N2 during the 1970s. Since during the same period there was a small reduction in the ^{210}Pb supply rate at BW14/N1, the difference may simply be due to a small local change in the pattern of sedimentation. Relatively few data points in BW89/5, combined with the effect of a possible slump event in the early part of the record, makes detailed comparisons with later cores difficult. The mean sedimentation rate from 1920 through to the mid-1960s (0.033 g cm^{-2} y^{-1}) was however very similar to that of the 2014 cores. Significantly higher post-1963 sedimentation rates are consistent with the ^{137}Cs record.

Uncertainties concerning the dry bulk density data, the relatively poor ^{137}Cs records and also the relationship between the cores analysed for ^{210}Pb and ^{137}Cs make detailed comparisons with the 1977 study problematic. In spite of these problems, there is a general level of consistency with the later studies. The mean ^{210}Pb supply rate (311 Bq m^{-2} y^{-1}) and sedimentation rate (0.10 g cm^{-2} y^{-1}) at the western core BWW are intermediate in value between the BW11/2 and the 1988/9 cores BW88/2 and BW89/2, and commensurate with its intermediate location. Estimates of the mean pre-1950

sedimentation rates for the central core BWC (0.041 g cm^{-2} y^{-1}) are very similar to those for BW12/9 and BW88/3. There is also evidence of a post-1950 increase. The eastern (BWE) and northern (BWN) are however outliers in that both appear to be from sites that have experience significantly higher sedimentation rates (and also ^{210}Pb supply) than nearby cores from the later studies. Since both were located in relatively shallow water, these results may be due to remobilization of sediments to the margins of the lake.

Discussion

The ^{137}Cs records shown in Figures 2-5 provide clear and direct evidence of the preservation and progressive burial of environmental records stored in the sediments of Brotherswater and, in this case, the reduction in concentration due to radioactive decay. The persistence over time of a relatively good agreement between ^{210}Pb dates calculated in this case using the CRS model and chronostratigraphic dates determined from the ^{137}Cs records provides evidence of the relative stability of ^{210}Pb records. Differences between ^{210}Pb and ^{137}Cs dates were relatively small at sites in the lake where the ^{210}Pb supply rate was comparable to the atmospheric flux. Discrepancies were however observed at sites where ^{210}Pb supply rates significantly exceeded the atmosphere flux. Calculations of pre-1963 and post-1963 ^{210}Pb supply rates showed that these discrepancies were attributable to changes in the ^{210}Pb supply rate due causes such as varying allochthonous inputs from the catchment and varying degrees of sediment focusing within the lake. Since the changes in sedimentation rates at these sites were not proportional to changes in the ^{210}Pb supply rates, in these cases neither of the standard simple (CRS and CIC) models were applicable to the ^{210}Pb record as a whole. Reliable chronologies spanning the ^{210}Pb period could however be constructed by applying these models in a piecewise way to different sections of the core. Although there were differences in detail, pre-1989 sedimentation rates determined from the recent study were generally similar to those determined for similar areas of the lake in the earlier study. This was not however the case for cores from the western side of the lake heavily impacted by catchment inputs where there were large differences between cores separated by relatively short distances.

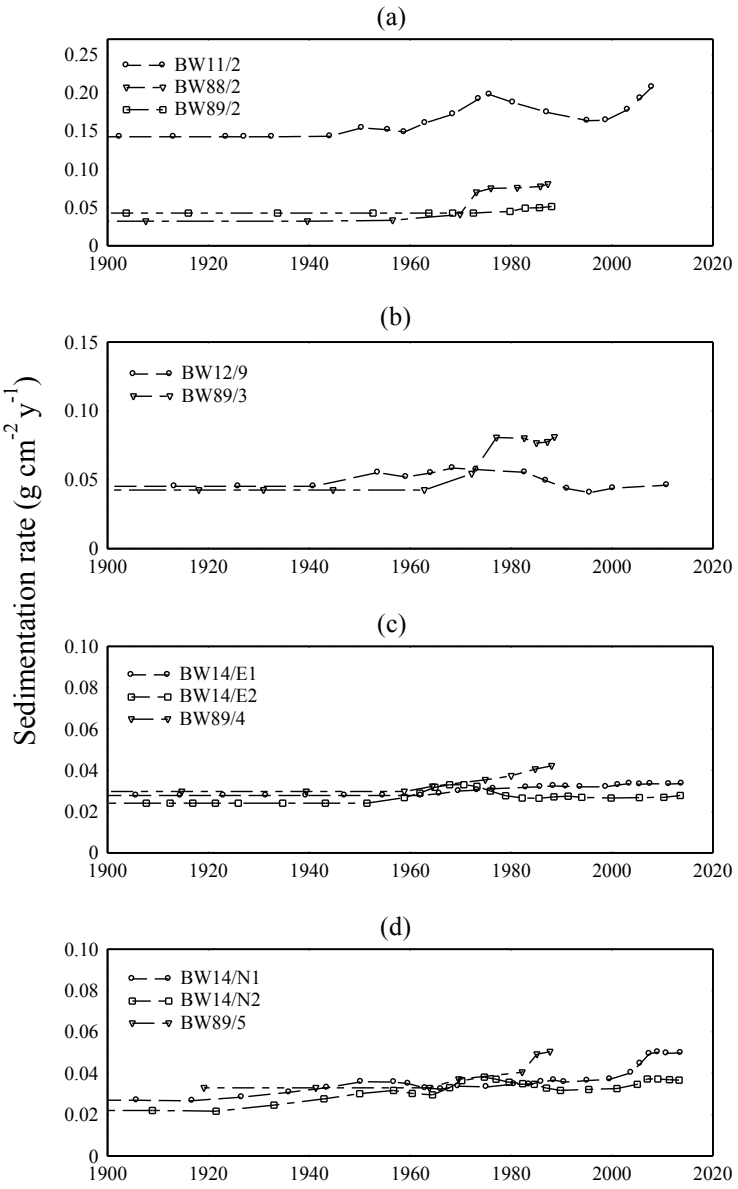

Fig 11. Sedimentation rates versus time in cores from (a) the western, (b) the central, (c) the eastern and (d) the northern areas of Brotherswater

References

Appleby PG (2001) Chronostratigraphic techniques in recent sediments. In: Last WM, Smol JP (eds) Tracking Environmental Change Using Lake Sediments Volume 1: Basin Analysis, Coring, and Chronological Techniques. Kluwer Academic, Dordrecht, pp 171-203

Appleby PG, Nolan PJ, Gifford DW, Godfrey MJ, Oldfield F, Anderson NJ, Battarbee RW (1986) Pb-210 dating by low-background gamma counting. Hydrobiologia, 143: 21-27

Appleby PG, Oldfield F (1978) The calculation of lead-210 dates assuming a constant rate of supply of unsupported ^{210}Pb to the sediment. Catena 5: 1-8

Appleby PG, Richardson N. Nolan PJ, (1991) ^{241}Am dating of lake sediments. Hydrobiologia, 214: 35-42.

Appleby, PG, Richardson N, Nolan PJ (1992) Self-absorption corrections for well-type germanium detectors. Nucl. Inst.& Methods B, 71: 228-233.

Bonnett PJP, Appleby PG, Haworth EY, Hilton J, Davison W, Oldfield F (1992). Environmental behaviour of radioactivity from Chernobyl: Brotherswater study. DOE Report No. DOE/RAS/92.004, 55pp.

Boyle JF (1995) A simple closure mechanism for a compact, large-diameter, gravity corer. Journal of Paleolimnology 13: 85–87.

Eakins JD, Cambray RS, Chambers KC, Lally AE (1981) The transfer of natural and artificial radionuclides to Brotherswater from its catchment. AERE-R 10375, AERE Harwell, UK, 26 pp.

Eakins JD, Cambray RS, Chambers KC, Lally AE (1984) The transfer of natural and artificial radionuclides to Brotherswater from its catchment. In: Haworth EY, Lund JW (eds) Lake sediments and Environmental History. Leicester University Press, Leicester, pp 94-114

Hilton J, Haworth EY, Davison W, Kelly M, Hamilton-Taylor J, Appleby PG (1992) Transport processes of ^{137}Cs in lake environments. DOE/RW/92.005

Maberly S, De Ville M, Thackeray S, Feuchtmayr H, Fletcher JM, James JB, Kelly JL, Vincent CD, Winfield IJ, Newton A, Atkinson D, Croft A, Drew H, Saag M, Taylor S, Titterington H (2011) A survey of the lakes of the English Lake District: The Lakes Tour 2010. Final report to the Environment Agency, Northwest region

Pennington W, (1981) Records of a lake's life in time: the sediments. Hydrobiologia, 79: 197-215

Robbins JA (1978) Geochemical and geophysical applications of radioactive lead. In Nriagu (ed) Biogeochemistry of Lead in the Environment. Elsevier Scientific, Amsterdam, pp 285-393.

Schillereff DN, Chiverrell RC, Macdonald N, Hooke JM, Welsh KE (2016) Quantifying system disturbance and recovery from historical mining-derived metal contamination at Brotherswater, northwest England. Journal of Paleolimnology, 56: 205-221. doi:10.1007/s10933-016-9907-1

Tables

Table 1 Brotherswater catchment-lake parameters

Location:	54.5ºN, 2.9ºW
Catchment area:	13 km^2
Altitude range:	158-800 m
Rainfall:	2530 mm
Lake area	1.8×10^5 m^2
Maximum depth:	17 m
Mean depth:	6.6 m
Lake volume:	2.1×10^6 m^3
Catchment Area to Lake ratio	72

Table 2 List of historical Brotherswater cores dated by ^{210}Pb and ^{137}Cs

	1976/7 study		1988/9 study	
Site	Core	Depth	Core	Depth
Inlet	BW1/76	8.5 m	BW89/1	8.5 m
Western	BWW	7.5 m	BW88/2	11 m
″			BW89/2	5 m
Central	BWC	17 m	BW89/3	17 m
Eastern	BWE	7.5 m	BW89/4	8.5 m
Northern	BWN	4 m	BW89/5	4.5 m

Table 3 List of 2011-2014 Brotherswater cores dated by ^{210}Pb and ^{137}Cs

Core	Date	Depth (m)	Map coordinates	
			North	East
BW11/2	2011	16.3	512678	340127
BW12/9	2012	15.1	512763	340206
BW14/E1	2014	12.5	512706	340423
BW14/E2	2014	13.5	512697	340404
BW14/N1	2014	11.5	512851	340215
BW14/N2	2014	13.5	512809	340232

Table 4 Chronostratigraphic dates for the 2011-2014 cores

	Depth (cm)		
	1986	1963	1867
BW11/2	11.25-12.75	21.75-23.25	51.25-54.25
BW12/9	4.0-5.5	9.75-10.75	23.5-25.0
BW14/E1	6.0-7.5	9.25-10.25	20.5-22.0
BW14/E2	4.75-6.25	7.75-9.0	19.25-20.75
BW14/N1	6.75-7.75	10.75-11.75	21-22.5
BW14/N2	5.0-6.5	10-11	19-20.5

Table 5 Chronostratigraphic dates for the 1988-1989 cores

	Depth (cm)	
	1986	1963
BW88/2	1-2	7.5-10
BW89/2	0.5-2.5	7-8.5
BW89/3	1-2	8.5-10.5
BW89/4	0-2	5-6.5
BW89/5	0-1	6-7.5

Table 6 Fallout ^{210}Pb parameters for the Brotherswater cores

Core and Date	Unsupported ^{210}Pb		
	Surface activity Bq kg^{-1}	Inventory Bq m^{-2}	Mean supply rate Bq m^{-2} y^{-1}
Western			
BWW (1977)	374	9990	311
BW88/2 (1988)	409	7998	249
BW89/2 (1989	396	6298	196
BW11/2 (2011)	286	19450	606
Central			
BWC (1977)	387	7772	242
BW89/3 (1989	412	7195	224
BW12/9 (2012)	346	5542	173
Northern			
BWN (1977)	381	15354	478
BW89/5 (1989)	394	6507	203
BW14/N1 (2014)	425	6884	214
BW14/N2 (2014)	506	5606	175
Eastern			
BWE (1977)	546	10360	323
BW89/4 (1989)	452	6222	194
BW14/E1 (2014)	579	6048	188
BW14/E2 (2014)	549	4634	144

Figure captions

Figure 1. Locations of the 2011-2014 core sites together with those from earlier studies.

Figure 2. ^{137}Cs records in cores from the western side of Brotherswater collected in (a) 1975, (b) 1988, (c) 1989, (d) 2011.

Figure 3. ^{137}Cs records in cores from the central area of Brotherswater collected in (a) 1977, (b) 1989, (c) 2012.

Figure 4. ^{137}Cs records in cores from the eastern side of Brotherswater collected in (a) 1977, (b) 1989, (c) and (d) 2014.

Figure 5. ^{137}Cs records in cores from the northern (outlet) end of Brotherswater collected in (a) 1977, (b) 1989, (c) and (d) 2014.

Figure 6. Stable Pb records in the Brotherswater cores collected for the present study

Figure 7. ^{210}Pb records in four cores from the western side of Brotherswater collected in (a) 1977, (b) 1988, (c) 1989, (d) 2011

Figure 8. ^{210}Pb records in three cores from the central area of Brotherswater collected in (a) 1977, (b) 1989, (d) 2012

Figure 9. ^{210}Pb records in cores from the eastern side of Brotherswater collected in (a) 1977, (b) 1989, (c) and (d) 2014

Figure 10. ^{210}Pb records in cores from the northern end of Brotherswater collected in (a) 1977, (b) 1989, (c) and (d) 2014

Figure 11. Sedimentation rates versus time in cores from (a) the western, (b) central, (c) eastern and (d) northern areas of Brotherswater

Figures

Figure 1. Locations of the 2011-2014 core sites together with those from earlier studies.

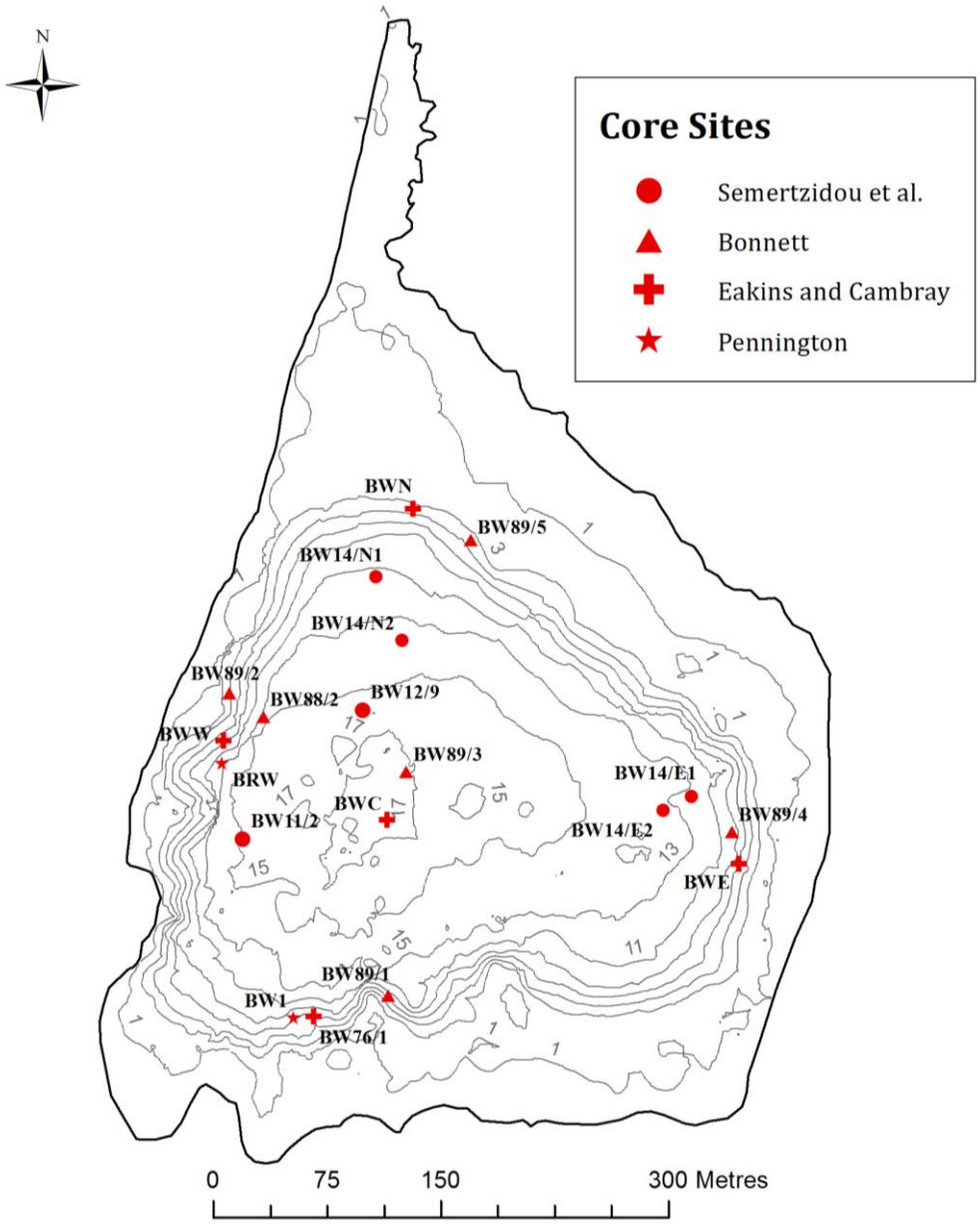

Figure 2. ^{137}Cs records in cores from the western side of Brotherswater collected in (a) 1975, (b) 1988, (c) 1989, (d) 2011.

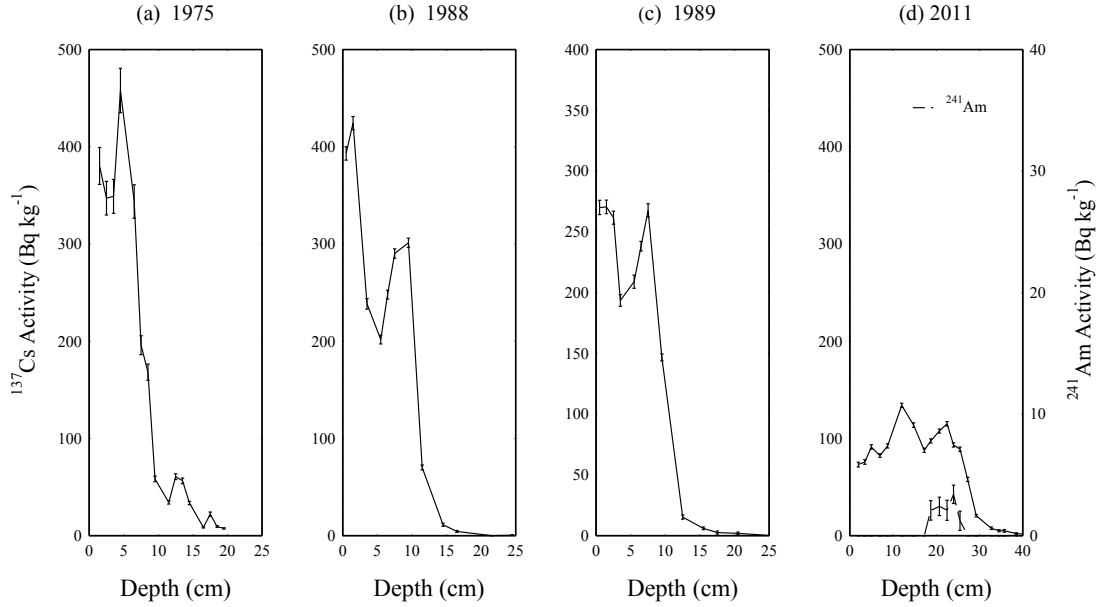

Figure 3. ^{137}Cs records in cores from the central area of Brotherswater collected in (a) 1977, (b) 1989, (c) 2012.

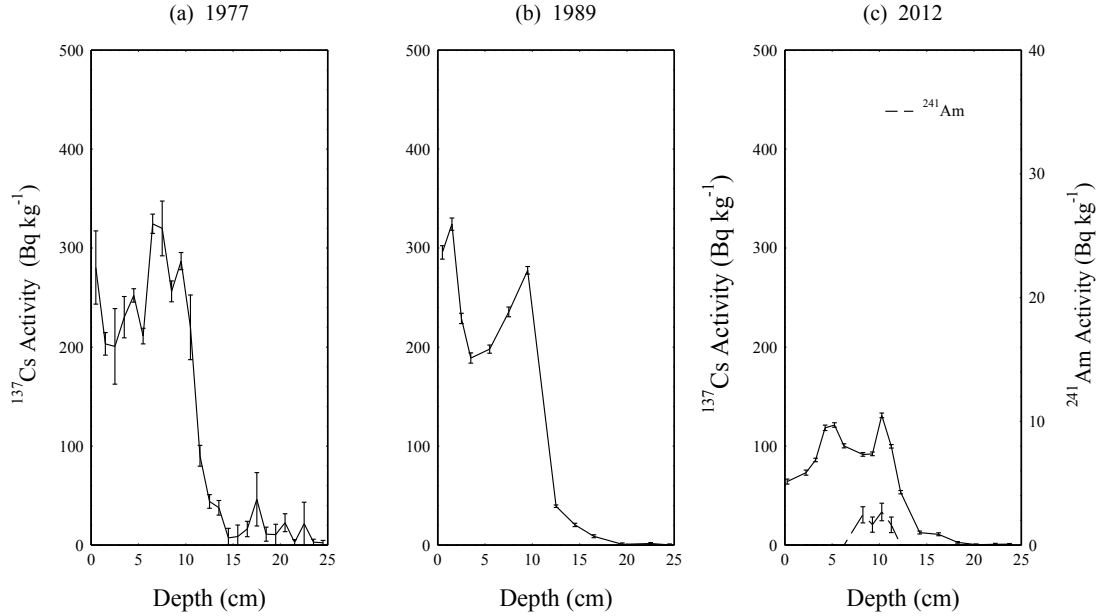

Figure 4. ^{137}Cs records in cores from the eastern side of Brotherswater collected in (a) 1977, (b) 1989, (c) and (d) 2014.

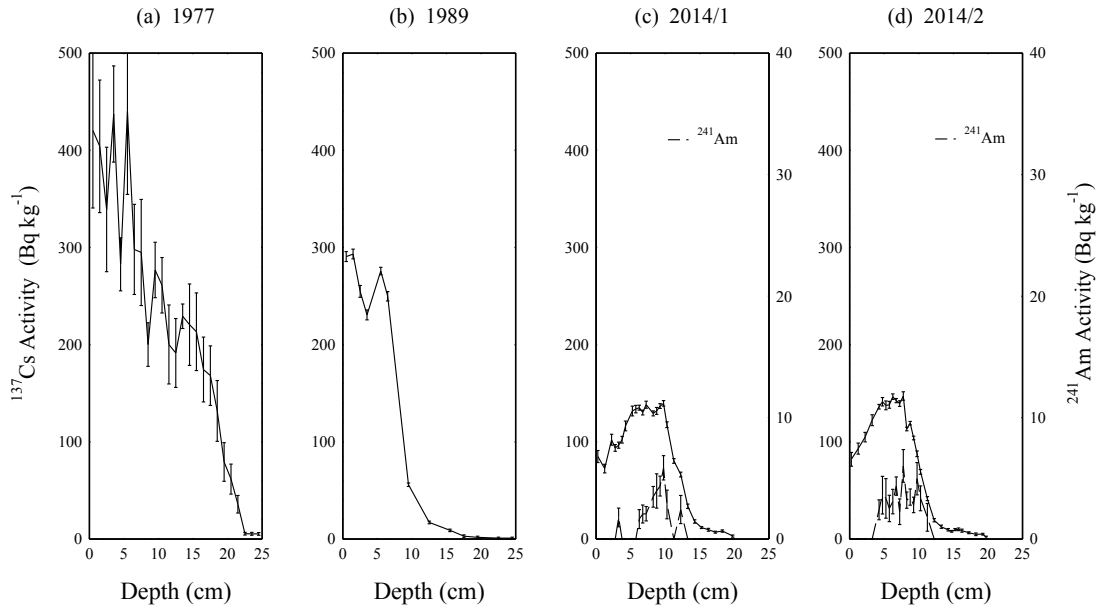

Figure 5. ^{137}Cs records in cores from the northern (outlet) end of Brotherswater collected in (a) 1977, (b) 1989, (c) and (d) 2014.

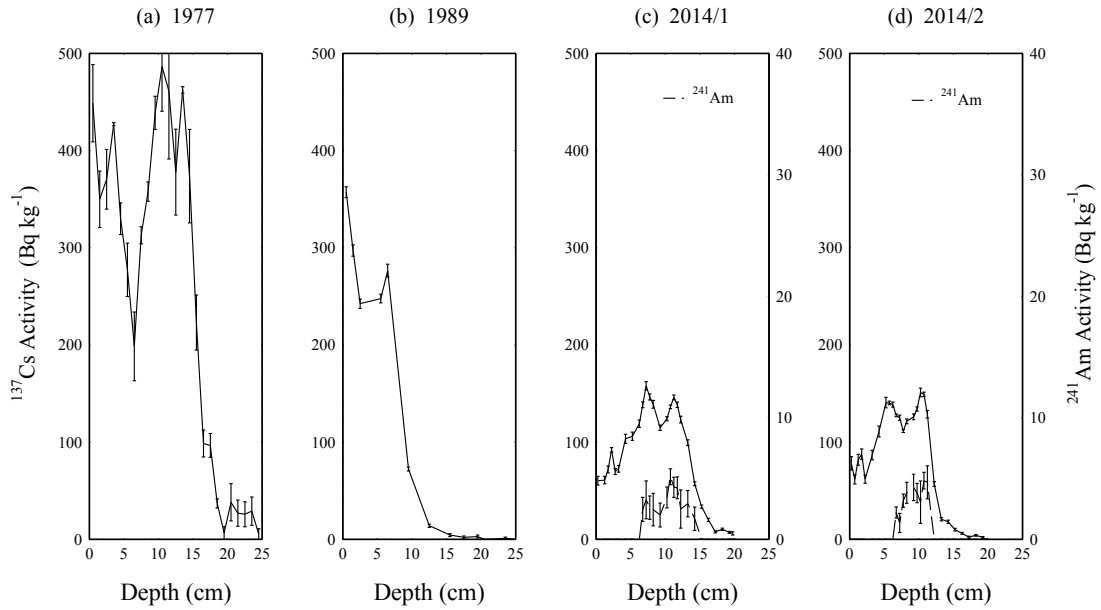

Figure 6. Stable Pb records in the Brotherswater cores collected for the present study

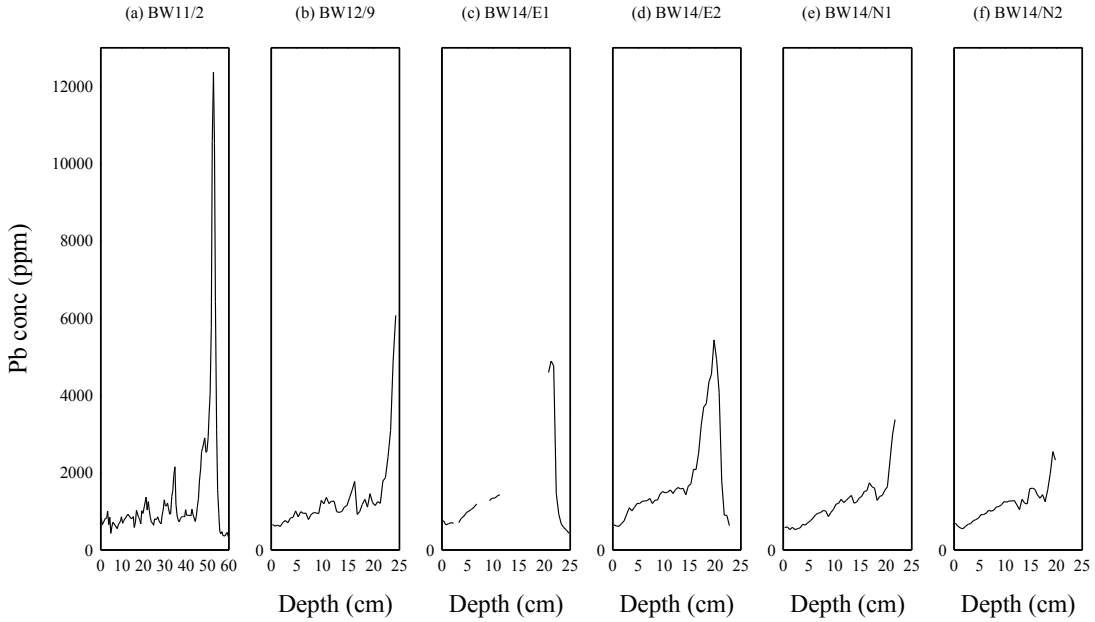

Figure 7. ^{210}Pb records in four cores from the western side of Brotherswater collected in (a) 1977, (b) 1988, (c) 1989, (d) 2011

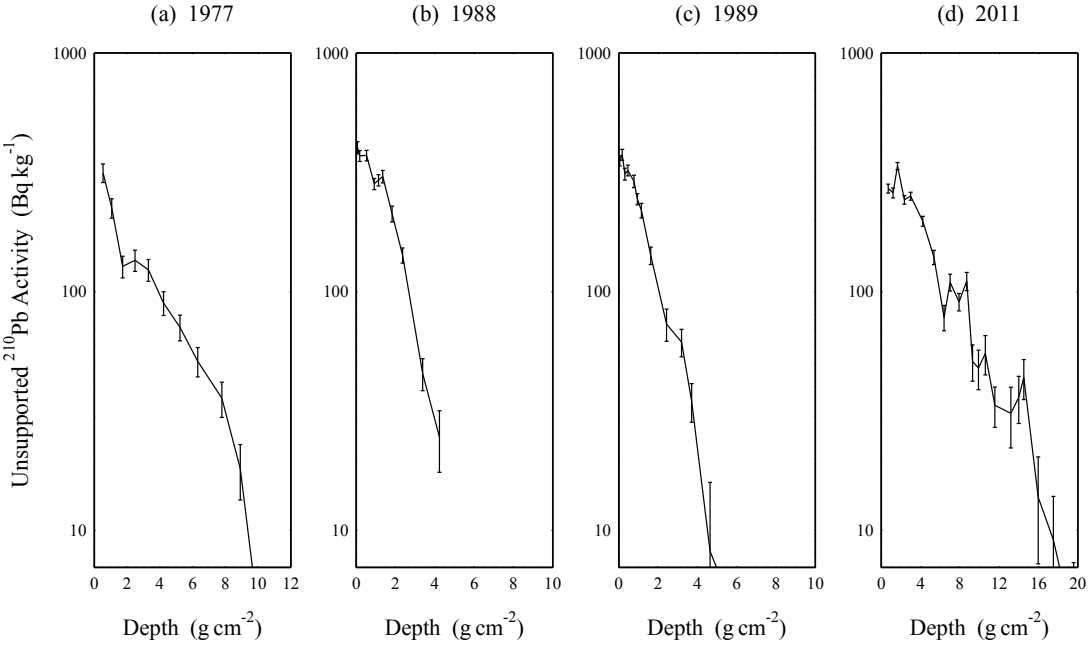

Figure 8. ^{210}Pb records in three cores from the central area of Brotherswater collected in (a) 1977, (b) 1989, (d) 2012

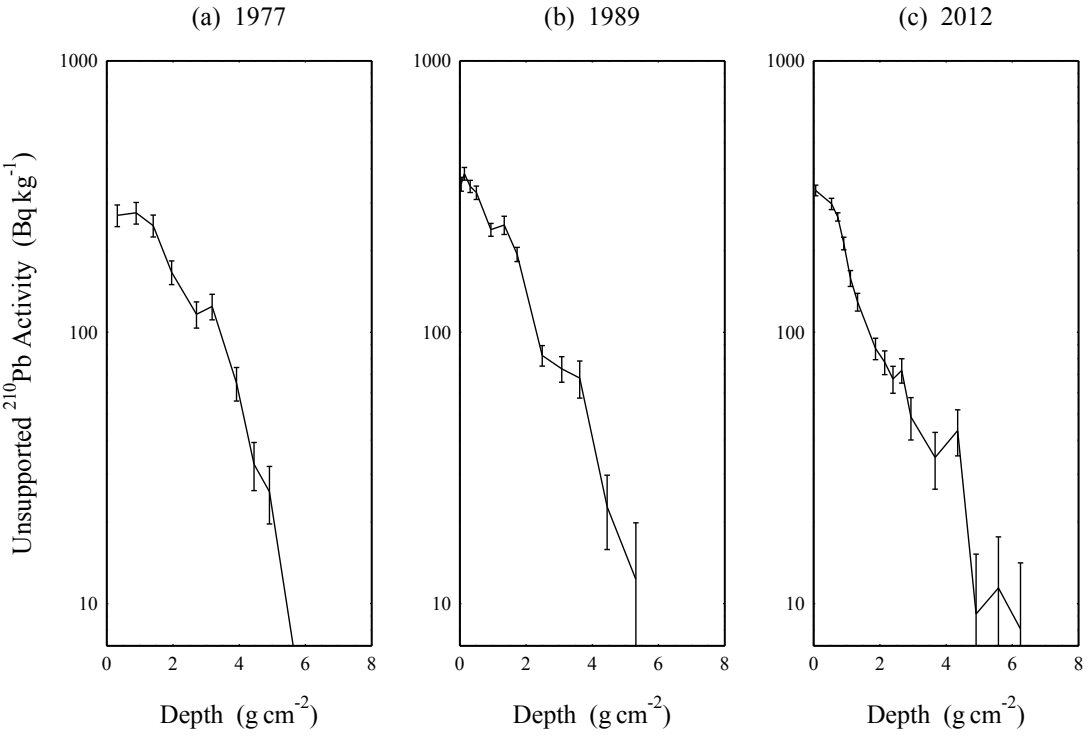

Figure 9. ^{210}Pb records in cores from the eastern side of Brotherswater collected in (a) 1977, (b) 1989, (c) and (d) 2014

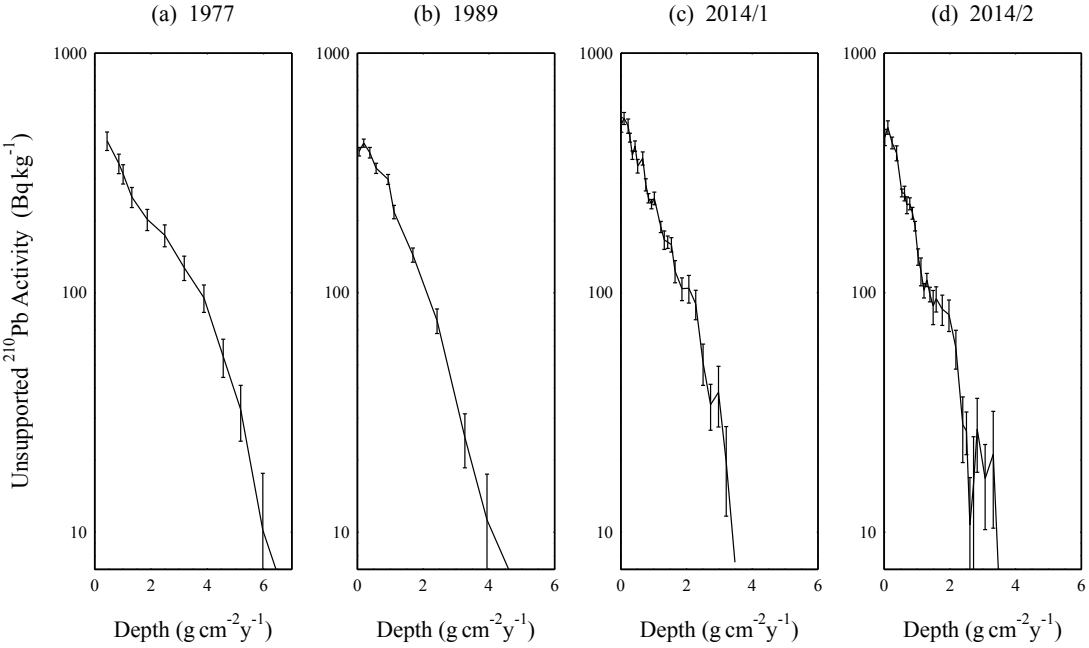

Figure 10. ^{210}Pb records in cores from the northern end of Brotherswater collected in (a) 1977, (b) 1989, (c) and (d) 2014

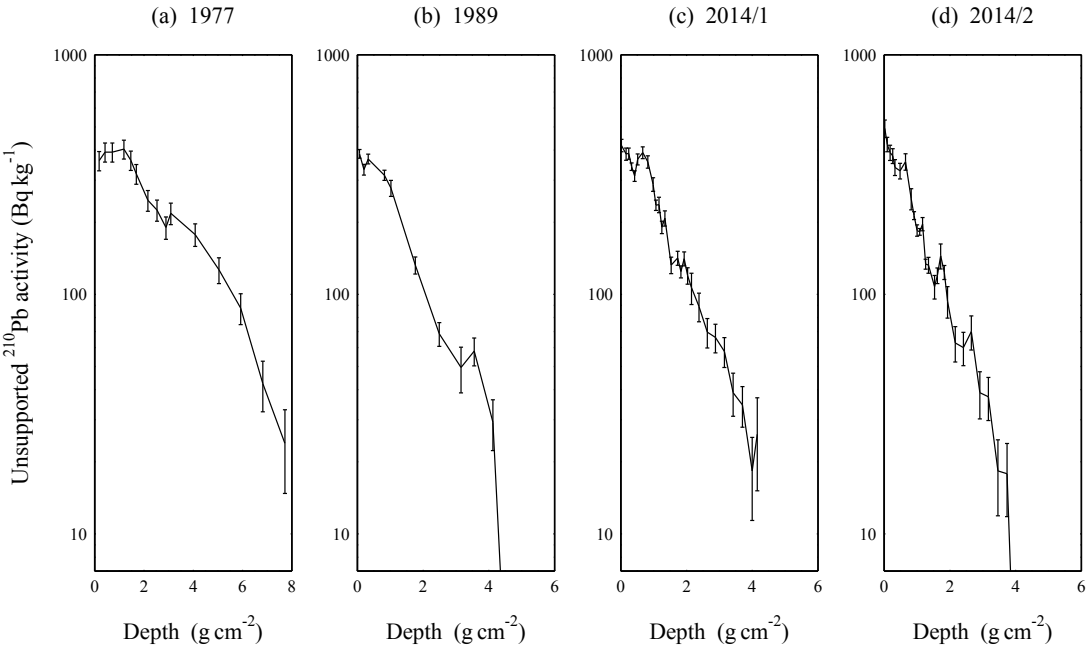

Figure 11. Sedimentation rates versus time in cores from (a) the western, (b) central, (c) eastern and (d) northern areas of Brotherswater